**Fakultät für Medizin**

**Institut/Klinik/Lehrstuhl für:**

**Institut für Medizinische Mikrobiologie, Immunologie und Hygiene**

# The interaction of hepatitis B or C virus infection and schistosomiasis in chronic pathogen-induced liver inflammation

**Eva Loffredo-Verde**

Vollständiger Abdruck der von der Fakultät für Medizin der Technischen Universität München zur Erlangung des akademischen Grades eines

**Doktors der Naturwissenschaften**

genehmigten Dissertation.

| | |
|---|---|
| Vorsitzende: | Univ.-Prof. Dr. U. Protzer |
| Prüfer der Dissertation: | 1. Priv.-Doz. Dr. C. U. I. Prazeres da Costa |
| | 2. Univ.-Prof. Dr. M. Klingenspor |

Die Dissertation wurde am 21.10.2015 bei der Fakultät für Medizin der Technischen Universität München eingereicht und durch die Fakultät für Medizin am 31.03.2016 angenommen.

# Content

## Abstract

One of the main complications of hepatitis C (HCV) and B virus (HBV) infection is the development of chronic hepatitis after the initial acute infection, since these individuals are at high risk to develop liver cirrhosis and hepatocellular carcinoma. Interestingly, chronicity develops at a higher frequency in developing countries in which co-infections with several helminth species, such as *S. mansoni*, are common. The underlying mechanisms leading to HCV/HBV chronicity are only partly understood but compromise $CD8^+$ and $CD4^+$ T cell responses, which might be affected in helminth co-infected patients due to dynamic schistosome-driven immune responses. These range from an initial $T_H1$- to $T_H2$-immunity and eventually to long-term immunosuppression. Thus, the effects of pre-existing helminth infections on concomitant HCV/HBV infection are hard to predict and need clarification. The central aims in this thesis were therefore to determine whether schistosome-induced immunomodulation could have an impact on the severity and course of another chronic liver disease, hepatitis C or B virus infection and whether this is associated with functional effector T cell and regulatory T cell (Treg) changes. To address the different questions we investigated *S. mansoni* and HCV co-infection in an epidemiological study and concomitant HBV and schistosomiasis in an experimental setting.

Regarding the interrelationship between *S. mansoni* and Hepatitis C virus infection, the parasite seems to accelerate the progression of the liver disease, as liver cirrhosis and hepatocellular carcinoma are more common within co-infected individuals. Since schistosome infections are renowned for their ability to induce regulatory networks such as Treg that control immune responses against homologous and heterologous antigens such as allergies, we hypothesized that expanding schistosome-induced Treg populations change their phenotype and could thereby suppress beneficial anti-HCV responses. We therefore analysed effector T cells and n/iTreg subsets applying the markers Granzyme B (GrzB) and Helios in Egyptian cohorts of HCV mono-infected (HCV), schistosome-co-infected (Sm/HCV) and infection-free individuals. Interestingly, viral load and liver transaminases were significantly elevated in Sm/HCV individuals when compared to HCV patients. Moreover, overall Treg frequencies and $Helios^{pos}$ Treg were not elevated in Sm/HCV individuals, but frequencies of $GrzB^+$ Treg were significantly increased. Simultaneously, $GrzB^+$ $CD8^+$ T cells were not suppressed in co-infected individuals. This study demonstrates that in Sm/HCV co-

infected cohorts, liver disease is aggravated with enhanced virus replication and Treg do not expand but rather change their phenotype with GrzB possibly being a more reliable marker than Helios for iTreg. Therefore, curing concurrent schistosome disease could be an important prerequisite for successful HCV treatment as co-infected individuals respond poorly to interferon therapy.

In contrast to concomitant *S. mansoni* and HCV infections, where an accelerated onset of the liver disease is observed in the majority of cases, the interrelationship between HBV and schistosomiasis is controversially discussed. We hypothesized that these diverging epidemiological observations result from fluctuating immune responses induced during schistosome infection, which influence the severity and outcome of a concomitant acute HBV co-infection. Therefore, to take our human study further and to expand on underlying mechanisms of interactions between hepatitis virus infections and schistosomiasis, we experimentally investigated, with the help of the AdHBV-$X^-$ mouse model, the development of an acute HBV infection acquired during the different immune phases ($T_H1$, $T_H2$, chronic) induced during *S. mansoni* infection. Compared to mice with an HBV mono-infection, we observed a faster viral clearance only in those animals who acquired the viral infection during IFN-γ-prone immune phases ($T_H1$ and chronic phase) of schistosomiasis. These animals displayed significantly decreased viral antigen levels and lower amounts of HBV genomes in the liver and had elevated frequencies of splenic and liver-resident HBV-specific $CD8^+$ IFN-$\gamma^+$ T cells when compared to HBV mono-infected counterparts. In addition, splenocytes and mesenterial lymph node cells of co-infected mice produced higher amounts of IFN-γ upon antigen-independent stimulation, showing that concomitant helminth infection boosts the production of this cytokine in an antigen-independent manner. In contrast, co-infected IFN-γ-deficient mice as well as animals infected with HBV during the early $T_H1$ and $T_H2$ phase, where the production of IFN-γ was hardly detectable failed to show an enhanced viral clearance. We therefore attributed suppressed viral replication rates in acutely and chronically schistosome co-infected animals to anti-viral and immunoregulatory properties of schistosome-induced IFN-γ.

A major effector cell population that is instigated already during the Th1 phase are Treg cells with strong immunosuppressive properties on bystander antigen-independent immune responses. We therefore hypothesized that these cells might effectively control antiviral immune responses. Therefore, we analysed the role of schistosome-induced Treg on the

establishment of anti-HBV immune responses during the chronic phase of helminth co-infection. For this purpose, a transgenic mouse model was used, that allowed the specific depletion of Treg cells. We found that loss of Treg cells during co-infection did not lead to a rise in decreased viral titers and antiviral immune responses. Accordingly, we concluded that the anti-viral effect of schistosome-induced IFN-γ dominates over possible Treg effects even during the chronic phase of infection.

In clinical terms, the scenario of a secondary schistosome infection acquired on top of a pre-existing chronic HBV infection is in some parts of the world at least as relevant as the scenario we addressed above. We had the possibility to infect HBV transgenic mice (HBVtg) with schistosomes to assess whether an additional helminth infection is able to break the evolving chronicity. We observed significantly lower viral replication rates exclusively during the $T_H1$ phase and found that the schistosome infection instigated the evolvement of anti-viral immunity. We conclude that co-infection could break the peripheral tolerance in HBVtg mice, possibly by induction of IFN-γ. Interestingly, neither acute nor chronic HBV infection influenced schistosome infection in terms of parasite development, fecundity or immunopathology.

Taken together, our data indicate a causal relationship between schistosome-induced IFN-γ production within the liver, the induction of antiviral T cells and clearance of HB/HC Virus. Importantly, we observe a much more significant role of this cytokine compared to the suppressive effects of the much discussed parasite induced Treg highlighted frequently in literature.

## Zusammenfassung

Eine große Problematik bei der Infektion mit Hepatitis C (HCV) und B-Viren (HBV) ist die Entwicklung von chronischer Hepatitis nach der anfänglichen akuten Infektion, da hier ein erhöhtes Risiko für die Entwicklung von Leberzirrhose und hepatozellulärem Karzinom besteht. Interessanterweise tritt eine höhere Chronizitätsrate in jenen Entwicklungsländern auf, in denen Co-Infektionen mit verschiedenen parasitären Helminthen, wie *S. mansoni* häufig sind. Obwohl die Mechanismen, die zur Entwicklung einer chronischen HCV/HBV Infektion führen, noch weitgehend ungeklärt sind, weiß man, dass vor allem insuffiziente $CD8^+$ und $CD4^+$ T-Zellantworten zur Chronifizierung beitragen. In Patienten mit einer simultanen Wurminfektion könnten dynamische schistosom-induzierte Immunantworten, die von einer anfänglichen $T_H1$- in eine $T_H2$ Phase übergehen, die virus-spezifische T-Zellantwort beeinflussen. Die Auswirkungen der bereits bestehenden Wurminfektionen auf die gleichzeitige HCV/HBV-Infektion sind daher schwer vorauszusagen. Deshalb war eines der Hauptziele dieser Arbeit zu untersuchen, ob die schistosom-induzierte Immunmodulation einen Einfluss auf die Schwere und den Verlauf einer anderen chronischen Lebererkrankung, nämlich Hepatitis C oder B-Virus-Infektion hat. Zudem sollte untersucht werden, ob dies mit phenotypischen und funktionellen Veränderungen der Effektor- und regulatorischen T-Zell (Treg) Populationen einhergeht. Um dies zu beantworten, untersuchten wir *S. mansoni* und HCV Co-Infektionen in einer epidemiologischen Studie und die gleichzeitige HBV und Bilharziose in einem Tiermodell.

Bei einer parallel auftretenden *S. mansoni* und Hepatitis-C-Virus Infektion, scheint der Parasit die Progression der Lebererkrankung zu beschleunigen, da das Auftreten von Leberzirrhose und hepatozellulärem Karzinom häufiger in co-infizierten Individuen zu beobachten ist. Schistosom-Infektionen sind im Allgemeinen dafür bekannt, regulatorische Netzwerke wie Tregs zu induzieren, welche die Immunantworten gegen homologe und heterologe Antigene wie Allergene kontrollieren können. Daher basiert diese Arbeit auf der Hypothese, dass in co-infizierten Patienten schistosom-induzierte Treg-Populationen ihren Phänotyp verändern und auf die HCV-spezifische Immunantwort ebenfalls suppressiv wirken. Wir untersuchten in ägyptischen Kohorten von HCV monoinfizierten (HCV), Schistosomen-co-infizierten (Sm/HCV) und gesunden Individuen die Effektor-T-Zell und n/iTreg Subpopulationen mit Hilfe der Marker Granzyme B (GrzB) und Helios. Im Gegensatz

zu HCV-monoinfizierten Patienten beobachteten wir deutlich höhere Viruslasten und Lebertransaminasewerte in Sm/HCV ko-infizierten Individuen. Während die allgemeine Treg- und Helios$^+$ Treg-Population in Sm/HCV co-infizierten Patienten nicht erhöht war, fanden wir jedoch einen deutlichen Anstieg an GrzB$^+$ Treg in diesen Individuen. Im Gegenzug blieben Populationen an GrzB$^+$ CD8$^+$ T-Zellen in allen Patientengruppen unverändert. Zusammenfassend zeigt diese Studie, dass bei Sm/HCV co-infizierten Kohorten die Lebererkrankung mit einer erhöhten Virusreplikation einher geht, und Treg-Populationen nicht durch ihre generelle Proliferation sondern durch ihren veränderten Phänotyp zu einem schwerwiegenderen Krankheitsbild führen. In co-infizierten Personen ist daher die Behandlung der Helmintheninfektion eine wichtige Voraussetzung für die erfolgreiche HCV-Behandlung, da im Allgemeinen bekannt ist, dass diese Individuen schlechter auf die Interferon-Therapie reagieren.

Im Gegensatz zur Co-Infektion mit *S. mansoni* und HCV, bei der ausschließlich ein beschleunigtes Voranschreiten der Lebererkrankung zu beobachten ist, wird die Interaktion zwischen HBV und Schistosomiasis kontrovers diskutiert. Die divergierenden epidemiologischen Beobachtungen ergeben sich vermutlich aus den dynamischen Immunreaktionen der Schistosom-Co-Infektion, die den Schweregrad und die Etablierung der HBV-Infektion unterschiedlich beeinflussen können. Daher untersuchten wir in einem Tiermodell die zugrundeliegenden Mechanismen der Wechselwirkungen zwischen Hepatitis-Virus-Infektionen und Bilharziose. Hierbei wurde mit dem AdHBV-X- Maus-Modell die Entwicklung einer akuten HBV-Infektion während der verschiedenen Immunphasen ($T_H1$, $T_H2$, chronisch) der *S. mansoni* Infektion erfasst. Im Gegensatz zu Mäusen mit einer HBV-Monoinfektion, beobachteten wir eine schnellere Viruseliminierung nur bei jenen Tieren, die die virale Infektion während der IFN-γ-dominanten Immunphasen ($T_H1$- und chronische Phase) der Schistosomiasis erwarben. In diesen Tieren fanden wir signifikant niedrigere Virusantigentiter und geringere Viruslasten in der Leber. Zudem wiesen diese Tiere eine erhöhte Frequenz an HBV-spezifischen CD8$^+$ IFN-γ$^+$ T-Zellen in Leber und Milz auf. Darüber hinaus reagierten bei antigen-unabhängiger Stimulation, Splenozyten und Zellen mesenterialer Lymphknoten von co-infizierten Tieren mit einer höheren Ausschüttung an IFN-γ. Dies deutet darauf hin, dass die gleichzeitige Wurminfektion die Produktion dieses Zytokins in einer antigen-unabhängigen Weise erhöht. Im Gegensatz dazu, zeigten co-infizierte IFN-γ-defiziente Mäuse sowie Tiere, die in der frühen, IFN-γ-unabhängigen $T_H1$ und

$T_H2$-Phase infiziert wurden, keine erhöhte Viruseliminierung. Die schnellere Viruseliminierung in akut und chronisch schistosom-co-infizierten Tieren lässt sich deshalb den antiviralen und immunregulatorischen Eigenschaften des schistosom-induzierten IFN-γ zuschreiben.

Eine weitere wichtige Effektorzell-Population, die bereits schon während der $T_H1$ -Phase der Helmintheninfektion induziert wird, sind Treg-Zellen. Da diese Zellen mit ihren ausgeprägten immunsuppressiven Eigenschaften auch antigenunabhängige Immunantworten beeinflussen können, nahmen wir an, dass diese auch antivirale Immunantworten kontrollieren. Deshalb wurde in einem weiteren Versuch der Einfluss dieser Schistosomen -induzierten Tregs auf die Entstehung und Etablierung der antiviralen Immunantwort während der chronischen Phase der Helmintheninfektion untersucht. Zu diesem Zweck verwendeten wir ein transgenes Mausmodell, dass die spezifische Depletion von Treg-Zellen erlaubt. Wir konnten zeigen, dass die Depletion dieser Zellen jedoch weder zu einer weiteren Beschleunigung der Viruseliminierung noch zu einer stärkeren Etablierung der antiviralen Immunantwort führt. Dementsprechend folgerten wir, dass auch während der chronischen Phase der Helmintheninfektion, die antivirale Wirkung des schistosom-induzierten IFN-γ über dem potentiellen Treg Effekt steht.

Das Szenario einer sekundär erworbenen Infektion mit *S. mansoni* auf einer bereits bestehenden, chronischen HBV Infektion ist klinisch in einigen Teilen der Welt auch von hoher Relevanz. In diesem Zusammenhang untersuchten wir mit einem HBV-transgenen Mausmodell (HBVtg), ob die zusätzliche Wurminfektion in der Lage ist, die bestehende Chronifizierung in diesen Tieren zu brechen. Da Co-infizierte Tiere eine signifikant niedrigere Virusreplikationsrate ausschließlich während der $T_H1$-Phase aufwiesen, vermuten wir, dass die Schistosomeninfektion, möglicherweise erneut durch die Induktion von IFN-γ, in der Lage war, die Etablierung einer antiviralen Immunantwort zu induzieren. Interessanterweise fanden wir im Gegensatz dazu, dass weder die akute, noch die chronische HBV Infektion die Helmintheninfektion in Bezug auf Immunpathologie, Fortpflanzung und Parasitenentwicklung beeinflusste.

Zusammenfassend zeigen unsere Daten, einen kausalen Zusammenhang zwischen schistosom-induzierter IFN- γ Produktion in der Leber, der Induktion von antiviralen T-Zellen und HB/HC-Viruseliminierung. Im Vergleich zu der in der Literatur viel beschriebenen

immunsuppressorischen Kapazität von schistosom-induzierten Tregs, scheint die Induktion von IFN-γ eine viel dominantere Rolle in der Viruseliminierung einzunehmen.

# 1 Introduction

## 1.1 Biology of Schistosomiasis

### 1.1.1 Taxonomy and geographical distribution

Parasites are microorganisms that live off of other organisms, or hosts, to survive. In tropical and subtropical regions parasitic infections are a large problem with Malaria being one of the deadliest diseases caused by a parasite. In general parasitic infections can be caused by three types of organisms: protozoa**,** helminths (worms)**,** and ectoparasites. Helminths are complex multi-cellular organisms that live alone or in humans. They are commonly known as worms and include roundworms (Nematodes)**,** tapeworms (Cestodes), ringworms (Tinea)**,** and flatworms (Trematodes)**.** Of the latter, *Schistosoma* species cause the tropical disease schistosomiasis, also known as bilharzia, which mainly affects either the intestine and the liver or the urogenital tract (Table 1). The most common human-pathogenic species are *S. mansoni* and *S. japonicum*, which cause intestinal and hepatosplenic schistosomiasis, or *S. haematobium*, which affects the urinary tract [1]. The geographical distribution differs by species and is depicted in Table 1.

| Manifestation | Species | Geographical distribution |
|---|---|---|
| **Intestinal Schistosomiasis** | *Schistosoma mansoni* | Africa, the Middle East, the Caribbean, Brazil, Venezuela, Suriname |
| | *Schistosoma japonicum* | China, Indonesia, the Philippines |
| | *Schistosoma mekongi* | Several districts of Cambodia and the Lao People's Democratic Republic |
| | *Schistosoma guineensis*<br>*Schistosoma intercalatum* | Rain forest areas of central Africa |
| **Urogenital Schistosomiais** | *Schistosoma heamtobium* | Africa, the Middle East |

**Table 1: Parasite species and geographical distribution of schistosomiasis** [1] updated February 2014.

According to the World Health Organisation (WHO) currently more than 249 million people worldwide in 78 tropical and subtropical countries are infected with *Schistosoma* species [1-3] and it is estimated that 732 million people are at risk of infection in endemic areas [1, 4, 5]. The parasite has a complex life cycle in which freshwater snails serve as the intermediate host. Due to the lack of access to proper water and sanitation facilities, individuals in developing countries are often exposed to water contaminated by infected snails. In endemic areas and especially in those with rising chemotherapeutic resistance or lack of proper health surveillance systems, these parasites have a detrimental impact on the financial and social sectors [6].

### 1.1.2 Lifecycle of *Schistosoma mansoni*

The complex lifecycle of *S. mansoni* provides an example for all species of schistosomes and includes six developmental stages within two hosts. Humans and other mammals function as definitive hosts, whereas freshwater snails such as *Biomphalaria glabrata* serve as intermediate host (Figure 1). After the eggs of the human-dwelling parasite are excreted via the feces into the water, a free-swimming larva, called miracidium, hatches from the egg and guided by light and chemical stimuli, pursues its intermediate host, the freshwater snail. Within the snail an asexual reproduction leads to the development of the second larval form, the cercariae, which is capable of infecting humans. The purpose of the growth in the snail is the numerical multiplication of the parasite, as from a single miracidium a few thousand cercaria will be released 4-6 weeks post infection. The free-swimming cercariae emerge from the snail during daylight, actively seek out their final host and penetrate the intact human skin by releasing proteolytic enzymes from its pre- and post-acetabular glands [7-9]. During the process of penetration, cercariae lose their tails, develop into schistosomulae and remain in the host epidermis for the next 24 hours [9]. Thereafter, schistosomulae migrate via dermal lymphatic vessels or blood venules into the pulmonary artery to reach the lung where they are located intra-vascularly (5-7 days post penetration) [9]. The parasites exit the lung in the direction of blood flow and polarize to the hepatic portal venous system (> 15 days post penetration), where they finally mature into adult female or male worms. Adult worms, also known as blood flukes, pair and migrate to the mesenteric veins where they reside and the females begin egg production (> 35 days post cercarial penetration). They are

able to survive within the human body for long periods of time by feeding on red blood cells [10]. Fecund female worms produce 300 - 3000 eggs per day which penetrate the intestinal wall by causing an inflammatory process to be released into the environment by stool passage and to continue the parasite's lifecycle [1, 3, 11-15].

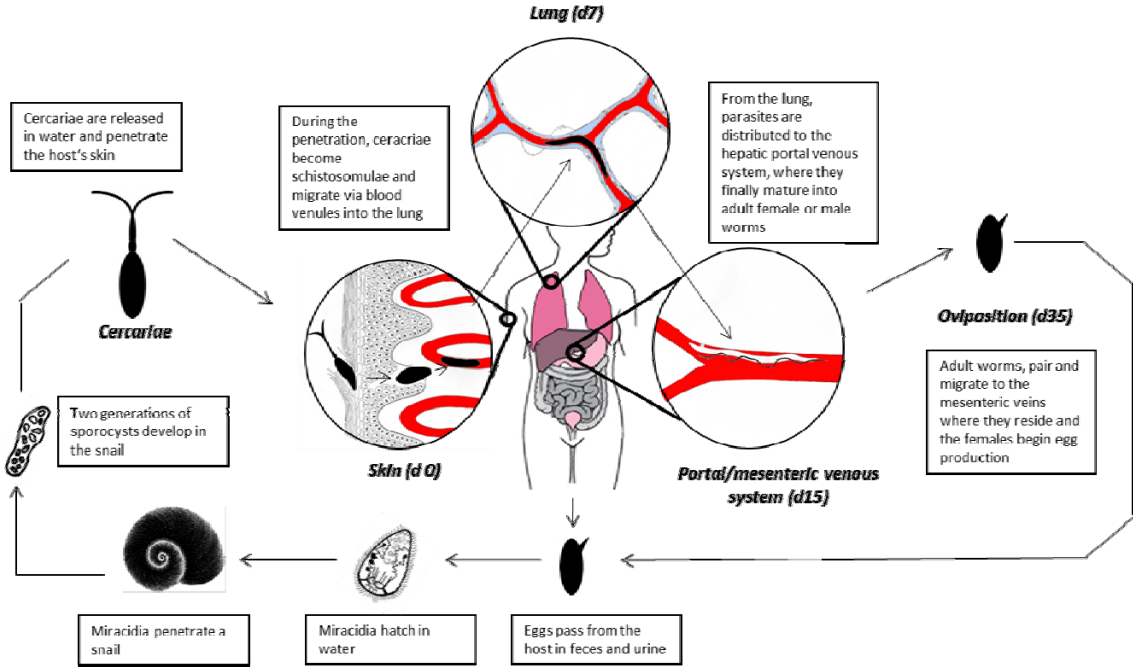


**Figure 1: Lifecycle of *S. mansoni*.** The complex lifecycle of *S. mansoni* starts with eggs containing miracidia and being released from infected individuals with feces into water. By contact with fresh water and in response to temperature and light the free-swimming miracidium hatches out of the eggs and searches for its intermediate snail host *(Biomphalaria glabrata).* Within the snail the parasite develops via a mother-sporocyst and daughter-sporocyst generation into cercariae. The free-swimming cercariae are released from the snail and actively search for their final host where penetration of the human skin is achieved by the use of proteoloytic enzymes. During penetration, the cercariae lose their forked tail and transform into an endoparasitic larvae, the schistosomula. The schistosomula, which are of male and female gender, are transported through the vasculature to the liver. There, they mature into adult worms and pair. The paired adult worms migrate to the mesenteric veins where they reside and begin to lay eggs. Released eggs penetrate the gut lumen and are released into the surrounding by stool passage again. Parasite eggs that become trapped within the host's tissues induce the pathology classically associated with schistosomiasis, such as liver fibrosis and portal hypertension. Adapted from [16] and Frahm, S. (2015), The influence of host serum factors on the development of *S. mansoni* in its definite host, *medical PhD thesis.*

Approximately 50% of eggs do not reach the intestinal lumen and are dispersed through the portovenal bloodflow into the liver and intestine where they become trapped in small blood vessels, the sinusoids [11, 17]. In the case of portovenous shunting, parasite eggs

accumulate also in the lung and other organs [18], where they finally cause immune reactions and progressive damage to organs. The continuous deposition of eggs into organ tissue is the underlying instigator of chronic inflammatory host immune responses, which are responsible for the pathology classically associated with schistosomiasis, such as liver fibrosis and portal hypertension.

Although humans are the main reservoir of infection also rodents such as *Mus musculus* or *Mesocricetus auratus* can be infected with the parasite and serve as animal models to study schistosomiasis [19].

### 1.1.3 Pathology of schistosomiasis

Infection with schistosomes leads to a variety of symptoms which correspond to various stages of infection. During penetration and migration through the skin, cercariae may cause temporary mild itching and dermatitis (schistosome cercarial dermatitis) [20]. Several weeks after infection, when maturing schistosomulae migrate through the lung, acute schistosomiasis can clinically present as Katayama's fever with symptoms including fever, cough, abdominal pain, hepatosplenomegaly development, eosinophilia, intestinal bleeding and diarrhea [11, 21-23]. In the chronic form of the disease, tissue-trapped eggs elicit the development of a cellular granulomatous reaction (see Figure 2) through the release of soluble egg antigen (SEA). This gives rise to the most serious disease symptoms of infection such as hepatosplenic inflammation, liver fibrosis, portal hypertension, bloody diarrhea, anemia and eventually undernutrition [1, 11, 22-24].

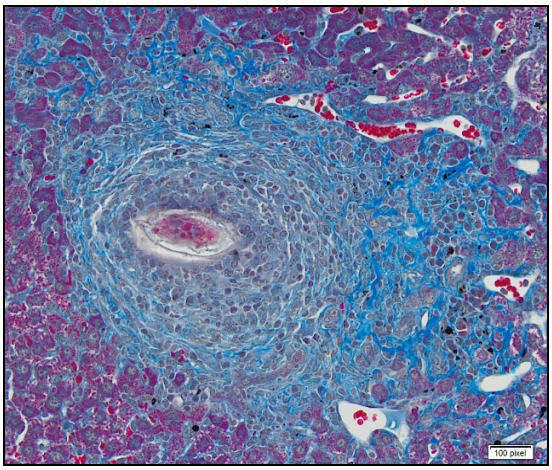


**Figure 2: Granuloma formation around tissue-trapped egg.** Accumulating infiltrating immune cells, such as eosinophils, lymphocytes and macrophages induce granuloma formation around *S. mansoni* egg in mouse liver tissue. Fibrotic tissue can be detected by staining tissue sections with Masson's blue, since collagen fibers turn blue during the staining procedure.

### 1.1.4 Immune responses during schistosomiasis

Due to prolonged dynamic co-evolution between host and parasite, adult worms are able to live for many years in its host's mesenteric vasculature. To achieve long-term persistent infection these helminths have adapted to their host environment by undergoing developmental changes that maintain a balanced host-parasite interplay for successful long-term transmission [3, 25, 26]. An example of this is their ability to escape immune recognition by the induction of regulatory $CD4^+$ T cells (Treg), which suppresses the host's specific immune response [27, 28]. Furthermore adult worms have the ability to coat themselves with host antigens and enzymatically cleave IgG antibodies bound on their surface via the release of metalloaminopeptidases or endoproteases with trypsin-like activity [3, 12, 29-31].

Another highly effective mechanism to achieve long-term persistent infection is the ability of schistosomes to modulate the host's immune system. Immunologically, the ability to drive the host's immune response through three different phases is one of the most interesting aspects of schistosome infection. It comprises of a dynamic switch from an initial pro-inflammatory $T_H1$ to a dominant helminth-beneficial $T_H2$ immune response, which eventually evolves into a regulatory immunosuppressive environment (Reg) 22 weeks post infection (see Figure 3) [3, 29].

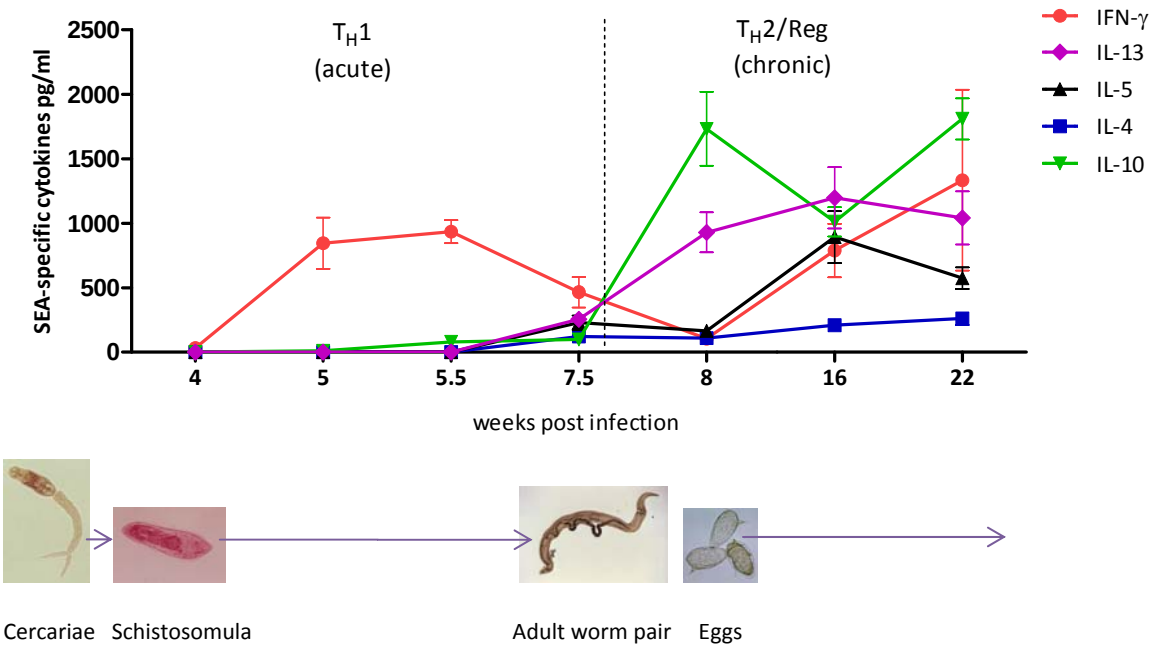


**Figure 3: Induction and development of $T_H1$- and $T_H2$ immune responses during *S. mansoni* infection in C57BL/6 mice.** Following cercariae penetration, a $T_H1$-cell response with high levels of IFN-γ production develops (acute phase). As the worms mature and eggs are deposited, a stronger $T_H2$-cell response with high levels of classical $T_H2$ cytokines such as IL-10, IL-13 and IL-5 arise (chronic phase) eventually ensuing in a regulatory immunosuppressive phase 22 weeks post infection (Reg).

### 1.1.4.1 The immune response during the acute phase of *S. mansoni* infection: $T_H1$ responses

As depicted in Figure 3 the $T_H1$ response is initiated during the first 7 weeks of infection, during which the host is exposed to migrating, immature parasites and is characterized by high levels of pro-inflammatory cytokines such as IL-1, IL-6, TNF-α (data not shown) and especially Interferon-γ (IFN-γ) [12, 32]. The pro-inflammatory $T_H1$ environment is caused by the infective schistosomes before egg production starts [33, 34] and is induced during the process when cercariae transform into schistosomula upon entry into the skin. The transformation process requires shedding and replacement of the tegument membranes [35] and previous studies have shown that whole schistosomula tegument induces the upregulation of co-stimulatory molecules such as the cluster of differentiation (CD)40 and CD86 on antigen-presenting cells (APC) provoking the production of pro-inflammatory cytokines such as TNF-α and IL-12p40 by dendritic cells (DC) [36]. Proinflammatory

responses during this phase of infection are further known to be triggered by the activation of the complement cascade through the carbohydrate enriched surface of cercariae and newly transformed schistosomula [37-39].

In contrast to people living in helminth endemic areas, the pronounced inflammatory response following cercarial penetration is mainly observed in individuals who have not been previously exposed to parasite antigens [40]. The milder inflammatory response in individuals living in endemic areas results from the constant exposure to parasite antigens and might be further explained by *in utero* sensitization and induction of tolerance against helminth antigens due to maternal infection with *S. mansoni* [41]. Furthermore, in rural endemic areas, schistosome infection is mainly acquired during childhood, and the constant exposure to helminth antigens favours the development of chronic schistosomiasis [2, 42-44]. Even though rates of chronic schistosome infections are higher in endemic areas, the clinical relevance of acute schistosomiasis still needs to be considered due to the burden of reinfection. Even though increasing masstreatment programs have been successful in diminishing chronic disease in patients (i.e. reducing adult worm numbers) they encourage little resistance to a repeated infection [45, 46]. Owing to unchanged living habits and unsuccessful or absent vector control, re-infection rates are high and patients are therefore continuously re-exposed to cercaries and migrating larvae after praziquantel treatment [47, 48]. These individuals will again undergo an acute phase of infection and this scenario will elicit initial $T_H1$ responses over again. Indeed, mouse studies have shown that re-exposure to cercaries after anti-schistosome treatment leads to either equal or even enhanced SEA-specific IFN-$\gamma$ responses, demonstrating the significance of schistosome-induced $T_H1$ responses [49, 50].

#### 1.1.4.2 Schistosoma-egg induced T helper type 2 ($T_H2$) immune responses

The more pronounced $T_H2$ response is initiated as soon as female worms become fecund and start releasing eggs (7-8 weeks post schistosome infection, see Figure 3) [33, 34]. It arises from granulomatous, immune-mediated responses raised against tissue-trapped, decaying eggs, which secrete SEA and thereby induce the production of classical $T_H2$ cytokines, such as IL-4, IL-13, IL-10 and IL-5 [33, 51]. This polarized $T_H2$ immunity comprises of an increased number of specific immune cells such as eosinophils, basophils, mast cells

and alternatively activated macrophages (AAM) as well as increased levels of circulating immunoglobulins, such as IgE [12]. It protects both the host and the parasite against overwhelming $T_H1$ and $T_H17$ cell mediated inflammation and potentially hepatotoxic products within egg antigens [33, 34, 51-53].

The following regulatory phase is initiated by the ongoing $T_H2$ type immune response itself in order to control the damage caused by this response. The elevated IL-10 levels suppress the proliferation and cytokine production of pro-inflammatory T cells in response to parasite and bystander antigens [54]. Additionally they induce the expansion of immunoregulatory cells such as Treg and regulatory B cells (Breg) [14, 55, 56], which dampen overall immune responses through their production of additional IL-10. Furthermore interfering with DC activity is another prominent way to induce a permissive environment that allows the parasite to survive for decades in its host [57]. In general, DCs control the development of adaptive immune responses by processing and presenting pathogen-derived antigens to naive T cells, which in turn get activated and provoke the appropriate response for the initial stimuli. Helminth-derived antigens, such as glycans found in SEA (core α-3-fucose, β2-xylose and Lewis X), have been shown to play an important role in dampening the function and maturation of DCs [58]. Previous studies have also shown that immature DCs pulsed with SEA do not show an increase in expression of costimulatory molecules (CD80 and CD86) or cytokines and rather inhibit LPS-induced activation, such as the upregulation of Major histocomatibility complex-I (MHC-I), costimulatory molecules and IL-12 production upon co-incubation [59-62]. Furthermore lipids from *S. mansoni*, particularly those containing phosphatidylserine additionally contribute to the immunoregulatory environment, since they block IL-12 production by DCs while promoting the development of IL-10 producing Treg cells [63]. More recently, *Everts et al.* and *Steinfelder et al.* demonstrated that also RNases (glycosylated T2 ribonuclease; Omega-1) abundantly present in SEA, are able to condition DCs to prime $T_H2$ responses. Mechanistically, Omega-1 binds via its glycan structure to the mannose receptor of DCs, is internalized and immediately suppresses protein synthesis by degrading both ribosomal and messenger RNA. Due to the impaired protein synthesis machinery, *in vitro* Omega-1-conditioned human DCs are largely refractory to respond to CD40 ligation by T cells, they fail to upregulate LPS-induced CD86 expression, and no longer secrete pro-inflammatory IL12p70 when co-cultured with naïve T cells. The low antigen presentation and the absence of IL-12 finally favour the induction of $T_H2$

responses in this scenario [64, 65]. In addition, *Klaver et al.* were able to show, that SEA glycans strongly induce the expression of the suppressor of cytokine signaling 1 (SOCS1) and SH2-containing protein tyrosine Phosphatase-1 (SHP-1), two negative regulators of Toll-like receptor 4 (TLR4) signalling in human DCs via interaction with the mannose receptor. Moreover, in this study, SEA was shown to induce the secretion of transforming growth factor β (TGF-β), and the surface expression of the costimulatory molecules Programmed Death Ligand-1 (PD-L1) and OX40 ligand (OX40L) on DCs. In co-culture, this DC subset had the ability to polarize naïve T cells into $T_H2$/regulatory T cell subsets [66]. Thus, during the ongoing $T_H2$ immune response, SEA appears to have a profound effect on Toll-like-receptor (TLR) ligand-induced DC maturation/activation, suppressing the inflammatory development of $T_H1$ type responses.

Other prominent mediators of the induction of regulatory mechanisms during the ongoing $T_H2$ type immune response are elevated IL-4 and IL-13 levels, which promote the development and recruitment of AAMs to sites of infection. Through their production of Chitinase, arginase-1 (Arg-1), resistin like molecule α (RELMα) and chitinase 3 like protein 3 (Ym1), AAMs are known to play an important role in wound-healing and tissue repair, and additionally dampen $T_H2$ cytokine-driven inflammation and fibrosis during schistosomiasis. Arg-1 expressing AAMs compete with $T_H2$ cells for arginine and thereby suppress $T_H2$ cell proliferation. Consequently, studies in Arg-1 deficient mice infected with *S. mansoni* demonstrated severe intestinal inflammation, liver fibrosis and portal hypertension [67-69]. More recently, *Jenkins et al.* showed that during $T_H2$-related pathologies, such as *Litomosoides sigmodontis* infection in mice, local macrophage proliferation, rather than recruitment from the blood led to an increase of the population density to sites of inflammation. In this study, tissue-resident macrophages started to proliferate in situ under the control of IL-4 and displayed an alternatively activated phenotype. The central role of IL-4 in this process was additionally shown in naïve mice, where exogenous administered IL-4 was sufficient to drive the accumulation of tissue macrophages through self-renewal [70]. Furthermore, a recent study using a $LysM^{Cre}$ mouse model (mice expressing a Cre recombinase from the lysozyme M-encoding locus (Lyz2)), demonstrated that distinct populations of alternatively activated macrophages control inflammation and fibrosis in chronic schistosomiasis. In *S. mansoni* infected IL-4R$\alpha^{flox/delta}$ $LysM^{Cre}$ mice, blood-derived macrophages, in comparison to tissue resident macrophages, expressed lower levels of Lyz2

(Lyz2$^{lo}$)and resisted LysM$^{Cre}$ mediated deletion of IL-4Rα. In response to IL-4 and IL-13, Lyz2$^{lo}$ IL-4Rα$^{+}$ macrophages differentiated into Arg1-expressing AAMs and were responsible to downregulate fibrosis. Tissue-resident Lyz2$^{high}$ IL-4Rα$^{+}$ macrophages were identified as the subset of AAMs controlling granulomatous inflammation [71]. Another recent study showed that during murine *S. mansoni* infection, elevated levels of IL-4 further induce the expression of high levels of retinal dehydrogenases (Raldh) in AAMs, which are required for the synthesis of the vitamin A metabolite retinoic acid (RA). In the presence of TGF-β, these *in vivo* derived AAMs had an enhanced capacity to induce the transcription factor forkhead box P3 (Foxp3) expression in CD4$^{+}$ T cells (see section 1.1.6) through an RA dependent mechanism and contributed therefore mainly in the regulation of effector immune responses during helminth infection [72].

### 1.1.5 Granuloma formation

Tissue-trapped schistosome eggs are the initial event in a complex pathophysiological cascade, which induce granuloma formation in the intestine and liver and may terminate in fibrosis. More specifically, granuloma formation describes the collection of host immune cells (mainly CD4$^{+}$ T cells, B cells, eosinophils and macrophages), which accumulate around tissue-trapped eggs as a result of the host's immune answer to a pathogen that can't be eliminated. In livers of chronically schistosome infected individuals, granulomas give rise to fibrosis and hepatosplenomegaly since intact liver tissue is replaced by collagen [73]. In general, symptoms and signs of the disease depend on the number and location of tissue-trapped eggs, where blood flow is impaired due to granuloma formation in the liver and, as a consequence develops into portal hypertension. With time, collateral circulation (portovenous shunting) is formed, allowing eggs to further move into the lungs, where they cause more granulomas and pulmonary arteritis [11, 73].

Granuloma formation is initiated by antigens secreted by the miracidium through microscopic pores within the egg shell. The strong granulomatous immune response of various immune cells raised against those decaying eggs, rather than parasite egg antigens themselves, is responsible for the pathologic tissue manifestations in schistosomiasis [3, 11, 73, 74]. During schistosomiasis, CD4$^{+}$ T cells are the main mediators of granuloma formation, in the absence of this T cell subset no granuloma formation occurs [3, 74, 75]. Interestingly,

the formation of granulomas within the liver differs from those developing in the intestine. Whilst the granulomas in the liver shrink and become fibrogenic in the chronic phase of infection, intestinal granulomas do not change in size and appearance [76]. Furthermore Layland *et al.* observed that the cellular infiltrate within granulomas changes with time. In granulomas becoming progressively older, increased populations of Treg and decreased numbers of $CD4^+$ T cells, macrophages and eosinophils could be detected. Treg cells accumulated hereby preferentially in the circumference of old granulomas, where they are believed to control the infiltration and response of other immune cells, such as eosinophils, at the site of inflammation [77, 78].

As mentioned above, a hallmark of chronic schistosomiasis is the granuloma-induced replacement of functional liver tissue by collagen. IL-13 is the main $T_H2$-type cytokine which plays a prominent role in granuloma formation and size. Several studies have shown that granuloma size is consistent with levels of IL-13 and that this cytokine seems to be the driving force of fibrosis development [79-82]. More specifically, schistosoma infected mice lacking IL-13 by either neutralization with an anti-IL-13 antibody treatment [81] or impairment of the IL-13 pathway using IL-4 and IL-13 receptor deficient mice [80, 82], fail to develop fibrosis resulting in prolonged host survival. Furthermore, a study with *Nippostrongylus brasiliensis* infected mice pointed out the important role of IL-13 receptor alpha 2 (IL-13R$\alpha$2) during nematode infection. In comparison to IL-13R$\alpha2^{-/-}$ mice, in wildtype animals infection-induced high levels of IL-13 led to an upregulation of the IL-13R$\alpha$2, which in turn served to limit the availability of IL-13, thereby regulating both the immune and biological effects of this cytokine [83]. Thus, regulatory mechansims, such as induced regulatory networks including Treg cells, are needed to balance $T_H1$ versus $T_H2$ immune responses and the arising immunopathology within the host during schistosomiasis. This process represents an excellent example of evolutionary evolved host-parasite interaction.

### 1.1.6 Role of regulatory T cells during schistosomiasis

As mentioned above, during the ongoing $T_H2$ immune response, elevated IL-10 levels as well as SEA- induced DCs promote the development of $T_H2$-type $CD4^+$ effector T cells and immunoregulatory cells such as Treg and Bregs which dampen overall immune responses through their production of additional IL-10 [14, 55, 56, 63]. However effector functions of

$CD4^+$ T cells are mainly known to be controlled by distinct populations of regulatory T cells and their soluble products, studies with B-cell deficient mice pointed out the additional regulatory role of this cell type during chronic *S. mansoni* infection, since the absence of this cell population led to enhanced $T_H2$ dependent immunopathology [84]. Despite this complexity of regulatory cell types, $CD4^+CD25^+Foxp3^+$ T cells remain the most prominent regulatory cells during helminth infection. As depicted in Figure 4, two types of $CD4^+$ Treg exist: 'natural' Tregs (nTreg) and 'induced' Tregs (iTreg), which are primarily defined by where they develop. nTreg arise from developing T cells in the thymus during the course of positive and negative selection. iTregs develop in the periphery from naïve $CD4^+$ T cells throughout infection, the exact site of induction is still unclear. Following antigenic stimulation and in the presence of TGF-$\beta$ and IL-2, naïve $CD4^+$ T cells start to express the transcription factor forkhead box P3 (Foxp3) and acquire suppressive capacity [85-87]. Even though nTregs and iTregs share similar cell surface markers such as CD25 and CTLA-4 (see Figure 4), there are cell surface markers such as Neuropilin-1 (see Figure 4) and intranuclear markers such as Helios, a transcription factor belonging to the Ikaros family of transcription factors, which are currently proposed to be exclusively expressed on/in nTreg, allowing the discrimination between these two Treg subsets [88-90].

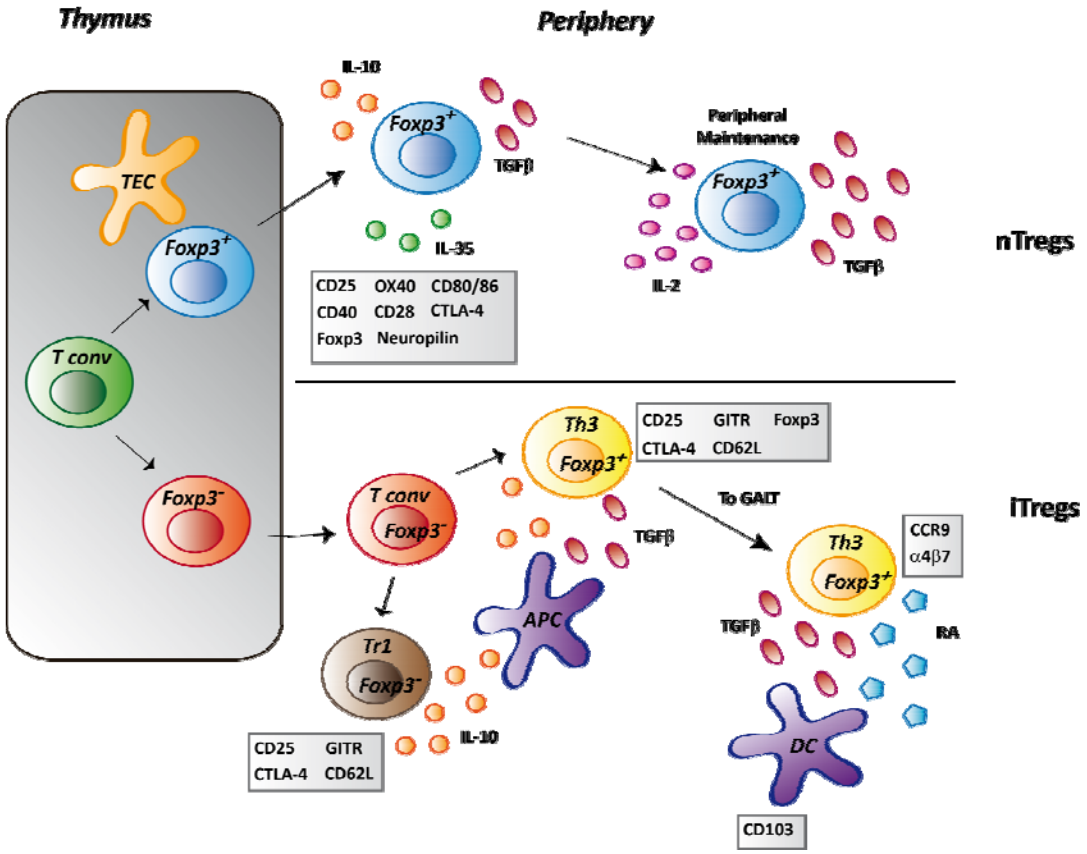


**Figure 4: Development of nTregs and iTregs and the relevant markers associated with each.** In the thymus, Foxp3$^+$ nTregs (top) arise from developing T cells during the course of positive and negative selection. Hereby, conventional T cells (T conv) undergo selection based on the strength of signal they receive from thymic APCs such as thymic epithelial cells (TEC) presenting self antigens. In general, strong signals due to high affinity or avidity interactions between the T cell receptor (TCR) and MHC:peptide complexes results in negative selection, whereas no or very low signal leads to thymocyte death. Positive selection of thymocytes that will survive and migrate to the periphery occurs when intermediate to weak signals are delivered via engaged TCR. nTregs are positively selected on a TCR affinity/signal strength that is between that required for the positive and negative selection for conventional T cells. In the periphery, nTregs express a various number of intranuclear- (Foxp3) and cell surface markers such as CD25, CTLA-4 and Neuropilin 1 (indicated in the box below) and secrete the cytokines IL-10, IL-35 and TGF-β to exert their suppressive effects on effector T cells (T conv). The central cytokines for Treg maintenance in the periphery are TGF-β and IL-2. Throughout infection, iTregs (bottom) develop from naïve conventional CD4$^+$ T cells (T conv) upon antigenic stimulation. Once in the periphery, naïve CD4$^+$ T cells can be induced to become Foxp3$^-$ Tr1 cells or Foxp3$^+$ Th3 cells via IL-10 and/or TGF-β secreted by APCs. Cell surface markers, such as CD25, CTLA-4 and GITR expressed by iTregs are depicted in the box below. Foxp3$^+$ iTregs can furthermore accumulate in the gut through upregulation of CCR9 and α4β7 via TGF-β and retinoic acid (RA) produced by CD103$^+$ dendritic cells. Adapted from [85, 87, 91].

Under steady state or physiological conditions, Treg cells control immune responses to self and foreign antigens by acting directly on effector T cells and furthermore avoid

autoimmunity by controlling autoreactive immune cells [92-94]. Regarding the function of Treg during Schistosomiasis, *Layland et al.* and others demonstrated their essential role in controlling exaggerated immunopathology as well as effector T cell responses by using the murine model of *S. mansoni* infection [77, 78, 95]: although Treg cannot prevent helminth infection per se they are beneficial for both, the host and the parasite - on the one hand Treg dampen liver inflammation to limit tissue damage in the host, and on the other hand Treg ensure parasite survival by suppressing effector immune responses against the helminth [78]. Furthermore, *ex vivo* isolated Treg specifically suppressed antigen-specific $CD4^+$ T cells from infected mice in an IL-10 independent manner [78] and, in comparison to Treg from naïve mice, had specifically upregulated genes such as granzyme B (GrzB), secretory leukocyte peptidase inhibitor (SLPI) or the homing marker CD103, implying that their phenotype changes during infection [77].

Functionally, the acquisition of e.g. cytotoxic activity [96] during the development of peripherally induced iTreg – as compared to nTreg - in different inflammatory environments is one of the many distinct features now proposed for iTreg [97]. Generally, Tregs suppress the proliferation of naïve T cells and their differentiation to effector T cells as well as the function of natural killer cells, B cells and APCs such as macrophages and dendritic cells [98, 99]. Treg-mediated suppression by n- and iTreg includes the secretion of immunosuppressive cytokines such as IL-10 and TGF-β. While IL-10 promotes the down regulation of pro-inflammatory cytokine production of effector cells, TGF-β leads to cell-cycle arrest and therefore decreased effector cell proliferation [94]. During *S. mansoni* infection, IL-10 is considered as the key mediator for immunosuppression, since several mouse studies using IL-10 deficient infected mice showed an excessive $T_H1$- and $T_H2$-type mixed immune response even late during the chronic phase of infection, which led to severe granulomatous liver damage and increased mortality [100-103]. Furthermore nTreg and iTreg express high levels of cytotoxic T-lymphocyte antigen 4 (CTLA-4) on their surface, which allows them to interact with APCs providing a down regulation of co-stimulatory molecules such as CD80/CD86 and thereby hindering the activation of other T cells by these APCs. While nTreg predominantly produce immunosuppressive IL-35 (see Figure 4) and compete with effector T cells for IL-2 leading to apoptosis of responder T cells, iTreg are able to kill effector T cells and APCs by cell-to-cell contact in a granzyme- or perforin-dependent manner [94, 97].

Since the importance of Treg during Schistosomiasis and other helminths is well documented [25, 104] there is increasing interest to study the role of these infection-induced Treg on immune responses during co-infection with other pathogens.

## 1.2 *S. mansoni* and viral co-infection in humans

Indeed, in rural areas endemic for schistosomiasis, chronically infected people are often exposed to other pathogens such as viruses [105, 106]. Due to the immune-modulatory ability of helminth infections, it is likely that pathogen interactions will occur on the systemic immunological level and on the level of the infected organ. A prominent example is the liver in the case of *S. mansoni* and hepatitis virus infections.

Since the liver has vital metabolic and clearance functions that involve the uptake of nutrients, waste products and pathogens from the blood, its microenvironment is set to prevent organ damage. The unique immunoregulatory function in the liver is mediated by local expression of co-inhibitory receptors and immunosuppressive mediators such as IL-10 or TGF-β, and helps to prevent inadvertent organ damage [107]. These tolerogenic properties however, render the liver an attractive target site for pathogens such as Hepatitis C- (HCV) and Hepatitis B virus (HBV) or schistosomes, but are altered upon infection and immune recognition.

In general, one of the main complications of hepatitis B and C virus infection is the development of chronic hepatitis after an acute infection and patients with chronic hepatitis B or C are at high risk to develop liver cirrhosis and hepatocellular carcinoma (HCC). Interestingly, chronic hepatitis B/C and also HCC develop at a higher frequency in developing countries in which co-infections with several helminth species such as *S. mansoni* are common [105, 106, 108-113]. Since helminths have developed strong immuneregulatory and even –suppressive capacities leading to chronic infections, during viral co-infection, these may contribute to HBV/HCV persistence by compromising anti-viral $CD8^+$ and $CD4^+$ effector T cell immune responses, and may lead to liver disease progression. As mentioned above, schistosome-induced immune responses, however, are very dynamic, ranging from an acute, inflammatory ($T_H1$) to a chronic, anti-inflammatory ($T_H2$) and immuneregulatory phase where suppressor cells like Treg play an important role. This circumstance as well as the fact that *S. mansoni* also causes mainly liver disease, might lead to very different outcomes of

concomitant acute and chronic HBV infection. More specifically, since Treg per se already delay the development of HBV-specific immune responses leading to prolonged viremia [114], schistosome-induced Treg with a pronounced immunosuppressive capacity [77, 78] as well as other inflammatory, liver-resident cell types such as macrophages and innate lymphoid cells might additionally influence viral clearance by interacting with antiviral immune responses and/or directly with infected liver cells.

Therefore, analysing co-infection under defined experimental conditions is of imminent importance to better understand plasticity of the liver microenvironment and its modulation by infection. Indeed, two very recent studies have addressed helminth-interaction with γ-herpesvirus and mouse-norovirus for the first time and demonstrated a helminth-mediated effect on viral replication on a systemic as well as mucosal level [115, 116]. In combination with *S. mansoni* infection, helminth-interaction with viruses has been so far mainly investigated with lymphocytic choriomeningitis virus (LCMV). In a murine *S. mansoni*/LCMV co-infection model, where the viral infection occurred during the $T_H2$ phase of schistosome infection, *Edwards et al.* reproduced the enhanced viral replication and liver pathology observed in human co-infections, and used this model to examine the mechanisms involved. The study demonstrated that both pathogens influenced each other in such a way that high numbers of infiltrating LCMV-specific IFN-$\gamma^+$ $CD8^+$ T cells suppressed the schistosome-induced production of $T_H2$ cytokines in the liver and led to an increased morbidity, linked to hepatotoxicity. On the other side, schistosome-egg antigens were found to suppress the type I Interferon response of bone-marrow-derived DCs locally in the liver and rendered the organ extremely susceptible to viral replication with ensuing immunopathological consequences [117, 118]. Another example for helminth interactions with viruses was shown in a study by *Scheer et al.* who analysed for the very first time the impact of *S. mansoni* infection on anti-viral immune responses in the upper respiratory tract. The study demonstrated that chronically schistosome infected mice were protected from a secondary viral respiratory challenge with influenza A virus, or with pneumonia virus of mice (PVM), a mouse virus to model respiratory syncital virus (RSV) infections. The enhanced immune protection to respiratory viruses during chronic murine schistosomiasis was attributed to elevated levels of serum $T_H2$ type cytokines, TNF-$\alpha$-mediated goblet cell hyperplasia and mucus secretion induced by the schistosome co-infection [119].

## 1.2.1 *S. mansoni* and Hepatitis C virus co-infection

### 1.2.1.1 Geographical distribution, transmission and associated disease of Hepatitis C virus infection

Hepatitis C virus (HCV) is the second most common viral infection worldwide and considered the most important agent of liver disease and liver carcinoma. In general, approximately 70% of acute HCV cases develop chronic hepatitis of which 15-20% will eventually evolve into cirrhosis with a 10% risk of hepatocellular carcinoma [120]. Currently, it is estimated that 180 million people are infected with HCV and interestingly, Egypt has the highest prevalence worldwide (31%) with 90% of those infected individuals being positive for the genotype 4 variant [121-124]. The Hepatitis C virus is predominantly a blood-borne virus and is most commonly transmitted amongst drug users through the sharing of injection equipment or people in health care settings via the transfusion of unscreened blood and blood products or the reuse and/or the inadequate sterilization of syringes and needles. Although HCV can also be transmitted sexually or vertically from mother to child, these modes of transmission are less common [125, 126].

Acute HCV infection is asymptomatic in approximately 80% of infected individuals and those who display symptoms exhibit fever, nausea, vomiting, fatigue, dark urine and jaundice [127]. The non-cytopathic virus infects and replicates mainly in hepatocytes, where entry into host cells is gained by viral binding to cell surface molecules such as CD81, Claudin-1 and Occludin. Furthermore, it has been reported that viral replication may also take place in peripheral blood mononuclear cells (PBMCs) and thereby interfering with their function, which might account for the high levels of immunological disorders found in chronically HCV infected patients [128, 129]. HCV has a wide variety of genotypes and its epitope structures mutate rapidly due to high error rates of the virus' RNA polymerase, leading to the production of many variants of the virus that are considered as quasispecies [128]. Due to the fact that no vaccine is available to prevent hepatitis C infection, infected individuals are generally treated with PEGylated Interferon-alpha (PEG-IFN-$\alpha$) in combination with agents inhibiting the viral NS3 and NS4 proteases, such as Boceprevir and Telaprevir, leading to decreased viral burden and consequently lower progression of the liver disease [130-132]. Since the administration of Interferones requires parenteral application and has various side-effects, in the HCV-drug development field, the oral or Interferon-free therapy is generally

seen as a major goal for the near-term or mid-term future [133]. Furthermore, numerous new inhibitors of the NS3/4 A protease are currently in clinical development, aiming to replace Boceprevir and Telaprevir. Here, Simeprevir and Faldaprevir in combination with PEG-IFN-$\alpha$ are shown to have a higher potency, higher genetic barriers to resistance and more favourable pharmacokinetic profiles, including once-daily dosing [133-138].

Immunologically, HCV infections induce both $CD4^+$ and $CD8^+$ T cell responses and during acute infection several studies have demonstrated that strong and sustained viral-specific $CD4^+$ and $CD8^+$ T cell responses are required for spontaneous and successful viral clearance. Individuals who fail to mount or sustain such virus-specific responses usually develop persistent viraemia and chronic infection [139]. Although the underlying mechanisms of dysfunctional virus-specific immune responses remain poorly understood, possible explanations have been proposed including the presence of HCV variants with altered epitope sequences, the induction of anergy by high antigen levels, the lack of different helper functions or the suppressive activity of regulatory T cells [94, 140]. Concerning the latter, research has shown that chronic HCV-infected individuals present higher levels of peripheral $CD4^+CD25^+Foxp3^+$ Treg, which, in response to HCV, are able to suppress virus-specific $CD8^+$ T cell responses by secretion of TGF-$\beta$ [140-142]. Furthermore, the presence of HCV-specific IL-$10^+$ Treg within isolated PBMCs and in the cellular infiltrate of liver tissue of chronically infected patients strengthened the involvement of Treg in controlling hepatic immune responses [143, 144].

#### 1.2.1.2 Concurrent *S. mansoni* and Hepatitis C virus infection

The high prevalence of HCV in Egypt stems from an iatrogenic epidemic that was introduced in the 1950s due to mass treatment with antimony against schistosomiasis [124, 145, 146]. Since then, concomitant human schistosomiasis and HCV infection are extremely common, especially in rural areas of Egypt [108, 109, 147] and co-infected individuals present an accelerated onset of liver cirrhosis and hepatocellular carcinoma [110, 148-151]. Indeed, 30% of HCV mono-infected individuals recovered from acute infections whereas all those with an additional *S. mansoni* infection progressed to a chronic state [152]. Moreover, compared to HCV mono-infected individuals, these patients exhibited higher HCV-positive RNA titres, higher necro-inflammatory and fibrotic scores in the liver and poor responses to interferon therapy [108, 151-156].

Therefore, one of the aims within this thesis is to investigate whether phenotypical changes of Foxp3$^+$ Treg, induced during human schistosomiasis, could be responsible for the reported failure to raise effective antiviral CD4$^+$ and CD8$^+$ T cell responses [140-142, 157, 158], which would lead to loss of viral replication control and eventually to more pronounced liver disease. Thus, we analysed liver function and viral load as well as Treg, T effector cell (Teff) frequencies and specifically the nTreg/iTreg distribution using the novel markers Helios and GrzB within patients with HCV mono-infection and those with concomitant Schistosoma infection.

## 1.2.2 *S. mansoni* and Hepatitis B virus co-infection

### 1.2.2.1 Geographical distribution, transmission and associated disease of Hepatitis B virus infection

Hepatitis B virus (HBV) infection is highly prevalent in Asia, Africa and South America. According to the WHO about a third of the world's population has been infected at one point in their lives with HBV, resulting in about 350 million chronic carriers [159]. The virus is transmitted by exposure to infectious blood, by sexual contact or vertically from infected mothers to their offspring. Acute perinatal infection (Asia) or acute infection during early childhood (Africa) are the major route of infection in these endemic countries and these children bear a much higher risk for chronic infection compared to adults (less than 5% vs. up to 90%) [160]. The virus infects hepatocytes by binding to the sodium/bile acid co-transporter (NTCP), a functional receptor expressed on liver cells [161]. Furthermore HBV is a non-cytopathic virus, and liver damage is mainly T-cell mediated [107]. Acute infection can cause liver inflammation, vomiting, jaundice and, in case of a fulminant immune response, to death. Chronic HBV infection develops in patients who fail to mount sustained HBV-specific CD8$^+$ and CD4$^+$ T cell immune responses [162]. Here, chronic inflammation is referred to as chronic hepatitis B, and bears a high risk for the patient to develop liver cirrhosis and hepatocellular carcinoma [163]. The main prerequisites for successful viral clearance are the killing of infected hepatocytes and purging of virus from viable liver cells [164] in order to prevent virus dissemination to intact, naïve liver tissue [165]. The first is mainly achieved by HBV-specific cytotoxic CD8$^+$ T cells that recognize HBV peptides on MHC-I of infected cells

and kill these in a perforin/GrzB-dependent manner [162, 166]. Virus purging, as part of the viral elimination process is mainly achieved by the induction of IFN-γ, a type II interferon produced mainly by $CD8^+$ and $CD4^+$ T cells [162, 166]. In response to the presence of viruses it binds to the IFN-γ receptor expressed on infected hepatocytes and activates the Janus kinase-STAT (JAK/STAT) signalling pathway leading to large amounts of protein kinase R (PKR) production [167]. This enzyme reduces protein synthesis within the cell and therefore the production of new viral particles is hampered. Another cellular enzyme, RNAseL, also induced following PKR activation, destroys RNA within the cells to further reduce protein synthesis of both viral and host genes. Inhibited protein synthesis finally destroys both the virus and infected host cells [168, 169]. Interferons activate a plethora of genes, known as interferon-stimulated genes (ISGs), which have additional roles in combating viruses such as Hepatitis B and C virus [170]. Finally, IFN-γ induces MHC-I and MHC-II up-regulation on APCs and promotes p53 activity within virus infected cells, promoting apoptosis and finally avoiding the spread of the virus to other cells [171].

Currently the prevalence of chronic HBV infection in Germany is about 0,6%, whereas in major parts of Africa and in China rates are about 8% and can reach up to 20% in some countries like Tanzania [172]. Acute infection with Hepatitis B usually does not require treatment as most adults are able to clear the infection spontaneously, however treatment of a chronic infection is necessary to reduce the risk of cirrhosis and liver cancer, especially in patients showing high viral titres and elevated serum alanine aminotransferase levels (ALT), which is a marker of liver tissue damage [173, 174]. In general, chronic HBV infection is treated by using antiviral drugs, such as Lamivudine or Tenofovir, which act directly on the viral reverse transcriptase [175] or PEGylated interferon alpha (Pegasys) that binds to the IFNα receptor activating the same JAK/STAT signalling pathway as IFN-γ [167]. The injection of PEG-IFN-α can further act as an additional immune system booster as it induces IFN-γ production by T cells [176]. Although direct antivirals cannot clear the infection, they stop viral replication and minimize progressing liver damage.

#### 1.2.2.2 Hepatitis B virus infection and concomitant schistosomiasis

As mentioned above, in rural areas endemic for schistosomiasis, chronically infected people are often co-infected with other pathogens such as HBV and interestingly, HBV chronicity

rates are much higher in these areas [105, 106]. Due to the lack of suitable animal models, the possible interactions between *S. mansoni* and HBV have up to now only been analysed epidemiologically and the results of these – rather few - studies are controversial: some studies demonstrate that co-infection with these two pathogens led to prolonged viremia and worsening of liver damage [105, 106, 111-113, 177]. For example, in Egyptian, Brazilian and Saudi-Arabian field studies higher prevalence of HBV infection and an aggravation of hepatic disease was observed in *S. mansoni* infected patients [111, 113, 177]. In addition, Brazilian patients with concurrent schistosome infection responded less prominently to vaccination against HBV [106]. In contrast, population based surveys from Egypt, Yemen and China revealed no higher HBV infection rates or higher probability of HBV chronicity in schistosome co-infected patients [178-180]. These diverging epidemiological observations clearly demand defined studies on the interaction of both pathogens and pathogen-induced immunity in controlled rodent models especially in the light of fluctuating immune resonses induced by schistosomes.

### 1.2.3 Animal models to study *S. mansoni* and Hepatitis B virus co-infection

Important issues to address in concurrent HBV and schistosome infection are for example the establishment of HBV infection, the contribution of innate and adaptive immune responses in the early phase of infection for viral clearance and persistence and the influence of both pathogens on the disease outcome. To address these questions cell based tools are not sufficient and lead to the necessity of animal models.

In general, HBV research has limited experimental models available due to the narrow host-range and organ-specificity of HBV. Besides humans only chimpanzees, tree shrews or macaques are naturally susceptible to the virus [181-183]. Since such studies are extremely limited due to ethical aspects, availability, and high costs, woodchucks and Peking ducks susceptible to B-like hepatitis viruses are alternatively used as natural animal models in HBV research [184, 185]. Like HBV, the woodchuck hepatitis virus (WHV) and the duck hepatitis virus (DHV) belong to the same family of *hepadnaviridae.* While the duck model has been extensively used for assessing antiviral strategies, the woodchuck model was utilized to learn about the immune response to mammalian hepadnaviral infection and the development of hepatocellular carcinoma [184-189]. Co-incidently woodchucks are also known to be

susceptible to schistosomes and are therefore considered as a good model to study *S. mansoni* and HBV co-infection [190]. The relevance of this unique model regarding hepatitis/schistosomiasis interactions was investigated by a study from *Andrade et al.* who infected woodchucks with *S. mansoni* before infecting them with WHV. In brief, the study showed no significant impact of schistosomiasis on WHV serum markers and no influence on viral replication in co-infected animals. Even though co-infected animals presented decreased numbers and smaller granuloma sizes, in general no aggravation of both diseases could be observed. The authors concluded that schistosomiasis and viral hepatitis in woodchucks run parallel courses, with neither apparent special histological features derived from the association of the two conditions, nor modulation of WHV replication [190].

Taken together, even though the woodchuck and Peking duck animal models brought fundamental knowledge into the biology of hepatitis B, the use of these models to study HBV infection has limitations. First, these animals are not convenient to keep due to the lack of inbred strains. Furthermore HBV- and WHV replication cycles are not completely comparable because the WHV DNA integrates into the host genome, whereas the HBV DNA remains as covalently-closed-circular DNA (cccDNA) in the cell nucleus. In addition, it is known that immunotherapeutic agents against WHV will not be effective against HBV, and vaccines against HBV can never be tested in woodchucks. Furthermore one of the main immunopathological features of HBV is the development of liver cirrhosis and HCC which cannot be investigated in woodchucks, since these animals do not develop cirrhosis [191-196].

All these limitations led to a new investigative approach which focuses on the acutal Hepatitis B virus. Therefore, HBV transgenic mouse lineages expressing partial or complete HBV genomes have been generated as an inbred animal model with a well defined immune system [197-199]. These transgenic mouse models are easy to handle at low-cost in the laboratory environment and can provide important insights into viral pathobiology and hepatocellular injury [200-204]. However, it is important to note that murine hepatocytes are not permissive to HBV infection, although they support the HBV lifecycle and secrete large amounts of virions upon transduction of viral genomes [199]. The reason why viral entry is hampered is currently under extensive research but first studies have already pointed out the important role of the human NTCP receptor for successful viral uptake into hepatocytes [161, 205]. The NTCP receptor is exclusively expressed on the surface of liver

cells and is normaly involved mostly in the uptake of conjugated bile salts and other molecules such as steroid and thyroid hormones [161, 206]. In humans, HBV as well as Hepatitis D virus (HDV) gain entry into liver cells by binding via their pre-S domain, a protein embedded in the lipid envelope of the virus, to the NTCP receptor [161, 205, 207]. Even though murine hepatocytes express this receptor, *in vitro* [208] and *in vivo* [209] experiments showed that its binding capacity to the viral pre-S domain was less efficient when compared to the human NTCP variant [210]. In general, the specific human NTCP receptor recognition, contributes to host specificity and tissue tropism of HBV and HDV [205, 211]. This fact was shown by a recent study of *Li et al.* who tested whether human NTCP can support HBV infection in non-susceptible murine hepatocyte cell lines. After exogenous introduction of the human NTCP, the study succeeded to render mouse cell lines AML-12, Hepa 1-6 and primary mouse hepatocytes susceptible to HDV but not to HBV and concluded that although human NTCP is a functional receptor that mediates HBV infection in human cells, it cannot support HBV infection in mouse hepatocytes [205]. It is therefore reasonable to speculate that additional human hepatocyte-specific factors are required for HBV infection of mice.

Besides the use of HBV transgenic mice, the species barrier of HBV can be overcome by either adenoviral HBV genome transfer or by hydrodynamic injection of plasmids carrying an HBV genome into mice. In the last years, two different mouse models of acute, self-limiting HBV infection have been independently developed with these two methods and allowed detailed studies of virus-host interactions in an immune competent environment [212-215]. Compared to HBV transgenic mice, which are immunotolerant to HBV and not able to clear HBV infection since the viral DNA is integrated into their genome, these new mouse models are suitable to analyse the onset, establishment and the dynamics of an acute HBV infection. In these mice, the transient genome transfer led to an extra-chromosomal organization of the HBV genome in the cell nucleus of murine hepatocytes which is comparable to the establishment of cccDNA in human liver cells [215, 216].

In the second part of this PhD thesis we took advantage of the adenoviral HBV genome transfer (AdHBV mouse model) to analyse the clearance of an acute HBV infection in animals with pre-existing *S. mansoni* infection. Furthermore, HBV transgenic mice were used to study the impact of a secondary acquired schistosome infection on top of a pre-existing chronic

HBV infection. The corresponding models are explained in detail in the respective result sections.

So far, the interrelationship between *S. mansoni* and HBV has only been addressed experimentally in a single study using a HBV transgenic (HBVtg) mouse model [217]. As mentioned above, in HBVtg mice, HBV DNA is integrated into the genome as a transgene and as a consequence these mice do not develop HBV-specific B and T cell responses, but serve as a model to study HBV replication in the liver microenvironment. The study investigated the influence of $T_H1$ or $T_H2$ type cytokines induced during *S. mansoni* infection on HBV replication. It demonstrated that HBV replication was suppressed during the $T_H1$ phase of *S. mansoni* infection and remained downregulated upon onset into the $T_H2$ phase 6-8 weeks post schistosome infection [217]. The authors attributed the suppressed HBV replication to the antiviral activity of schistosome-induced IFN-$\gamma$ and showed that the first appearance of $T_H2$ type cytokines does not counteract with the antiviral effect of IFN-$\gamma$ [217]. However, *Guidotti et al.,* only monitored HBV replication up to the 8th week of schistosome infection, and did not provide any information on whether this suppression persisted during the successive immune-suppressive phases of schistosome infection. Therefore, it is very important to study whether HBV replication re-occurs upon progression into the $T_H2$ and regulatory phases of schistosome infection. Furthermore, this mouse model is not suitable to address the consequences of an acute HBV infection acquired on top of an already existing *S. mansoni* infection, which would reflect the situation in schistosome endemic areas more appropriately especially because young children are infected with the helminth before acquiring an additional HBV infection during adolescence. Therefore, in this thesis, besides the HBVtg mouse model we additionally use the AdHBV mouse model to address these important epidemiological aspects. More specifically, we experimentally investigate the outcome of an acute HBV infection acquired during the different immune phases ($T_H1$, $T_H2$) induced during *S. mansoni* infection and address the question whether an already existing helminth infection drives an acute HBV infection towards chronicity.

## 1.2.4 AdHBV mouse model

### 1.2.4.1 The hepatitis B virus particle and its replication cycle

HBV belongs to the family of *hepadnaviridae* (hepatitis-DNA-viruses), and as mentioned above, related viruses such as WHV and DHV were found in rodents and birds [218]. The major characteristics of hepadnaviruses are their hepatotropism, strict species-specificity, their capacity to persist and to induce a chronic infection. Furthermore, they have a similar mode of replication including a reverse-transcription step and similar genome structure and –organization [219, 220]. The infectious virion is termed as Dane particle after its discoverer D.S. Dane, and is about 42 nm in size [221]. It has a spherical structure and consists of the nucleocapsid, enveloped in a host-derived lipoprotein membrane (see Figure 5). As depicted in Figure 5, three different hepatitis B surface (HBs) glycoproteins are integrated into the lipid-envelope termed small (S), middle (M) and large (L) proteins with the domains S, pre-S2 and pre-S1 which are necessary for viral binding and entry into susceptible cells. Together, these proteins are often referred to as hepatitis B surface antigen (HBsAg) [222-225]. The icosahedral nucleocapsid consists of 180 - 240 viral core proteins, termed hepatitis B core antigen (HBcAg), and encloses the partially double-stranded viral DNA as well as the viral DNA polymerase with reverse-transcriptase activity [226, 227].

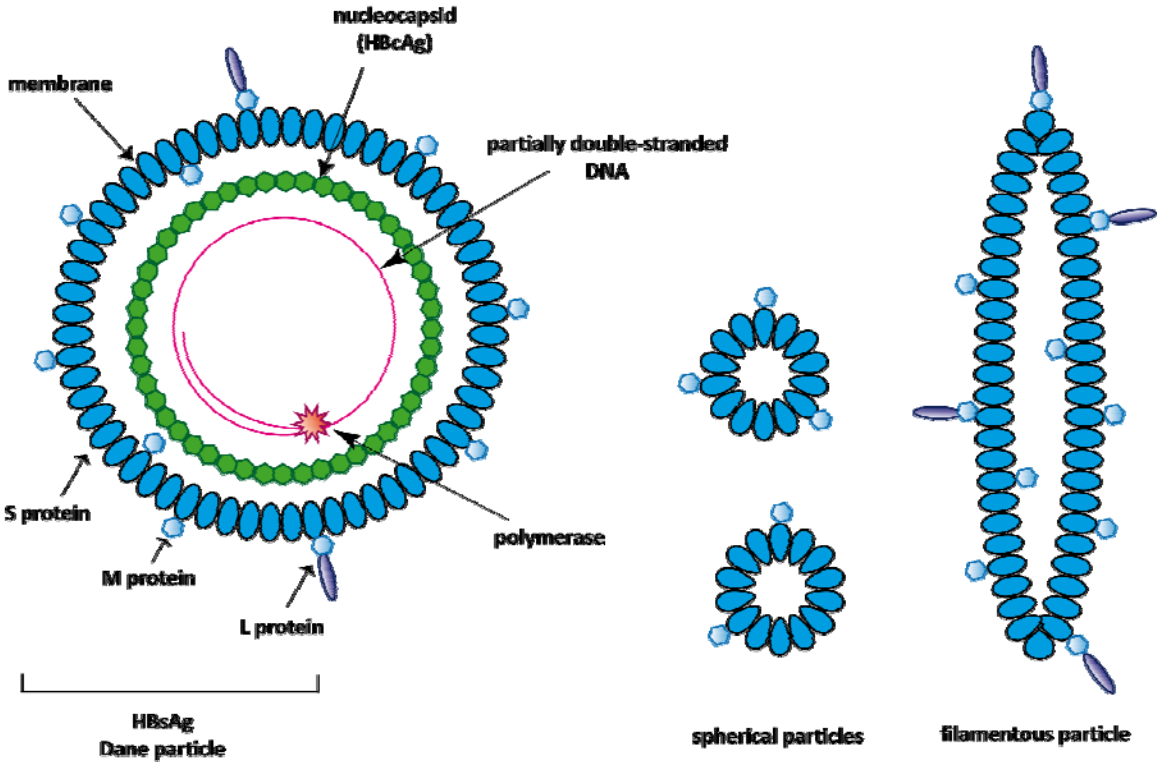


**Figure 5: Schematic representation of the HBV virion.** The hepatitis B virus particle is composed of an outer lipid-envelope containing the three embedded surface proteins S-, M- and L-protein, which are necessary for viral binding and entry into susceptible cells. The icosahedral nucleocapsid is enveloped by the lipid-membrane, and encloses the partially double-stranded viral DNA and the viral DNA polymerase. It is composed of viral core proteins termed HBcAg. Besides the infectious Dane particle, two different forms of non-infectious subviral particles (SVP), termed spheres and filaments, are secreted from HBV infected hepatocytes. These SVPs are produced in excess during the lifecycle of the virus and are composed of the viral lipid envelope with embedded surface proteins (HBsAg), lacking the nucleocapsid with the viral genome. Adapted from: Sirma H, Funk A and Will H. Molekulare Virologie von Hepatitis B- und –D-Viren. In: Hepatitis B Infektion – Therapie – Prophylaxe. Georg Thieme Verlag, 2006. Chapter 1.5, p.4.

In addition to the Dane particle, two different forms of non-infectious subviral particles (SVP), termed spheres and filaments, are secreted from HBV replicating hepatocytes (Figure 5). They are composed of the viral lipid envelope with embedded HBsAg and lack the nucleocapsid with the viral DNA. These non-infectious particles are secreted in 10,000 – to 100,000-fold excess over virions and are needed to escape the host's immune system, since they trap the majority of antibodies produced against HBV (anti-HBsAg) [228].

The lifecycle of the hepatitis B virus is complex and starts when viral particles get trapped on the surface of hepatocytes either by unspecific binding to heparan sulfate proteoglycans or specific binding to the NTCP receptor (Figure 6) [229]. The specific interaction of the viral

large surface protein (L-protein) with the sodium/bile acid co-transporter (NTCP) finally leads to clathrin-dependent endocytosis or membrane fusion of the virion [161, 230]. Upon entry, the nucleocapsid enclosing the viral DNA is released and transported by host chaperons to the nucleus, where the core protein is able to bind to nuclear pores and finally releases the relaxed circular (rc) DNA into the nucleus [231, 232]. Here, the partially double stranded DNA (rcDNA) is made fully double stranded and transformed into covalently closed circular DNA (cccDNA), representing a highly stable episomal mini-chromosome which is usually not integrated into the host genome and has the potential to persist in the host cell over years [233].

The cccDNA serves as a template for the transcription of four viral messenger (m) RNAs which are transported from the nucleus to the cytoplasm where they are used to generate the new copies of the viral genome, the capsid core and surface proteins and the viral DNA polymerase [234, 235]. The new copies of the viral genome derive from one of the largest RNAs (pre-genomic or pgRNA) which are used as template for the viral DNA polymerase to synthesize rcDNA via its reverse transcriptase activity. The newly synthesized rcDNA is then encapsidated together with the new viral DNA polymerase in the self-assembled core capsids [236, 237]. The synthesized viral surface proteins are afterwards integrated into the endoplasmic reticulum and either form empty subviral particles or interact with viral core capsids carrying the new copies of the viral rcDNA, to finally form enveloped Dane particles [238]. While the majority of infectious virions and SVPs are transported to the cell surface and released via multivesicular bodies, some of them are recycled back into the nucleus, where they establish and maintain a persistent infection by constantly filling up the cccDNA pool within the infected liver cell [239, 240]. Within the cell nucleus itself, the viral X-gen, encoding a transcription factor, is necessary for the formation of cccDNA. In the absence of this gene, cccDNA cannot be generated, resulting in no viral persistance within the nucleus of hepatocytes. The function of the protein coded for by gene X is furthermore associated with the development of liver cancer. It stimulates genes that promote cell growth and inactivates growth regulating molecules [161, 238, 241].

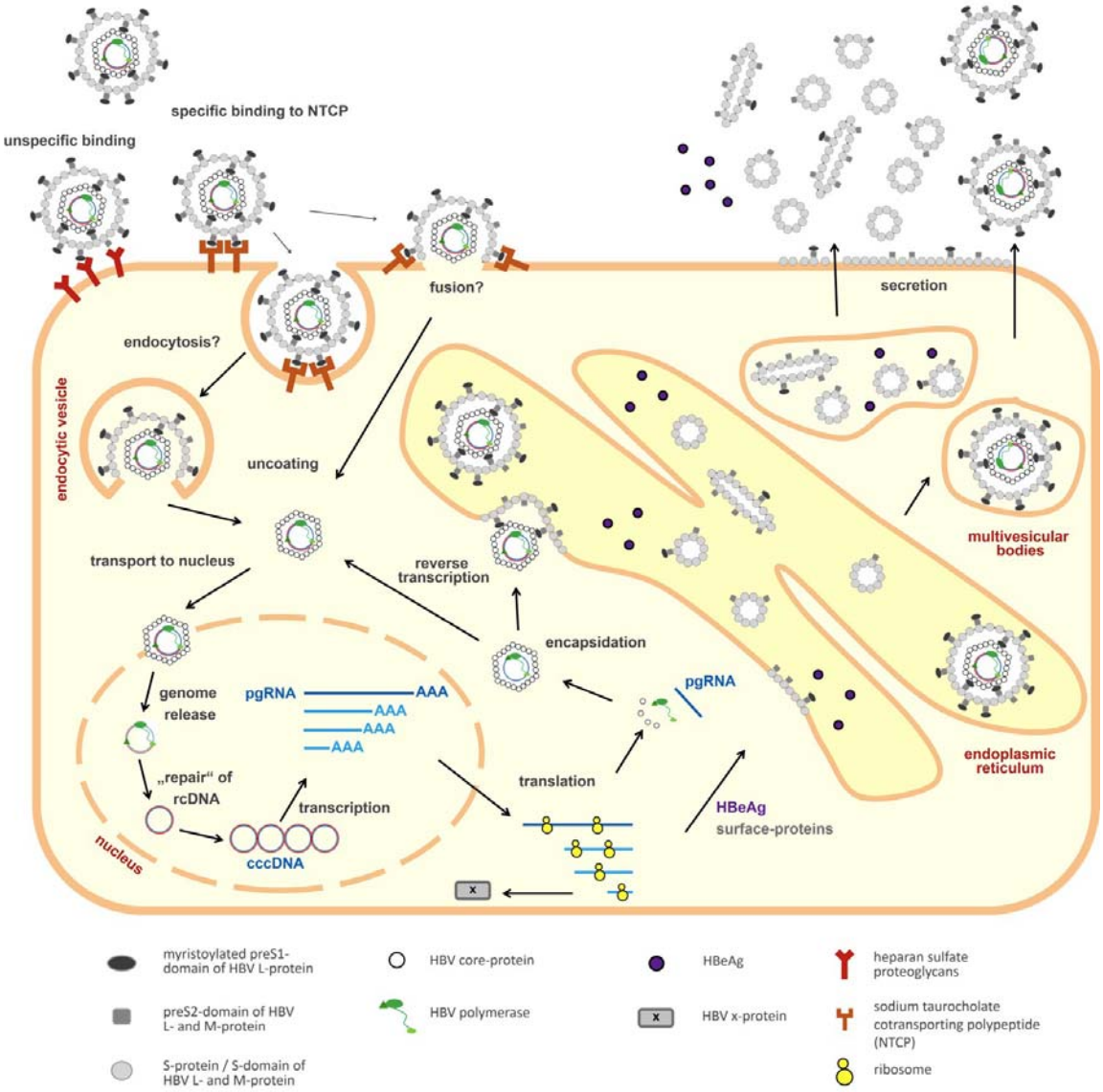


**Figure 6: The replication cycle of HBV.** Hepatitis B virions gain entry into hepatocytes by either unspecific or specific binding to heparan sulfate proteoglycans or the NTCP receptors expressed on the cell surface. Following endocytosis, uncoating of the virions and release of the capsid into the cytosol is initiated, where the nucleocapsid carrying the viral DNA is transported via host chaperons to the cell nucleus. Here the partially double stranded rcDNA is released into the nucleus, is made fully double stranded and transformes into covalently closed circular DNA (cccDNA) by the help of host enzymes. Within the cell nucleus itself, the viral X-gen, encoding a transcription factor, is necessary for the formation of cccDNA. The cccDNA is used as template for the transcription of pre-genomic (pg) RNA and three other messenger RNAs that are translocated into the cytoplasm where the translation of the HBV polymerase, HBV x-protein, HBV core-protein and surface proteins takes place. Encapsidation of the pgRNA and viral polymerase enables reverse transcription to rcDNA. Within the endoplasmic reticulum newly synthesized surface proteins either assemble to form empty subviral particles (SVP) or interact with viral core capsids carrying the new copies of the viral rcDNA, to finally form enveloped Dane particles. Infectious virions and SVPs either recycle back to the nucleus and thereby filling up the cccDNA pool or are secreted via multivesicular bodies from infected hepatocytes. Taken (with personal communication and permission) from Jäger, C. (2015). Therapeutic vaccination using MVA-vectors in a murine model of chronic HBV infection, *PhD Thesis*.

### 1.2.4.2 Adenoviral HBV genome transfer

As mentioned above, to actively infect mice with HBV, an adenoviral genome transfer using an adenoviral vector carrying replication competent HBV genomes is used to overcome the species barrier of HBV. Adenoviruses are medium-sized (80-110 nm), non-enveloped viruses with a nucleocapsid carrying a double stranded, linear DNA which does not integrate into the host genome [242]. They have a broad range of vertebrate hosts and 57 different serotypes have been found to mainly cause infections of the upper respiratory tract in humans [243, 244]. So far, in gene therapy, adenoviruses have long been used as a popular viral vector due to their potential to carry large transgenes and their ability to affect both replicating and non-replicating cells. Here, they serve as a vehicle to administer targeted therapy in the form of recombinant DNA or protein [245]. In general, the advantages of using adenoviral vectors are their high transduction efficiency in a pleiority of cells, their capacity to carry large amounts of DNA of interest and to maintain the DNA insert. Their active import of the contained DNA into the nucleus and their high stability especially against desinfectants is an additional benefit [246]. Strong host immune responses against expressed adenoviral proteins however, are one of the main disadvantages of adenoviral vectors, which can be overcome by using genetically modified adenoviruses carrying deletions in genes encoding for the majority of adenoviral proteins, such as early region 1 (E1A and E1B) and early region 3 (E3) genes [213, 247, 248].

Given that adenoviruses additionally display a strong liver tropism after intravenous injection (i.v.), in HBV research, they are used as viral shuttles to transfer replication competent HBV DNA in murine hepatocytes. 2001, *Sprinzl et al.* constructed for the first time, adenoviral vectors containing a 1.3-fold-overlength of human and duck hepatitis B virus genomes. Here, the adenovirus-mediated HBV genome transfer initiated HBV replication in primary hepatocytes from various species and in the livers of mice, since high titers of infectious virions were found in the culture medium of infected cells and in the sera of mice [213].

In this thesis, an acute HBV infection in mice was carried out with an adenoviral vector transferring a 1.3-fold overlength HBV genome with a deletion in the viral X-gen (AdHBV-$X^-$) (Figure 7). As mentioned above, the X-gen encodes for proteins which are necessary for the formation of cccDNA. Thus, following adenoviral transfer of HBV-$X^-$ DNA, no cccDNA can be

established, leading to an acute, self-limiting HBV infection, where the hepatitis B virus is able to replicate only once and cannot persist in infected murine hepatocytes.

As depicted in Figure 7, the replication-competent HBV-X$^-$ genome was inserted into the E1 region of an adenovirus type 5 genome with deleted E1 and E3 regions, in order to prevent adenoviral replication and immune evasion strategies [247, 248].

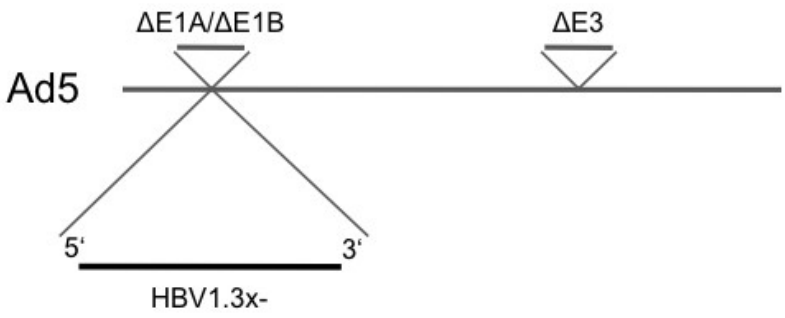


**Figure 7: The recombinant adenovirus genome used to generate AdHBV-X$^-$.** First-generation adenoviral vector derived from adenovirus serotype 5 (Ad5) with deletions (Δ) in the early regions of E1A, E1B and E3. The HBV 1.3-fold overlength genome containing a stop codon in the open reading frame of the X-gene is inserted into the ΔE1A/E1B regions of the adenoviral vector. Adapted from [215].

Following HBV-X$^-$-genome transfer, an acute, self-limiting hepatitis B infection is established and infectious HBV virions are efficiently produced and secreted by murine hepatocytes *in vivo*. Since the adenoviral vector is genetically modified, it immediately degrades upon uptake into hepatocytes, avoiding the persistent circulation of adenovirus in the bloodstream and the establishment of adenoviral-specific immune responses [213, 215]. Taken together, this vector has various advantages: (1) it allows to induce HBV replication in a broad range of cell types and species from an extrachromosomal template as in the natural infection; (2) it allows to control the strength of infection by varying the dose of the inoculum; (3) adenoviruses are hepatotropic viruses targeting hepatocytes very efficiently upon intravenous injection. Thus, AdHBV-X$^-$ is a valuable tool to study HBV infection in well-defined model organisms.

## 1.3 Aims of the thesis

One of the main complications of hepatitis C and B virus infection is the development of chronic hepatitis after an acute infection, since these individuals are at high risk to develop liver cirrhosis and hepatocellular carcinoma. Interestingly, chronic hepatitis B and C develop at a higher frequency in developing countries in which co-infections with several helminth species, such as *S. mansoni* are common. The underlying mechanisms leading to HCV and HBV chronicity are only partly understood but they compromise $CD8^+$ and $CD4^+$ T cell responses, which might be affected in helminth co-infected patients due to dynamic schistosome driven immune responses. These range from an initial $T_H1$- to $T_H2$-immunity and eventually to long-term immunosuppression. Thus, the effects of pre-existing helminth infections on concomitant HCV/HBV infection are hard to predict and need clarification. Therefore, in this thesis we investigate in more detail *S. mansoni* infections with either concurrent HCV or HBV infections.

The first part of this thesis addresses the interrelationship between *S. mansoni* and Hepatitis C virus infection. Here, the parasite seems to accelerate the progression of the liver disease, as liver cirrhosis and hepatocellular carcinoma are more common within co-infected individuals. Since the underlying mechanisms leading to the aggravated liver disease outcome are still not understood, our human study aims to investigate whether phenotype changes of $Foxp3^+$ Treg, induced during human schistosomiasis, could be responsible for the reported failure to raise effective antiviral $CD4^+$ and $CD8^+$ T cell responses. Impaired antiviral immune responses would then lead to loss of viral replication control and eventually to a more pronounced liver disease. Thus, in collaboration with the University of Cairo in Egypt, we analysed liver function and viral load as well as Treg, T effector cell frequencies and specifically the nTreg/iTreg distribution using the novel markers Helios and GrzB within patients with HCV mono-infection and those with concomitant Schistosoma infection.

The central questions in this study are:

1. Do schistosome-induced Treg change their phenotype in human schistosomiasis and contribute to the failure to raise effective anti-viral T cell responses?
2. Is the n/iTreg distribution altered in infected individuals and how do these different Treg compartments contribute to the impaired anti-viral immune response?

3. Is the frequency and function of effector T cells altered in co-infected individuals?

Regarding concomitant *S. mansoni* and HBV infections, in the second part of this thesis, we experimentally investigate with the help of the AdHBV-$X^-$ mouse model, the outcome of an acute HBV infection acquired during the different immune phases ($T_H1$, $T_H2$, chronic) induced during *S. mansoni* infection. Here we address the question whether an already existing helminth infection drives an acute HBV infection towards chronicity. The impact of a secondary acquired schistosome infection on top of a pre-existing chronic HBV infection will be additionally investigated with the use of the HBV transgenic mouse model.
The central questions in this study are:

1. Does the phase of immune response during *S. mansoni* infection determine the outcome of an acute hepatitis B virus co-infection or its severity by changing the liver microenvironment?
2. Does the acute *S. mansoni* infection break the chronicity/tolerance in a chronically HBV infected host by immune cell infiltration and local production of IFN-γ in the liver?
3. Does chronic *S. mansoni* infection lead to resurgence of HBV replication in a persistent HBV infection and long-term disease progression via schistosome-induced Treg?

The results will deepen our understanding as to why HCV and HBV chronicity rates are much higher in third-world (helminth-endemic) countries compared to industrialized ones. In the future, this may have a direct impact on worldwide treatment and vaccination efforts of HCV/HBV, which currently disregard the role of helminth co-infections.

# 2 Material and Methods

## 2.1 Materials

### 2.1.1 Equipment

| | |
|---|---|
| Agarose gel documentation system | Bio-Rad |
| Agarose gel electrophoresis system (Sub-Cell® GT) | Bio-Rad |
| anti-HBsAg and anti-HBeAg ELISA (Murex®; AXSYM assay system) | Abbott Laboratories |
| Automatic ice machine (Scotsman MF36) | Gastro |
| Automatic pipettes (2-1000µl) | Gilson |
| Balance (440-33N) | Kern |
| Balance (XB120A) | Precisa |
| BD LSRII™ flow cytometer | BD |
| BD FACSCalibur™ flow cytometer | BD |
| Biological safety cabinet (Hera safe) | Thermo Scientific® |
| Centrifuge (Biofuge fresco) | Heraeus |
| Centrifuge (Eppendorf 5424) | Eppendorf |
| Centrifuge (Megafuge 3.0R) | Thermo Scientific® |
| Cooling plate (COP 30) | Medite |
| CyAn ADP Lx P6 | DakoCytomation |
| CyAn ADP Lx P8 | DakoCytomation |
| Disperser (T10 basic Ultra-Turrax®) | IKA |
| ELISA microplate reader (Sunrise™) | Tecan |
| Freezer (-20°C) | Bosch |
| Freezer (-80°C) | Thermo Scientific® |
| Freezing container (Nalgene® Mr. Frosty) | Sigma® |
| Fridge | Bosch |
| Glassware | Schott |
| Haematocytometer (Neubauer chamber) | Karl Hect KG |
| Homogeniser (5ml) | B Braun |
| Incubator (BBD 6220) | Heraeus |
| Laminar Flow Hera Safe ClassII, Type A7B3 | Heraeus |
| Light Cycler 480 II | Roche Diagnostic® |

| | |
|---|---|
| LumiNunc™ 96-well plates (white) | Nunc |
| Microscope (Axioscop) | Zeiss |
| Microscope (Axiovert) | Zeiss |
| Microwave (1100W) | Panasonic |
| Milli-Q Integral System | Millipore™ |
| Mini-PROTEAN electrophoresis system | Bio-Rad |
| Mini-Pump variable flow | Neolab® |
| MoFlo™ XDP | Beckman Coulter |
| Multichanel pipettes (Acura® 855; 5-350µl) | Socorex |
| Multipette® plus | Eppendorf |
| NanoDrop® 1000 Spectrophotometer | Thermo Scientific® |
| Orbital shaker (3005) | GFL |
| Paraffin embedding system (TB 588) | Medite |
| Paraffin oven | Memmert |
| pH-meter (MultiCal®) | WTW |
| Pipetboy (acu) | IBS |
| Power supply (Power Pac 3000) | BioRad |
| Power supply (EV231) | Peqlab |
| Reflovet Plus System | Roche Diagnostics® |
| Rotary microtome automatic (RM 2245) | Leica |
| Rotating mixer (RM 5) | Assistant |
| Shandon Excelsior ES tissue processor | Thermo Scientific® |
| Stericup® filter units (500ml) | Millipore™ |
| Thermocycler (T3000) | Biometra |
| Thermomagnetic stirrer (IKAMAG® REO) | IKA |
| Thermomixer (compact) | Eppendorf |
| Tissue cool plate (COP 20) | Medite |
| Tissue flotation bath (TFB 35) | Medite |
| Ultracentrifuge (Optima™ L-100 XP) | Beckman Coulter |
| Vi-CELL® Cell Viability Analyser | Beckman Coulter |
| Vortex mixer (Reax top) | Heidolph |
| Water bath | Memmert |

### 2.1.2 Software

| | |
|---|---|
| CELLQuest Pro™ software (Flow Cytometry) | BD |
| FlowCytomix™ Pro 3.0 Software | Affymetrix |
| (sample analysis of multiplex immunoassay) | |
| FlowJo v9.5.3 (Flow cytometry analysis software) | TreeStar |
| GraphPad Prism 5 | GraphPad Software |
| (Biostatistics, curve fitting and scientific graphing programme) | |
| Magellan™ (Data analysis software for microplate reader) | Tecan |
| Nanodrop® 1000 V 3.7.0 | Kisker |

### 2.1.3 Consumables

| | |
|---|---|
| Blood agar plates | BD |
| Cell scraper | TPP® |
| Cell strainer (40-100µm) | BD |
| Centripreps® | Amicon |
| Combitips plus® (0.2-2.5ml) | Eppendorf |
| Cover slips | Roth® |
| Cryo vials | Alpha Laboratories |
| Culture plates (6-, 12-, 24-, 96-well) | BD |
| Disposable bags | Roth® |
| ELISA plates (96 well) | Nunc |
| Eppendorf tubes (0.5-2ml) | Eppendorf |
| FACS tubes (Microtubes, 1.2ml) | Alpha Laboratories |
| Fast-Read 102® | Biosigma |
| Glass slide | Langenbrinck |
| Gloves | Meditrade® |
| Hypodermic needles (Sterican®) | B Braun |
| Leucosep-Tubes | Greiner |
| MacConkey agar plates | BD |

| | |
|---|---|
| Parafilm M® | Pechiney |
| Petri dishes | Greiner |
| Pipet tips (10-1000µl) | Starlab |
| Reaction tubes | Zefa-Laborservice |
| Scalpels | Feather |
| Slidescanner SCN400 | Leica |
| Sterile filters (0.22µm, 0.4µm) | VWR Lab Shop |
| Serological pipettes (5-50ml) | Greiner |
| Sub-Q syringes (1ml) | BD |
| Syringes (1-25ml) | B Braun |
| Syringe filter (0.2µm, 0.45µm) | Sartorius |
| Tissue culture flask (50-500ml) | BD |
| Tubes (15ml, 50ml) | Greiner |

### 2.1.4 Reagents

| | |
|---|---|
| Acetic acid | Roth® |
| Acetone | Fischer Scientific |
| Acid fuchsin | Morphisto |
| Agarose | Sigma® |
| Ammonium chloride ($NH_4Cl$) | Roth® |
| Aniline blue | Morphisto |
| Bicoll, Ficoll separating solution (density 1.077g/mL) | Biochrom AG |
| Brefeldin A (5mg/mL in DMSO) | Sigma-Aldrich |
| Bovine serum albumin (BSA) | PAA |
| Bromophenol blue | Roth®, Sigma® |
| Chloroform | Roth® |
| Collagenase (from *Clostridium histolyticum*) | Sigma® |
| Collagenase Type IV (240 u/mg) | Worthington® |
| Cytofix/Cytoperm reagent | BD |
| Deoxynucleoside triphosphate (dNTPs) | Promega |
| Deoxyribonuclease I from bovine pancreas (DNAse) | Sigma® |

| | |
|---|---|
| Dimethylsulfoxid (DMSO) | Sigma® |
| Diphteria toxin (DTX) | Merck |
| DirectPCR-tail lysis reagent | Peqlab |
| Dithiothreitol (DTT) | Roth® |
| Dulbecco's PBS (Endotoxin-free) | PAA |
| Ethidium monoazide bromide (EMA) | Invitrogen |
| Entellan® | Merck |
| Eosin 1% (v/v) | Morphisto |
| Ethanol 70%-99.8% (v/v) | MRI Pharmacy |
| Ethidium bromide | Roth® |
| Ethylenediaminetetraacetic acid (EDTA) | Roth® |
| Forene® | Abbott |
| Formaldehyde solution 37% (v/v) | Sigma®, Merck |
| Gentamicin (10 mg/ml) | PAA |
| Herculase II | Stratagene |
| Hydrogen chloride (HCl) | Roth® |
| 4-(2-Hydroxyethyl)-1-piperazineethanesulfonic acid (HEPES) | Sigma® |
| Isopropanol | MRI Pharmacy |
| Light Cycler® 480 Probes Master | Roche |
| Mayer`s haematoxylin | Morphisto |
| Methanol | Roth® |
| β-Mercaptoethanol | Roth®, Sigma® |
| Narcoren® | Merial |
| Paraformaldehyde (PFA) | Sigma® |
| Percoll™ | GE Healthcare |
| Periodic acid | Morphisto |
| Perm/Wash Solution | BD |
| Phenol | Roth® |
| Phosphate buffered saline (PBS) | MRI |
| Phosphomolybdic acid | Morphisto |
| Potassium hydroxide (KOH) | Merck |
| Powdered PBS (Phosphate buffered saline) | Biochrom |

| | |
|---|---|
| Proteinase K (20 mg/ml) | Peqlab |
| RNAlater® | Ambion® |
| Roti®-Histofix 4% (v/v) | Roth® |
| Roti®-Safe GelStain | Roth® |
| Schiff reagent | Morphisto |
| Sodium chloride (0,9% v/v NaCl) | B Braun |
| Sucrose | Roth® |
| Sulphuric acid ($H_2SO_4$) | Merck |
| 3,3',5,5'-Tetramethylbenzidine (TMB) substrate | BD |
| Tris(hydroxymethyl)aminomethane (Tris) | Merck, Roth® |
| Trisodium citrate dihydrate | Roth® |
| Trypan blue solution 0.4% (v/v) | Sigma® |
| Tween® 20 | Sigma® |
| Vancomycin hydrochloride (VANCO-cell® 500 mg) | Cellpharm |
| Weigert`s haematoxylin | Morphisto |

### 2.1.5 Medium supplements

| | |
|---|---|
| Fetal calf serum (FCS) | PAA |
| β-Mercaptoethanol for cell culture | Gibco® |
| Non-essential amino acids (100x) | PAA |
| Penicillin/Streptomycin (100x) | PAA |
| RPMI 1640 (with L-Glutamine) | PAA |
| Sodium pyruvate solution (100 mM) | PAA |

### 2.1.6 Kit systems

| | |
|---|---|
| anti-HBsAg and anti-HBeAg ELISA (Murex®; AXSYM assay system) | Abbott Laboratories |
| BD OptEIA™ (TMB substrate) | BD |
| DC protein assay | Bio-Rad |
| DNeasy Blood & Tissue Kit | Quiagen |
| Foxp3 staining buffer set | Affymetrix |

| | |
|---|---|
| GoTaq® DNA polymerase (including 5x Green GoTaq® reaction buffer) | Promega |
| Herculase II reaction buffer | Stratagene |
| Human Th1/Th2/Th8/Th17/Th22 13plex Kit FlowCytomix | Affymetrix |
| Mouse ELISA Kits (Duo Set®; IL-13, IL-10) | R&D |
| Mouse ELISA Kits (Ready-Set-Go) IFN-γ, IL-4, IL-5 | Affymetrix |
| QuantiTect Reverse Transcription Kit | Quiagen |
| QIAmp DNA Stool Mini Kit | Quiagen |
| RNeasy Mini Kit | Quiagen |
| Taq buffer | Invitrogen |
| T cell activation/expansion Kit (mouse) | Miltenyi Biotec |

### 2.1.7 Size standards

| | |
|---|---|
| Gene Ruler™ 100 bp DNA ladder | LifeTechnologies |

### 2.1.8 Antibodies

Table 2 depicts all antibodies which were used for the data presented in this study. ELISA antibodies from the Affymetrix and R&D ELISA-Kits, 13plex Kit FlowCytomix (section 2.1.6) as well as for the AXSYM assay systems (section 2.1.1) are not included.

| ***Name*** | ***Antigen*** | ***Conjugate*** | ***Species*** | ***Dilution*** | ***Producer*** | ***Method*** |
|---|---|---|---|---|---|---|
| ***α-human CD8 FITC*** (Clone RPA-T8) | *CD8* | *FITC* | *Mouse* | *1:50* | *BD* | *FACS* |
| ***α-human CD8 PE*** (Clone RPA-T8) | *CD8* | *PE* | *Mouse* | *1:200* | *BD* | *FACS* |
| ***α-human CD8 AmCyAn*** | *CD8* | *AmCyAn* | *Mouse* | *1:20* | *BD* | *FACS* |

| | | | | | | |
|---|---|---|---|---|---|---|
| (Clone SK1) | | | | | | |
| ***α-human CD19 ECD*** (Clone J3-119) | *CD19* | *ECD* | *Mouse* | *1:20* | *Beckman Coulter* | *FACS* |
| ***α-human CD4 PE-Cy5*** (Clone OKT4) | *CD4* | *PE-Cy5* | *Mouse* | *1:20* | *BioLegend* | *FACS* |
| ***α-human CD8 PB*** (Clone SK1) | *CD8* | *PB* | *Mouse* | *1:400* | *BioLegend* | *FACS* |
| ***α-human CD3 PE-Cy7*** (Clone UCHT-1) | *CD3* | *PE-Cy7* | *Mouse* | *1:400* | *Affymetrix* | *FACS* |
| ***α-human CD4 A700*** (Clone OKT4) | *CD4* | *A700* | *Mouse* | *1:800* | *Affymetrix* | *FACS* |
| ***α-human CD127 PE*** (Clone HIL-7R-M21k) | *CD127* | *PE* | *Mouse* | *1:100* | *BD* | *FACS* |
| ***α-human CD103 PE-Cy5*** (Clone Ber-ACT8) | *CD103* | *PE-Cy5* | *Mouse* | *1:50* | *BioLegend* | *FACS* |
| ***α-human CD25 PE-Cy7*** (Clone BC96) | *CD25* | *PE-Cy7* | *Mouse* | *1:10* | *Affymetrix* | *FACS* |
| ***α-human Granzyme B FITC*** (Clone GB11) | *Granzyme B* | *FITC* | *Mouse* | *1:20* | *BD* | *FACS* |
| ***α-human Foxp3 PB*** (Clone 206D) | *Foxp3* | *PB* | *Mouse* | *1:20* | *BioLegend* | *FACS* |

| | | | | | | |
|---|---|---|---|---|---|---|
| ***α-human Helios FITC*** (Clone 22F6) | *Helios* | *FITC* | *Mouse* | *1:20* | *BioLegend* | *FACS* |
| ***α-mouse CD4 PE-TexasRed*** (Clone RM4-5) | *CD4* | *PE-TexasRed* | *Rat* | *1:800* | *LifeTechnologies* | *FACS* |
| ***α-mouse Neuropilin1 PerCP*** | *Neuropilin1* | *PerCP* | *Goat* | *1:10* | *R&D* | *FACS* |
| ***α-mouse CD8 APC*** (Clone 53-6.7) | *CD8* | *APC* | *Rat* | *1:200* | *Affymetrix* | *FACS* |
| ***α-mouse Foxp3 PE*** (Clone FJK-16s) | *Foxp3* | *PE* | *Rat* | *1:200* | *Affymetrix* | *FACS* |
| ***α-mouse CD4 PE-Cy7*** (Clone RM4-5) | *CD4* | *PE-Cy7* | *Rat* | *1:200* | *Affymetrix* | *FACS* |
| ***α-mouse CD8 PerCP*** (Clone 53-6.7) | *CD8* | *PerCP* | *Rat* | *1:100* | *BD* | *FACS* |
| ***α-mouse CD19 PE*** (Clone eBio1D3) | *CD19* | *PE* | *Rat* | *1:300* | *Affymetrix* | *FACS* |
| ***α-mouse Helios PB*** (Clone 22F6) | *Helios* | *PB* | *Goat* | *1:20* | *BioLegend* | *FACS* |
| ***α-mouse CD8 FITC*** (Clone 53-6.7) | *CD8* | *FITC* | *Rat* | *1:200* | *Affymetrix* | *FACS* |
| ***α-mouse CD8 APC-Cy7*** (Clone 53-6.7) | *CD8* | *APC-Cy7* | *Rat* | *1:100* | *BD* | *FACS* |
| ***α-mouse IL-4*** | *IL-4* | *APC* | *Rat* | *1:200* | *BioLegend* | *FACS* |

| | | | | | | |
|---|---|---|---|---|---|---|
| ***APC***<br><br>(Clone 11B11) | | | | | | |
| ***α-mouse IL-2 APC***<br><br>(Clone JES6-5H4) | *IL-2* | *APC* | *Rat* | *1:200* | *Affymetrix* | *FACS* |
| ***α-mouse IL-10 FITC***<br><br>(Clone JES5-16E3) | *IL-10* | *FITC* | *Rat* | *1:200* | *Affymetrix* | *FACS* |
| ***α-mouse Foxp3 FITC***<br><br>(Clone FKJ-16s) | *Foxp3* | *FITC* | *Rat* | *1:200* | *Affymetrix* | *FACS* |
| ***α-mouse Foxp3 eF450***<br><br>(Clone FKJ-16s) | *Foxp3* | *eF450* | *Rat* | *1:200* | *Affymetrix* | *FACS* |
| ***α-mouse IFN-γ PE***<br><br>(Clone XMG 1.2) | *IFN-γ* | *PE* | *Rat* | *1:200* | *Affymetrix* | *FACS* |
| ***α-mouse CD16/CD32***<br><br>Fc receptor block<br><br>(Clone 93) | *CD16/32* | - | *Rat* | *1:1000* | *Affymetrix* | *FACS* |
| ***α-mouse CD3e***<br><br>(Clone 17A2) | *CD3* | - | *Rat* | *1µg/ml* | *Affymetrix* | *In vitro stimulation* |
| ***α-mouse CD28***<br><br>(Clone 37.51) | *CD28* | - | *Golden Syrian Hamster* | *1µg/ml* | *Affymetrix* | *In vitro stimulation* |

**Table 2: Antibodies used for FACS and *in vitro* stimulation.**

## 2.1.9 Buffers and solutions

All buffers and solutions were prepared with Millipore Q distillated water.

### 2.1.8.1 Buffers and solutions for egg preparation

| | | |
|---|---|---|
| Vancomycin solution: | 500 mg | Vancomycin hydrochloride |
| | 10 ml | 0.9% NaCl (w/v) |
| Collagenase solution: | 500 mg | Collagenase |
| | 5 ml | Dulbecco`s PBS (1x) |
| DNase solution: | 1 g | DNase I |
| | 146 ml | Dulbecco`s PBS (1x) |
| Egg-PBS solution: | 1x | Dulbecco`s PBS (1x) |
| | 0.1% (v/v) | Vancomycin solution |
| | 0.5% (v/v) | Gentamicin |
| Liver digestion solution: | 25 ml | Egg-PBS solution |
| | 1 ml | Collagenase solution |
| | 3 ml | DNase solution |
| | 500 µl | Penicillin/Streptomycin |
| Percoll solution: | 8 ml | Percoll™ |
| | 32 ml | 0.25M Sucrose |

### 2.1.9.2 Buffers for erythrocyte lysis

| | | |
|---|---|---|
| ACT buffer: | 17 mM | Tris |
| | 160 mM | $NH_4Cl$ |
| | pH 7.2 | |

### 2.1.9.3 Buffers for liver-associated lymphocytes isolation

| | | |
|---|---|---|
| Liver digestion solution: | 10 mg/liver | Collagenase Type IV |

| | | |
|---|---|---|
| | 12,5 ml/liver | RPMI + 10% (v/v) Penicillin/Streptomycin |
| Percoll solution: | 8 ml | Percoll™ |
| | 32 ml | 0.25 M Sucrose |

**2.1.9.4 Buffers and solutions for FACS**

| | | |
|---|---|---|
| FACS buffer: | 1x | PBS (pH 7.2-7.4) |
| | 2% (v/v) | FCS |
| Fc block solution: | 1x | FACS buffer |
| | 0.1% (v/v) | α-mouse CD16/32 |

**2.1.9.5 Buffers and solutions for ELISA**

| | | |
|---|---|---|
| Reagent diluents: | 1x | PBS (pH 7.2-7.4) |
| | 1% (w/v) | BSA |
| Washing buffer: | 1x | PBS (pH 7.2-7.4) |
| | 0.05% (v/v) | Tween® 20 |
| Stopping solution: | 2 M | $H_2SO_4$ |

**2.1.9.6 Buffers for IFN-γ genotyping PCR**

| | | |
|---|---|---|
| Polymerase buffer: (including loading buffer) | 400 µl | 5x Green GoTaq® reaction buffer |
| | 40 µl | 10mM dNTPs |
| | 40 µl | 1% BSA (w/v) |
| | 1260 µl | $H_2O$ |
| TAE buffer: | 40 mM | Tris-Acetic acid (pH8.3) |
| | 1 mM | EDTA |
| Tail-digestion solution: | 250 µl | DirectPCR-tail lysis reagent |

| | | |
|---|---|---|
| | 4 µl | Proteinase K (20mg/ml) |

## 2.1.10 Cell culture medium

| | | |
|---|---|---|
| Complete medium: | 1x | RPMI 1640 |
| | 10% (v/v) | FCS |
| | 1% (v/v) | Penicillin/Streptomycin |
| | 1% (v/v) | Non-essential amino acids |
| | 1% (v/v) | Sodium pyruvate solution |
| | 0.1% (v/v) | β-Mercaptoethanol for cell culture |

## 2.1.11 Primer sequences

### 2.1.11.1 IFN-γ genotyping primer

| | | |
|---|---|---|
| oIMR6218 | 5’-CCT TCT ATC GCC TTC TTG ACG-3’ | (mutant) |
| oIMR8284 | 5’-AGA AGT AAG TGG AAG GGC CCA GAA G -3’ | (wt) |
| oIMR8285 | 5’-AGG GAA ACT GGG AGA GGA GAA ATA T -3’ | (common) |

### 2.1.11.2 Primer for *S. mansoni* specific qPCR

Forward tandem repeat (FP): 5’ CAACCGTTCTATGAAAATCGTTGT 3’

Reverse tandem repeat (RP): 5’ CCACGCTCTCGCAAATAATCT 3’

Dual labeled probe tandem repeat (labeled probe) with 5’ and 3’ modifications:

5’ [6FAM]TCCGAAACCACTGGATTTTTATGAT[BHQ1] 3’

### 2.1.11.4 Primer for HBV- and Adenovirus specific qPCR

HBV:

Forward primer (HBV1745+): 5’-GTTGCC-CGTTTGTCCTCTAATTC-3’

Reverse primer (HBV1844-): 5’-GGAGGGATACATAGAGGTTCCTTGA-3’

Adenovirus:

Forward primer (Ad156+): 5'-TAAGCGACGGATGTGG-3'

Reverse primer (Ad388-): 5'-CCACGTAAACGGTCAAAG-3'

Murine reference gene (non-coding region located 1345 bp downstream of 3' end of protein kinase C-binding protein NELL1 precursor on chromosome 7; amplicon 154 bp):

Forward primer: 5'- GGATCAAGGTCAGAGGACCA -3'

Reverse primer: 5'- GGGTTTCTCTCTGGCATTTG-3'

## 2.2 Methods

### 2.2.1 Animals

#### 2.2.1.1 Mouse strains and housing

C57BL/6 and NMRI mice (the latter were used as mammalian host for *Schistosoma mansoni* cycle and to obtain infected livers for the preparation of eggs or SEA) were obtained from Harlan Winkelmann GmbH (Germany), whereas DEREG C57BL/6 mice were bred and housed at the Institute of Medical Microbiology, Immunology and Hygiene (MIH), TU Munich. C57BL/6 IFN-$\gamma^{-/-}$ mice were purchased from The Jackson Laboratory (Charles River Laboratories, Bar Harbor, Maine) and HBV transgenic mice (HBV1.3xfs) on a C57BL/6 background were kindly provided by Prof. Dr. Ulrike Protzer (TU Munich). All mouse strains were bred and maintained under specific pathogen-free (spf) conditions in the animal house of the MIH. Experimental mice were sex- and age-matched and the experiments were performed in accordance with local government regulations (license number for animal testing 55.2.1.54-2532-112-13).

#### 2.2.1.2 Screening of DEREG mice

In some experiments of this study, DEREG-mice ("**de**pletion of **reg**ulatory T cell" mice) were used, bacterial artificial chromosome (BAC)-transgenic mice on C57BL/6 background in which an enhanced GFP (eGFP)-human *diphtheria*-toxin receptor (hDTR) fusion protein is expressed under the control of the *foxp3*-locus [249]. In DEREG mice, Foxp3$^{+}$Tregs can be depleted systemically and specifically, but only transiently by injecting *diphtheria*-toxin

(DTX), which does not affect other cell populations lacking the receptor [249]. Additionally, Foxp3-expressing Tregs can easily be detected by GFP-fluorescence.

Between 25% and 50% of the female offspring in the DEREG mouse breeding show a transgene-positive phenotype, indicated by eGFP-expression of regulatory T cells. Therefore, the offspring of each breeding pair had to be screened for GFP-positive regulatory T cells in order to gain mice for experiments and for further breeding. DEREG-mice were bled at the facial vein and approximately 10 µL blood were dissolved in 10 µL heparin solution and stored on ice. Lysis of erythrocytes (2.1.9.2) was performed and cells were washed 2x with 200 µL FACS-buffer. Thereafter, cells were stained with anti-mouse CD4 APC 1:200 as described below (section 2.3.4.2). After 2x washing of the stained PBMCs with 200 µL FACS-buffer, flow cytometry was performed to detect the $CD4^+eGFP^+$ regulatory T cells.

#### 2.2.1.3 Depletion of $CD4^+Foxp3^+$regulatory T cells in DEREG mice

For Treg-depletion, DEREG mice received daily injections of 1µg *diphtheria* toxin in 200 µl PBS intraperitonially (i.p.) on two consecutive days.

#### 2.2.1.4 IFN-γ genotyping PCR

For the present study PCR reactions were performed to verify the genotype of the specific knockout-strain of mice namely, IFN-γ-deficient mice.

Therefore, approximately 0.5 cm of a mouse`s tail was digested with 250 µl tail-digestion solution (DirectPCR-tail lysis reagent, Peqlab) and 4 µl (0.4 mg/ml) Proteinase K (Peqlab) overnight using a thermomixer (55°C, 450 rpm). The lysate was then heat inactivated at 85°C for 45 min, centrifuged (10 sec, 13000 rpm) and the resulting supernatant stored at -20°C or directly used for genotyping PCR reactions.
Genotyping primers were re-suspended in Millipore Q distilled water to a concentration of 100 pmol/µl and the genotyping PCR reaction mix was prepared as follows:

| *Volume* | *Component* |
|---|---|
| 1 µl | Lysate (including mouse DNA) |
| 2,6 µl | Primer (mutant) |
| 0,4 µl | Primer (wt) |
| 1,2 µl | Primer (common) |
| 22 µl | Polymerase buffer (see section 2.1.9.6) |
| 0,1 µl | GoTaq® DNA polymerase |

The corresponding primers for the PCR reaction are depicted in section 2.1.11.1. The PCR reactions were performed on a Thermocycler T3000 (Biometra) as follows:

| | *Temperature* | *Time* | |
|---|---|---|---|
| Initiation | 94°C | 3 min | |
| Denaturation | 94°C | 30 sec | |
| Annealing | 67°C | 1 min | 35cycles |
| Elongation | 72°C | 1 min | |
| Final elongation | 72°C | 2 min | |
| Storage | 10°C | ∞ | |

Expected results:

| | *Mutant allele* | *Wildtype allele* |
|---|---|---|
| Amplification products | 500 bp | 210 bp |

To determine the specific size (length) of DNA fragments, amplification products were separated using agarose-gel electrophoresis.

For the present study, agarose gels (1.5%) were prepared by boiling up agarose (Sigma ®) in TAE buffer (section 2.1.9.6). After cooling to approximately 50°C, a DNA-intercalating agent, such as ethidium bromide (300 µg/l; Roth®) or Roti®-Safe GelStain (5 µl/100 ml; Roth®), was added to the agarose gel solution. The final polymerization was then performed in a horizontal gel chamber (Bio-Rad) at room temperature, in which a comb was placed to form pockets for sample application. Afterwards 15 µl of PCR product (including the synthesized DNA fragments) and 5 µl of Gene Ruler$^{TM}$ 100 bp DNA ladder (LifeTechnologies) were loaded into the gel pockets. The DNA fragments were separated at 130 mA for 40-60min within a TAE buffer filled agarose gel electrophoresis system (Bio-Rad). Detection of separated DNA fragments occurred by exciting the intercalating agents with UV light at 254 nm. The emission of the DNA fragments was measured and photographed using the agarose gel documentation system (Bio-Rad). The length of the new synthesized DNA fragments was determined by comparing the size of the different fragments to the applied standard with defined DNA fragment lengths (Gene Ruler$^{TM}$ 100 bp DNA ladder), resulting in confirmation of the mouse genotype.

### 2.2.2 *S. mansoni* lifecycle maintenance

Murine infection of *S. mansoni* reflects both the immunological and parasitological consequences that arise in humans as it is one of only a few helminthes that infect both mouse and man. To maintain the *S. mansoni* cycle at the MIH, NMRI mice were used as mammalian hosts and were regularly (every 3 weeks) infected intraperitoneal (i.p.) with 140-200 cercariae of a Brazilian strain of *S. mansoni,* which had been released previously from *Biomphalaria glabrata* snails after exposure to light and a temperature of 31°C. 8 weeks post infection, mice were sacrificed to obtain their intestines and to isolate miracidiae, which were used to infect new snails to continue the infectious cycle (section 1.1.2). In addition, livers of infected mice were used for the preparation of eggs and SEA (section 2.2.3).

## 2.2.3 SEA preparation

### 2.2.3.1 Egg preparation from liver tissue

To prepare fresh eggs from liver tissue, NMRI mice were sacrificed 8 weeks post *S. mansoni* infection and livers were removed using sterile scissors and tweezers. Obtained livers were washed in pre-cooled 1.2% (v/v) NaCl solution and bile ducts and gallbladders were removed. Afterwards livers were minced using a scalpel and transferred into a 50 ml tube containing 25 ml liver digestion solution (section 2.1.8.1). The tube was then filled up with PBS to 50 ml and incubated under continuous agitation at 37°C overnight using an orbital shaker. Thereafter, digested livers were washed twice by centrifugation at 400 g for 5 min at 4°C and the remaining pellet was re-suspended in 25 ml PBS and filtered twice through a 250 µm sieve. The filtrate was layered on a Percoll gradient (section 2.1.8.1) and centrifuged at 800 g for 10 min at 4°C, to finally separate the eggs from liver tissue. Eggs were washed three times with 15 ml and 30 ml of 1 mM EDTA solution, respectively, and finally with 30 ml PBS as previously described. After these washing steps, the egg pellet was re-suspended in 700 µl PBS and 5 µl were microscopically analysed (x10 magnification) to confirm the purity and to calculate the total egg count with the following formula:

*total egg count = (counted eggs x 700 µl) / 5 µl*

Finally, isolated eggs were either frozen at -80°C or directly used for SEA preparation (section 2.2.3.2). Contaminations of the obtained egg suspension were analysed by standard microbiological assessments on blood – and MacConkey agar plates containing 1-2 µl of the egg suspension (incubation at 37°C for 48 hours).

### 2.2.3.2 SEA preparation from liver-derived eggs

The egg suspension (section 2.2.3.1) was transferred to a glass homogenizer and pestled for at least 20 min on ice. During this procedure egg shells were destroyed and a mixture of different (glyco-)proteins and (glyco-)lipids, namely the soluble egg antigens (SEA), were released. To separate the egg shells from the SEA, an ultracentrifugation step at 100,000 g for 1h (4°C) using the Optima™ L-100 XP ultracentrifuge was performed. The supernatant, containing the SEA, was then collected and transferred to a cryotube, whereas the remaining

egg shell pellet was re-suspended in 200 µl PBS. Possible contaminations were excluded by plating 1-2 µl of both suspensions on a blood - and MacConkey agar plates (incubation at 37°C for 48 hours). The protein concentration of both, the SEA solution and egg shell pellet solution was measured by using the DC protein assay kit (Bio-Rad) according to the manufacturer's instructions. Finally, both suspensions were frozen at -80°C.

## 2.2.4 Experimental *Schistosoma mansoni* and Hepatitis B virus co-infection

### 2.2.4.1 Infection protocols

#### 2.2.4.1.1 Investigation of immune phases and cytokine responses during *S. mansoni* infection in C57BL/6 mice

To determine differential cytokine responses induced during the different immune phases of *S. mansoni* infection, C57BL/6 mice were infected with *S. mansoni* by injection of 180 cercariea i.p.. Immune responses were analysed at week 4, 5, 5.5, 7.5, 8, 16 and 22 weeks post infection.

#### 2.2.4.1.2 Protocol for investigating the outcome of a secondary acquired acute HBV infection during the acute phase of *S. mansoni* infection

The outcome of a secondary acquired acute HBV infection during the acute phase of *S. mansoni* infection was analysed by infecting 6-8-week-old female C57BL/6 and C57BL/6 IFN-$\gamma^{-/-}$ mice with 180 cercariae i.p. before infecting them intravenously (i.v.) with either an adenoviral vector containing HBV DNA (AdHBV-X$^-$, section 2.2.5.1) or with an empty adenoviral vector, lacking HBV DNA (AdEmpty, section 2.2.5.1), 4 or 5 weeks post schistosome infection. Post viral infection, successful virus infection and ongoing viral clearance was monitored by bleeding mice at day 3, 7, 14 and 21 followed by measuring viral antigen levels, such as Hepatitis B surface antigen (HBsAg) and Hepatitis B early antigen (HBeAg), within mice sera with a microparticle enzyme immunoassay (section 2.2.5.4). Final analysis of mice took place 3 days and 3 weeks post viral infection.

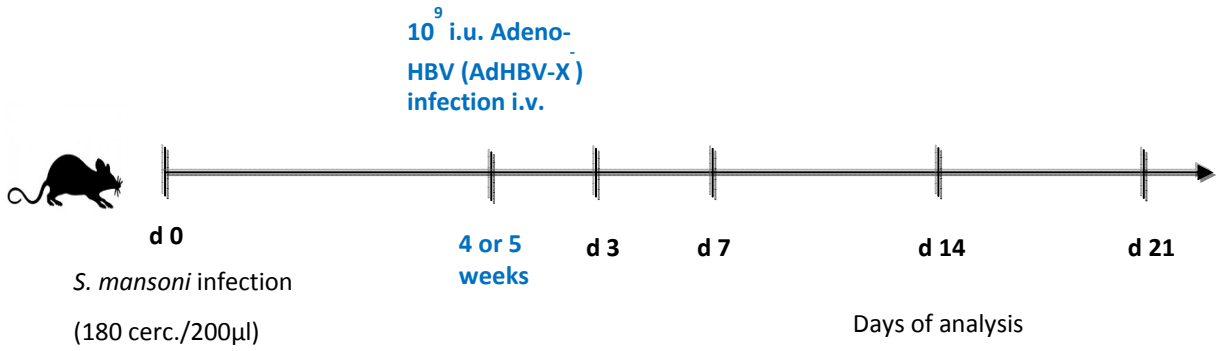


#### 2.2.4.1.3 Protocol for investigating the outcome of a secondary acquired acute HBV infection during the chronic phase of *S. mansoni* infection

Acute HBV infection acquired during the chronic phase of *S. mansoni* infection was analysed by infecting C57BL/6 and DEREG C57BL/6 mice with 180 cercariae i.p.. AdHBV-X$^-$ infection (section 2.2.5.1) followed 16 weeks post schistosome infection and final analysis of mice took place 3 days and 3 weeks post viral infection. Viral replication and elimination was monitored by bleeding mice at 3, 7, 14 and 21 days post viral infection and by measuring viral antigens within sera of mice. Diphteria Toxin was injected i.p. in DEREG mice on two consecutive days post viral infection to investigate the influence of Treg depletion on viral clearance (detailed experimental protocol for DEREG experiment see section 3.2.5.1).

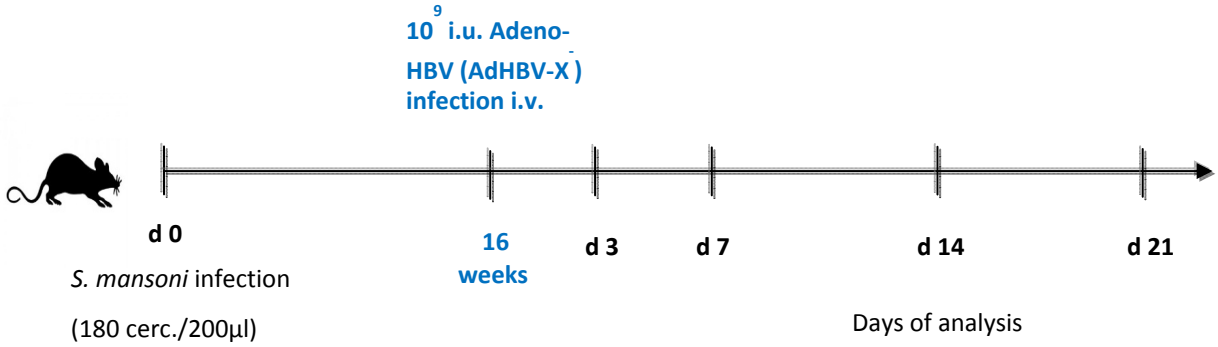


#### 2.2.4.1.4 Impact of a secondary acquired schistosome infection on liver disease outcome in chronically HBV infected mice

The impact of a secondary acquired schistosome infection on top of a pre-existing chronic HBV infection was investigated by infecting HBV transgenic mice (HBV1.3xfs) on a C57BL/6

background with 180 cercariae i.p.. Viral replication was monitored by bleeding mice at day 42, 56, 70, 84, 98 and 112 and by measuring viral antigens within mice sera. Final analysis of mice took place at 6.5 and 16 weeks post schistosome infection.

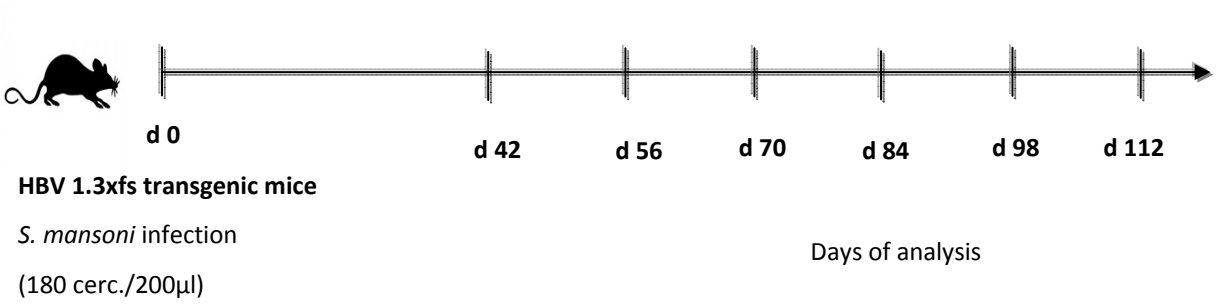


Age-, strain- and sex-matched uninfected mice were used as controls in all experiments.

### 2.2.4.2 Evaluation of *S. mansoni* infection

The general infection status was scored by the degree of visual infection and organ damage. Specifically, the liver was examined for signs of fibrosis, changes in colour and visible granulomas. The infection status was graded on a scale from 0 to 3 DOI (degree of infection) with 3 denoting the highest level of infection. In addition, total body weight of each individual mouse and organ weight (liver, intestine and spleen) were obtained and compared with uninfected mice.

#### 2.2.4.2.1 *S. mansoni* egg count analysis within liver

Weighed liver samples from individual mice were digested in 5 ml of 5% (w/v) KOH solution under continuous agitation at 37°C for at least 2 hours. After incubation, the released eggs were centrifuged at 400 g for 10 min and 4.5 ml of the supernatant was immediately removed. 10 µl of the re-suspended remaining eggs (within 500 µl) were counted trice under the microscope (x10 magnification) and the number of eggs in the liver was calculated as follows:

*eggs/mg tissue = (average of counted eggs x 50) / weight of tissue sample (mg)*

#### 2.2.4.2.2 Histological methods

Infection of *S. mansoni*, especially chronic infection, is characterized by chronic local inflammatory responses to tissue-trapped schistosome eggs within the liver and intestine. Around tissue-trapped decaying eggs granuloma formation is induced, leading to a unique form of liver and intestine fibrosis, which is the main elicitor of morbidity and mortality (section 1.1.5). For the present study, liver granuloma formation and infiltration of immune cells within granulomas were analysed and compared to wildtype controls.

#### 2.2.4.2.3 Tissue preparation for histological staining

The left liver lobe from each individual mouse was fixed in Roti®-Histofix (4%), dehydrated using the Shandon Excelsior ES tissue processor and embedded in paraffin using the TB 588 paraffin embedding system. 3 µm sections were cut using the RM 2245 automatic rotary microtome and fixed on glass slides for staining techniques (section 2.2.4.2.3.1 and section 2.2.5.5).

##### 2.2.4.2.3.1 Staining techniques

For analysis of granuloma formation and immune cell infiltration within the liver, trichrome Masson`s blue and heamatoxylin/eosin (HE) stains were performed. The trichrome Masson`s blue stain was used to differentiate between collagen and smooth muscle and to visualize the increase of collagen during granuloma formation, since the aniline component in the staining buffer turns collagen fibers blue. Liver sections stained with Masson`s blue stain were furthermore used for size analysis of the granulomas. The Masson`s blue staining procedure is depicted in Table 3.

| Reagent | Producer | Incubation time | Function |
|---|---|---|---|
| Xylene | Engelbrecht | 10 min | Dissolving of paraffin |
| Ethanol (96%) | MRI | 2 min | Rinsing with mounting water content (watering) |
| Ethanol (80%) | MRI | 1 min | |
| Ethanol (70%) | MRI | 1 min | |
| Aqua bidest. | MRI | 1 min | |
| Weigert's heamatoxylin | Morphisto | 2 min | Complexation of positive heamatoxylin to the negative nucleic acids phosphate groups (nuclear staining) |
| Tap water | - | Constant rinsing for 5 min | Achievement of deep blue staining due to pH alteration |
| Acid fuchsin | Morphisto | 2 min | Staining of the smooth muscle tissue |
| Phospho-molybdic acid | Morphisto | 5 min | Differentiation and increasing of contrast between collagen and smooth muscle tissue |
| Aniline blue | Morphisto | 4 min | Staining of collagen |
| Tap water | - | Rinsing until water becomes clear | Dissolving of aniline blue |
| Ethanol (96%) | MRI | 2 min | Rinsing with mounting alcohol content (dehydration) |
| Isoporopanol | MRI | 1 min | |
| Xylene | Engelbrecht | 10 min | Fixation |
| Entellan® | Merck | - | Fixation and covering with coverslip |

**Table 3: Masson`s blue staining protocol.**

The HE staining is a combined staining method and was used in this study to analyse immune cell infiltration within granulomas. Hemalum, a complex formed from aluminium ions and

oxidized haematoxylin, colours the nuclear of cells blue, whereas the eosin solution stains eosinophilic structures within tissues in various shades of red. The HE staining procedure is depicted in Table 4.

| Reagent | Producer | Incubation time | Function |
|---|---|---|---|
| Xylene | Engelbrecht | 10 min | Dissolving of paraffin |
| Ethanol (96%) | MRI | 2 min | Rinsing with mounting water content (watering) |
| Ethanol (80%) | MRI | 2 min | |
| Ethanol (70%) | MRI | 2 min | |
| Ethanol (60%) | MRI | 2 min | |
| Aqua bidest. | MRI | 2 min | |
| Mayer's heamatoxylin | Morphisto | 5 min | Complexation of positive heamatoxylin to the negative nucleic acids phosphate groups (nuclear staining) |
| Tap water | - | Constant rinsing for 12 min | Achievement of deep blue staining due to pH alteration |
| 1% (v/v) Eosin | Morphisto | 5 min | Staining of eosinophilic structures |
| Tap water | - | Rinsing until water becomes clear | Dissolving of eosin |
| Ethanol (80%) | MRI | 1 min | Rinsing with mounting alcohol content (dehydration) |
| Ethanol (96%) | MRI | 4 min | |
| Xylene | Engelbrecht | 10 min | Fixation |
| Entellan® | Merck | - | Fixation and covering with coverslip |

**Table 4: Heamatoxylin and eosin staining protocol.**

#### 2.2.4.2.3.2 Microscopical analysis of stained liver sections

Masson`s blue stained liver sections were analysed microscopically for granuloma formation and size, whereas HE stained sections were used to monitor immune cell infiltration. Granuloma sizes were determined by measuring the diameters of granulomas with the help of an ocular micrometer along the longitudinal axis of the eggs at x10 magnification with the Axioscop microscope. Up to 40 granulomas of each individual liver section were evaluated and the average size of granulomas from each liver section was calculated.

### 2.2.4.3 *S. mansoni* specific qPCR

#### 2.2.4.3.1 Isolation of parasite DNA from stool

Stool samples from *S. mansoni* infected mice were collected into 2 ml reaction tubes. According to the protocol provided in the QIAmp DNA Stool Mini Kit, DNA was isolated from approximately 100 mg stool. The method was performed as recommended by the manufacturer with little alterations. In brief, collected stool samples were re-suspended in 500 µl InhibitEX buffer, homogenized by vortexing and incubated at 95°C for 20 min in a shaker in order to lyse stable parasite eggs and release parasite DNA. To purify the DNA-containing supernatant from remaining stool particles, lysed samples were centrifuged at 13000 rpm for 1 min (RT). Afterwards 200 µl supernatant was collected from each sample and mixed with 15 µl proteinase K and 200 µl buffer AL for digestion of proteins. Optimal working conditions for the proteinase K were reached by incubating samples for 10 min at 70°C. Afterwards, samples were loaded onto QIAmp spin columns, followed by two washing steps with buffer AW1 and AW2. Finally, the purified DNA was eluted from the spin column in 50 µl buffer AE and the yield and purity of DNA was determined using Nanodrop® 1000 (Kisker). DNA samples were then stored at –20°C for use in qPCR.

#### 2.2.4.3.2 *S. mansoni* specific qPCR and running conditions

In order to verify the infection with *S. mansoni*, DNA isolated from stool (section 2.2.4.5.1) was amplified by qPCR. Reverse and forward primers and the labeled probe for this experiment were based on findings of Wichmann *et al* [250]and lead to the amplification of a 86 bp fragment of the *S. mansoni* DNA tandem repeat unit as described in section 2.1.11.2.

The qPCR reaction mix was prepared as follows:

| ***PCR-Mix*** | ***Volume*** |
|---|---|
| LightCycler®480 Probes Master | 10 µl |
| Forward primer (10µM) | 1.0 µl |
| Reverse primer (10µM) | 1.0 µl |
| Probe (6µM) | 1.0 µl |
| Target DNA | 2.0 µl |
| DEPC $H_2O$ | 5.0 µl |

The corresponding primers as well as the schistosome specific dual labeled probe tandem repeat for the PCR reaction are depicted in section 2.1.11.1. As positive control DNA isolated from stool of previously schistosome infected mice was used. The PCR was runned on the LightCycler®480 (Roche) with the following settings:

| | ***Temperature*** | ***Time*** | |
|---|---|---|---|
| Hot Start | 95°C | 5 min | |
| Denaturation | 95°C | 10 sec | |
| Annealing/Extension | 58°C | 30 sec | 45 cycles |
| Measurement of fuorescence | | | |
| Cooling | 45°C | 15 sec | |

## 2.2.5 Experimental Hepatitis B Virus infection

### 2.2.5.1 Adeno-HBV-X$^-$ (AdHBV-X$^-$) and Adeno-Empty (AdEmpty)

Since HBV cannot infect murine hepatocytes, an adenoviral vector transferring a 1.3-fold overlenght HBV-genome with a deletion in the X-gen (AdHBV-X$^-$), was used in this study to introduce HBV into the mouse liver across the species barrier [213]. As control groups, mice were infected with an empty adenoviral-vector lacking HBV DNA (AdEmpty). Based on the Gateway/AdEasy pENTR system from Invitrogen the replication-competent HBV-genome was inserted into the E1 region of a human adenovirus type 5 genome with deleted E1 and E3 regions (Fig. 7). These deleted regions, which originally encode for the majority of adenoviral genes, lead to degradation of the adenoviral vector upon uptake into hepatocytes, whereas HBV DNA is carried into the cell nucleus via host chaperons. Due to the mutated X-gen, the HB-virus is able to replicate only once in infected liver cells, as no covalently-closed-circular DNA (cccDNA) can be formed (section 1.2.4.2).

In general, application of AdHBV-X$^-$ allows efficient and dose-dependent HBV-replication in various cells of different species [213]. Following HBV-genome transfer, infectious HBV virions are also efficiently produced and secreted by murine hepatocytes *in vivo*. Infection with AdHBV-X$^-$ induces an acute, self-limiting hepatitis B infection in mice, without persistent circulation of adenovirus in the bloodstream [213, 215]. The adenoviral constructs used in this thesis were produced and kindly provided by Prof. Dr. Ulrike Protzer (TU Munich).

| Vector name | Description |
|---|---|
| AdHBV-X$^-$ | Insert of HBV1.3 overlength genome (subtype awy) under the HBV promotor with a premature stop codon in the HBx ORF preventing HBx expression (see Freyend et al. 2011) |
| AdEmpty | No insert |

**Table 5: Overview of Ad vector constructs with their characteristics that were used during this thesis.**

### 2.2.5.2 Intravenous injection (i.v.)

Mice were intravenously injected into the tail vain. Therefore, mice were warmed under a heating light to dilate the veins facilitating injection. The mouse was placed in a mouse holder, the tail was disinfected with 70% ethanol and hold firmly. A 25gauge attached to a syringe was inserted into the lumen of the vein; if no resistance was felt by pushing the plunger, the material (virus (AdHBV-X$^-$ 1x10$^9$ IU/ml) or an empty adenoviral vector lacking HBV (AdEmpty 1x10$^9$ IU/ml)) was injected in a total volume of 100 µl (adjusted by sterile, physiological natrium chlorid solution). Upon retraction of the needle, the tail was disinfected a second time and pressure was applied to the site of injection for 5 seconds to ensure hemostasis.

### 2.2.5.3 Submandibular collection of blood samples

Mice have a small vascular bundle at the back of the jaw where the orbital vein, submandibular vein, and other facial veins join. This area can be punctured to obtain blood with minimal pain or distress. Therefore, to obtain blood samples from the facial vein, mice were hold firmly with the left hand. With the free hand, a 4-5 mm lancet was punctured at the base of the far ear or at the base of the far side of the mouse's mouth. Immediately after, 4-7 drops of blood were collected in small heparinized blood collection tubes and stored at room temperature. Mice were afterwards released into their cages, where bleeding ceases immediately. In general, collection of blood samples with the facial vein technique requires no anesthetic of mice.

### 2.2.5.4 Serological analysis

Collected blood samples (section 2.2.5.3) were centrifuged at 10.000 rpm for 5 min at RT, to obtain the sera. Within serum samples viral antigen levels such as Hepatitis B surface antigen (HBsAg) and Hepatitis B early antigen were measured and quantified in 1:500 dilutions (HBsAg, diluted in 1x PBS) and 1:10 dilutions (HBeAg, diluted in 1x PBS), by using AXSYM$^{TM}$ assays (Abbott Laboratories, Abbott Park, IL,USA).

#### 2.2.5.5 Immunohistochemical detection and quantification of viral antigens

Paraffin-embedded liver tissue samples (section 2.2.4.2.3) were cutted into 3µm tissue sections and were stained with Horseradish-Peroxidase labelled antibodies (Diagnostic Biosystems, Pleasanton, CA, USA) against HBsAg and HBV core antigen (HBcAg) by using the staining kit of BOND-MAX (Leica Biosystems, New Castle, United Kingdom). The staining was performed on a BOND-MAX immunohistochemistry robot (Leica Biosystems) using BOND polymer refine detection solution for DAB. Evaluation and pictures of the stainings were performed on an Olympus BX53 microscope with a Leica SCN400 slide scanner in 10x magnification. Semiquantitative analysis of stained sections was performed by counting localization, intensity, distribution and percentage of positive cell staining throughout the whole tissue specimen using SlidePath TissueIA image analysis software (Leica) [251] on whole tissue sections and normalized to tissue area or hepatocyte number, respectively. Immnuohistochemical detection and quantification of viral antigens was performed in collaboration with Prof. Dr. Mathias Heikenwälder (TU Munich).

#### 2.2.5.6 Quantification of viral DNA

##### 2.2.5.6.1 DNA Isolation

DNA from liver tissue samples (~3x3 mm) was isolated by using the DNeasy Blood & Tissue Kit according to manufacturer's instructions.

##### 2.2.5.6.2 HBV- and Adenovirus specific qPCR

Adenoviral- and HBV genomes were detected in DNA isolated from liver tissue samples (section 2.2.5.6.1) by real-time PCR performed on a Light Cycler$^{TM}$ 480 II (Roche) using the SYBR Green I Master Mix. For absolute quantification of HBV- and adenoviral genomes in murine liver tissue, HBV- and adenoviral DNA was quantified using an external plasmid standard that contained either HBV-or adenoviral DNA sequences. Additionally a relative quantification of viral DNA compared to a murine reference gene (non-coding region located 1345 bp downstream of 3' end of protein kinase C-binding protein NELL1 precursor on chromosome 7) was performed. Samples were prepared as follows:

| *PCR-Mix* | *Volume* |
|---|---|
| LightCycler®480 II Probes Master | 5 µl |
| Forward primer (10µM) | 0.5 µl |
| Reverse primer (10µM) | 0.5 µl |
| DNA template | 2.0 µl |
| DEPC $H_2O$ | 2 µl |

The corresponding primers for the HBV-, adenoviral and murine reference gene specific PCR reaction are depicted in section 2.1.11.4. The running parameters for the PCR reaction are depited below:

| | *Temperature* | *Time* | |
|---|---|---|---|
| Hot Start | 95°C | 5 min | |
| Denaturation | 95°C | 15 sec | |
| Annealing | 60°C | 5 sec | 45 cycles |
| Extension | 72°C | 15 sec | |
| Cooling | 40°C | 30 sec | |

## 2.3 Cell biological methods

### 2.3.1 Preparation of immune cells

#### 2.3.1.1 Preparation of spleen and mesenteric lymph node cells

All mice were euthanized by carbon dioxide inhalation for harvesting of organs. Spleen and mesenteric lymph node (MLN) were removed using scissors and tweezers under sterile conditions. Thereafter, to obtain single cell suspensions, spleen and MLNs were placed in separate petri dishes filled with PBS and crushed with a plunger. The resulting cell suspension was transferred to a 50 ml tube and centrifuged at 230 g for 10 min (4°C). The pellet was re-suspended in 5 ml ACT buffer (section 2.1.9.2) and incubated for approximately 5 min at room temperature to lyse erythrocytes. Immediately after incubation, the cell suspensions were filtered through a 100 µm cell strainer into a new 50 ml tube and washed with PBS. After centrifugation at 230 g for 10 min (4°C), the supernatant was discarded and the cell pellet dissolved in the appropriate buffer or culture medium. Finally, the cells were counted (section 2.3.2.1) and used for cell stimulation assays (section 2.3.3.1) and flow cytometry (section 2.3.4.2).

#### 2.3.1.2 Isolation of liver-associated lymphocytes

Liver-associated lymphocytes (LALs) were prepared after PBS-perfusion of livers. Livers were minced through 100 µm cell strainers and washed with RPMI1640/10% FCS medium. After centrifugation at 300x g for 5 min at 4°C, the cell pellets were re-suspended in 12.5 ml liver digestion solution (section 2.1.9.3) and digested for 20 min at 37°C. The digested liver solutions were afterwards centrifuged at 300x g for 10 min at 4°C and the obtained cell pellets were re-suspended in 3 ml 40% Percoll solution and layered onto 3 ml 80% Percoll separating solution for gradient centrifugation at 300x g for 20 min (RT) without breaks. After gradient centrifugation, hepatocytes were discarded, whereas liver-associated lymphocytes were collected and washed three times in 5 ml RPMI1640. After erythrocyte lysis in 3 ml ACT buffer (section 2.1.9.2) for 3 min, cells were centrifuged (300x g, 5 min, 4°C) to finally obtain the enriched liver-associated lymphocytes, which were re-suspended in cell culture medium (section 2.1.10). Finally, the cells were counted (section 2.3.2.1) and used for cell stimulation assays (section 2.3.3.1) and flow cytometry (section 2.3.4.2).

## 2.3.2 Cell handling

### 2.3.2.1 Cell counting

Cells were counted either manually in a Neubauer hemocytometer or automatically with the Vi-CELL® Cell Viability Analyser (Beckman Coulter). A small aliquot of the cell suspension was added to Trypan blue solution in a dilution 1:10, to further distinguish between dead and viable cells. Total living cells were then counted in 16 quadrants of the grid. The cell titer (cell/ml) of the original suspension was then calculated using the following formula:

*cell/ml = counted cells x dilution factor (Trypan blue dilution) x $10^4$ x $ml^{-1}$*

## 2.3.3 Stimulation of immune cells

### 2.3.3.1 Stimulation of splenocytes and MLN cells

Isolated and counted splenocytes and MLN cells (section 2.3.1.1 and 2.3.2.1) were seeded in a round-bottom 96-well plate at a concentration of 2x$10^5$ cells/ml in a total volume of 200 µl complete medium (section 2.1.10) per well. For *S. mansoni* specific stimulation cells were stimulated with SEA (20µg/ml) (section 2.2.3.2), whereas as positive control cells were stimulated with biotinylated αCD3 and αCD28 coated MicroBeads (Miltenyi Biotec, Germany) in a cell to bead ratio 1:1. Afterwards cells were incubated for 48 hours at 37°C. Culture supernatant (150-175 µl) was collected and stored at –20°C for cytokine measurement by ELISA (section 2.3.3.2).

### 2.3.3.2 Enzyme-Linked ImmunoSorbent Assay (ELISA)

For the measurement of cytokine production in the culture supernatants from stimulated cells (section 2.3.3.1) Ready-Set-Go® ELISAs (Affymetrix) and Duo Set® ELISAs (R&D) were performed according to the manufacturer's instructions. In brief, 96-well ELISA plates were coated with 50 µl/well capture antibody diluted (as indicated by the manufacturer) in coating buffer and incubated overnight at 4°C. Before blocking with 100 µl blocking buffer for 1 hour at room temperature, plates were washed thrice with washing buffer (section 2.1.9.5). After blocking, plates were washed again three times with washing buffer. Samples and serial standard dilutions (highest standard concentration: 2000 pg/ml) were prepared in

blocking buffer and added in 50 µl/well to the antibody-pre-coated plates. Afterwards, plates were incubated for at least 2 hours at room temperature to allow cytokines within the samples to specifically bind to capture antibodies. After three additional washing steps, 50 µl/well of biotinylated detection antibody diluted (as indicated by the manufacturer) in blocking buffer was applied and incubated for a further 1 hour at room temperature. Surplus detection antibodies were then washed away (three times with washing buffer), before adding 50 µl/well of streptavidin-horseradish peroxidase (HRP) conjugate diluted (as indicated by the manufacturer) in blocking buffer. Afterwards, the plates were incubated for 30 min at room temperature in the dark. Following this incubation, plates were washed thrice with washing buffer before adding 50 µl/well of substrate solution (TMB substrate). The occurring enzymatic colour reaction was stopped by adding 50 µl/well of stopping solution (section 2.1.9.5). Immediately after stopping the reaction, the plates were measured at 450 nm using the Sunrise$^{TM}$ ELISA microplate reader. Cytokine concentrations within samples were the calculated according to the standard curve.

## 2.3.4 Flow Cytometry

### 2.3.4.1 Stimulation of LALs and splenocytes for intracellular cytokine staining

LALs (section 2.3.1.2) and splenocytes (section 2.3.1.1) were seeded in a round-bottom 96-well plate at a concentration of $1x10^6$ cells/ml in a total volume of 200 µl complete medium (section 2.1.10) per well. To monitor HBV-specific immune responses, cells were stimulated at 37°C in the presence of 13.5 µg/ml brefeldin A (BFA) for 4.5 hours with a peptide pool derived from an HBV-core-peptide library (HBV core pool 3; concentration of peptide: 2 µg/ml). The HB virus particle is composed of an outer lipid envelope and a nucleocapsid core, which is composed of different peptides, such as the core peptide 3. Each peptide consists of 15 aminoacids and overlaps the next peptide with 4 aminoacids. The core peptide 3 is the most immunogenic peptide and induces virus-specific immune responses. To monitor immune responses raised against the empty adenoviral vector, cells were stimulated with Adeno hexon derived peptide pools (AdH; 8 µM/ml). The HBcP3 as well as the AdH were kindly provided by Prof. Dr. Ulrike Protzer (TU Munich). As positive controls, LALs and

splenocytes were stimulated in the presence of BFA with PMA (50 ng/ml) and Ionomycin (1 µg/ml).

#### 2.3.4.2 Multicolour surface and intracellular cytokine staining

After antigen-specific (HBcP3) and antigen-unspecific stimulation (PMA/Ionomycin) (section 2.3.4.1), cells were centrifuged at 300 x g and 4°C for 5 min. The supernatant was discarded and the cell pellets re-suspended in 50 µL FACS buffer each + ethidium monoazide bromide (EMA, 1:1000) as a marker for discrimination of live/dead cells. The plate was then exposed to light for 10 min on ice to allow EMA staining reaction. Afterwards cells were washed by adding 150 µL FACS buffer and by centrifuging them as described above (2x wash). To avoid undesired antibody-binding by Fc-receptors (e.g. on macrophages), cell pellets were re-suspended in 50 µL Fc-blocking solution (antibody dilutions in FACS buffer see section 2.1.8, table 2.1) and incubated for 20 min in the dark on ice. Afterwards, cells were washed twice in 150 µl FACS buffer as described above. For surface staining, such as CD4 and CD8, cell pellets were re-suspended in 50 µL/well fluorophore-conjugated antibody solution (section 2.1.8, Table 2.1) and incubated for 30 min in the dark on ice. After washing twice cell pellets were re-suspended in 100 µL Cytofix/Cytoperm (BD) each and incubated in the dark at 4°C for 20 min, in order to permeabilize cells for intracellular cytokine staining. After washing with 200 µl 1x Perm/Wash solution (BD), cells were re-suspended in 50 µL/well intracellular antibody solution (intracellular staining antibodies such as e.g. IFN-γ, IL-4, IL-10, IL-2 diluted in 1x Perm/Wash; section 2.1.8, Table 2.1) and incubated for 30 min on ice in the dark. Cells were washed twice in 1x Perm/Wash solution afterwards. At last, the cell pellets were taken up in 250 µL FACS buffer, transferred to FACS tubes and acquired by using the LSRII flow cytometer (Becton Dickinson) equipped with a high-throughput system. Sample analysis was performed using FlowJo version 9.5.3 (Tree Star, Ashland, OR, USA) according to the gating strategy illustrated in Figure 10.

#### 2.3.4.3 Intranuclear Foxp3 staining

To stain Foxp3 (Forkhead box P3), which is the transcription factor and master control gene

for the development and function of regulatory T cells (section 1.1.6), α-mouse Foxp3-FITC, Foxp3-eF450
or Foxp3-PE antibodies (Table 2.1) were used. For intranuclear staining, immune cells were fixed and permeabilized with the Foxp3 staining buffer set from Affymetrix (section 2.1.6). Therefore, CD4 stained cells (section 2.3.4.2) were centrifuged at 300 g for 5 min (4°C) and re-suspended in 100 µl fixation/permeabilization working solution (Affymetrix) before incubating them for 30 min at 4°C in the dark. Afterwards cells were washed twice with 200 µl 1x Perm/Wash buffer (Affymetrix) and re-suspended in either 50 µl FITC or PE conjugated Foxp3 antibodies, diluted in permeabilization buffer. An incubation period of 30 min at 4°C in the dark followed. After washing twice, stained cells were re-suspended in 250 µl FACS buffer and acquired with the previously described FACS scan (section 2.3.4.2). Data analysis was done using FlowJo (section 2.3.4.2).

## 2.4 Human *S. mansoni* and Hepatitis C co-infection study

### 2.4.1 Study subjects and collection of cell samples

In collaboration with the Hepatology Outpatient Clinic of Cairo University Hospital in Egypt in 2009, chronic hepatitis C patients were recruited and further classified into HCV mono-infected (n = 15 – HCV) or co-infected with *S. mansoni* (n = 16 – Sm/HCV). Schistosome infection was diagnosed on the presence of *S. mansoni* eggs within the stool with the Kato-Katz method and/or the presence of high titres of schistosomal antibodies (>1/640) against adult worms (Fumouze Diagnostics, Levallois-Perret, France). The study protocol was in accordance with the ethical guidelines of the 1975 Declaration of Helsinki, and ethical clearance was given by the Scientific Research Ethics Committee at the Faculty of Medicine, Cairo University in Egypt and by the Ethics Commission of the Faculty of Medicine at the Technischen Universität München (TUM) in Germany. Patients exhibiting other viral hepatic infections, hepatic cirrhosis, prolonged partial prothrombin time (PPT) and hepatocellular carcinoma were excluded, as well as other intestinal parasitic infections diagnosed by sodium-acetate-formalin (SAF) enrichment method and microscopy. As the areas of patient recruitment in Egypt are considered malaria free, individuals were not tested for malaria. Peripheral blood mononuclear cells (PBMC) were isolated immediately after the collection of fresh heparinized blood using Ficoll-Hypaque density gradient centrifugation. Cell samples

were subsequently cryopreserved in 10% DMSO (dimethyl sulphoxide) and 90% fetal calf serum (Sigma Chemicals, Hamburg, Germany; PAA Laboratories Inc., Cölbe, Germany) at - 80°C and shipped to Germany on dry ice. Before shipping, HCV viral loads in plasma were quantified using real-time PCR [252]. Further blood analysis of all study participants included routine laboratory tests such as liver enzymes AST, ALT and AFP (Reflovet Plus Reader, Roche, Penzberg, Germany), kidney function and coagulation tests, and a blood count. For comparison, further samples were collected from age-matched, infection-free volunteers, which were mainly relatives of the patient cohort and resided therefore in the same endemic area (n = 13). They are denoted in this study as 'healthy donors' (HD).

## 2.4.2 Multicolour surface and intracellular staining of human PBMCs

### 2.4.2.1 Thawing of cells

The freezing medium contains DMSO, which is toxic for cells after extended amounts of exposure at warm temperatures. Therefore, frozen cells were rapidly thawed by warming the cryotube between the hands and immediately after thawing added to 50 ml of warmed complete medium (section 2.1.10). After centrifugation at 230 g for 10min (4°C), the supernatant was discarded, the pellet re-suspended in 20 ml complete medium and centrifuged once again. After centrifugation the pellet was re-suspended in the appropriate buffer or culture medium and counted (section 2.3.2.1). Cells were then used for flow cytometry (section 2.3.6).

### 2.4.2.2 Multicolour surface and intracellular staining

Phenotypic and functional characteristics of regulatory and effector T-cell subsets were investigated using multicolour surface and intracellular stainings based on flow cytometry technology. The following staining panel was designed in order to characterize Treg and T effector cells: CD8 AmCyAn, CD127 PE, Granzyme B FITC (Becton Dickinson, Heidelberg, Germany), CD3 APC-A750, CD25 PE-Cy7 (Beckmann Coulter, Krefeld, Germany), CD103 PE-Cy5, Foxp3 PB, Helios FITC (BioLegend, San Diego, CA, USA) and CD4 A700 (Affymetrix, Vienna, Austria). Dilutions of human antibodies are depicted in section 2.8.1, Table 2. Viability was assessed by addition of ethidium monoazide ([EMA], Molecular

Probes/Invitrogen, Karlsruhe, Germany) and did not differ between patient groups (average mean of viable cells in % ± SD: HD 76.6% ± 11.7%; Sm/ HCV: 77.3% ± 14.1%; HCV: 74.0% ± 16.2%). In short, following surface staining (section 2.3.4.2), PBMCs were fixed and permeabilized for 20 min at 4°C in 100 µL fixation/permeabilization working solution using the Foxp3 staining buffer set (section 2.3.4.3). After washing, cells were re-suspended in permeabilization buffer containing antihuman antibodies specific to intracellular, such as Granzyme B, (section 2.8.1, Table 2.1) and intranuclear proteins, such as Foxp3 and Helios (section 2.8.1, Table 2.1) for 30 min at 4°C. Cell acquisition was performed using the LSRII flow cytometer. Sample analysis was performed using FlowJo version 9.5.3.

### 2.4.3 Serum cytokine detection

Levels of IL-6 and IL-8 were measured in individual plasma samples using the human Th1/Th2/Th8/Th17/Th22 13plex Kit FlowCytomix according to manufacturer's instructions (Affymetrix) (section 2.1.6). Acquisition of the multiplex immunoassay was performed using the LSRII flow cytometer. Sample analysis was performed with Flowcytomix$^{TM}$ Pro 3.0 Software (Affymetrix).

### 2.4.4 Statistical analysis

All statistical tests were performed with PRISM® 5.01 (Graph- Pad Software Inc., San Diego, CA, USA). D'Agostino and Pearson omnibus normality tests were performed, and parametrically distributed data were analysed with unpaired t-test (2 groups) and Mann-Whitney U-test was used for nonparametric data. For more than two groups, 1-way ANOVA test was conducted and if data were nonparametric, a Kruskal–Wallis test with a confidence interval of 95% was employed. Results with a *P* value of <0.05 were considered as significant and *P* values <0.01 as highly significant.

# 3 Results

## 3.1 Human *Schistosoma mansoni* and hepatitis C virus co-infection

Schistosome infections are renowned for their ability to induce regulatory networks such as regulatory T cells that control immune responses against homologous and heterologous antigens such as allergies. However, in the case of co-infection with hepatitis C virus, schistosomes seems to accentuate disease progression, as liver cirrhosis and hepatocellular carcinoma are more common within co-infected individuals. Since the underlying mechanisms leading to such liver disease aggravation are still not understood, we hypothesized that expanding Treg populations, known to be induced during schistosome infection, aquire a phenotype that suppress beneficial anti- HCV responses. Impaired antiviral immune responses would then lead to loss of viral replication control and eventually to a more pronounced liver disease. To address our hypotheses, we designed in collaboration with the Hepatology Outpatient Clinic of Cairo University Hospital in Egypt a study in which we analysed the liver pathology and viral load as well as effector T cells and n/iTreg subsets in patients with HCV mono-infection (HCV) and schistosome-co-infection (*Sm*/HCV). Infection-free, age-matched individuals from the same endemic area were used as control groups (HD = healthy donors). The study was published in the journal *Parasite Immunology* in February this year, and is reproduced in this thesis with permission from John Wiley and Sons [253].

### 3.1.1 Schistosome infection aggravates HCV-related liver disease and induces changes in the regulatory T-cell phenotype

#### 3.1.1.1 Co-infected patients present higher viral load and stronger liver pathology

To determine whether co-infected individuals indeed display an aggravated liver disease, patients were recruited based on the following parameters: viral titers, liver transaminases levels, ultrasonography and schistosoma infection. Within the three different groups, the base-line characteristics such as age, gender and body mass index (BMI) were similar (Table 6). Basic haematological parameters such as complete blood count, coagulation rates and partial thromboplastin time (PTT) were all comparable as well (data not shown). *S. mansoni*

eggs and specific antibodies were only detected in the *Sm*/HCV groups (Table 6). The percentage of lymphocytes was also comparable between the groups (Table 6). Liver function was assessed by measurement of total bilirubin, alpha fetoprotein (AFP) and liver transaminases (AST/ALT) in plasma. Whereas levels of the total bilirubin and AFP did not significantly differ between the groups (Table 6), both ALT (Figure 8a) and AST (Figure 8b) levels were significantly higher in the *Sm*/HCV group. Furthermore, HCV-RNA titers were also significantly higher in the co-infected patient group (Figure 8c) indicating that this cohort had an aggravated disease state.

| | **Healthy Donors (HD)** | ***S. mansoni*-HCV co-infected patients (*Sm*/HCV)** | **HCV mono-infected patients (HCV)** |
|---|---|---|---|
| **Number** (Male: Female) | 13 (8:5) | 16 (10:6) | 15 (8:7) |
| **Age, years** | 37.0 ± 8,9 | 40,5 ± 7,9 | 40.5 ± 9,7 |
| **Body mass index** | 25.5 ± 3,9 | 26.7 ± 2,9 | 26,6 ± 3,6 |
| **Total Bilirubin** | 0.7 ± 0.2 | 0.8 ± 0.4 | 0.7 ± 0.2 |
| **AFP** (U/ml) | n.d. | 5,2 ± 5,2 | 6,7 ± 3,8 |
| **Lymphocytes** (%) | 40,7 ± 8,7 | 44.7 ± 10.1 | 51,4 ± 14,6 |
| **Stool (Kato Katz)** | 0/13 | 8/16 | 0/15 |
| **Schistosome mAb** | 0/13 | 16/16 | 0/15 |

**Table 6: Baseline characteristics of healthy donors, *Schistosoma mansoni*/HCV co-infected and HCV mono-infected patients.** Gender, age and body mass index (BMI) of healthy donors (HD, n = 13), *S. mansoni* and HCV co-infected (*Sm*/HCV, n = 16) and HCV mono-infected (HCV, n = 15) are shown. Liver damage was evaluated by measuring levels of total bilirubin and alpha fetoprotein (AFP). Schistosome infection was diagnosed by counting *S. mansoni* eggs/g stool and the detection of antischistosomal antibodies (schistosome mAb) within plasma. Percentages of total leucocytes are indicated for each patient as lymphocytes %. Data are shown as mean ± SD; n.d., not determined [253].

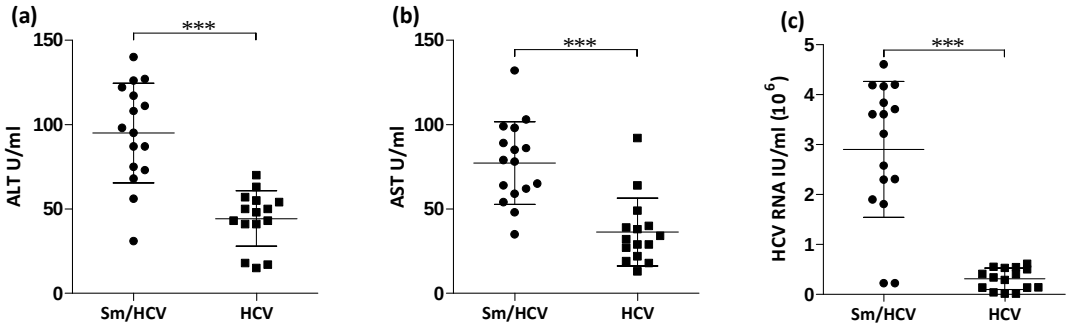


**Figure 8: Elevated HCV-RNA and liver transaminases (ALT/AST) in the plasma of Schistosoma/HCV-co-infected patients.** To determine the extent of liver damage between HCV mono-infected and S. mansoni/HCV (*Sm*/HCV) co-infected individuals, liver transaminases (a) ALT and (b) AST were measured in plasma. (c) HCV-RNA levels were ascertained by real-time PCR. Symbols show individual measurements within the patient groups and graphs show mean ± SD. Asterisks show statistical differences (Student's t-test (c) or Mann– Whitney U-test (a, b)) between the groups indicated by the brackets (***$P < 0.001$) [253].

### 3.1.1.2 Co-infected and HCV mono-infected patients present higher levels of circulating IL-8 when compared to healthy individuals

To analyse whether the differential outcomes of liver inflammation between HCV mono-infected and schistosome co-infected individuals might result from the exposure to a more inflammatory environment, we analysed the cytokine milieu within plasma by using a multiplex cytokine assay (section 2.4.3). Figure 9a shows that in comparison to HD, *Sm*/HCV co-infected and HCV mono-infected individuals had significantly higher levels of circulating IL-8. No differences between the two HCV-infected groups could be determined. Some HCV-infected individuals did, however, present high amounts of IL-6 (Figure 9b). No differences were found in IL-12p70, IFN-$\gamma$, IL-17A, IL-2, IL-10, IL-22, IL-13, IL-4, IL-1$\beta$, TNF$\alpha$ and IL-5 (data not shown).

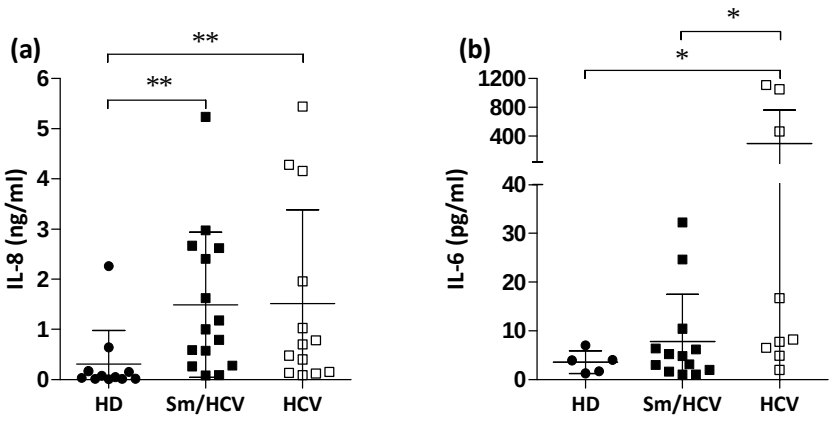


**Figure 9: HCV infected patients produce more IL-8 and IL-6 than healthy individuals.**
(a) IL-8 and (b) IL-6 levels in individual infection-free volunteers (HD), HCV and Sm/HCV were analysed in the plasma with a multiplex cytokine assay. Symbols show individual data and graphs depict mean ± SEM. Statistical significances between the indicated groups were obtained after Kruskal–Wallis test and Mann-Whitney U-test (*$P < 0.05$; **$P < 0.01$). Taken from [253].

### 3.1.1.3 Frequency of effector $CD4^+$ and $CD8^+$ T cells is increased in infected patients, whereas the distribution of GrzB-producing $CD4^+$ and $CD8^+$ effector T cells is not altered

Since aggravation of liver disease in HCV infection is associated with decreased effector T cell function, we first analysed alterations in the frequency of $CD4^+$ and $CD8^+$ T effector cells. For that, PBMCs from individuals in all three groups were analysed using a 9-colour ICS assay Teff/Treg panel (section 2.4.2.2). As effector T cells do not express the Treg-specific transcription factor Foxp3, frequencies of total $CD4^+$ and $CD8^+$ T-cell populations were defined using the marker combination $CD4^+Foxp3^-$ and $CD8^+Foxp3^-$. The portion of the different leukocyte subtypes, such as $CD4^+$, $CD8^+$ T effector cells, Treg and n/iTreg was evaluated according to the gating strategy in Figure 10.

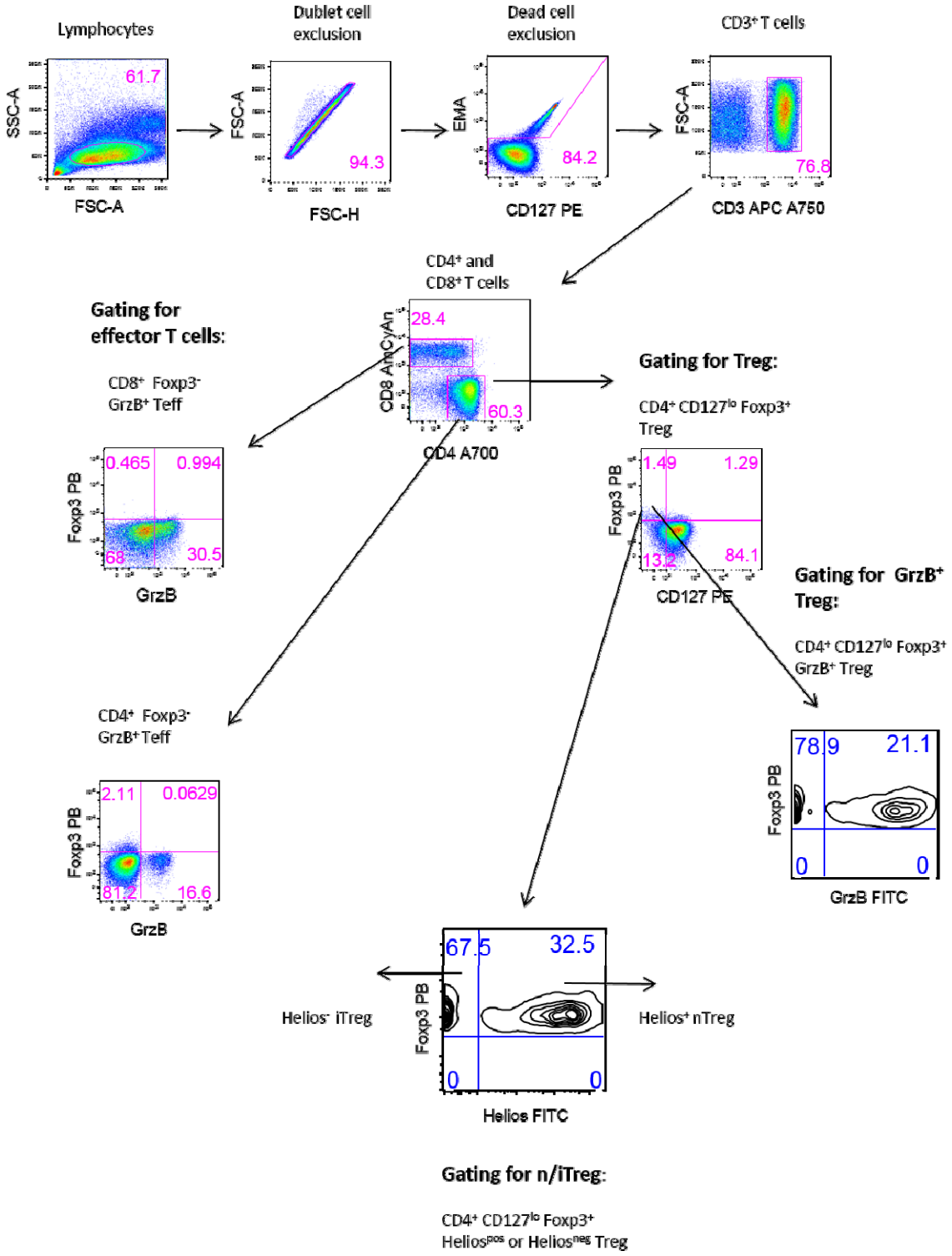


**Figure 10: Gating strategy for flow cytometric analysis of lymphocyte populations in peripheral blood mononucleated cells based on multi-parameter staining panels.** Analysis covered markers for T cells (CD4, CD8, GrzB) and Treg cells (CD4, CD127, Foxp3, Helios, GrzB). Frequencies of distinct cell subsets were analysed within PBMCs by Flow Cytometry using the LSRII cytometer (BD). Acquisition was done with 100.000 – 500.000 cells. The gating strategy is shown on PBMCs of a healthy donor.

As shown in Figure 11a and 11b, the frequency of $CD4^+Foxp3^-$ and $CD8^+Foxp3^-$ T effector cells was significantly higher in both HCV-infected cohorts when compared to HD. Viral infections are known to induce both $CD4^+$ and $CD8^+$ immune responses, and as the majority of $CD8^+$ effector T cells produce the serine protease Granzyme B, the prevalence of these effector T-cell populations was further assessed by staining GrzB intracellularly (Figure 11c, d). Since frequencies of GrzB-producing $CD8^+Foxp3^-$ and $CD4^+Foxp3^-$ effector T cells were not altered within the different groups (Figure 11c, d, respectively), we asked whether the production of the serine protease differs. The mean fluorescence intensity (MFI) of GrzB, however, was again similar between the three different study groups (data not shown).

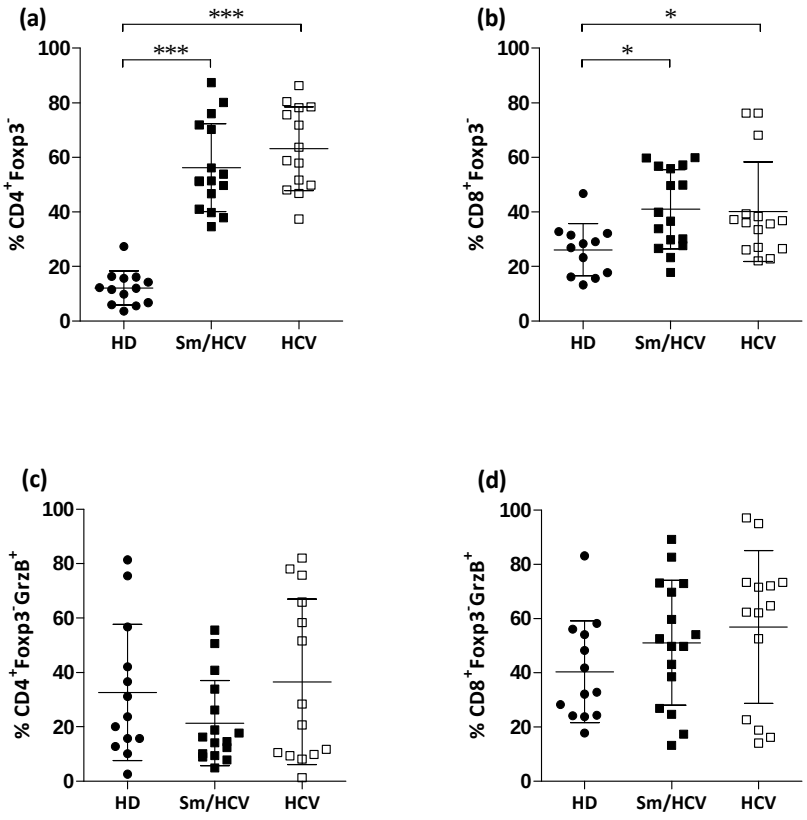


**Figure 11: Frequency of effector $CD4^+$ T and $CD8^+$ T cells is increased within HCV-infected patients.** Frequencies of T-cell subsets were analysed within PBMCs using a 9-colour ICS assay 'Teff' panel. Frequency of (a) $CD4^+Foxp3^-$ T cells and (b) $CD8^+Foxp3^-$ T cells in all three groups. The function of effector T cell populations was further assessed by determining the frequencies of (c) $CD4^+Foxp3^-GrzB^+$ and $CD8^+Foxp3^-GrzB^+$ T cells (d). Symbols show individual T cell frequencies, and graphs show data as mean ± SD. Statistical significances between the indicated groups were calculated using ANOVA (a, b, c) and Kruskal– Wallis test (d) (*$P < 0.05$, ***$P < 0.001$). Taken from [253].

### 3.1.1.4 nTreg/iTreg ratio is altered in HCV-infected patients but only *Sm*/HCV co-infected individuals display increased frequencies of GrzB-producing $CD4^+CD127^{lo}Foxp3^+$ Treg

As we have shown previously that during murine *S. mansoni* infection $Foxp3^+$ Treg increase homeostatically with effector T cell populations [77, 78] and moreover that GrzB is upregulated in Treg from schistosome-infected mice, we investigated whether this is the case in human schistosomiasis as well. To characterize Treg in PBMCs from all three groups of individuals, we defined this cell subset using the marker combination: $CD4^+$ $CD127^{lo}$ $Foxp3^+$ (see gating strategy Figure 10). The Treg phenotype was then expanded upon by additionally analyzing intracellular expression of GrzB or Helios, which allows the discrimination between nTreg and infection-induced iTreg (see Figure 10 and section 1.1.6) [88]. As shown in Figure 12a, the frequency of $CD4^+CD127^{lo}Foxp3^+$ Treg was comparable between the three groups. However, upon further characterization of the Treg phenotype using the novel marker Helios, we detected significantly higher frequencies of $CD4^+CD127^{lo}Foxp3^+Helios^{pos}$ Treg within the HCV mono-infected group when compared to HD (Figure 12b). This phenotype was further reflected in the frequency of $CD4^+CD127^{lo}Foxp3^+Helios^{neg}$ cells as this population was significantly reduced in the HCV mono-infected group compared to HD individuals (Figure 12c). However, levels of $CD4^+CD127^{lo}Foxp3^+$GrzB-producing Treg within the *Sm*/HCV group were significantly increased when compared to both the HCV mono-infected individuals and HD (Figure 12d). The MFI of GrzB, however, was again similar in Tregs of the three different study groups, showing that frequencies of GrzB-producing Treg expand per se, but do not produce more GrzB (data not shown).

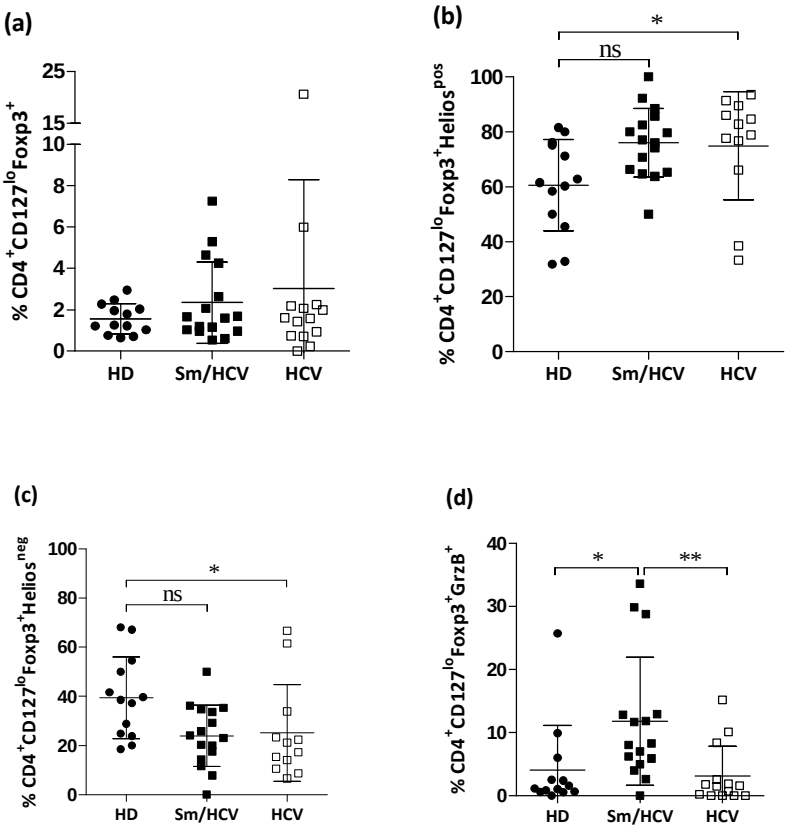


**Figure 12: Pronounced increase of CD4$^+$CD127$^{lo}$Foxp3$^+$GrzB$^+$ Treg in *Sm*/HCV-infected individuals.** (a) The frequency of CD4$^+$CD127$^{lo}$Foxp3$^+$ Treg was determined in all three groups. Treg subsets were then further differentiated into CD4$^+$CD127$^{lo}$Foxp3$^+$Helios$^{pos}$ (b) and CD4$^+$CD127$^{lo}$Foxp3$^+$Helios$^{neg}$ (c). The Treg phenotype was further analysed using the marker combination CD4$^+$CD127$^{lo}$Foxp3$^+$GrzB$^+$ within PBMCs of individual donors (d). Symbols show T cell frequencies of each individual, and data are displayed as mean ± SD. Statistical significances between the indicated groups were obtained after Kruskal–Wallis test and Mann–Whitney U-test (*$P$ < 0.05 and **$P$ < 0.01). Taken from [253].

Taken together, this study shows that in HCV co-infected individuals the additional schistosome infection indeed aggravates the liver disease and inhibits virus elimination, since stronger liver pathology and higher viral loads were observed in the *Sm*/HCV group. According to our data, a potential regulatory scenario is that schistosome-induced Treg have an influence on the effector T cell populations by acting directly on virus-specific effector T cells via GrzB.

## 3.2 *Schistosoma mansoni* and hepatitis B virus co-infection in mice

As mentioned in the introduction (section 1.2), one of the main complications of hepatitis B and C virus infection is the development of chronic hepatitis after an acute infection, since these individuals are at high risk to develop liver cirrhosis and hepatocellular carcinoma. Interestingly, chronic hepatitis B and C develop at a higher frequency in developing countries in which co-infections with helminths, such as *S. mansoni* are common. In co-infected individuals, dynamic schistosome driven immune responses range from an initial $T_H1$- to $T_H2$- and eventually long-term immunosuppression, and might influence the establishment of an effective anti-viral immune response in a phase-dependent manner. Thus, the effects of pre-existing helminth infections on concomitant HBV/HCV infection are hard to predict and need clarification.

Therefore, to further corroborate our findings in humans and to expand on underlying mechanisms of interactions between hepatitis virus infections and schistosomiasis, we experimentally investigated, with the help of the AdHBV-$X^-$ mouse model, the outcomes of an acute HBV infection acquired during the different immune phases ($T_H1$, $T_H2$, chronic) induced during *S. mansoni* infection. So far, murine HCV infections can only be analysed in T- and B cell deficient mice with human chimeric livers, where the liver is repopulated with human hepatocytes. Since these animals lack an adaptive immune system, the establishment of an anti-viral immune response and the resulting viral clearance can't be investigated [254, 255]. Consequently, to study the establishment of virus-specific immune responses in the presence of a concomitant schistosome infection, we switched to a fully immuno-competent mouse model where an acute HBV infection can be established via adenoviral genome transfer (AdHBV-$X^-$ mouse model, see section 1.2.4). This helped to address the question whether an existing helminth infection drives an acute HBV infection towards chronicity. On the other hand, the impact of a secondary acquired schistosome infection on top of a pre-existing chronic HBV infection was investigated by the use of the HBV transgenic mouse model.

## 3.2.1 Immune response during *S. mansoni* infection

### 3.2.1.1 *S. mansoni*- specific cytokine profile in C57BL/6 mice

Even though the dynamics of immune responses in ongoing schistosome infection are already described in the literature [3], in this study we re-evaluated the course of infection in C57BL/6 mice, since differences in mouse and helminth strains as well as animal housing conditions have to be considered. The re-evaluation of immune responses in *S. mansoni* infected C57BL/6 mice allowed us furthermore to clearly characterize time frames of the immune phases induced during infection ($T_H1$, $T_H2$ phases). This in turn enabled us to accurately study the outcome of the additional acute HBV infection during these distinct immune phases. As shown in Figure 13, SEA-specific immune responses start to be detectable after the first 4 weeks of infection and were determined until the 22nd week post infection. Initial IFN-γ release (designated as "$T_H1$ phase") from SEA-restimulated splenocytes was successively replaced by $T_H2$ cytokines such as IL-4, IL-5, IL-13 and IL-10 (designated as "$T_H2$ phase") 7.5 to 8 weeks post infection. Interestingly, 16 and 22 weeks post schistosome infection, apart from increased levels of the predominant cytokine IL-10, rising IFN-γ levels were detected again in SEA-re-stimulated splenocytes. This may be attributed to the general $T_H1$-prone phenotype of C57BL/6 mice.

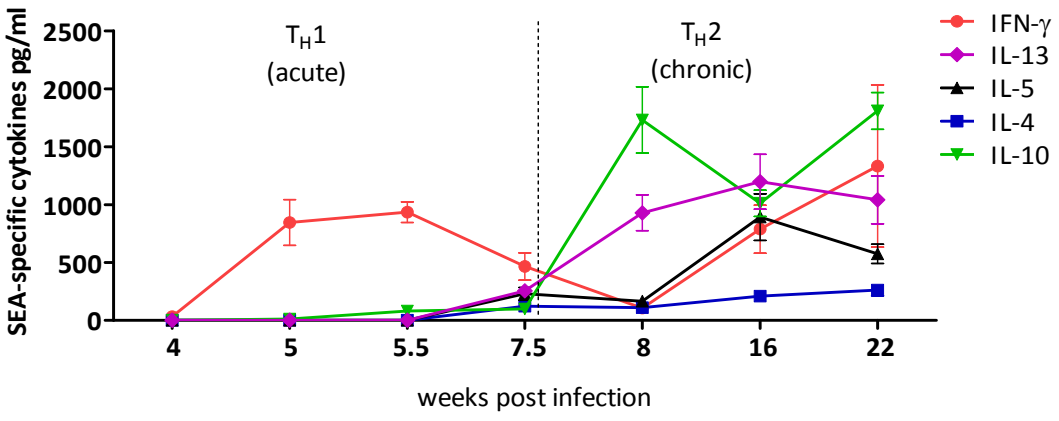


**Figure 13: Induction and development of $T_H1$- and $T_H2$ immune responses during *S. mansoni* infection in C57BL/6 mice.** Splenocytes from *S. mansoni* infected mice ($2x10^5$ cells/ml) were re-stimulated with SEA (20 µg/ml) at 4, 5, 5.5, 7.5, 8, 16 and 22 weeks post-infection. IL-5, IL-4, IL-10, IL-13 and IFN-γ were measured in the supernatant 48 hours after culture by ELISA. A minimum of three mice were analysed at each time point. Results are shown as mean ± SEM.

These results constitute the basis for all further HBV co-infection experiments in which the "$T_H1$ phase" corresponds to 5, the "$T_H2$ phase" to 8 and the "chronic phase" to 17 weeks of schistosome infection.

Besides systemic schistosome-specific immune responses we additionally monitored immunohistochemically (see section 2.2.4.2.3.1) the formation of $CD4^+$ T cell-mediated granulomas, which stem from inflammatory responses around schistosome eggs trapped in the liver or intestine (section 1.1.3 and 1.1.5). The granuloma formation and size were evaluated microscopically and the results are shown in Figure 14.

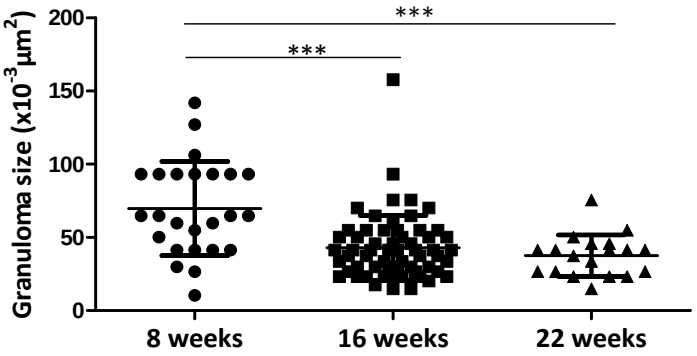


**Figure 14: Granuloma sizes shrink throughout the course of infection.** *S. mansoni* infected mice were sacrificed 8 (n = 5), 16 (n = 5) and 22 (n = 3) weeks post infection and left liver lobes from individually infected mice were fixed and embedded in paraffin. Thereafter, 3µm sections were fixed on glass slides for Masson`s blue staining and microscopically assessed (x10 magnification) to calculate the average granuloma size per mouse. 30-40 granulomas per section from each infected mouse were analysed. The results are shown as mean ± SD and asterisks show significant differences between brackets *** $P < 0.001$.

The assessment of liver immunopathology showed that throughout the course of infection granuloma sizes shrink (Figure 14) and become more fibrogenic (Figure 15), since the largest granulomas with the lowest amount of collagen were observed 8 weeks post schistosome infection (Figure 14 and 15).

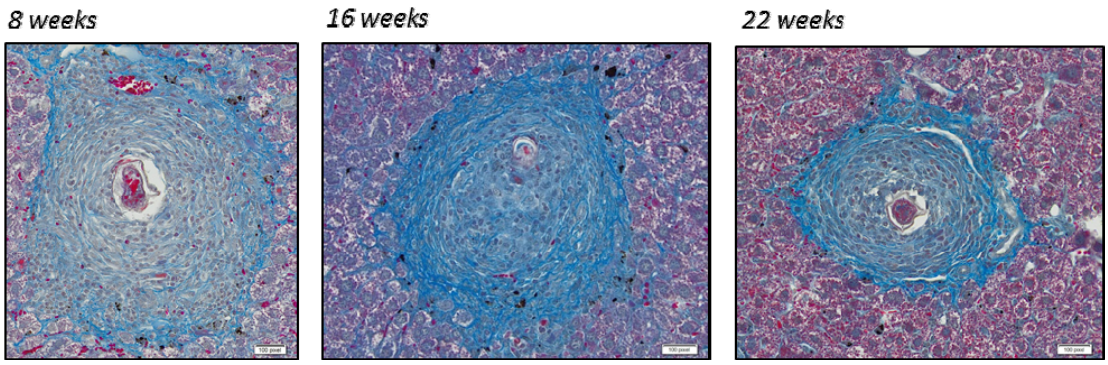


**Figure 15: Granuloma size become smaller and more fibrogenic throughout the course of infection.** Fibrotic tissue can be detected by staining tissue sections with Masson's blue, since collagen fibers turn blue during the staining procedure. For that, *S. mansoni* infected mice were sacrificed 8 (n = 5), 16 (n = 5) and 22 (n = 3) weeks post infection and left liver lobes from individually infected mice were fixed and embedded in paraffin. Thereafter, 3µm sections were fixed on glass slides for Masson`s blue staining and microscopically assessed (scale: 100 pixels).

### 3.2.2 Impact of distinct immune phases induced during *S. mansoni* infection on the outcome of a secondary acquired, acute HBV infection

Important issues to address in concurrent HBV and schistosome infection are for example the establishment of HBV infection, the contribution of innate and adaptive immune responses in the early phase of infection for viral clearance and persistence and the influence of both pathogens on the disease outcome. With the help of an adenoviral HBV genome transfer, we investigated the outcomes of an acute HBV infection acquired during the different immune phases ($T_H1$, $T_H2$, chronic) of *S. mansoni* infection. Additionally we addressed the question whether an already existing helminth infection drives an acute HBV infection towards chronicity.

#### 3.2.2.1 Outcome of secondary acquired, acute HBV infection during the $T_H1$ phase of *S. mansoni* infection

The outcome of a secondary acquired acute HBV infection during the acute phase of *S. mansoni* infection was analysed by infecting C57BL/6 mice with *S. mansoni* cercariae before infecting them intravenously with an adenoviral vector containing HBV DNA

(AdHBV $X^-$, section 2.2.5.1), 4 (early phase of acute *S. mansoni* infection) or 5 (proper $T_H1$ phase) weeks post schistosome infection. The detailed experimental protocol is described in section 2.2.4.1.2.

#### 3.2.2.1.1 Schistosome infected animals can be equally infected with HBV at an early stage of helminth infection

To analyse the development of HBV infection during the early phase of acute schistosome infection, mice were infected with AdHBV-$X^-$ 4 weeks post helminth infection, where IFN-$\gamma$ production is only instigated (see *S. mansoni* kinetic, section 3.2.1.1). Post viral infection, successful HBV infection and ongoing viral clearance were monitored by bleeding mice at day 3, 7, 14 and 21, followed by measuring viral antigen levels such as HBsAg and HBeAg, within mice sera (Figure 16). Furthermore, at the day of final analysis (21 days post viral infection) schistosome infection was confirmed in all mice by detection of parasite eggs and granuloma formation in the liver (see section 3.2.3.1, Figure 38). As depicted in Figure 16a and b, between co-infected (S.m./HBV) and HBV mono-infected (HBV) animals no differences in viral antigen levels were detected three days post viral infection. Additionally, throughout the course of HBV infection, viral antigen levels remained unaltered (Figure 16c and d).

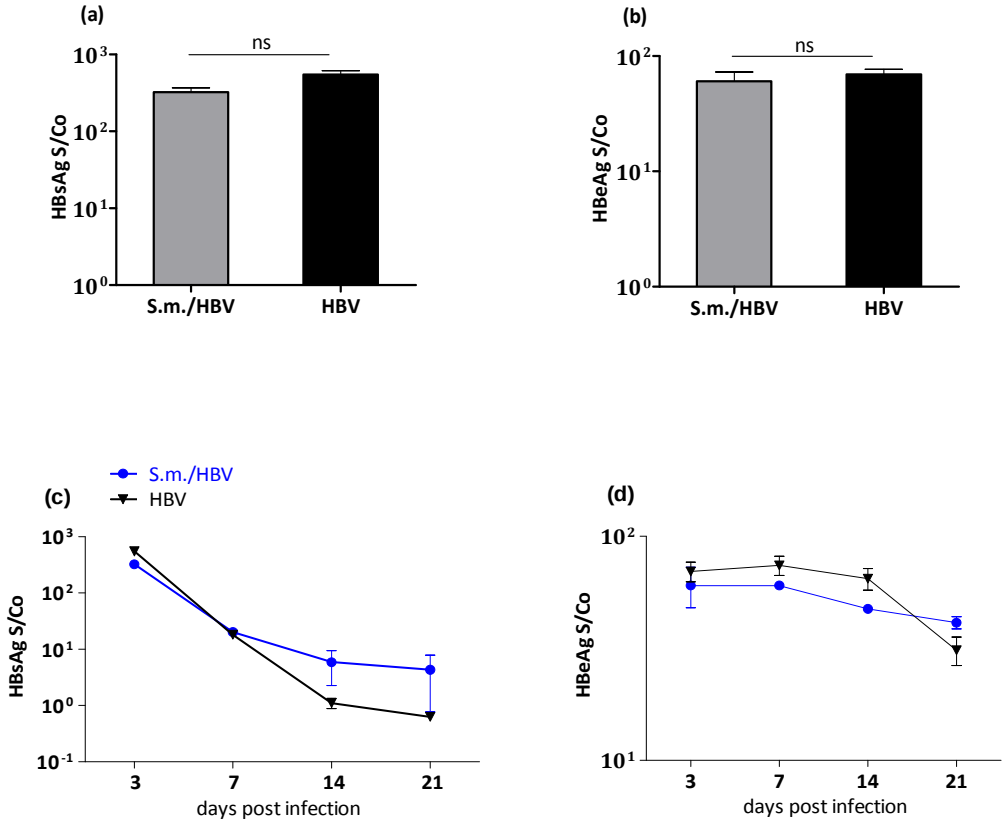


**Figure 16: No differences in viral antigen levels between co-infected and HBV mono-infected animals.** Qualitative detection of viral antigens in mice sera was performed with a microparticle enzyme assay (Abbott Axsym System) and is shown as ratio of fluorescent product formation rate of the sample (S) to cutoff rate (Co). (a) Levels of HBsAg and (b) HbeAg within S.m./HBV co-infected and HBV mono-infected mice 3 days post viral infection. (c) Fluctuations of HBsAg and (d) HbeAg levels throughout the course of HBV infection in sera of co-infected and HBV mono-infected mice. A minimum of three mice were analysed at each time point. Data is shown as mean ± SEM (a,b) and mean and error ± SEM (c,d). Statistical evaluation was calculated using the Mann-Whitney U-test for nonparametric distributed data (n.s, not significant).

Adenoviral- and HBV genomes were detected by real-time PCR in DNA isolated from liver tissue samples of co-infected and HBV mono-infected mice (see section 2.2.5.6). The relative quantification of viral DNA was performed in comparison to a murine non-coding region located 1345 bp downstream of the 3' end of the protein kinase C-binding protein NELL1 precursor on chromosome 7 (= reference gene) and is displayed in Figure 17 as target (viral DNA) to reference (reference gene) ratio (Tgt/Ref).

As shown in Figure 17, three days post viral infection the amount of HBV genomes was equal in both animal groups and did not change in *S. mansoni* co-infected animals upon 3 weeks of

viral infection. HBV mono-infected mice, however, displayed a tendency towards elevated HBV genomes 3 weeks post viral infection. These results indicate that while both animal groups can be equally infected with the virus, later during the course of infection, HBV replication seems to be suppressed in the schistosome co-infected animal group. Of note, the amount of adenoviral genomes did not differ between both animal groups, indicating that an equal amount of adenoviral vectors carrying HBV DNA arrives into hepatocyte nuclei.

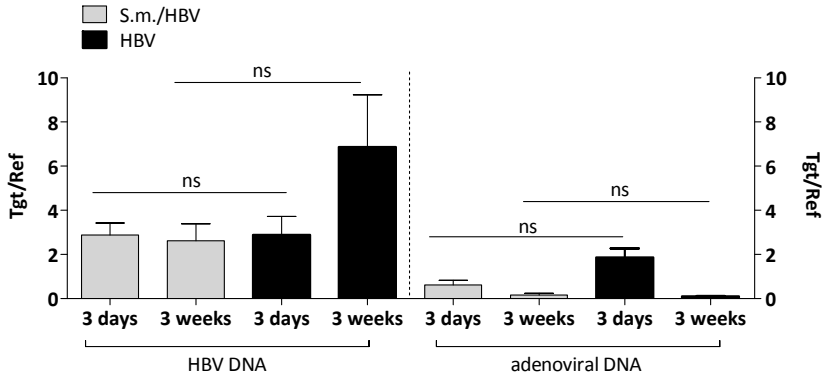


**Figure 17: Amount of HBV- and adenoviral DNA is not altered within co-infected and HBV mono-infected livers at an early timepoint during co-infection.** Adenoviral- and HBV genomes were detected in DNA isolated from liver tissue samples by real-time PCR performed on a Light Cycler™ 480 II. The relative quantification of viral DNA compared to the murine reference gene (Tgt/Ref) is shown in co-infected and HBV mono-infected livers 3 days and 3 weeks post viral infection. A minimum of three mice were analysed at each time point. Bar graphs show data as mean ± SEM. Statistical evaluation between the indicated groups was performed by using the Mann-Whitney U-test for nonparametric distributed data (n.s, not significant).

The extend of HBV infection in livers of both animal groups was additionally investigated with an immunhistochemical technique (see section 2.2.4.2.3), where the localization and quantity of the virus was determined in paraffin-embedded liver tissue samples 3 days and 3 weeks post viral infection. Livers of naïve mice were used as a negative control for the specificity of the staining. For this purpose, 3µm tissue sections were stained with antibodies against HBsAg and Hepatitis B core antigen (HBcAg) (see section 2.2.5.5). Three days post viral infection, equal amounts of positively HBsAg- and HBcAg-stained liver cells were detected in livers of co-infected and HBV mono-infected mice (Figure 18a, b, e, f). Three weeks post HBV infection, however, schistosome-induced granuloma formation and only some hepatocytes positively stained for HBsAg (Figure 18c) and HBcAg (Figure 18g) were

detected in livers of co-infected mice. In comparison, many more HBsAg (Figure 18d) and core antigen (Figure 18h) stained hepatocytes were found in livers of HBV mono-infected animals.

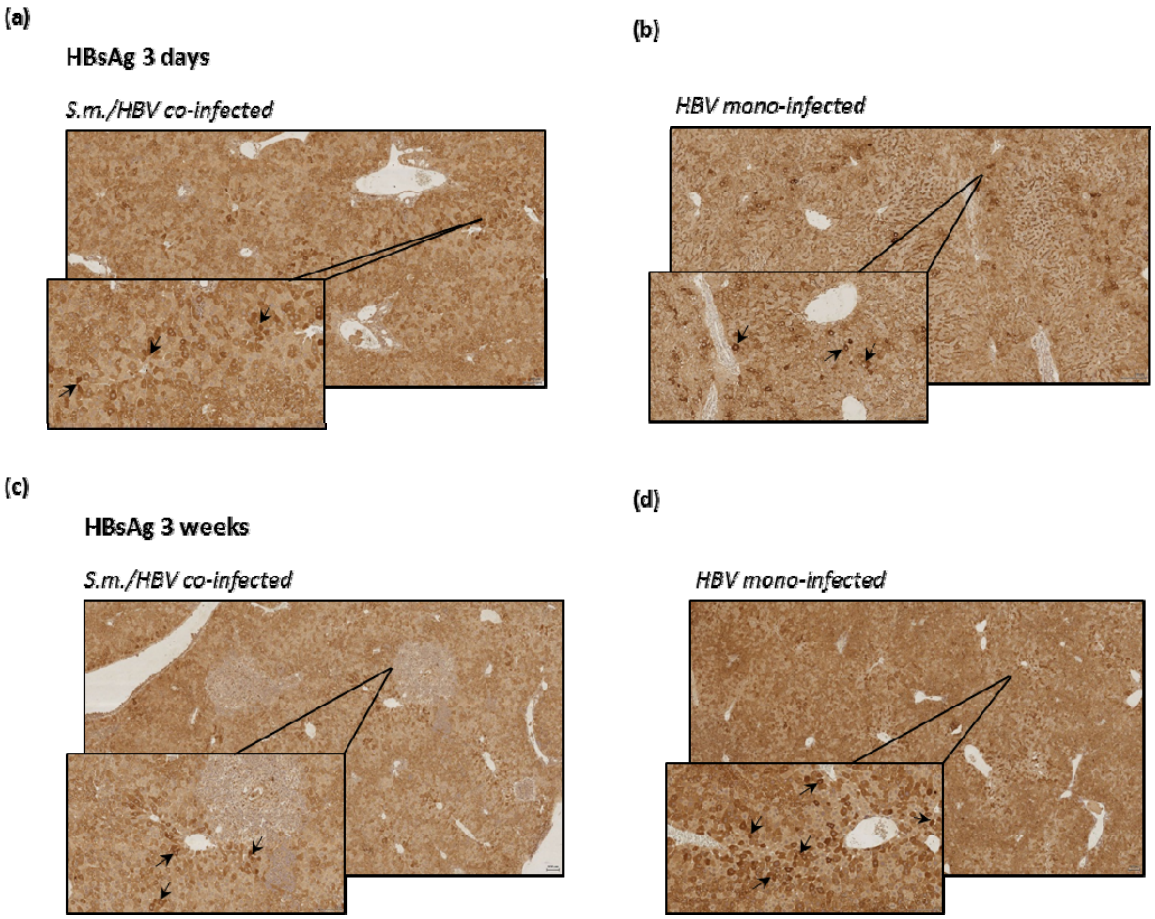

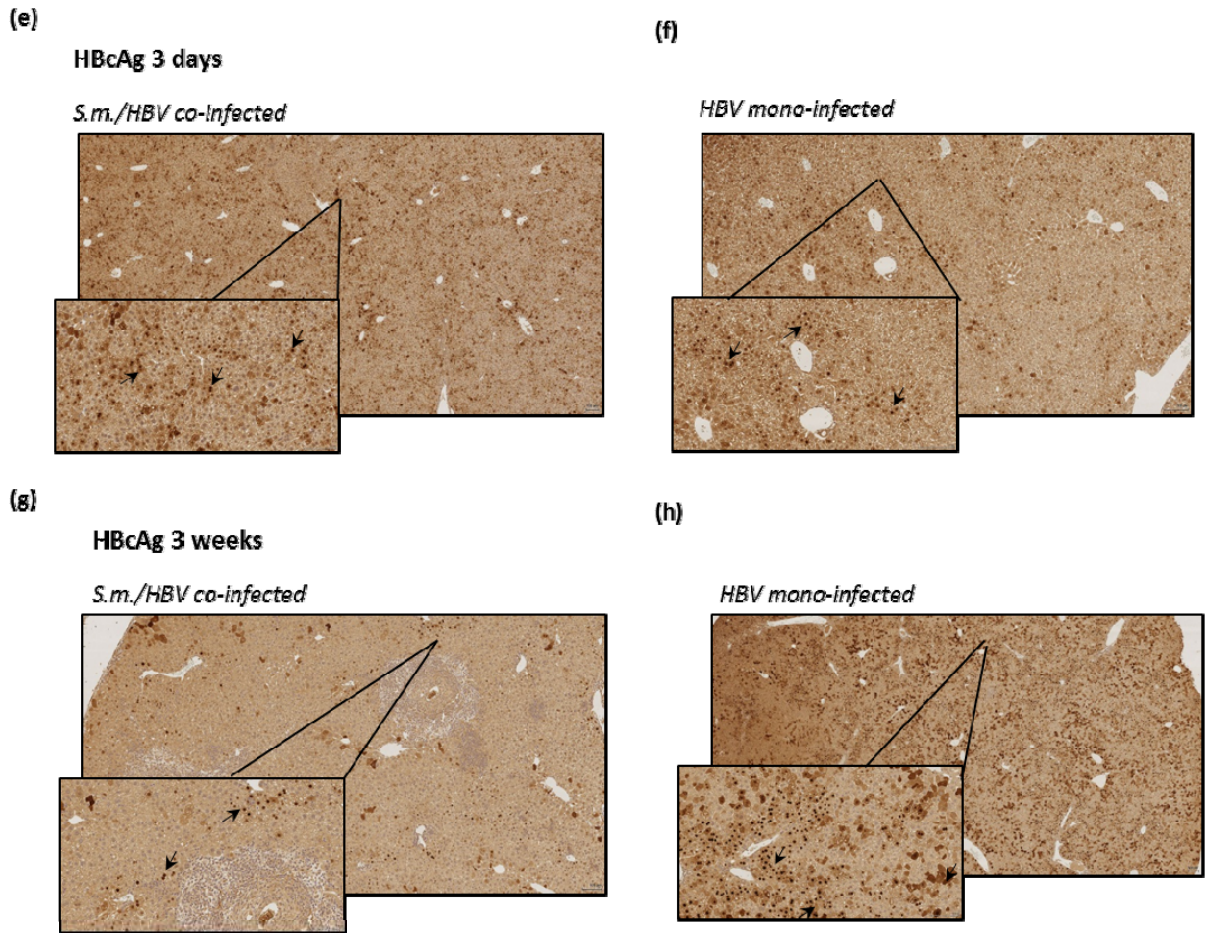


**Figure 18: Immunhistochemical detection of HBsAg and HBcAg in hepatocytes of co-infected and HBV mono-infected mice.** Detection of HBsAg (a- d) and HBcAg (e - h) within S.m./HBV co-infected and HBV mono-infected liver sections three days (a, b, e, f) and three weeks (c, d, g, h) post viral infection. Immunohistochemical stainings were performed with Horseradish-Peroxidase labelled antibodies against HBsAg and HBcAg by using the staining kit of BOND-MAX and were performed on a BOND-MAX immunohistochemistry robot (Leica Biosystems) using BOND polymer refine detection solution for DAB. Evaluation and pictures of the stainings were carried out on an Olympus BX53 microscope with a Leica SCN400 slide scanner in 10x magnification.

The semiquantitative analysis of stained sections was performed by counting the localization, intensity, distribution and percentage of positive cell staining throughout the whole tissue specimen using SlidePath TissueIA image analysis software (Leica) [251] on whole tissue sections and normalized to tissue area or hepatocyte number, respectively. Since the hepatitis B surface antigen accumulates in the cytoplasm of infected liver cells (see Figure 18a-d), the amount of positively HBsAg-stained hepatocytes is depicted in Figure 19a as HBsAg-positive area/liver tissue area in percentage. The hepatitis B core antigen is produced in the endoplasmic reticulum located in the proximity of the cell nucleus (see Figure 18e-h).

Consequently, in Figure 19b, infected liver cells are quantified and shown as % HBcAg positive nuclei. The evaluation of all stained liver sections revealed almost equal percentages of HBsAg- and HBcAg-stained hepatocytes three days post viral infection (Figure 19a and b). While three weeks post infection, the amount of HBsAg-stained liver cells remained almost equal between both animal groups, percentages of HBcAg-stained hepatocytes were significantly elevated in HBV mono-infected liver sections. As expected, in livers of naïve animals no positive staining for HBs-and HBcAg was observed. The results indicate that at an early stage of helminth infection, schistosome-infected livers can be equally infected with HBV but throughout the course of viral infection, HBV replication seems to be suppressed in co-infected mice.

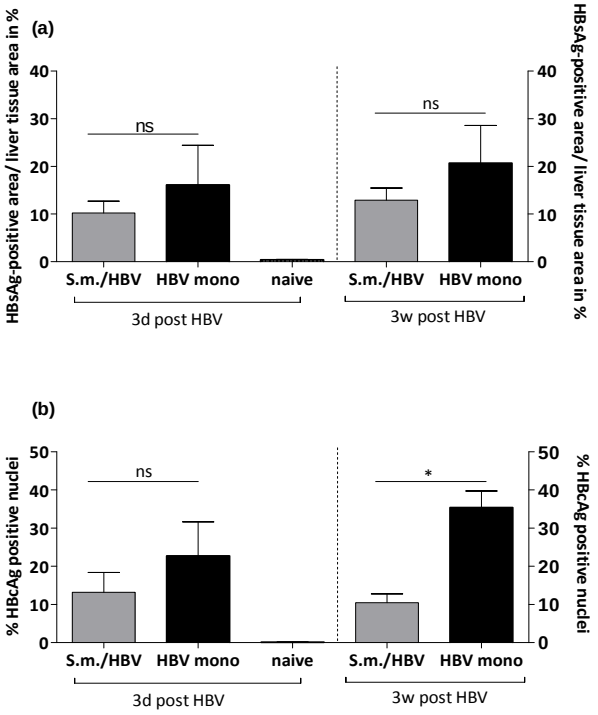


**Figure 19: Equal amounts of HBsAg- and HBcAg-stained hepatocytes in livers of co-infected and HBV mono-infected mice at an early stage of helminth infection.** The semiquantitative analysis of stained sections was performed by counting the localization, intensity, distribution and percentage of positive cell staining throughout the whole tissue specimen by using SlidePath TissueIA image analysis software (Leica) on whole tissue sections and normalized to tissue area or hepatocyte number, respectively. (a) Percentages of positively HBsAg-stained hepatocytes depicted as HBsAg-positive area/liver tissue area in % after 3 days and 3 weeks of HBV infection. (b) Positively HBcAg-stained liver cells shown as % HBcAg positive nuclei 3 days and 3 weeks post viral infection. Uninfected livers of naïve mice were used as control. A minimum of three livers of the indicated animal groups were analysed at each time point and the data is shown as mean ± SEM. Statistical evaluation was calculated using the Mann-Whitney U-test for nonparametric distributed data (*$P < 0.05$; n.s, not significant).

Since the additional *S. mansoni* infection seemed to hinder the production of HBcAg, and this is known to be controlled by virus-specific T cells, we analysed different cell populations present in the periphery (spleen) and within the liver three weeks post viral infection. An example of the gating strategy to detect the different liver-associated lymphocyte (LAL) populations is shown from one co-infected mouse (Figure 20). Frequencies of total $CD4^+$, $CD8^+$ (a) and Treg (e) were measured within unstimulated LALs and splenocytes, whereas frequencies of IFN-γ-producing $CD4^+$ and $CD8^+$ effector cells were measured either within unstimulated cells (b), PMA/Ionomycin (c) or HBV core peptide library stimulation, containing HBV core Pool 3 (HBcP3) (d). The core peptide 3 is the most immunogenic peptide and induces virus-specific immune responses (see section 2.3.4.1).

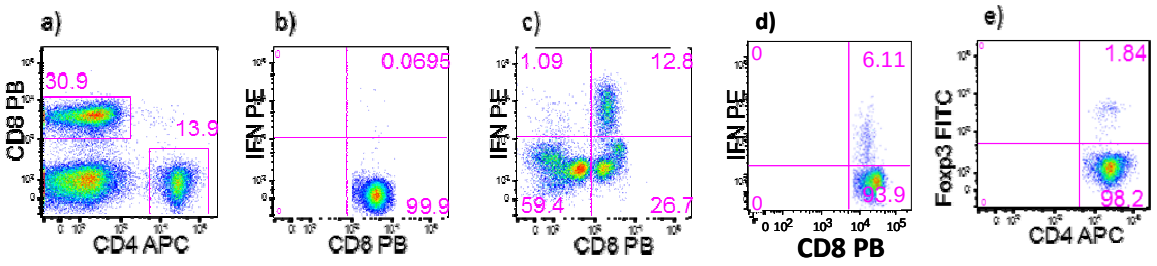


**Figure 20: Gating strategy to detect frequencies of total $CD4^+$ and $CD8^+$ T cells and virus specific T cell responses shown on an example within LALs from a co-infected mouse.** Virus specific-T cell responses, frequencies of total $CD4^+$ and $CD8^+$ T cells and frequencies of Treg were analysed within splenocytes and LALs by Flow Cytometry using the LSRII cytometer. Acquisition was done with 100.000 – 500.000 cells. (a) Frequencies of total $CD4^+$ and $CD8^+$ T cells measured within living lymphocytes. Frequencies of IFN-γ producing $CD8^+$ effector cells within living lymphocytes measured within the upper right quadrant either (b) within unstimulated cells, (c) PMA/Ionomycin or (d) HBcP3 stimulated cells. e) Frequencies of $CD4^+$ $Foxp3^+$ Treg cells, gated within all living lymphocytes.

Besides a slight increase in splenic $CD4^+$ T cells in HBV mono-infected animals, no differences were detected in $CD8^+$ and Treg frequencies in spleen and LALs (data not shown). In comparison to HBV mono-infected animals, upon antigen-specific stimulation with HBcP3 co-infected mice tend to respond with slightly elevated frequencies of virus-specific $CD8^+$ IFN-$\gamma^+$ T cells in the liver and the spleen (Figure 21). *S. mansoni* mono-infected and naïve mice showed no virus-specific $CD8^+$ responses to the HBV peptide library, showing that HBcP3 induces only HBV-specific immune responses in HBV infected mice (Figure 21).

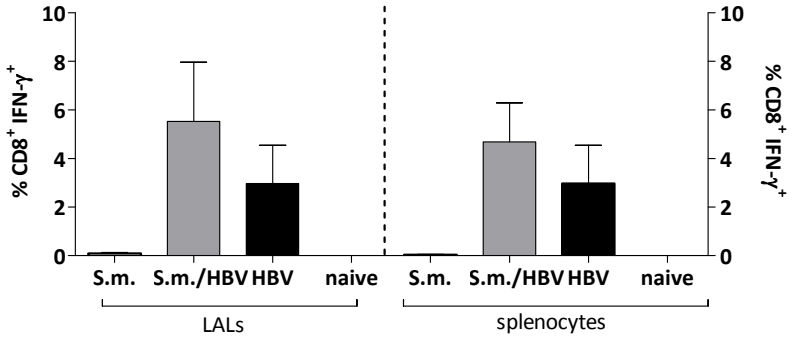


**Figure 21: Elevated frequencies of virus-specific CD8$^+$ IFN-γ$^+$ T cells in livers and spleens of co-infected mice.** Frequencies of CD8$^+$ IFN-γ$^+$ T cells upon HBcP3 are shown in livers and spleens of indicated animal groups. A minimum of three mice per group were analysed and the graphs are shown as mean ± SEM. No statistical differences between the indicated groups could be obtained after Mann-Whitney U-test for nonparametric distributed data.

Taken together, these results indicate that at an early stage of helminth infection, schistosome infected animals can be equally infected with HBV. A possible HBV entry-inhibition in the schistosome pre-infected liver can be excluded, since three days post viral infection - which corresponds to 4.5 weeks of schistosome infection - viral load and viral antigen levels were similar to those obtained from HBV mono-infected mice. Throughout the course of viral infection, however, a tendency towards schistosome mediated suppression of viral replication was observed owing to the fact that the viral load and specific viral antigens, such as HBcAg did not rise like in HBV mono-infected mice. In co-infected animals viral replication is presumably controlled by elevated frequencies of antigen-specific CD8$^+$ IFN-γ$^+$ T cells.

### 3.2.2.1.2 HBV infection acquired during the $T_H1$ phase of schistosome infection is cleared faster in co-infected mice

To analyse the development of HBV infection during the proper acute phase of schistosome infection, mice were infected with HBV 5 weeks post helminth infection, where very high levels of IFN-γ are reached (see *S. mansoni* kinetic, section 3.2.1.1). Post viral infection, successful HBV infection and ongoing viral clearance was monitored by bleeding mice at day 3, 7 and 21, followed by measuring viral antigen levels within mice sera (Figure 22). Furthermore, at the day of final analysis (21 days post viral infection) schistosome infection

was confirmed in all mice by detection of parasite eggs and granuloma formation in the liver (see section 3.2.3.1, Figure 38). As depicted in Figure 22a and b, three days post viral infection co-infected animals already showed significantly decreased viral antigen levels when compared to HBV mono-infected mice. Throughout the course of infection viral antigen levels did not significantly differ anymore between both animal groups, even though a tendency towards decreased viral antigen levels was still detectable in co-infected mice (Figure 22c and d).

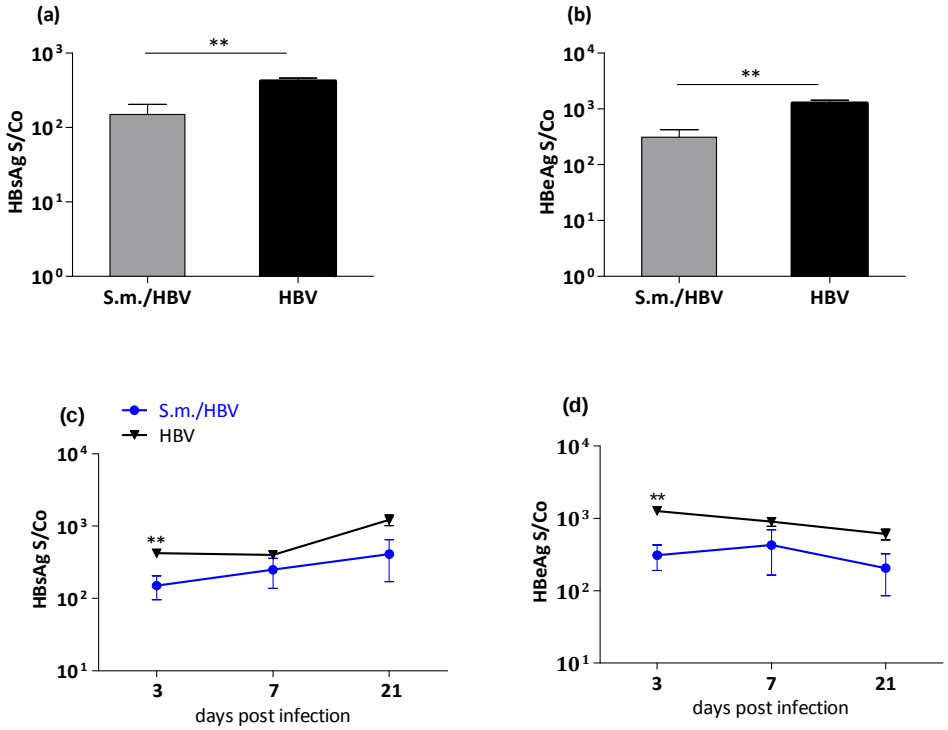


**Figure 22: Decreased viral antigen levels in sera of co-infected mice.** Qualitative detection of viral antigens in mice sera. (a) Levels of HBsAg and (b) HbeAg within S.m./HBV co-infected and HBV mono-infected mice 3 days post viral infection. (c) Fluctuations of HBsAg and (d) HBeAg levels throughout the course of HBV infection in sera of indicated animal groups. A minimum of four mice were analysed at each time point. Data show representative results from two independent experiments and is depicted as mean ± SEM (a, b) and mean and error ± SEM (c, d). Statistical evaluation was calculated using the Mann-Whitney U-test for nonparametric distributed data (**$P < 0.01$).

Furthermore, a clear tendency towards decreased amounts of HBV genomes was detected in livers of co-infected mice three days and three weeks post viral infection (Figure 23). At both timepoints, however, adenoviral genomes were comparable (Figure 23).

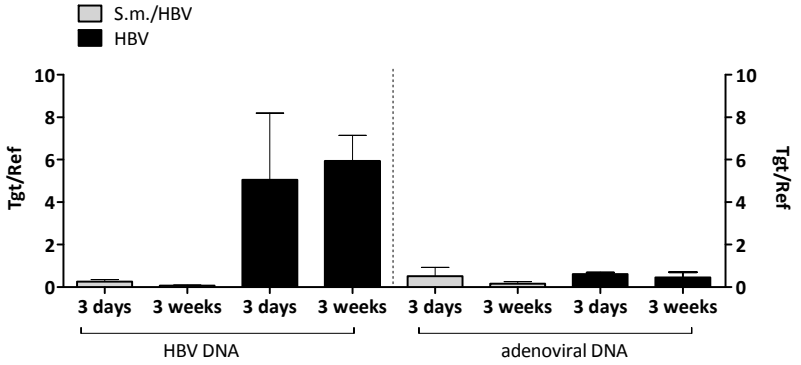


**Figure 23: Decreased amounts of HBV genomes in livers of co-infected mice.** Adenoviral- and HBV genomes were detected in DNA isolated from liver tissue samples by real-time PCR. The relative quantification of viral DNA compared to the murine reference gene (Tgt/Ref) is shown in co-infected and HBV mono-infected livers 3 days and 3 weeks post viral infection. A minimum of three mice were analysed at each time point. Bar graphs show representative results from two independent experiments and data is illustrated as mean ± SEM. Statistical evaluation between the indicated groups was performed by using the Mann-Whitney U-test for nonparametric distributed data (n.s, not significant).

The semiquantitative analysis of immunohistochemically stained HBsAg and HBcAg within liver sections of co-infected and HBV mono-infected mice also revealed a clear tendency towards lower amounts of antigen-positive hepatocytes (Figure 24a and b) which reached significance at 3 weeks post viral infection in HBcAg-positive cells of co-infected animals (Figure 24b).

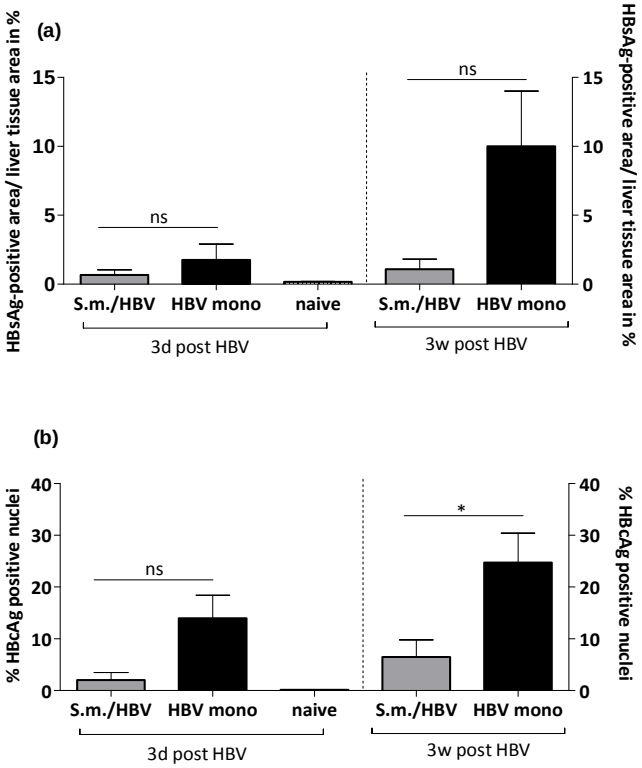


**Figure 24: Lower amounts of antigen-positive hepatocytes in livers of co-infected animals.** The semiquantitative analysis of stained sections was performed by counting the localization, intensity, distribution and percentage of positive cell staining throughout the whole tissue specimen by using SlidePath TissueIA image analysis software (Leica) on whole tissue sections and normalized to tissue area or hepatocyte number, respectively. (a) Percentages of positively HBsAg-stained hepatocytes depicted as HBsAg-positive area/liver tissue area in % after 3 days and 3 weeks of HBV infection. (b) Positively HBcAg- stained liver cells shown as % HBcAg positive nuclei 3 days and 3 weeks post viral infection. Uninfected livers of naïve mice were used as control. A minimum of three livers of the indicated animal groups were analysed at each time point and the data is shown as mean ± SEM. Statistical evaluation was calculated using the Mann-Whitney U-test for nonparametric distributed data (*$P < 0.05$; n.s, not significant).

These data indicate that an acute HBV infection acquired during the $T_H1$-prone phase of schistosome infection is cleared faster in co-infected animals. This is inferred by the fact that three days post viral infection these mice already displayed a lower viral replication rate when compared to their HBV mono-infected counterparts. To assess whether IFN-γ release from co-infected splenocytes is responsible for the observed decreased viral load, we analysed splenic IFN-γ secretion upon *S. mansoni*-specific (SEA)- and antigen-independent stimulation of the T cell receptor with biotinylated αCD3 and αCD28 coated MicroBeads (section 2.3.3.1 and 2.3.3.2). After an incubation period of 48 hours, IFN-γ was measured in the culture supernatant (section 2.3.3.2). Three days post viral infection, both schistosome-

infected groups (*S. mansoni* mono-infected and S.m./HBV co-infected) produced equal amounts of IFN-γ after SEA stimulation. However, upon αCD3/CD28 stimulation the splenocytes of co-infected mice produced higher levels of this cytokine than both mono-infected groups (Figure 25). These results indicate that schistosome specific immune responses are not influenced by the additional HBV infection, and that the helminth infection possibly boosts the production of this cytokine in an antigen-independent manner. This circumstance could contribute to lower viral loads. Of note, unstimulated splenocytes of all indicated animal groups produced equal levels of the cytokine at levels < 20 pg/ml (data not shown).

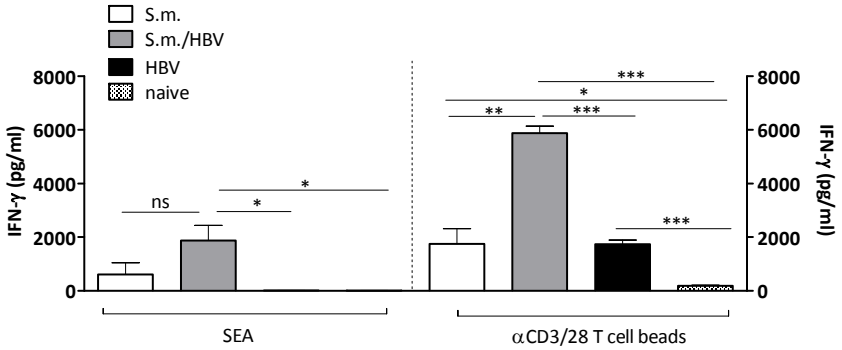


**Figure 25: Splenocytes from co-infected animals produce more IFN-γ when compared to HBV mono-infected mice.** Three days post viral infection, splenocytes ($2x10^5$ cells/ml) of *S. mansoni* mono-infected (n = 3), S.m./HBV co-infected (n = 3), HBV mono-infected (n = 3) and uninfected, naïve mice (n = 3) were either restimulated with SEA (20µg/ml) or αCD3/CD28 T cell beads (cell to bead ratio 1:1). After 48 hours IFN-γ levels were measured in the supernatant by ELISA. Bar graphs show representative results from two independent experiments and data is illustrated as mean ± SEM. Asteriks show statistical differences (Student's t test) between the groups indicated by the brackets (**P* < 0.05, ***P* < 0.01 and ****P* < 0.001; not significant, n.s.).

Upon HBcP3 stimulation of LALs and splenocytes frequencies of $CD8^+$ IFN-$\gamma^+$ T cells were elevated in the liver and spleen of co-infected mice when compared to HBV mono-infected mice (Figure 26). Again, upon HBV-specific stimulation no virus-specifc $CD8^+$ IFN-$\gamma^+$ T cell response was detected in *S. mansoni* mono-infected and naïve mice (Figure 26).

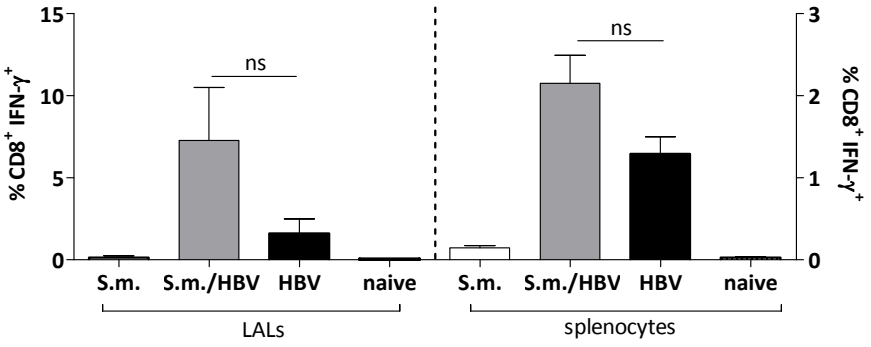


**Figure 26: Frequencies of virus-specific CD8$^+$ IFN-γ$^+$ T cells are elevated in livers and spleens of co-infected mice.** Frequencies of CD8$^+$ IFN-γ$^+$ T cells upon HBcP3 stimulation in livers and the spleen of indicated animal groups. A minimum of three mice per group were analysed and the graphs show representative results from two independent experiments. The data is depicted as mean ± SEM. No statistical differences between the groups were obtained (Student's t test) (not significant, n.s.).

Taken together, these results indicate, that an HBV infection acquired during the proper $T_H1$ phase of schistosome infection, is cleared faster when compared to HBV mono-infected mice. Higher levels of local schistosome-induced IFN-γ, which can immediately act on viral replication, might be responsible for the lower viral load present in co-infected mice. In addition, increased levels of schistosome-induced IFN-γ might induce a faster priming and/or enhanced proliferation of virus-specific T cells, since upon HBcP3 stimulation a clear tendency towards elevated frequencies of CD8$^+$ IFN-γ secreting T cells were detected in both organs of co-infected animals. The increased population of virus-specific T cells might additionally contribute to the faster viral clearance observed in co-infected mice.

### 3.2.2.2 Outcome of secondary acquired, acute HBV infection during the $T_H2$ phase of *S. mansoni* infection

#### 3.2.2.2.1 Acute HBV infection acquired during the $T_H2$ phase of schistosome infection develops equally in co-infected and HBV mono-infected mice

Since we observed a faster viral clearance of an acute HBV infection acquired during the $T_H1$ phase of schistosome infection, we asked whether $T_H2$ cytokines during the $T_H2$ phase could skew this observation. For that, mice were infected with HBV 8 weeks post schistosome

infection, where high levels of $T_H2$-type cytokines such as IL-10 and IL-13 and low levels of IFN-γ are present (see *S. mansoni* kinetic, section 3.2.1.1). Successful HBV infection and ongoing viral clearance was monitored by bleeding mice at day 3, 7, 14 and 21, followed by measuring viral antigen levels within mice sera (Figure 27). In addition, at the day of final analysis (21 days post viral infection) schistosome infection was confirmed in all mice by detection of parasite eggs and granuloma formation in the liver (see section 3.2.3.1, Figure 38). Three days post viral infection, equal levels of HBsAg (Figure 27a) and HBeAg (Figure 27b) were measured in the serum of co-infected and HBV mono-infected mice. Additionally, throughout the course of infection, viral antigen levels did not differ between both animal groups (Figure 27c and d).

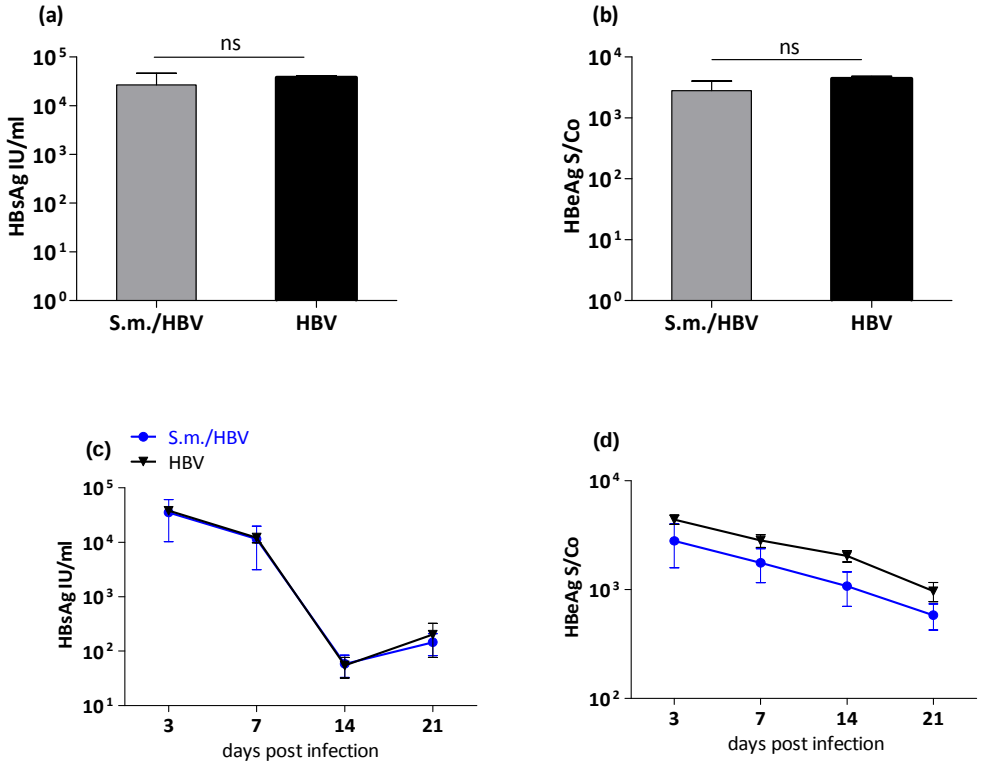


**Figure 27: Equal viral antigen levels in sera of co-infected and HBV mono-infected mice.** Quantitative (HBsAg) and qualitative (HBeAg) detection of viral antigens in mice sera were performed with a microparticle enzyme assay and are illustrated for HBsAg as international units/ml (IU/ml) and S/Co for HBeAg. (a) Levels of HBsAg and (b) HBeAg within S.m./HBV co-infected and HBV mono-infected mice 3 days post viral infection. (c) Fluctuations of HBsAg and (d) HBeAg levels throughout the course of HBV infection in sera of indicated animal groups. A minimum of two mice were analysed at each time point and data is depicted as mean ± SEM (a, b) and mean and error ± SEM (c, d). Statistical evaluation was calculated using the Mann-Whitney U-test for nonparametric distributed data (n.s.; not significant).

Three weeks post viral infection, the relative quantification of HBV and adenoviral genomes revealed a tendency towards higher amounts of HBV DNA in livers of co-infected mice when compared to HBV mono-infected animals. However, numbers of adenoviral genomes were similar in both groups (Figure 28).

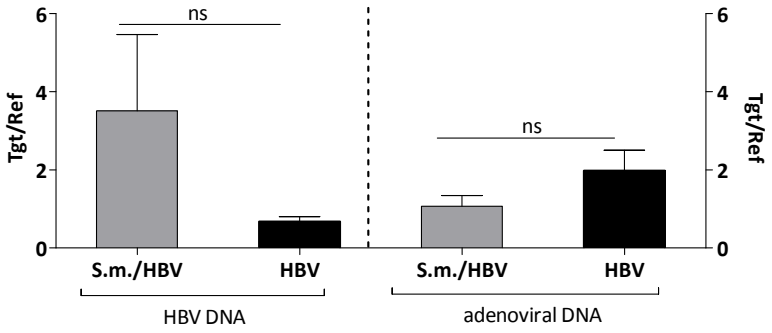


**Figure 28: Higher numbers of HBV genomes in livers of co-infected mice.** Adenoviral- and HBV genomes were detected in DNA isolated from liver tissue samples by real-time PCR The relative quantification of viral DNA compared to the murine reference gene (Tgt/Ref) is shown in co-infected and HBV mono-infected livers 3 weeks post viral infection. A minimum of three mice were analysed at each time point and bar graphs are shown as mean ± SEM. Statistical evaluation between the indicated groups was performed by using the Mann-Whitney U-test for nonparametric distributed data (n.s, not significant).

Flow cytometric analyses revealed no differences in the frequency of total $CD4^+$ and $CD8^+$ T cells and no alterations in the Treg frequency in both organs of all mice (data not shown). Populations of eosinophils and monocytes, however, slightly increased, whereas frequencies of neutrophils remained unaltered in livers and spleens of co-infected mice (data not shown).

Furthermore, upon antigen-specific stimulation with HBcP3 a tendency towards higher frequencies of $CD8^+$ IFN-$\gamma^+$ T cells was detected in both organs of co-infected mice as well as the HBV mono-infected counterparts. Upon HBV-specific stimulation no virus-specific $CD8^+$ T cell responses were detected in livers and spleens of naïve mice (Figure 29).

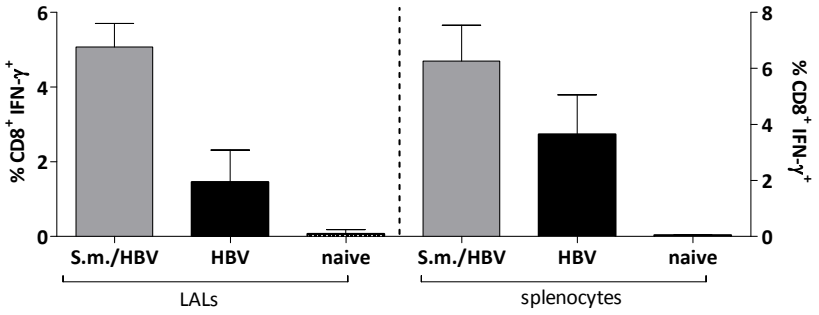


**Figure 29: Elevated frequencies of virus-specific CD8$^+$ IFN-γ$^+$ T cells in livers and spleens of co-infected mice.** Frequencies of CD8$^+$ IFN-γ$^+$ T cells upon HBcP3 stimulation in livers and the spleen of indicated animal groups. A minimum of two mice per group were analysed and the graphs are shown as mean ± SEM. Statistical analyses calculated with the Mann-Whitney U-test revealed no significant differences between the indicated groups.

Taken together, these results demonstrate that an HBV infection acquired during the $T_H2$ phase of schistosome infection seems to develop equally when compared to HBV mono-infected mice. Even though a tendency towards elevated frequencies of CD8$^+$ IFN-γ secreting T cells was detected upon HBcP3 stimulation in organs of co-infected mice, throughout the course of infection these mice had similar levels of serum viral antigens and no significantly altered viral load when compared to HBV mono-infected animals.

### 3.2.2.3 Outcome of secondary acquired, acute HBV infection during the chronic phase of *S. mansoni* infection

Since we observed a faster viral clearance of an acute HBV infection acquired during the $T_H1$ phase of schistosome infection, we asked whether high levels of $T_H2$-type cytokines such as IL-10, IL-5 and IL-13 as well as high frequencies of Treg known to be present during the chronic phase of schistosome infection, might influence the supposed anti-viral activity of schistosome induced IFN-γ, which interestingly rose again during this late phase of infection (see *S. mansoni* kinetic, section 3.2.1.1).

#### 3.2.2.3.1 Faster viral clearance of acute HBV infection acquired during the chronic phase of schistosome infection

To investigate the impact of the chronic phase of schistosome infection on the course of an acute, secondary acquired HBV infection, mice were infected with HBV 16 weeks post schistosome infection. The detailed experimental protocol is described in section 2.2.4.1.3. Viral infection and ongoing clearance were subsequently monitored by bleeding mice at indicated time points post HBV infection (see section 2.2.4.1.3), followed by measuring serum viral antigen levels (Figure 30). In addition, at the day of final analysis (21 days post viral infection) schistosome infection was confirmed in all mice by detection of parasite eggs and granuloma formation in the liver (see section 3.2.3.1, Figure 38). Three days post viral infection, co-infected mice had significantly decreased levels of HBsAg (Figure 30a) and HBeAg (Figure 30b) when compared to HBV mono-infected animals. Furthermore, while levels of HBeAg remained significantly decreased throughout the whole course of infection, lower levels of HBsAg were detected in sera of co-infected mice at days 7 and 21 post viral infection (Figure 30c and d). Two weeks post HBV infection, co-infected and HBV mono-infected mice had equal serum HBsAg titers (Figure 30c and d).

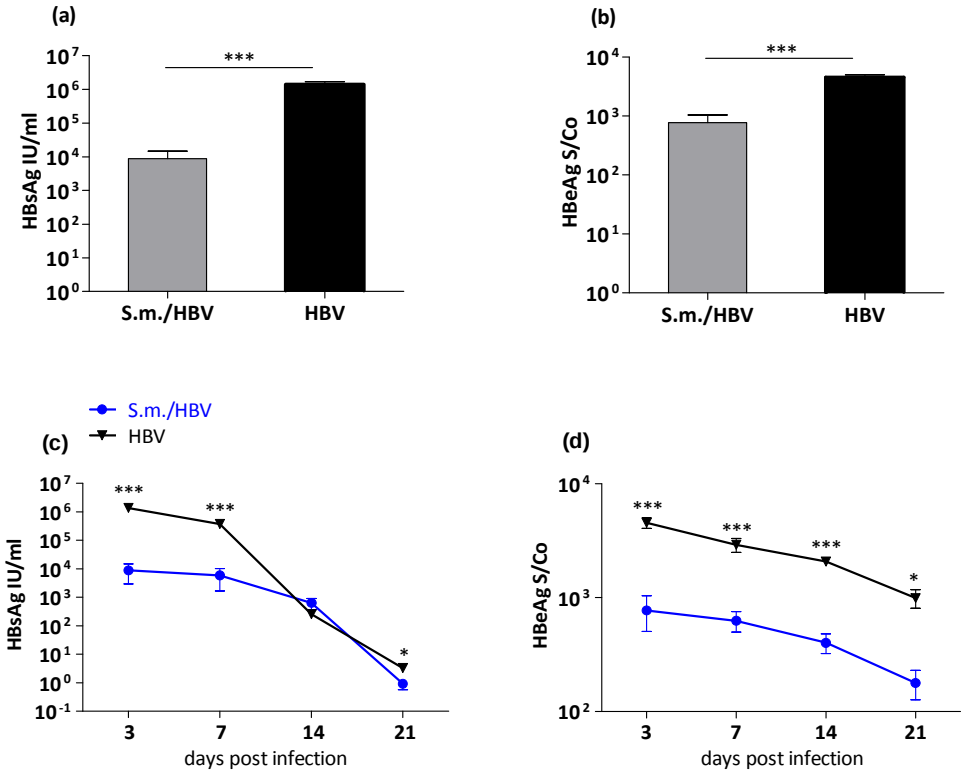


**Figure 30: Decreased viral antigen levels in sera of co-infected mice.** Quantitative (HBsAg) and qualitative (HBeAg) detection of viral antigens in mice sera was performed with a microparticle enzyme assay and is shown for HBsAg as IU/ml and S/Co for HBeAg. (a) Levels of HBsAg and (b) HBeAg within S.m./HBV co-infected and HBV mono-infected mice 3 days post viral infection. (c) Fluctuations of HBsAg and (d) HBeAg levels throughout the course of HBV infection in sera of indicated animal groups. A minimum of six mice were analysed at each time point. Data show representative results from two independent experiments and is depicted as mean ± SEM (a, b) and mean and error ± SEM (c, d). Statistical evaluation was calculated using the Mann-Whitney U-test for nonparametric distributed data (*$P < 0.05$ and ***$P < 0.001$; not significant, n.s.).

Three weeks post viral infection, the relative quantification of HBV and adenoviral genomes revealed significantly lower amounts of HBV DNA and unaltered levels of adenoviral DNA in livers of co-infected mice when compared to HBV mono-infected animals (Figure 31).

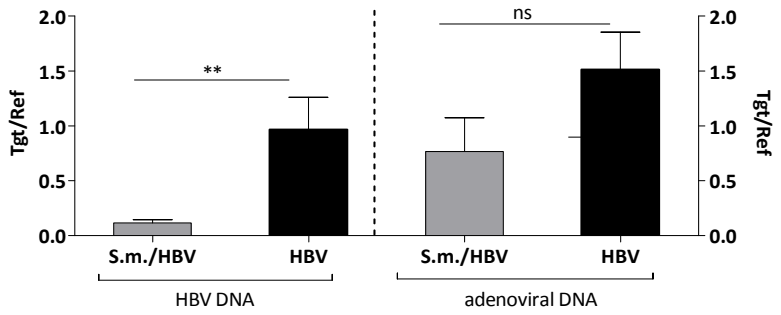


**Figure 31: Decreased amounts of HBV genomes in livers of co-infected mice.** Adenoviral- and HBV genomes were detected in DNA isolated from liver tissue samples by real-time PCR. The relative quantification of viral DNA compared to the murine reference gene (Tgt/Ref) is shown in co-infected and HBV mono-infected livers 3 weeks post viral infection. A minimum of six mice were analysed at each time point. Data show representative results from two independent experiments and bar graphs are shown as mean ± SEM. Statistical evaluation between the indicated groups was performed by using the Mann-Whitney U-test for nonparametric distributed data (**$P < 0.01$, n.s, not significant).

Since chronically schistosome infected mice interestingly cleared the additional HBV infection faster than their HBV mono-infected counterparts, we asked whether rising IFN-γ levels detectable along with $T_H2$-type cytokines, such as the immunosuppressive cytokine IL-10, might still be responsible for the observed decreased viral load present in co-infected animals. Therefore, three weeks post viral infection, we analysed levels of IFN-γ (Figure 32a) and IL-10 (Figure 32b) in isolated mesenteric lymph node cells (MLNs), upon antigen-specific and antigen-independent stimulation (section 2.3.3.1 and 2.3.3.2). In contrast to the $T_H1$ phase experiment, where IFN-γ levels were measured in restimulated splenocytes (section 3.2.2.1.2, Figure 25), during the chronic phase of schistosome infection, the cytokine response is measured in MLNs since adult worms reside in the mesenteric veins and MLNs function as the draining lymph nodes. Both schistosome infected animal groups secreted similar levels of IL-10 under both stimulation conditions, indicating that also in the chronic phase of helminth infection, the additional HBV infection does not influence schistosome specific immune responses. In comparison to HBV mono-infected mice, MLNs of schistosome infected mice produced significantly higher levels of IL-10 (Figure 32b). Interestingly, even though elevated levels of IL-10 were present, MLNs of co-infected animals still produced significantly higher levels of IFN-γ upon antigen-independent stimulation when compared to HBV mono-infected mice (Figure 32a). Between both schistosome-infected animal groups IFN-γ production did not differ upon SEA- or αCD3/CD28 stimulation (Figure 32a). These

results show that even late during the chronic phase of schistosome infection, elevated levels of IFN-γ coexist with anti-inflammatory IL-10. In chronically schistosome infected mice, these rising IFN-γ levels might then again be responsible for the faster viral clearance when compared to HBV mono-infected animals.

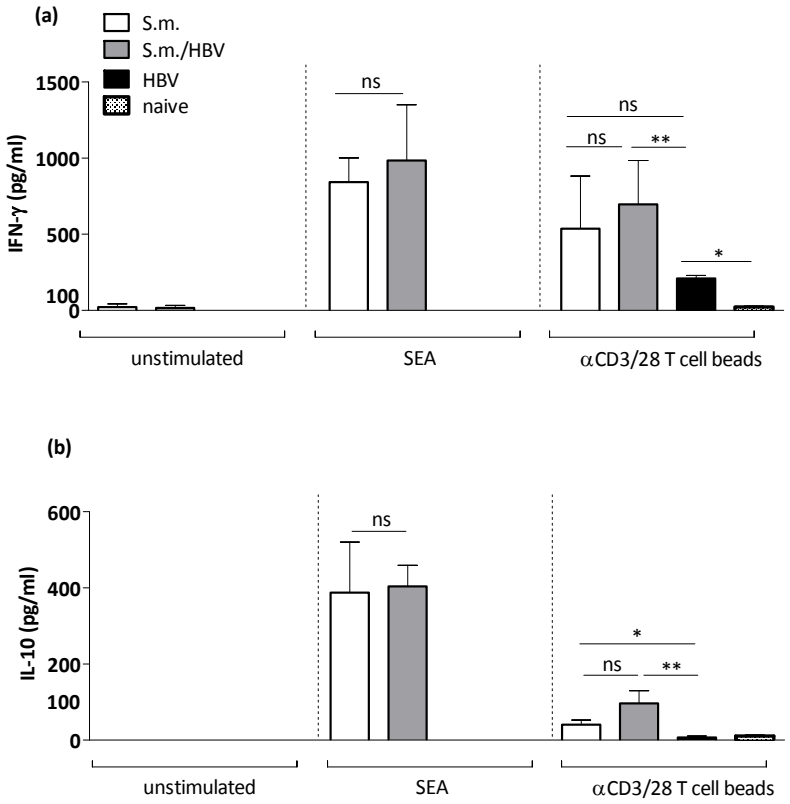


**Figure 32: MLNs of co-infected animals still produce higher levels of IFN-γ when compared to HBV mono-infected mice.** Three weeks post HBV infection, MLNs ($2x10^5$ cells/ml) of *S. mansoni* mono-infected (n = 3), S.m./HBV co-infected (n = 5), HBV mono-infected (n = 6) and uninfected, naïve mice (n = 3) were either restimulated with SEA (20μg/ml) or αCD3/CD28 T cell beads (cell to bead ratio 1:1). After 48 hours levels of IFN-γ (a) and IL-10 (b) were measured in the supernatant by ELISA. Bar graphs show representative results from two independent experiments and data is illustrated as mean ± SEM. Asteriks show statistical differences (Mann-Whitney U-test) between the groups indicated by the brackets (*$P < 0.05$ and **$P < 0.01$; not significant, n.s.).

Flow cytometric analysis revealed unaltered frequencies of $CD4^+$ and $CD8^+$ T cells as well as Treg in the liver and spleen of all animal groups (data not shown). LALs from co-infected animals respond better to antigen-specific stimulation with HBcP3, since in comparison to HBV mono-infected counterparts, significantly elevated frequencies of $CD8^+$ IFN-$\gamma^+$ T cells were detected. Co-infected splenocytes restimulated with HBcP3 responded with a clear

tendency towards higher proportions of $CD8^+$ IFN-$\gamma^+$ T cells when compared to mice with HBV mono-infection. *S. mansoni* mono-infected and naïve mice showed no virus-specific $CD8^+$ responses to the HBV peptide library (Figure 33).

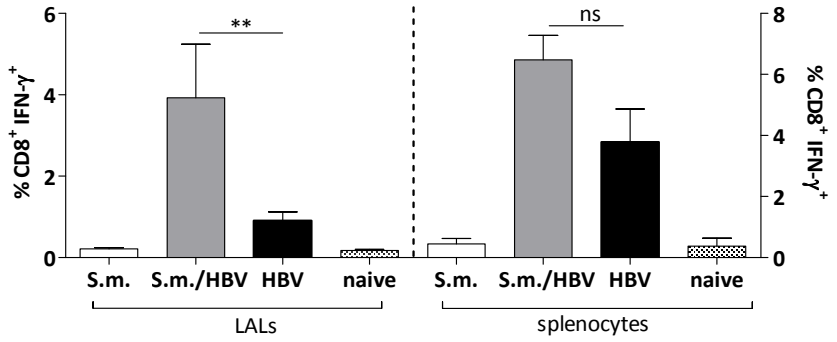


**Figure 33: Increased frequencies of virus-specific $CD8^+$ IFN-$\gamma^+$ T cells in livers of co-infected mice.** Frequencies of $CD8^+$ IFN-$\gamma^+$ T cells upon HBcP3 stimulation in livers and the spleen of indicated animal groups. A minimum of three mice per group were analysed and the data show representative results from two independent experiments. Graphs are shown as mean ± SEM. Asteriks show statistical differences (Mann-Whitney U-test) between the groups indicated by the brackets (**$P < 0.01$; not significant, n.s.).

Taken together, these results indicate, that an HBV infection acquired during the chronic phase of schistosome infection, is cleared faster when compared to HBV mono-infected mice. Elevated $T_H2$-type cytokines present during this phase of infection, seemed neither to suppress the production nor the anti-viral activity of IFN-$\gamma$, since co-infected animals responded with high levels of IFN-$\gamma$ to SEA- and $\alpha$CD3/CD28 stimulation and had decreased viral antigen levels and lower viral loads in general. Furthermore, in comparison to HBV mono-infected animals, increased frequencies of $CD8^+$ IFN-$\gamma^+$ virus-specific T cells were observed in the liver of co-infected mice which might additionally contribute to the faster viral clearance.

### 3.2.2.4 Impact of a secondary acquired schistosome infection on liver disease outcome in chronically HBV infected mice

As described in the introduction, the impact of a secondary acquired schistosome infection on top of a pre-existing chronic HBV infection, has so far only been addressed experimentally

in a single study using an HBV transgenic (HBVtg) mouse model [217]. The study investigated the influence of $T_H1$ or $T_H2$ type cytokines induced during *S. mansoni* infection on HBV replication. It demonstrated that HBV replication was suppressed during the $T_H1$ phase of *S. mansoni* infection and remained downregulated upon onset into the $T_H2$ phase 6-8 weeks post schistosome infection. The authors attributed the suppressed HBV replication to the antiviral activity of schistosome-induced IFN-γ and showed that the first appearance of $T_H2$ type cytokines does not counteract with the antiviral effect of IFN-γ [217]. However, *Guidotti et al.,* only monitored HBV replication up to the 8th week of schistosome infection during which the $T_H2$ phase has just begun to establish itself and did not provide any information on whether this suppression persisted during the successive immune-suppressive phases of schistosome infection. In order to take *Guidotti's* studies further and to study whether HBV replication re-occurs upon progression into the $T_H2$ and regulatory phases of schistosome infection we repeated the experiment with HBVtg mice co-infected with *S. mansoni* and followed these mice over an extended infection period up to 16 weeks. Animals were bled on a weekly basis to assess fluctuations in virus replication, cytokine milieu and virus-specific T cells during the successive Th2 phase.

#### 3.2.2.4.1 Co-infected HBVtg mice show decreased HBV replication exclusively during the $T_H1$ phase of *S. mansoni* infection

The impact of a secondary acquired schistosome infection on the liver disease outcome in chronically HBV infected mice was analysed by using the mouse line HBV1.3xfs [256] on a C57BL/6 background because they are less susceptible to transgene silencing compared to the HBV 1.3.32 transgenic mice used by *Guidotti et al*. Of note, all HBVtg mice only start expressing HBV-antigen shortly before birth and therefore do not show clonal deletion of HBV-specific T cells. Thereby, tolerance on a T cell level evolves and can be broken, e.g. by depletion of regulatory T cells or the induction of HBV-specific T cells [257]. At an age of 6-8 weeks, these mice were either infected with *S. mansoni* (HBVtg/Sm) or left uninfected (HBVtg) and viral replication was monitored on a weekly basis by measuring serum viral antigen levels. In addition, at the timepoints of final analysis (6.5 and 16 weeks post *S. mansoni* infection) schistosome infection was confirmed in all mice by detection of

parasite eggs and granuloma formation in the liver (see section 3.2.3.2, Figure 40). The detailed experimental protocol is described in section 2.2.4.1.4.

Like *Guidotti et al.*, in co-infected animals we detected significantly lower viral antigen (HBsAg, HBeAg) secretion during the $T_H1$ phase of *S. mansoni* infection (5.5 and 6.5 weeks post infection), indicating that compared to uninfected HBVtg mice, in these animals HBV replication was suppressed (Figure 34). Interestingly, after the third bleeding round (timepoint 6.5 weeks post schistosome infection), the drop in viral antigen levels was also observed in HBVtg mice without an additional schistosome infection (Figure 34). This is a result known to stem from repetitive bleeding of these animals and the generally slow reproduction of new viral antigens. Furthermore, over the course of schistosome infection, measured viral antigen titers were very low and did not differ anymore between both animal groups. Consequently, an eventual relapse in viral replication was difficult to determine and not observed during the chronic phase of schistosome infection (up to 12 weeks) (Figure 34).

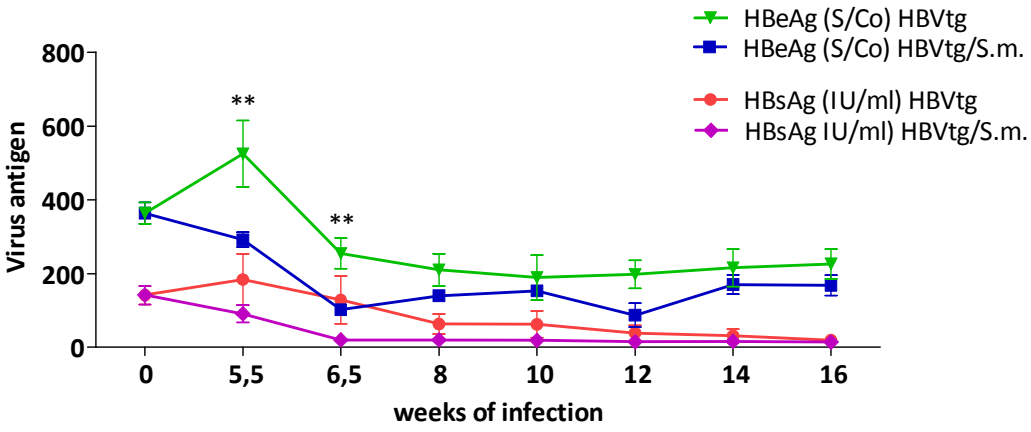


**Figure 34: Decreased HBV replication in co-infected HBVtg mice during the $T_H1$ phase of *S. mansoni* infection.** Quantitative (HBsAg IU/ml) and qualitative (HBeAg S/Co) detection of viral antigens in sera of HBVtg mice with (HBVtg/S.m.) or without (HBVtg) additional *S. mansoni* infection. Fluctuations of viral antigens in both animal groups were monitored over an infection period of 16 weeks. A minimum of four mice were analysed at each time point and data is depicted as mean and error ± SEM. Statistical evaluation was calculated using the Mann-Whitney U-test for nonparametric distributed data (**$P < 0.01$).

Even though significantly decreased viral antigen levels were detected in co-infected HBVtg mice during the $T_H1$ phase of schistosome infection, the amount of HBV genomes did not differ in livers of both animals groups during the acute (6.5 weeks post infection, Figure 35

left side) and chronic phase (16 weeks post infection, Figure 35 right side) of helminth infection. These results indicate that during the $T_H1$ phase, the antiviral activity of schistosome-induced IFN-γ directly acts on viral replication but does not result in viral elimination.

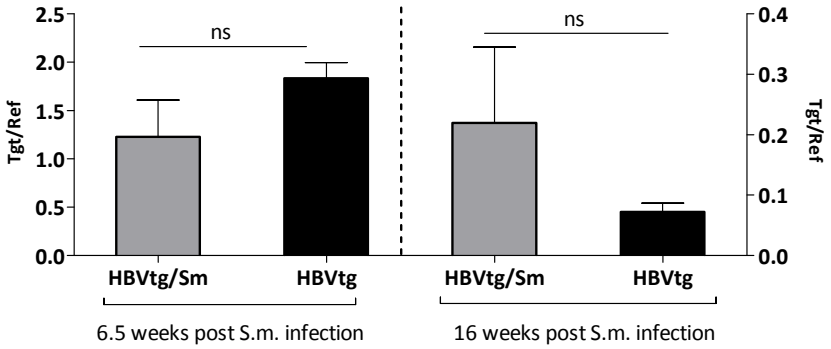


**Figure 35: Unaltered amounts of HBV genomes in livers of HBVtg mice with or without additional *S. mansoni* infection.** HBV genomes were detected in DNA isolated from liver tissue samples by real-time PCR. The relative quantification of viral DNA compared to the murine reference gene (Tgt/Ref) is shown in livers of HBVtg mice with or without additional *S. mansoni* infection 6.5 and 16 weeks post helminth infection. A minimum of three mice were analysed at each time point and bar graphs are shown as mean ± SEM. No statistical differences between the indicated groups were obtained after Mann-Whitney U-test for nonparametric distributed data (n.s, not significant).

Next, 6.5 and 16 weeks post helminth infection, schistosome-specific and independent immune responses were analysed in both animal groups to determine the effects of co-infection on the cytokine milieu. Splenocytes (Figure 36a) and MLNs (Figure 36b and c) of HBVtg mice with or without an additional schistosome infection were stimulated with SEA or anti-CD3/CD28 beads and levels of IFN-γ and IL-10 were measured in the culture supernatant. At both indicated time points and stimulation conditions, a tendency towards higher IFN-γ production was observed in splenocytes and MLNs of co-infected animals (Figure 36a and b). In addition, during the chronic phase of schistosome infection, MLNs of co-infected mice secreted significantly higher levels of IL-10 upon both stimulation conditions (Figure 36c). The altered cytokine milieu might be responsible for the overall observed decreased viral antigen titres present in co-infected mice.

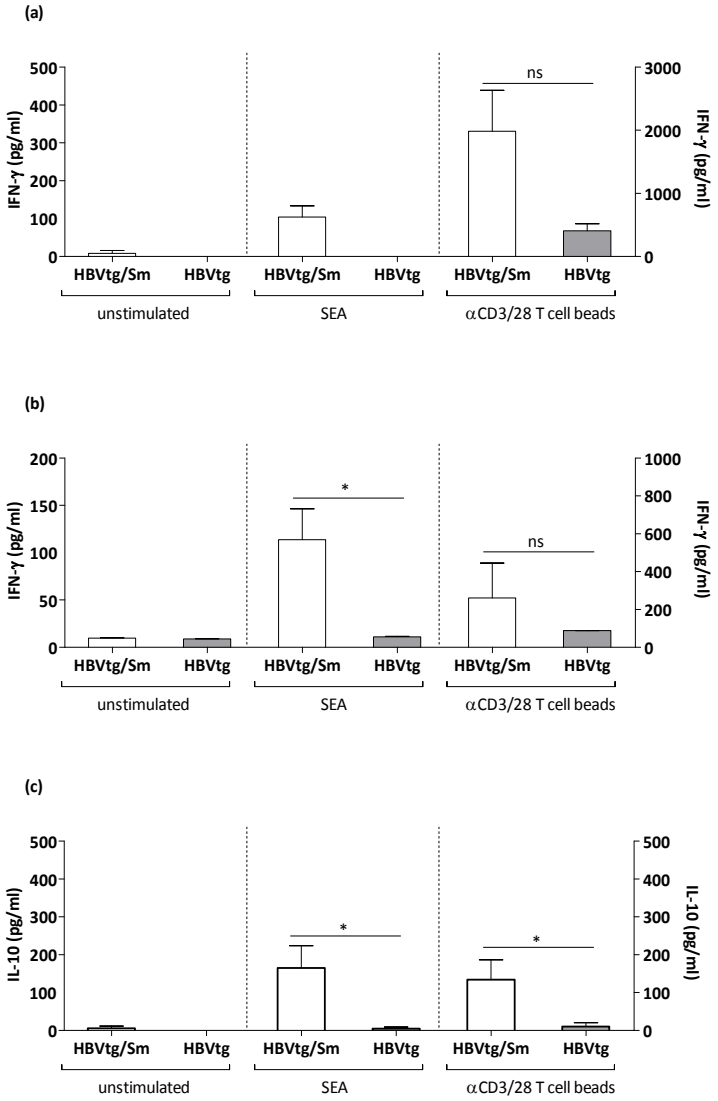


**Figure 36: Cytokine milieu in co-infected HBVtg mice is altered towards significantly higher levels of IL-10 and increased IFN-γ production.** Cytokine milieu in antigen-specific (SEA 20µg/ml) and independent (αCD3/CD28 beads) restimulted splenocytes and MLNs ($2x10^5$ cells/ml) of HBVtg/Sm and HBVtg mice was determined by ELISA. Levels of IFN-γ were either measured in re-stimulated splenocytes during the acute phase of schistosome infection (6.5 weeks) (a) or after 16 weeks of helminth infection in MLNs (b). IL-10 secretion was measured in re-stimulated MLNs only in the chronic phase of helminth infection (16 weeks) (c). A minimum of three mice were analysed at each timepoint and bar graphs are shown as mean ± SEM. Asteriks show statistical differences (Mann-Whitney U-test) between the groups indicated by the brackets (*$P < 0.05$; not significant, n.s.).

As mentioned above, HBVtg mice do not show clonal deletion of HBV-specific T cells, since these animals only start to express HBV-antigen shortly before birth. Consequently, only a peripheral tolerance on a T cell level evolves, which can be broken. We therefore asked whether the additional acute schistosome infection can break the tolerance evolved in HBVtg mice by local production of IFN-γ in the liver and monitored virus-specific T cell

frequencies in this organ and in the periphery such as the spleen. As depicted in Figure 37a, during the acute phase of schistosome infection (6.5 weeks) we indeed find a clear tendency towards elevated frequencies of $CD8^+$ IFN-$\gamma^+$ T cells locally in the liver and in the spleen of co-infected mice upon HBcP3 stimulation. During the chronic phase of schistosome infection the trend towards elevated frequencies of virus-specific $CD8^+$ IFN-$\gamma^+$ T cells was still observed in LALs of co-infected mice (Figure 37b).

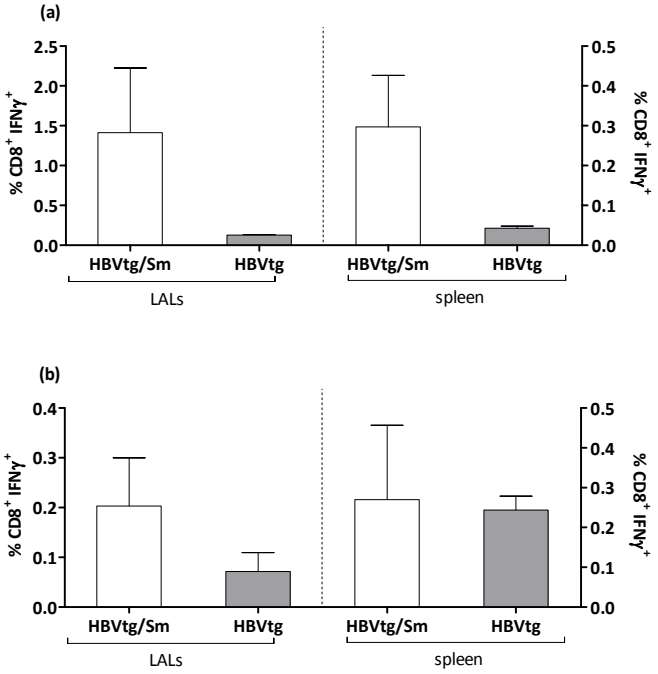


**Figure 37: Higher frequencies of virus-specific $CD8^+$ IFN-$\gamma^+$ T cells in organs of co-infected mice during the acute phase of schistosome infection.** Upon HBcP3 stimulation frequencies of $CD8^+$ IFN-$\gamma^+$ T cells were monitored either during (a) the acute phase of schistosome infection (6.5 weeks) or (b) 16 weeks post helminth infection in livers and spleens of indicated animals groups. A minimum of three mice per group were analysed at each timepoint and the data is illustrated as mean ± SEM. No statistical differences between the indicated groups were obtained after Mann-Whitney U-test for nonparametric distributed data.

Taken together, these results indicate that an additional acute schistosome infection is able to break the chronicity evolved in HBVtg mice, since lower viral antigen levels and higher frequencies of virus-specific T cells were detected exclusively in co-infected animals. Like *Guidotti et al.* we believe that high levels of schistosome-induced IFN-$\gamma$, present during the $T_H1$ phase of helminth infection, led to the drop of viral antigen levels in co-infected mice.

Elevated levels of this cytokine might furthermore be responsible for the induction of virus-specific T cells, since upon HBV specific re-stimulation only co-infected animals had increased frequencies of $CD8^+$ IFN-$\gamma^+$ T cells locally in the liver and in the periphery.

### 3.2.3 Impact of Hepatitis B virus infection on *S. mansoni* disease outcome

We previously observed that the distinct immune phases of *S. mansoni* infection led to differential outcomes in the case of acute and chronic HBV co-infection. This in turn prompted us to investigate if the latter had an impact on the helminth disease outcome as well. For this purpose different parasitological parameters were analysed in *S. mansoni* infected animals with or without concomitant HBV infection.

#### 3.2.3.1 Acute HBV infection acquired during the distinct immune phases of *S. mansoni* infection does not influence the helminth disease outcome

As described in section 2.2.4.2, the schistosome infection was evaluated by scoring for parasitological parameters such as, degree of infection (DOI), organ weight (spleen and liver), egg count and granuloma formation within livers of co-infected or schistosome mono-infected mice. Since both animal groups presented equal parasite egg burdens (Figure 38a) and granuloma sizes (Figure 38b) at all indicated time points (4 weeks – 16 weeks post *S. mansoni* infection), we concluded that the acute HBV infection acquired during the different immune phases of *S. mansoni* infection had no influence on the helminth disease outcome.

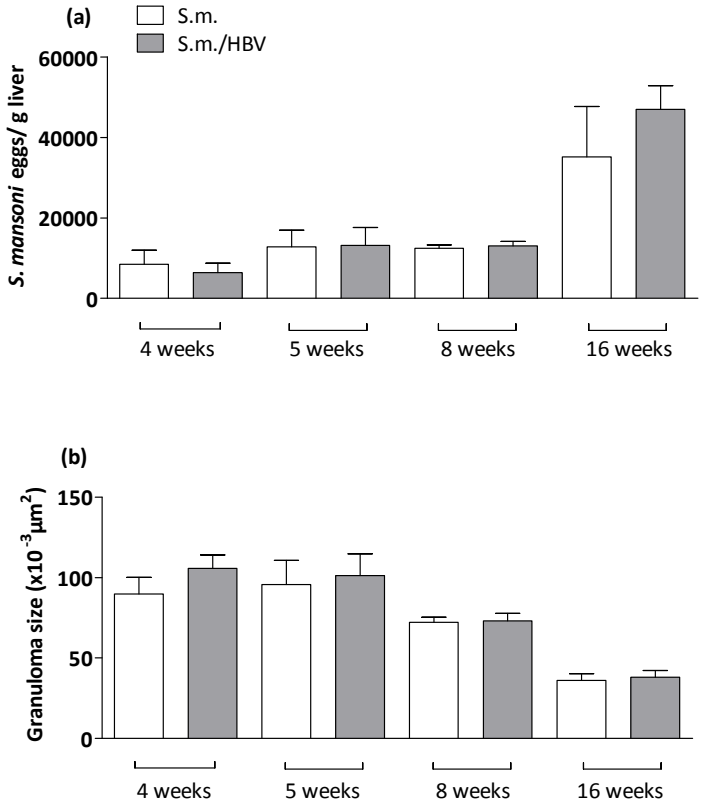


**Figure 38: Parasite egg burdens and granuloma sizes are not altered in mice with an additional acute HBV infection.** *S. mansoni*/HBV co-infected or schistosome mono-infected mice were sacrificed at indicated timepoints post schistosome infection (4 – 16 weeks) and the parasitological parameters such as egg count (a) and granuloma sizes (b) were evaluated within the liver. A minimum of three mice per group were analysed at each timepoint and the results are shown as mean ± SEM. No statistical differences between the indicated groups were obtained after Mann-Whitney U-test for nonparametric distributed data.

To determine if the additional, acute HBV infection has an impact on schistosome-specific immune responses, we compared antigen-specific and independent immune responses raised in both animal groups during the acute and chronic phase of helminth infection. For that, we restimulated splenocytes (Figure 39 left side) and MLNs (Figure 39 right side) of co-infected and schistosome mono-infected mice with SEA or anti-CD3/CD28 beads and levels of IFN-γ were measured in the culture supernatant. As illustrated in Figure 39, upon antigen-specific stimulation, both animal groups responded with similar levels of IFN-γ during the acute (5 weeks *S. mansoni* infection + 3 weeks HBV infection) and chronic phase (16 weeks *S. mansoni* infection + 3 weeks HBV infection) of schistosome infection. Antigen-independent stimulation revealed significantly higher levels of IFN-γ in splenocytes of co-

infected mice during the acute phase of helminth infection, whereas obtained cytokine responses between MLNs of both animal groups did not differ later during the chronic phase (Figure 39). The absent effect of the additional viral infection on schistosome-specific immune responses was furthermore also shown in section 3.2.2.3.1, Figure 32, where both chronically schistosome infected groups (*S. mansoni* mono-infected and S.m./HBV co-infected) responded with similar levels of IL-10 to SEA and antigen-independent stimulation.

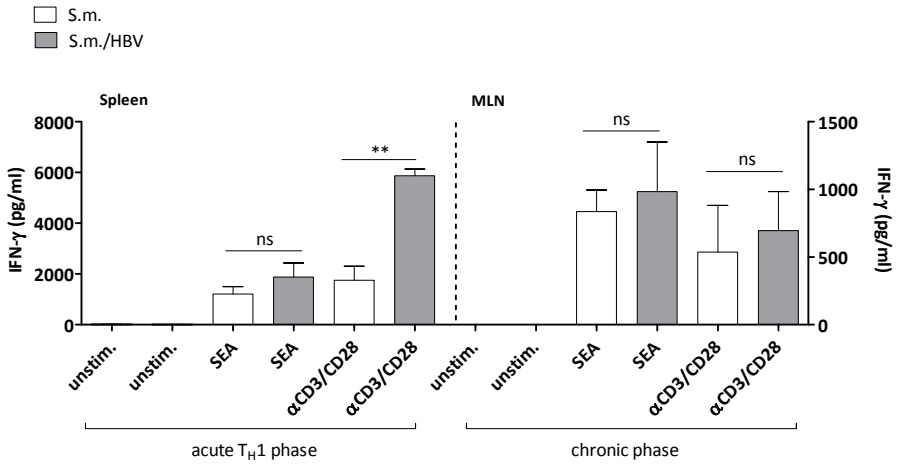


**Figure 39: Splenocytes and MLNs of co-infected mice respond with similar cytokine secretion to schistosome-specific stimulation.** Cytokine milieu in antigen-specific (SEA 20µg/ml) and independent (αCD3/CD28 beads) restimulted splenocytes and MLNs ($2x10^5$ cells/ml) of Sm/HBV co-infected and Sm mono-infected mice was determined by ELISA. Levels of IFN-γ were either measured in restimulated splenocytes during the acute phase of schistosome infection (5 weeks *S. mansoni* infection + 3 weeks HBV infection) or after 19 weeks of helminth infection (16 weeks *S. mansoni* infection + 3 weeks HBV infection) in MLNs. A minimum of three mice per group were analysed at each timepoint and bar graphs are shown as mean ± SEM. Asteriks show statistical differences (Mann-Whitney U-test) between the groups indicated by the brackets (**$P < 0.01$; not significant, n.s.).

Taken together these results indicate, that an acute HBV infection acquired during the acute or chronic phase of schistosome infection does not influence the helminth disease outcome, since co-infected and schistosome mono-infected mice responded equally to antigen-specific stimulation and had unaltered parasitological parameters.

### 3.2.3.2 *S. mansoni* infection develops normally in chronically HBV infected mice

Following up these results, we analysed the outcome of a secondary acquired schistosome infection on top of a pre-existing chronic HBV infection as well. 16 weeks post schistosome infection, we found equal parasite egg burdens and granuloma sizes in livers of co-infected HBV transgenic mice (HBVtg/Sm) when compared to livers of schistosome mono-infected animals (S.m.) and those with a concurrent acute HBV infection (S.m./HBV) (Figure 40a and b).

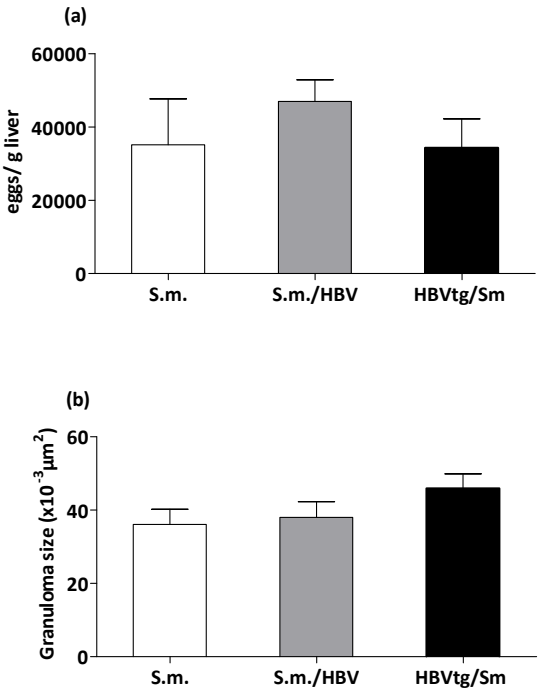


**Figure 40: Parasite egg burdens and granuloma sizes are not altered in chronically HBV infected mice with concurrent schistosome infection.** Co-infected HBVtg mice (HBVtg/S.m.), schistosome mono-infected (S.m.; 16 weeks *S. mansoni* infection) and those with an additional acute HBV infection (S.m./HBV, 16 weeks *S. mansoni* and acute HBV co-infection) were sacrificed 16 weeks post schistosome infection and the parasitological parameters such as egg count (a) and granuloma sizes (b) were evaluated within the liver. A minimum of three mice per group were analysed and the results are shown as mean ± SEM. No statistical differences between the indicated groups were obtained after Kruskal-Wallis and Dunn's Test for nonparametric distributed data.

In addition, 16 weeks post helminth infection re-stimulated MLNs of all indicated animal groups responded with similar levels of IFN-γ (Figure 41a) and IL-10 (Figure 41b) to schistosome-specific and antigen-independent stimulation conditions.

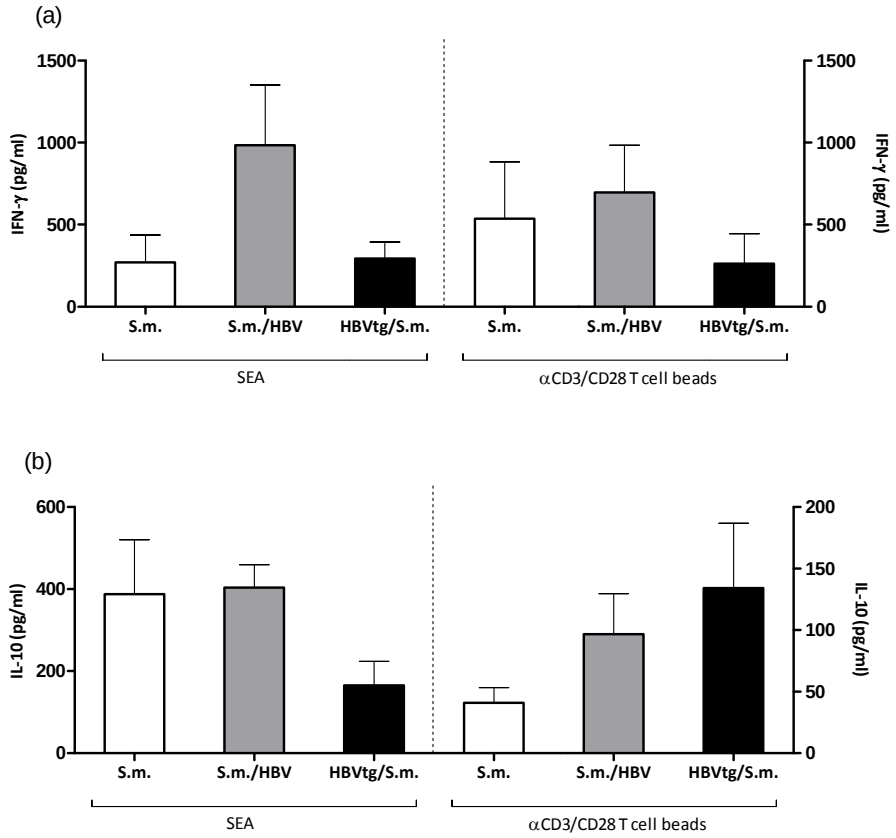


**Figure 41: Schistosome-specific immune responses are unaltered in co-infected HBVtg mice.** IFN-γ responses in antigen-specific (SEA 20µg/ml) and independent (αCD3/CD28 beads) restimulted MLNs (2x10$^5$ cells/ml) of co-infected HBVtg mice (HBVtg/S.m.), schistosome mono-infected (S.m.; 16 weeks *S. mansoni* infection) and those with an additional acute HBV infection (S.m./HBV, 16 weeks *S. mansoni* and acute HBV co-infection) were determined by ELISA 16 weeks post helminth infection. A minimum of three mice per group were analysed and data are shown as mean ± SEM. No statistical differences between the indicated groups were obtained after Kruskal-Wallis and Dunn's Test for nonparametric distributed data.

Taken together these results indicate, that a secondary acquired *S. mansoni* infection develops normally in chronically HBV infected mice, since schistosome-specific immune responses as well as parasitological parameters were comparable to those obtained from schistosome mono-infected animals and those with concomitant acute HBV infection.

## 3.2.4 Impact of the 'empty' adenoviral vector on *S. mansoni* disease outcome

To exclude a possible impact of the adenoviral vector itself on schistosome specific immune responses, we administered the 'empty' adenoviral vector, lacking HBV DNA (10$^9$ i.u.

Ad-Empty intravenously; section 2.2.5.1), instead of the AdHBV-X$^-$ vector (section 2.2.5.1) to 5 weeks schistosome-infected mice. The detailed experimental protocol is described in section 2.2.4.1.2.

### 3.2.4.1 Ad-Empty vector has no influence on schistosome specific immune responses and disease outcome

Three weeks post adenoviral infection – which corresponds to 8 weeks of schistosome infection – we found equal numbers of parasite eggs and similar granuloma sizes in livers of schistosome mono-infected mice (S.m.) and in those with an additional 'empty' adenoviral infection (S.m./Ad-Empty) (Figure 42a and b).

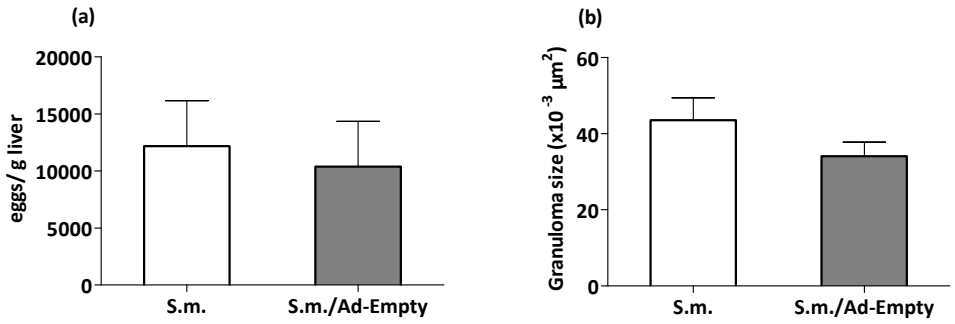


**Figure 42: Equal numbers of parasite eggs and similar granuloma sizes in schistosome infected animals with concomitant 'empty' adenoviral infection.** Co-infected (S.m./Ad-Empty) and schistosome mono-infected (S.m.) mice were sacrificed 8 weeks post schistosome infection and the parasitological parameters such as egg count (a) and granuloma sizes (b) were evaluated within the liver. A minimum of three mice per group were analysed and the results are shown as mean ± SEM. No statistical differences between the indicated groups were obtained after Mann-Whitney U-Test for nonparametric distributed data.

Furthermore, 8 weeks post helminth infection MLNs from schistosome mono-infected and S.m./Ad-Empty co-infected mice responded with equal levels of IFN-γ (Figure 43a) and IL-10 (Figure 43b) to antigen-specific and unspecific stimulation. Animals with Ad-Empty mono-infection (Ad-Empty) and uninfected mice (naïve) showed very low IFN-γ and no IL-10 secretion in both stimulation conditions (Figure 43a and b).

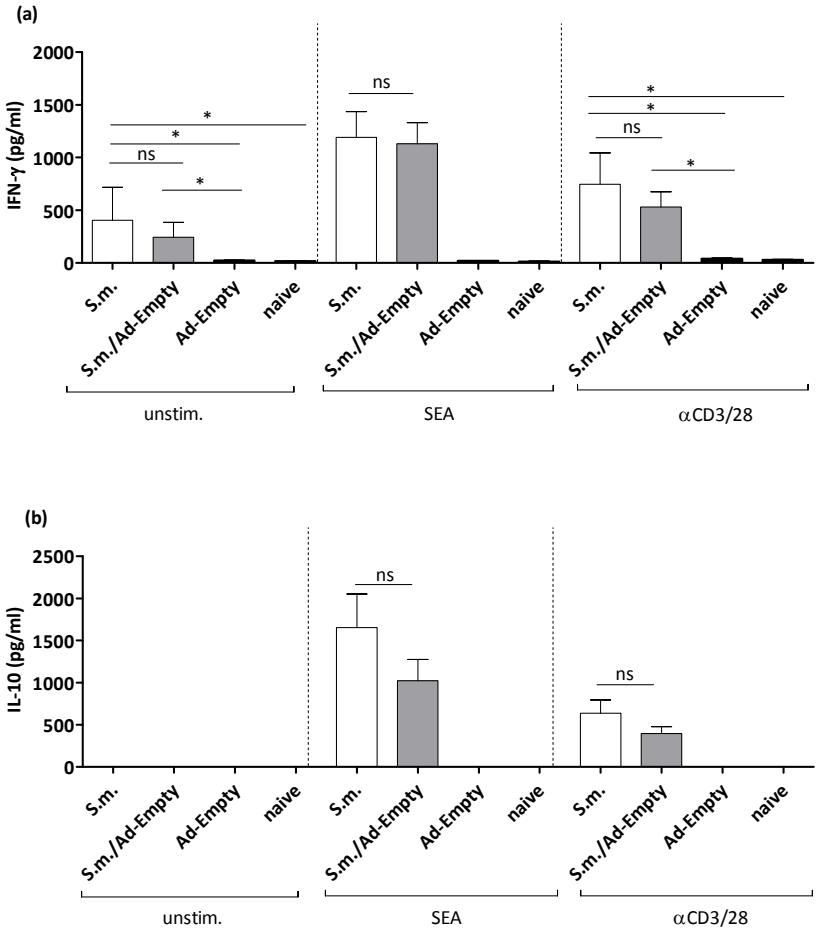


**Figure 43: No influence of empty adenoviral vector on *S. mansoni* specific immune responses.** Three weeks post adenoviral infection, MLNs ($2x10^5$ cells/ml) of *S. mansoni* mono-infected (n = 5), S.m./Ad-Empty co-infected (n = 4), Ad-Empty mono-infected (n = 5) and uninfected, naïve mice (n = 3) were either restimulated with SEA (20µg/ml) or αCD3/CD28 T cell beads. After 48 hours IFN-γ (a) and IL-10 levels (b) were measured in the supernatant of indicated animal groups by ELISA. Bar graphs are illustrated as mean ± SEM. Asteriks show statistical differences (Mann Whitney-U test for nonparametric distributed data) between the groups indicated by the brackets (*$P < 0.05$; not significant, n.s.).

Taken together, these results indicate that the empty adenoviral vector itself has no influence on immune responses generated during helminth infection and has no impact on parasitological parameters in co-infected mice.

## 3.2.5 Role of schistosome-induced regulatory T cells and IFN-γ production on viral clearance

Our HBV/*S. mansoni* co-infection experiments demonstrated a faster viral clearance of the acute HBV infection during the $T_H1$ and chronic phase of schistosome infection. In both cases we hypothesized that schistosome-induced IFN-γ secretion immediately acts on viral replication and induces a faster priming and proliferation of virus-specific T cells, leading to decreased viral loads observed in co-infected mice. Interestingly, during the chronic phase of schistosome infection, we showed that elevated levels of immunosuppressive, anti-inflammatory IL-10, neither suppressed the production nor the anti-viral activity of IFN-γ. During this phase, however, the role of schistosome-induced regulatory T cells on viral clearance needs to be considered, since previous studies of Prof. Protzer's group with HBV infected mice showed, that Treg cells per se delay viral clearance [114]: *Stross et al.* showed that 7 days post HBV infection Treg numbers increased locally in the liver of infected mice and delayed the development of virus-specific immune responses. In Treg-depleted DEREG mice virus elimination occurred faster (lower viral load and viral antigen levels) when compared to wildtype mice infected with HBV, demonstrating a role for Treg in the liver in controlling virus-specific immune responses rather than acting directly on hepatocytes. In this context it is important to investigate the impact of schistosome-induced Treg with a unique phenotype (section 1.1.6) on virus-specific immune responses.

### 3.2.5.1 The role of schistosome-induced regulatory T cells during the chronic phase of *S. mansoni* infection on viral replication in co-infected animals

To study the role of schistosome-induced Treg during the chronic phase of *S. mansoni* infection on viral replication we intraveniously administered $10^9$ i.u. AdHBV-$X^-$ to 17 weeks schistosome infected C57BL/6 and DEREG C57BL/6 mice. The DEREG (DEpletion of REGulatory T cells) mouse model is a BAC (bacterial artificial chromosome) transgenic mouse line which allows the specific depletion of $eGFP^+$ $Foxp3^+$ cells at specific timepoints during the infection through the administration of diphtheria toxin (DT) [249]. To deplete $Foxp3^+$ Treg we injected DT (1µg/mouse) i.p. into co-infected and HBV mono-infected DEREG mice on two consecutive days post viral infection (scheme 1). Viral replication and elimination was

subsequently monitored by measuring serum viral antigen levels 3 and 7 days post HBV infection. Schistosome infection was confirmed in all mice by detection of parasite eggs and granuloma formation in the liver and did not differ between the groups (data not shown).

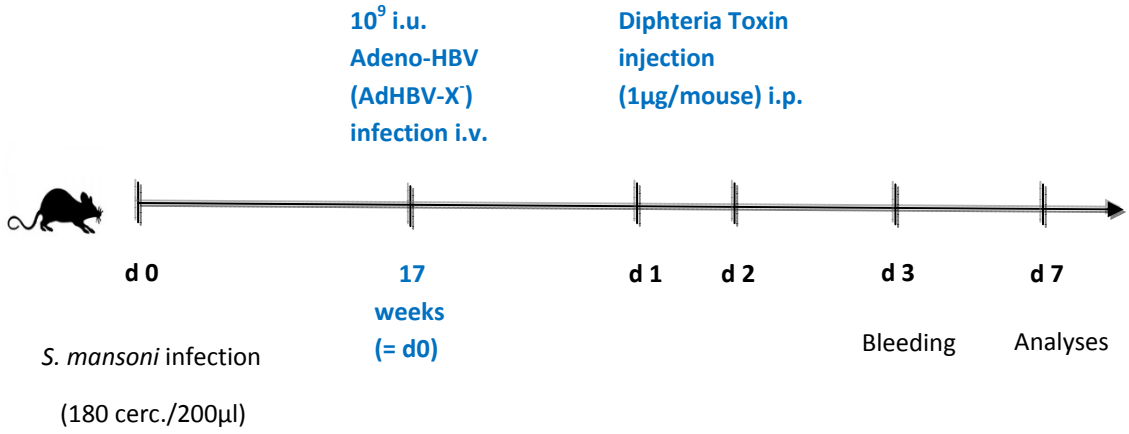


**Scheme 1: Experimental setup to analyse the role of schistosome-induced Treg on viral replication during the chronic phase of helminth infection.** *S. mansoni* infection in C57BL/6 and DEREG mice was performed with 180 cercariae i.p.. Acute AdHBV-X$^-$ ($10^9$ i.u. AdHBV-X$^-$) infection followed intraveniously 17 weeks post schistosome infection. Treg depletion in DEREG mice occurred on day 1 and 2 post viral infection via administration of DT (1µg/mouse i.p.) and viral serum-antigen levels were measured at day 3 and 7 in all mice. One week post HBV infection, animals were sacrificed and immunological parameters were investigated.

As depicted in Figure 44a, three days post viral infection the lowest HBsAg levels were measured in schistosome co-infected animals in general when compared to their HBV mono-infected counterparts. Here co-infected animals either Treg depleted (S.m./HBV $^{DT}$) or not (S.m./HBV), had significantly decreased HBsAg levels in comparison to HBV mono-infected mice without Treg depletion (HBV) (Figure 44a). Between both schistosome co-infected animal groups, viral antigen levels (HBsAg and HBeAg) remained unaltered at both time points post HBV infection. This indicates that the Treg depletion does not additionally enhance the typically observed faster viral clearance in co-infected mice (Figure 44a-d). Between both HBV mono-infected animal groups, significantly lower levels of HBeAg were observed only after 7 days of infection in Treg depleted mice (HBV $^{DT}$) (Figure 44d).

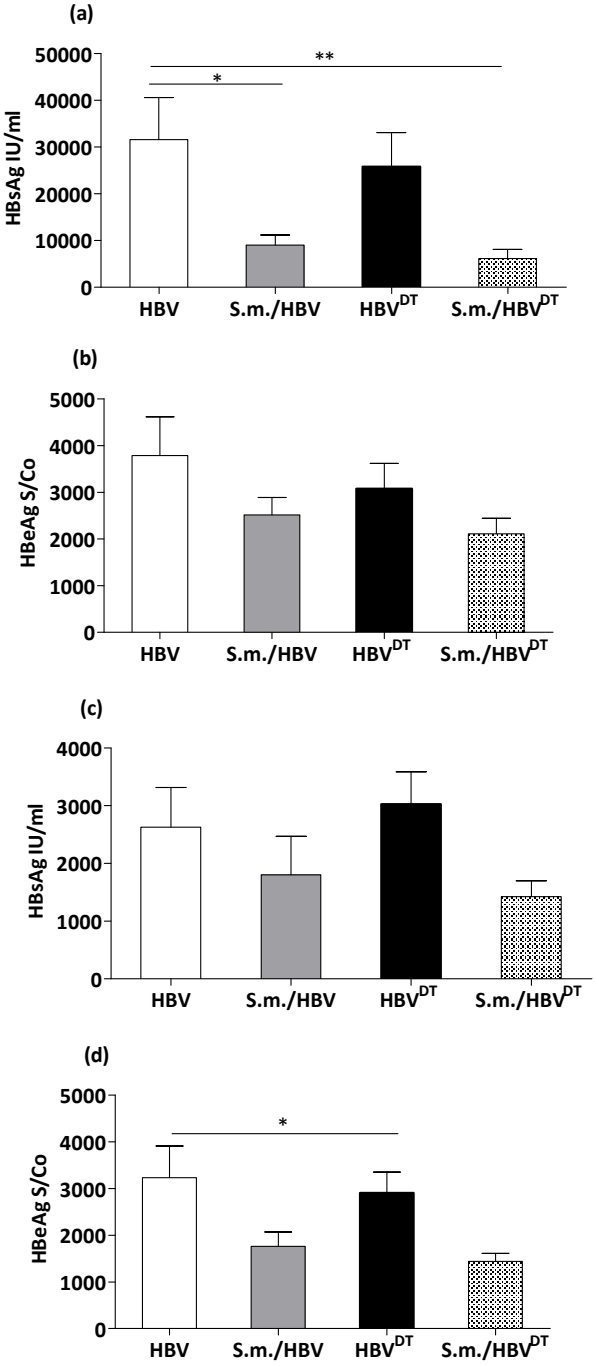


**Figure 44: Schistosome co-infection leads to lower viral replication rates independent of Treg.** Quantitative (HBsAg) and qualitative (HBeAg) detection of viral antigens in sera of co-infected, Treg depleted (S.m./HBV $^{DT}$ ; n=11), co-infected (S.m./HBV; n=11), HBV mono-infected, Treg depleted (HBV $^{DT}$; n=8) and HBV mono-infected (HBV; n=8) mice was performed with a microparticle enzyme assay and is shown for HBsAg as IU/ml and S/Co for HBeAg. (a, c) Levels of HBsAg and (b, d) HBeAg within sera of indicated animal groups 3 days (a, b) and 7 days (c, d) post viral infection. Results show data pooled from two independent experiments and are depicted as mean ± SEM. Statistical evaluation was calculated using ANOVA and Bonferroni's Multiple Comaprison Test for parametric distributed data (*$P < 0.05$ and **$P < 0.01$).

Furthermore, one week post viral infection, in comparison to HBV mono-infected mice without Treg depletion, a tendency towards lower amounts of HBV DNA was observed in livers of both co-infected (S.m./HBV and S.m./HBV$^{DT}$) and HBV$^{DT}$ animal groups (Figure 45). These results were in line with adenoviral DNA levels, where the lowest titers were found in S.m./HBV$^{DT}$ mice (Figure 45).

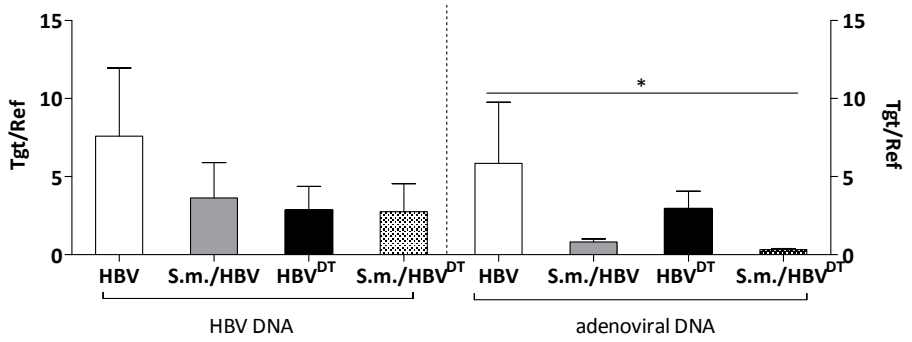


**Figure 45: Schistosome co-infected and HBV$^{DT}$ animal had lower amounts of HBV and adenoviral genomes.** Adenoviral- and HBV genomes were detected in DNA isolated from liver tissue samples by real-time PCR. The relative quantification of viral DNA compared to the murine reference gene (Tgt/Ref) is shown in co-infected, Treg depleted (S.m./HBV $^{DT}$ ; n=11), co-infected (S.m./HBV; n=11), HBV mono-infected, Treg depleted (HBV $^{DT}$; n=8) and HBV mono-infected (HBV; n=8) livers one week post viral infection. Results show data pooled from two independent experiments and are illustrated as mean ± SEM. Statistical evaluation between the indicated groups was calculated after Kruskal-Wallis and Dunn's Test for nonparametric distributed data (*$P$ < 0.05).

To determine the effects of Treg depletion on the cytokine milieu in co-infected and HBV mono-infected mice, we next analysed schistosome-specific and independent immune responses in all animal groups. As depicted in Figure 46a, splenocytes of both schistosome infected animal groups (S.m./HBV and S.m./HBV$^{DT}$) produced similar amounts of IFN-γ upon SEA stimulation. Upon antigen-independent stimulation, however, splenocytes of S.m./HBV$^{DT}$ mice secreted significantly higher amounts of IFN-γ when compared to their co-infected counterparts without Treg depletion (S.m./HBV). As expected, we further detected significantly higher IFN-γ secretion in antigen-independent restimulated splenocytes of HBV$^{DT}$ animals in comparison to HBV mono-infected counterparts (HBV). Moreover, like in previous co-infection experiments, we observed significantly higher IFN-γ secretion in antigen-independent restimulated splenocytes of S.m./HBV animals when compared to HBV mono-

infected counterparts. Upon Treg depletion however, IFN-γ levels did not differ between S.m./HBV$^{DT}$ and HBV$^{DT}$ animal groups (Figure 46a).

In addition, upon SEA stimulation mesenterial lymph node cells of both schistosome infected groups (S.m./HBV and S.m./HBV$^{DT}$) responded with equal levels of IFN-γ. Antigen-independent stimulation, however revealed significantly higher IFN-γ secretion in MLNs of S.m./HBV$^{DT}$ animals when compared to S.m./HBV mice (Figure 46b). Of note, like in previous experiments, MLNs of schistosome co-infected mice (S.m./HBV and S.m./HBV$^{DT}$) secreted higher cytokine levels in comparison to MLNs of HBV mono-infected counterparts (HBV and HBV$^{DT}$) (Figure 46b).

In contrast to unaltered IFN-γ levels, between both schistosome infected animal groups (S.m./HBV and S.m./HBV$^{DT}$) IL-10 secretion was significantly increased in SEA- and antigen-independent restimulated splenocytes (Figure 46c) and MLNs (Figure 46d) of S.m./HBV$^{DT}$ mice. The increased IL-10 production was furthermore also seen in antigen-independent restimulated splenocytes of S.m./HBV co-infected animals in comparison to HBV mono-infected mice (Figure 46c). Between both HBV mono-infected animal groups (HBV and HBV$^{DT}$), Treg depletion (HBV$^{DT}$) led to an increased IL-10 secretion in antigen-independent restimulated splenocytes (Figure 46c).

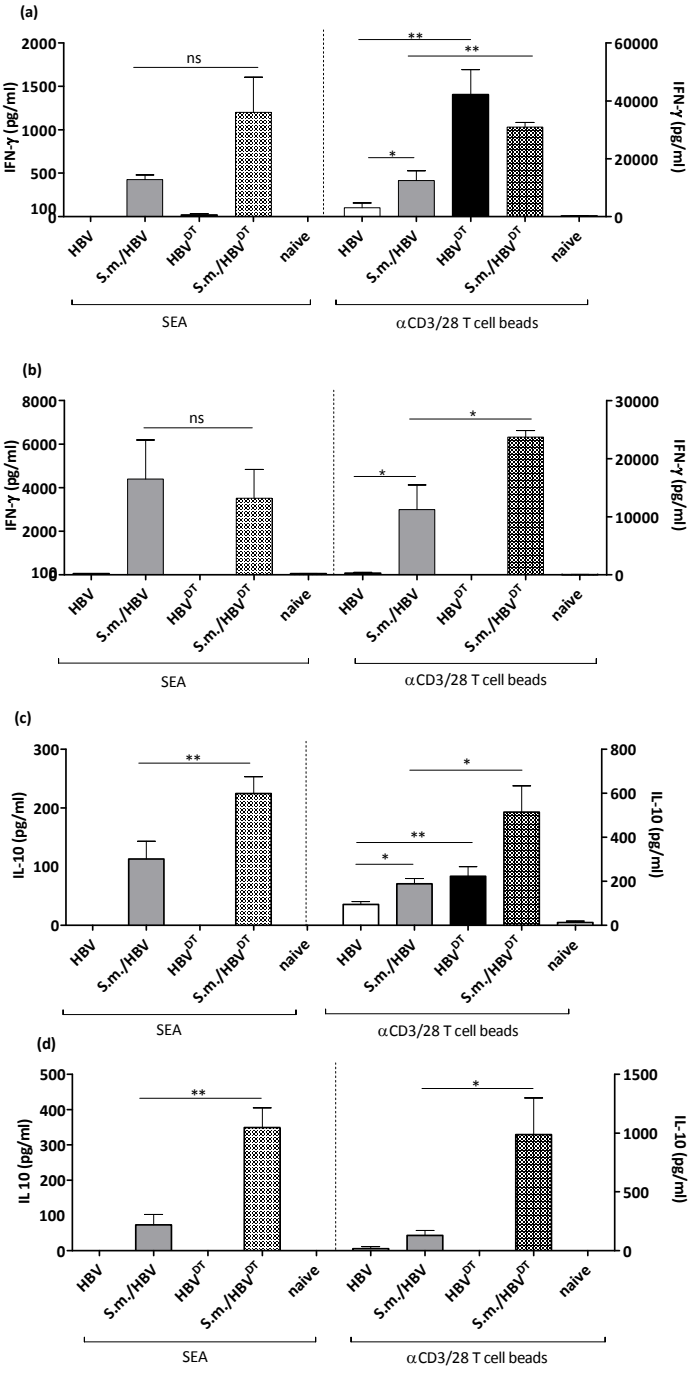


**Figure 46: Treg depletion during schistosome infection leads to enhanced IL-10 secretion independent of HBV co-infection.** One week post HBV infection, splenocytes and MLNs ($2x10^5$ cells/ml) of co-infected, Treg depleted (S.m./HBV $^{DT}$ ; n=5), co-infected (S.m./HBV; n=6), HBV mono-infected, Treg depleted (HBV $^{DT}$; n=3), HBV mono-infected (HBV; n=5) and uninfected (naïve, n=3) mice were either re-stimulated with SEA (20µg/ml) or αCD3/CD28 T cell beads (cell to bead ratio 1:1). After 48 hours IFN-γ (a, b) and IL-10 (c, d) secretion were measured in the supernatant of either splenocytes (a, c) or MLNs (b, d) by ELISA. Bar graphs show representative results from two independent experiments and data is illustrated as mean ± SEM. Asteriks show statistical differences (Mann-Whitney U-test) between the groups indicated by the brackets (*$P < 0.05$, **$P < 0.01$ and ***$P < 0.001$; not significant, n.s.).

To determine the effects of Treg depletion on the establishment of virus-specific peripheral and liver-resident T cell responses, we analysed frequencies of $CD8^+$ and $CD4^+$ IFN-$\gamma^+$ as well as $CD4^+$ IL-$2^+$ T cells upon HBcP3 stimulation. Flow cytometric analysis revealed significantly higher frequencies of $CD4^+IL\text{-}2^+$ effector T cells in livers of Treg depleted co-infected mice (S.m./$HBV^{DT}$) when compared to co-infected animals without DT administration (S.m./HBV) (Figure 47a). Within splenocytes, however, similar $CD4^+IL\text{-}2^+$ responses were detected in all indicated animal groups (Figure 47a).

HBV-specific $CD4^+IFN\text{-}\gamma^+$ T cell responses were significantly elevated in livers of S.m./$HBV^{DT}$ mice when compared to LALs of S.m./HBV animals (Figure 47b). LALs of Treg depleted HBV mono-infected mice ($HBV^{DT}$) did also respond with a clear tendency towards elevated frequencies of $CD4^+IL\text{-}2^+$ T cells to HBcP3 stimulation (Figure 47b). Splenocytes of indicated animal groups responded with equal frequencies of $CD4^+IFN\text{-}\gamma^+$ T effector cells to HBV-specific restimulation (Figure 47b).

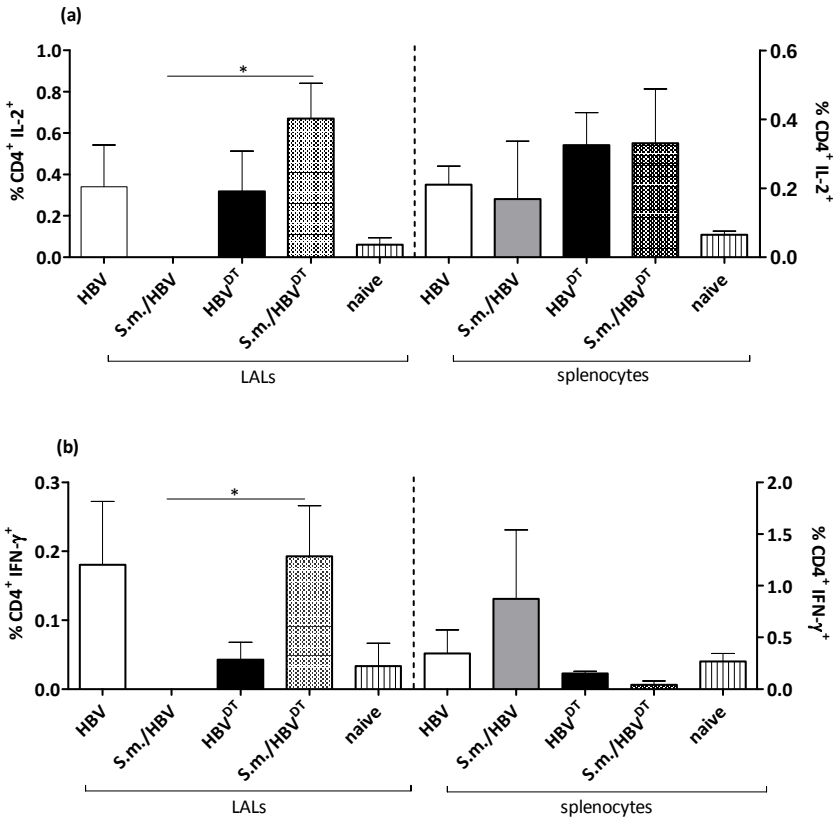


**Figure 47: Increased frequencies of HBV-specific $CD4^+IL2^+$ and $CD4^+IFN\text{-}\gamma^+$ T cells in livers of co-infected Treg depleted mice.** Frequencies of $CD4^+$ IL-$2^+$ (a) and $CD4^+IFN\text{-}\gamma^+$ T cells (b) upon HBcP3 stimulation in livers and the spleen of co-infected, Treg depleted (S.m./$HBV^{DT}$; n=5), co-infected (S.m./HBV; n=6), HBV mono-infected, Treg depleted ($HBV^{DT}$; n=3), HBV mono-infected

(HBV; n=5) and uninfected (naïve, n=3) mice. Bar graphs are illustrated as mean ± SEM and show representative results from two independent experiments. Statistical evaluation between the indicated groups was calculated after Kruskal-Wallis and Dunn's Test for nonparametric distributed data (*$P < 0.05$).

Populations of HBV-specific CD8$^+$IFN-$\gamma^+$ T cells did not differ in both organs of indicated animal groups, however a tendency towards elevated frequencies of virus-specific CD8$^+$IFN $\gamma^+$ T cells were observed in splenocytes of S.m./HBV animals (Figure 48).

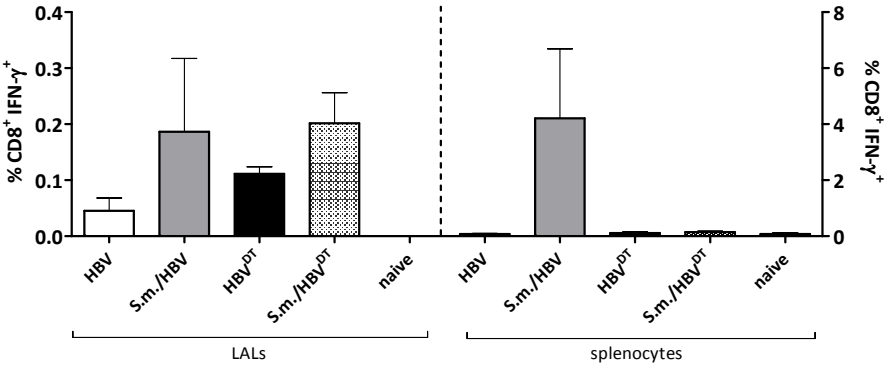


**Figure 48: Unaltered HBV-specific CD8$^+$IFN-$\gamma^+$ T cell response in livers and increased response in spleens of co-infected mice without Treg depletion.** Fequencies of CD8$^+$IFN-$\gamma^+$ T cells upon HBcP3 stimulation in livers and the spleen of co-infected, Treg depleted (S.m./HBV $^{DT}$ ; n=5), co-infected (S.m./HBV; n=6), HBV mono-infected, Treg depleted (HBV $^{DT}$; n=3), HBV mono-infected (HBV; n=5) and uninfected (naïve, n=3) mice. Bar graphs are illustrated as mean ± SEM and show representative results from two independent experiments. No statistical differences between the indicated groups were obtained after Kruskal-Wallis and Dunn's Test for nonparametric distributed data.

Taken together, these results show no prominent role of schistosome-induced Treg on viral clearance. In comparison to HBV-mono-infected mice (HBV$^{DT}$ and HBV), lower viral loads were observed in both schistosome co-infected animal groups (S.m./HBV$^{DT}$ and S.m./HBV), indicating that Treg depletion per se does not further enhance the accelerated viral clearance in co-infected mice. It is more likely that in these mice the lower viral replication rates are again attributed to the anti-viral effect of schistosome-induced IFN-$\gamma$.

### 3.2.5.2 The role of schistosome-induced IFN-γ production on viral clearance

To clarify the question whether decreased viral antigen levels within co-infected animals result from the impact of elevated schistosome-induced IFN-γ production we therefore performed experiments in C57BL/6 IFN-$\gamma^{-/-}$ mice either co-infected with *S. mansoni* (5 weeks) and HBV or HBV alone. Groups of wildtype C57BL/6 mice either co-infected or HBV mono-infected served as control. The detailed experimental protocol is described in section 2.2.4.1.2.

#### 3.2.5.2.1 Schistosome infection in IFN-γ-deficient C57BL/6 mice develops normally in terms of parasite development and dynamics of $T_H2$ responses

*Straubinger et al.* recently showed that the schistosome infection in IFN-γ-deficient BALB/c mice develops normally in terms of parasite development and dynamics of $T_H2$ T cell responses [258]. To figure out if this is the case also in C57BL/6 IFN-$\gamma^{-/-}$ animals, we analysed whether schistosome-specific immune responses in *S. mansoni* mono-infected and co-infected C57BL/6 IFN-$\gamma^{-/-}$ animals were comparable to those of infected wildtype counterparts. As depicted in Figure 49, three days post viral infection, SEA-restimulated splenocytes of schistosome mono-infected IFN-$\gamma^{-/-}$ mice produced equal amounts of IL-13 (Figure 49a) and IL-10 (Figure 49b) when compared to *S. mansoni* mono-infected wildtype mice. In addition, also co-infected IFN-$\gamma^{-/-}$ and wildtype mice responded with similar levels of both cytokines to antigen-specific restimulation (Figure 49). At this time point during helminth infection, no schistosome-specific IL-4 secretion was observed in all animal groups (data not shown).

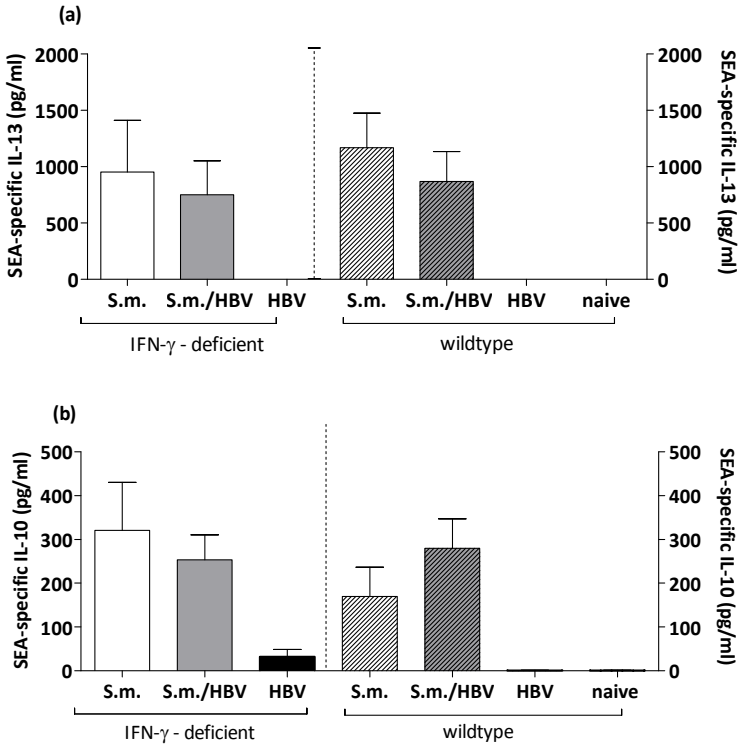


**Figure 49: Schistosome-specific cytokine production is unaltered in C57BL/6 IFN-γ $^{-/-}$ mice.** Three days post HBV infection – which corresponds to 5.5 weeks of schistosome infection, splenocytes (2x10$^5$ cells/ml) of indicated animal groups were restimulated with SEA (20µg/ml). After 48 hours levels of IL-13 (a) and IL-10 (b) were measured in the supernatant by ELISA. A minimum of three mice were analysed and data is illustrated as mean ± SEM. No statistical differences were obtained after Kruskal-Wallis and Dunn's Test for nonparametric distributed data.

Three weeks post HBV infection – which corresponds to 8 weeks of schistosome infection, splenocytes of schistosome infected IFN-$\gamma^{-/-}$ and wildtype mice still responded with similar levels of IL-4, IL-13 and IL-10 upon antigen-specific and antigen-independent restimulation (Figure 50). The same situation was reflected in restimulated MLNs (data not shown).

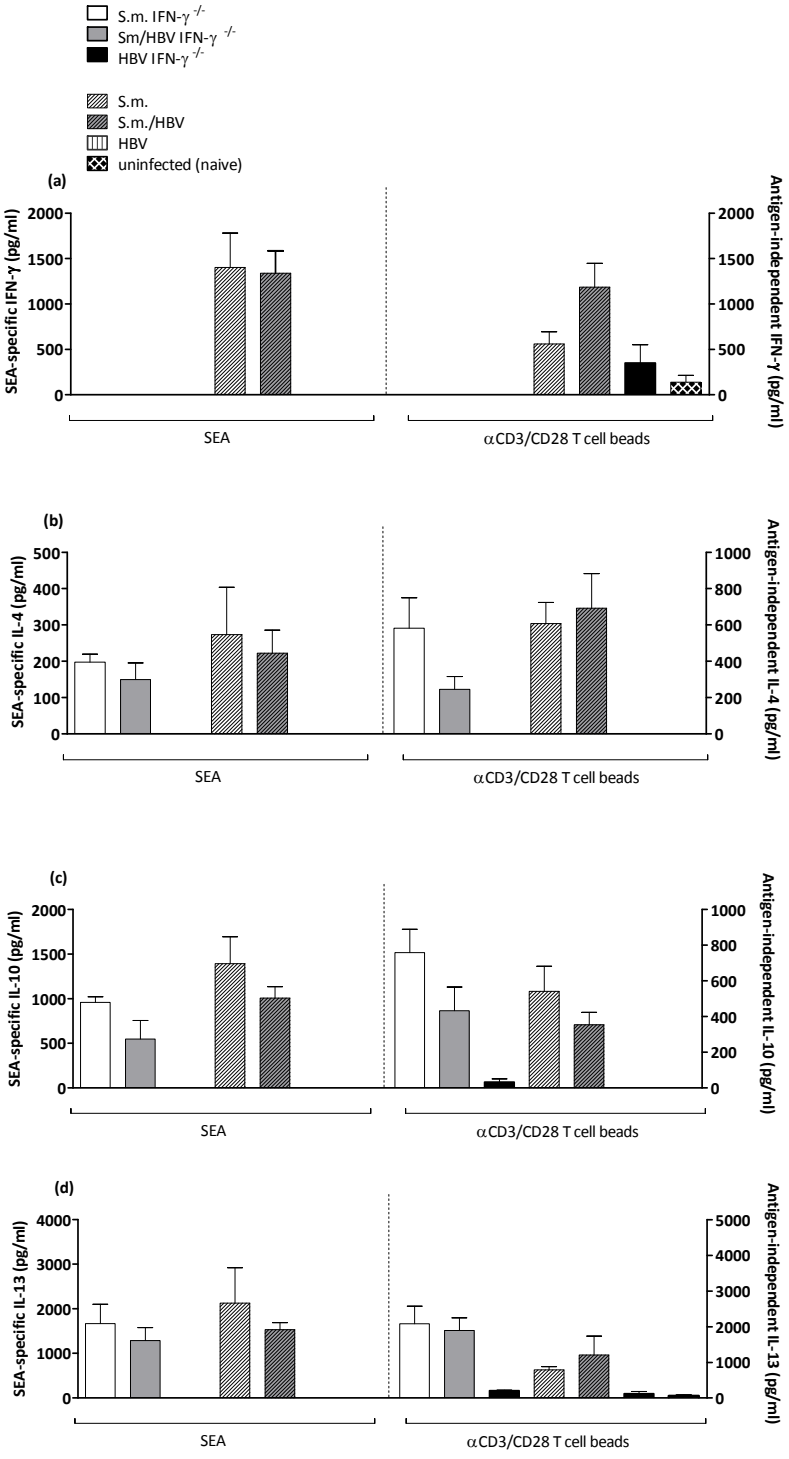


**Figure 50: Splenocytes of C57BL/6 IFN-γ $^{-/-}$ mice respond similar to schistosome-specific and antigen-independent stimulation.** Three weeks post HBV infection – which corresponds to 8 weeks of schistosome infection, splenocytes (2x10$^5$ cells/ml) of indicated animal groups were either restimulated with SEA (20µg/ml) or αCD3/CD28 T cell beads (cell to bead ratio 1:1). After 48 hours levels of IFN-γ (a), IL-4 (b), IL-10 (c) and IL-13 (d) were measured in the supernatant by ELISA. A minimum of three mice were analysed and data is shown as mean ± SEM. No statistical differences were obtained after Kruskal-Wallis and Dunn's Test for nonparametric distributed data.

Furthermore, three weeks post viral infection (corresponding to 8 weeks of schistosome infection) we found equal numbers of parasite eggs and similar granuloma sizes in livers of schistosome infected IFN-$\gamma^{-/-}$ and wildtype mice (Figure 51). These data demonstrate that the schistosome infection in IFN-γ-deficient C57BL/6 mice develops normally in terms of parasite development and dynamics of $T_H1/T_H2$ T cell responses.

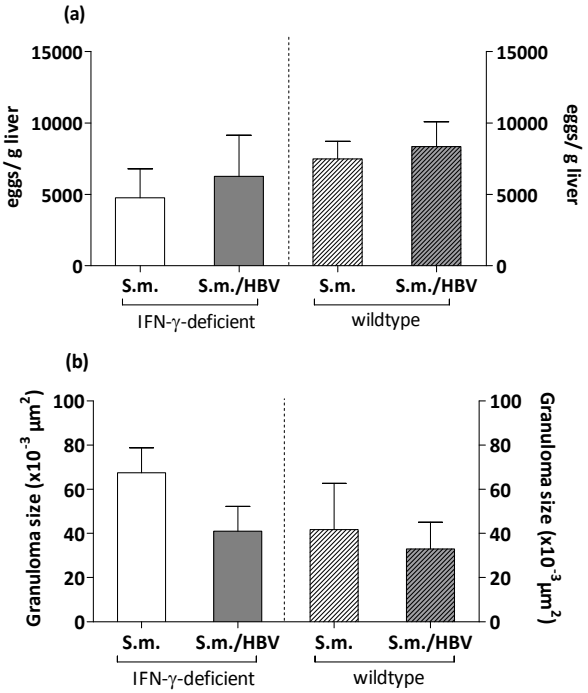


**Figure 51: Parasite egg burdens and granuloma sizes were comparable in schistosome infected C57BL/6 IFN-γ $^{-/-}$.** Schistosome infected IFN-$\gamma^{-/-}$ and wildtype mice were sacrificed 8 weeks post schistosome infection and the parasitological parameters such as egg count (a) and granuloma sizes (b) were evaluated within the liver. A minimum of three mice per group were analysed and the results are shown as mean ± SEM. No statistical differences between the indicated groups were obtained after Kruskal-Wallis and Dunn's Test for nonparametric distributed data.

### 3.2.5.2.2 Co-infected IFN-γ-deficient C57BL/6 mice fail to show enhanced viral clearance

To point out the central role of schistosome-induced IFN-γ on viral clearance, like in previous experiments, we bled mice at day 3, 7, 14 and 21 post HBV infection, and monitored the viral replication rates by measuring serum viral antigen levels. Schistosome infection was confirmed in all mice by detection of parasite eggs and granuloma formation in the liver (Figure 51).

As depicted in Figure 52 co-infected IFN-$\gamma^{-/-}$ mice failed to show enhanced viral clearance when compared to co-infected wildtype mice and had serum virus antigen levels comparable to HBV mono-infected groups (Figure 52a - d). Between both HBV mono-infected animal groups, viral antigen levels did not differ throughout the first two weeks of infection (data not shown). 21 days post viral infection, however, IFN-$\gamma^{-/-}$ mice had elevated levels of HBeAg and failed to clear the virus as fast as their mono-infected wildtype counterparts (Figure 52d). Throughout the whole course of infection, S.m./HBV co-infected wildtype mice presented the lowest viral antigen titers and consequently the fastest viral clearance (Figure 52a - d).

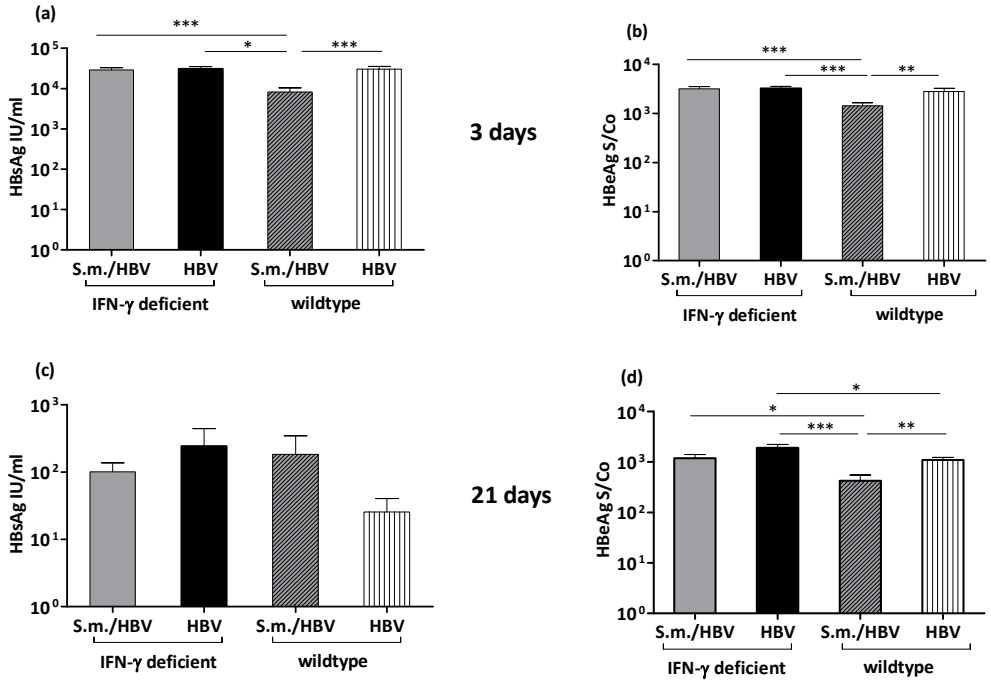


**Figure 52: Increased viral antigens in sera of co-infected IFN-$\gamma^{-/-}$ mice.** (a, c) Levels of HBsAg and (b, d) HBeAg in sera of S.m./HBV co-infected IFN-$\gamma^{-/-}$ (n=8), co-infected wildtype (n=8), HBV mono-infected IFN-$\gamma^{-/-}$ (n=5) and HBV mono-infected wildtype (n=5) mice at indicated timepoints post viral infection. Data is shown as mean ± SEM. Statistical evaluation was calculated using ANOVA and Bonferroni's Multiple Comaprison Test for parametric distributed data (*$P$ < 0.05, **$P$ < 0.01 and ***$P$ < 0.001).

Three days (Figure 53a) and three weeks (Figure 53b) post viral infection, the relative quantification of HBV and adenoviral genomes revealed significantly higher amounts of HBV DNA in livers of co-infected and HBV mono-infected IFN-$\gamma^{-/-}$ mice when compared to co-

infected wildtype mice. In comparison to HBV mono-infected wildtype livers, however, both IFN-$\gamma^{-/-}$ groups presented similar HBV genome numbers in their livers (Figure 53). Of note, at both indicated time points adenoviral DNA titers did not differ between the animal groups (Figure 53).

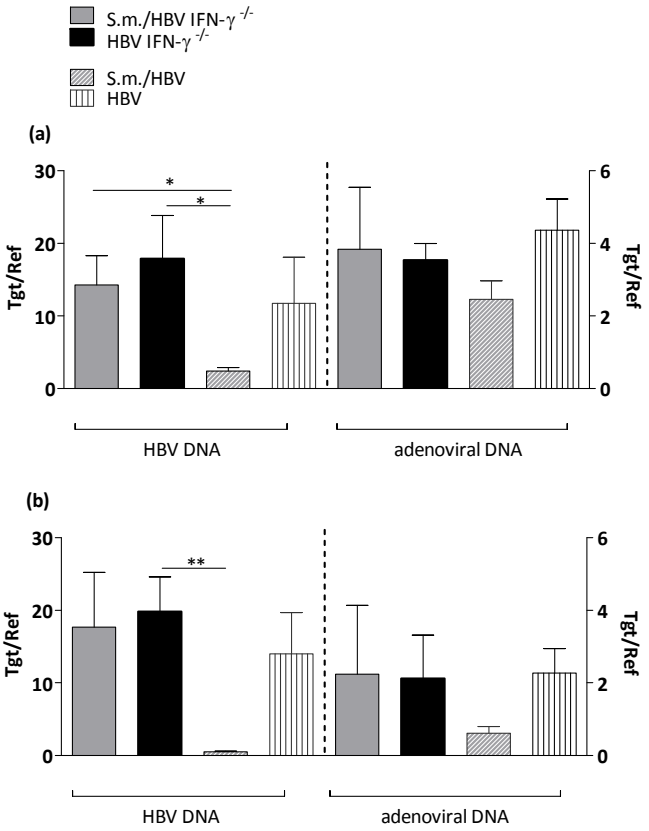


**Figure 53: Increased numbers of HBV genomes in livers of co-infected IFN-$\gamma^{-/-}$ mice.** Adenoviral- and HBV genomes were detected in DNA isolated from liver tissue samples by real-time PCR. The relative quantification of viral DNA compared to the murine reference gene (Tgt/Ref) is shown in S.m./HBV co-infected IFN-$\gamma^{-/-}$ (n=5), co-infected wildtype (n=4), HBV mono-infected IFN-$\gamma^{-/-}$ (n=5) and HBV mono-infected wildtype (n=4) livers 3 days (a) and 3 weeks (b) post viral infection. Bar graphs show data as mean ± SEM. Statistical evaluation between the indicated groups was performed by using the Kruskal-Wallis and Dunn's Test for nonparametric distributed data (*$P < 0.05$ and **$P < 0.01$).

These data indicate that the lack of IFN-$\gamma$ leads to increased viral antigen levels and elevated numbers of HBV genomes in co-infected IFN-$\gamma$-deficient mice and point towards a major role of schistosome induced IFN-$\gamma$ in viral clearance.

To analyse whether the absence of IFN-γ has an impact on the cell composition present in the spleen and in the liver, we analysed different effector cell populations upon HBV-specific stimulation via Flow Cytometry. Virus-specific peripheral and liver-resident T effector cell responses revealed elevated frequencies of $CD4^+$ $Foxp3^-$ $IL\text{-}10^+$ responses in both organs of S.m./HBV co-infected and HBV mono-infected IFN-γ-deficient animals as well as in co-infected and HBV mono-infected wildtype counterparts (Figure 54a and b). Furthermore, upon HBV-specific restimulation, a tendency towards elevated proportions of $CD4^+$ $IL\text{-}2^+$ effector T cells were detected in livers of co-infected IFN-γ-deficient mice when compared to livers of co-infected wildtype mice (Figure 54a). LALs from both HBV mono-infected animal groups, however, displayed similar frequencies of HBV-specific $CD4^+$ $IL\text{-}2^+$ T cells (Figure 54a). HBcP3-restimulated splenocytes of co-infected and HBV mono-infected animal groups responded with similar proportions of $CD4^+$ $IL\text{-}2^+$ effector T cells (Figure 54b). Of note, upon antigen-specific restimulation no $CD4^+$ $IL\text{-}4^+$ T effector cells were detected in both organs of all animal groups (data not shown).

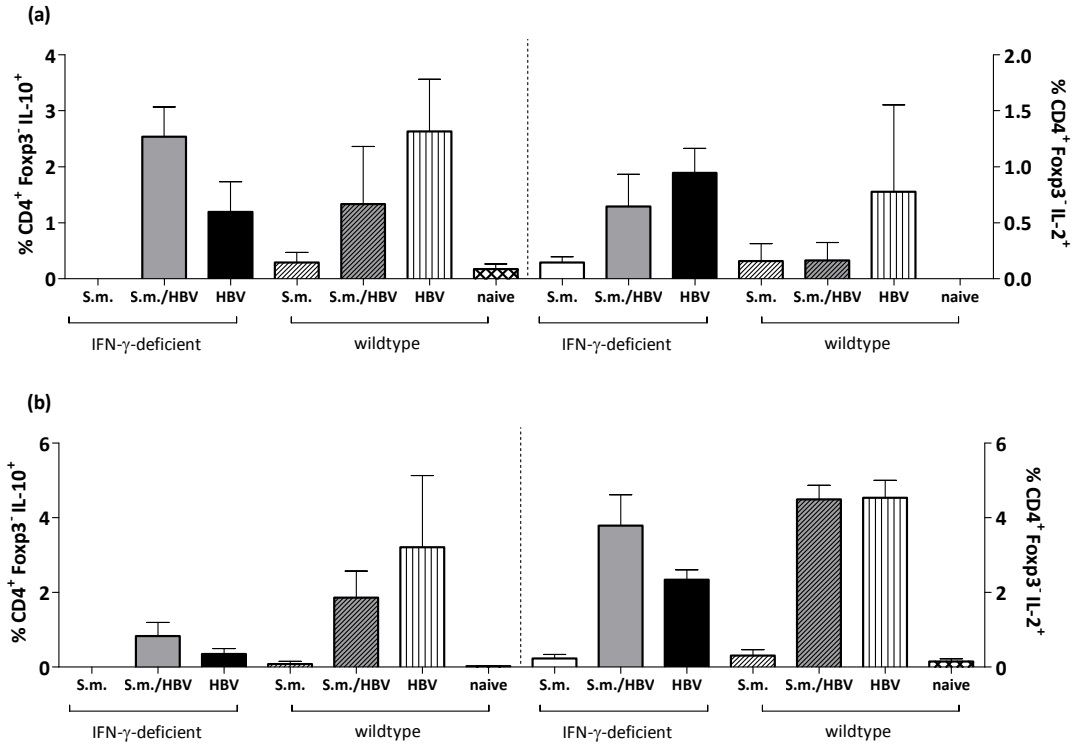


**Figure 54: Unaltered frequencies of virus-specific $CD4^+$ $Foxp3^-$ $IL\text{-}10^+$ / $IL\text{-}2^+$ T effector cells in organs of infected mice.** Frequencies of $CD4^+$ $Foxp3^-$ $IL\text{-}10^+$ and $CD4^+$ $Foxp3^-$ $IL\text{-}2^+$ T cells upon HBcP3 stimulation in livers (a) and the spleen (b) of indicated animal groups. A minimum of three mice per group were analysed and graphs are shown as mean ± SEM. Asteriks show statistical differences

(Kruskal Wallis and Dunn's Test) between the groups indicated by the brackets (*$P < 0.05$).

Finally, we monitored frequencies of liver-resident and splenic virus-specific $CD4^+$ and $CD8^+IFN\text{-}\gamma^+$ T cells. Like in previous co-infection experiments, in LALs and splenocytes of co-infected wildtype mice we observed a tendency towards higher frequencies of HBV-specific $CD4^+$ $IFN\text{-}\gamma^+$ (data not shown) and $CD8^+IFN\text{-}\gamma^+$ T cells when compared to HBV mono-infected wildtype mice (Figure 55).

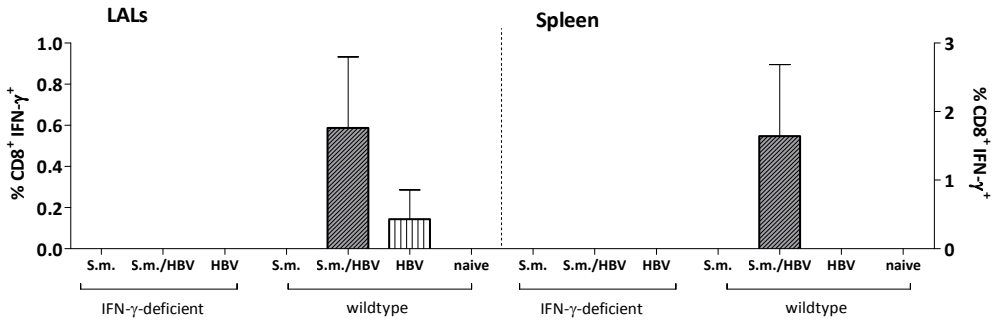


**Figure 55: Elevated frequencies of virus-specific $CD8^+IFN\text{-}\gamma^+$ T cells in livers and spleens of co-infected wildtype mice.** Frequencies of $CD8^+$ $IFN\text{-}\gamma^+$ T cells upon HBcP3 stimulation in livers (right side) and the spleen (left side) of indicated animal groups. A minimum of three mice per group were analysed and graphs are shown as mean ± SEM. No statistical differences were observed after Kruskal Wallis and Dunn's Test for non-parametric distributed data.

In summary, we found comparable serum virus antigen and DNA amounts between co-infected $IFN\text{-}\gamma^{-/-}$ mice and HBV mono-infected mice, since no schistosome-induced $CD4^+IFN\text{-}\gamma^+$ immune response and no virus-specific $CD4^+$ and $CD8^+$ $IFN\text{-}\gamma^+$ immune response has developed. Taken together, these data point towards a major role of schistosome induced IFN-γ in viral clearance because in comparison to co-infected wildtype mice, co-infected IFN-γ-deficient mice failed to show enhanced viral clearance.

# 4 Discussion

One of the main complications of hepatitis C and B virus infection is the development of chronic hepatitis after an acute infection, since these individuals are at high risk to develop liver cirrhosis and hepatocellular carcinoma. Interestingly, epidemiological studies reported that chronic hepatitis C and B develop at a higher frequency in developing countries in which co-infections with several helminth species, such as *S. mansoni* are common [105, 106, 108, 109, 111-113, 152, 177, 180]. Since helminths rely on their host's survival for a successful life cycle they have co-evolutionally adopted several mechanisms to evade and modulate the host's immune response [3, 25, 26]. In schistosomiasis or Bilharzia, it has been shown that for the parasite, a balanced immune response by the host is more acceptable than no immune response at all. This balance or even 'tolerance' is maintained by strong immune regulatory processes such as regulatory T cells induced during the chronic infection [27, 28]. We have previously shown that during schistosome infection, Tregs expand in parallel with effector T cell populations and change their phenotype acquiring stronger suppressive properties and expressing molecules like cytotoxic GrzB [54, 77, 78]. However, little remains known about the impact of schistosome infection on other chronic diseases in humans, which is of imminent importance since especially in rural areas endemic for schistosomiasis, chronically infected individuals are often exposed also to other pathogens such as viruses [106, 152]. Since chronic hepatitis C and B virus infections usually develop in individuals who fail to mount a strong and sustained virus-specific $CD8^+$ and $CD4^+$ immune response [139, 259] in schistosome co-infected individuals, the question arises whether the strong immune regulatory- and even suppressive capacities of helminths might contribute to HCV and HBV persistance by compromising anti-viral immune responses. In addition it has to be considered that dynamic schistosome-specific immune responses, ranging from an initial $T_H1$- to $T_H2$- and eventually long-term immunosuppression (see section 3.2.1.1) might additionally influence the establishment of an effective anti-viral immune response in a phase-dependent manner. Thus, the effects of pre-existing helminth infections on concomitant HCV/HBV infection are hard to predict and the question arises how the cell composition and the cytokine milieu present during the different immune phases of schistosome infection (see section 3.2.1.1), influence the outcome of a secondary acquired hepatitis C or B virus infection.

The central aims in this study were therefore to determine whether schistosome-induced immunomodulation could have an impact on the severity and course of another chronic liver disease, hepatitis C or B virus infection and whether this is associated with functional effector T cell and nTreg/iTreg changes. To address the different questions we had the opportunity to investigate *S. mansoni* and HCV co-infection in a human study and concomitant HBV and schistosomiasis in a mouse study.

## 4.1 Human *Schistosoma mansoni* and hepatitis C virus co-infection

The first part of this thesis addressed the interrelationship between *S. mansoni* and Hepatitis C virus infection. Here, the parasite seems to accelerate the progression of the liver disease, as liver cirrhosis and hepatocellular carcinoma are more common within co-infected individuals [110, 148-151]. Whilst 30% of HCV mono-infected individuals recovered from acute infections, all those with an additional *S. mansoni* infection progressed to a chronic state [152]. Moreover, compared to HCV mono-infected individuals, these patients exhibited higher HCV-positive RNA titres, higher necro-inflammatory and fibrotic scores in the liver and poor responses to interferon therapy [108, 151-156] (see section 1.2.1.2). Since the underlying mechanisms leading to the aggravated liver disease outcome are still not understood, our human study aimed to investigate whether phenotypic changes of $Foxp3^+$ Treg, induced during human schistosomiasis, could be responsible for the reported failure to raise effective antiviral $CD4^+$ and $CD8^+$ T cell responses [140-142, 157, 158]. Impaired antiviral immune responses would then lead to loss of viral replication control and eventually to a more pronounced liver disease. Thus, we analysed liver function and viral load as well as Treg, T effector cell frequencies and specifically the nTreg/iTreg distribution within patients with HCV mono-infection and those with concomitant Schistosoma infection.

### 4.1.1 Schistosome infection aggravates HCV-related liver disease and induces changes in the regulatory T-cell phenotype

Within our study, we found that HCV patients with schistosoma co-infection had significantly higher liver transaminases levels as well as elevated HCV-RNA titres, indicating that concomitant schistosome infection indeed aggravates liver disease and inhibits virus

elimination (see section 3.1.1.1). As previous studies revealed that ALT and AST levels in endemic normals and *S. mansoni* mono-infected individuals were comparable [260], our current findings substantiate other studies performed in Egypt demonstrating aggravated liver disease and less controlled viral replication in schistosome co-infected HCV patients [105, 106, 108, 110, 151, 154, 156]. Viral clearance is known to correlate with strong and sustained virus-specific $CD4^+$ and $CD8^+$ T cell responses during acute HCV infection [261], and chronicity develops in such individuals who fail to mount or sustain such responses [139]. Mechanisms responsible for such dysfunctional HCV-specific $CD8^+$ T cells are still not understood, and several explanations have been proposed, including the lack of different $CD4^+$ helper T cell functions or the suppressive activity of Treg [262]. Indeed, chronic HCV infection per se can lead to the expansion of $CD4^+CD25^+Foxp3^+$ T cells that reportedly suppress $CD8^+$ T-cell responses to different viral antigens [140, 141, 261, 263]. As liver biopsies from chronic HCV-infected individuals showed an influx of Treg, it has been suggested that such cells aid in controlling hepatic immune responses [144]. In association, *Bolacchi et al.* detected peripheral $CD4^+CD25^{hi}$ Treg that secreted TGF-β in response to HCV peptides, and in turn, this was inversely correlated to liver inflammation [142]. Concerning the expansion or even the change of phenotype of Treg during human schistosomiasis, controversial data have been put forward in contrast to the consistent findings in mice [27, 78, 103, 264]. When compared to both HCV mono-infected and healthy donors, the frequency of $CD4^+CD127^{lo}Foxp3^+$ Tregs in this study was not elevated in the schistosome co-infected group. However, we did find a higher frequency of GrzB-positive Treg within the Sm/HCV group, which confirmed our previous findings in *S. mansoni* infected mice where GrzB was upregulated in schistosome- induced Treg which simultaneously had an enhanced suppressive capacity on antigen-specific effector T cells [77, 78] (see section 3.1.1.4). Therefore, a potential regulatory scenario is that schistosome-induced Treg have an influence on the effector T-cell populations by acting directly on virus-specific effector T cells via GrzB. As this study revealed no correlations between GrzB-producing Treg and effector T-cell populations, future studies should concentrate on elucidating possible interactions between $GrzB^+$Treg and distinct effector T-cell subsets that have phenotypes unique in their expression of cytokines (IFN-γ, IL-2) or activation markers (CD44, CD69). In our study, we further analysed the phenotype of effector $CD4^+$ and $CD8^+$ T cells using GrzB as a functional marker. Even though there were significantly increased frequencies of $CD4^+$ and $CD8^+$

effector T cells within Sm/HCV and HCV mono-infected patients, frequencies of GrzB-secreting $CD8^+$ and $CD4^+$ effector T cells were not altered (see section 3.1.1.3). This could be due to the fact that all HCV patients were chronically infected and therefore lacked appropriate cytotoxic effector responses as described before [139, 261]. As GrzB expression is not the only hallmark of $CD8^+$ and $CD4^+$ T-cell activation, future studies should for example aim at deciphering whether viral-specific $CD8^+$ and $CD4^+$ T-cell responses are modulated in co-infected individuals by using an HCV genotype 4a peptide library. Such findings would expand on previous studies that have demonstrated that co-infected patients exhibit either completely absent or transiently weak HCV-specific IFN-$\gamma$ secretion by $CD4^+$ T cells [28, 265]. In addition, all HCV-infected patients had significantly elevated frequencies of total $CD4^+$ and $CD8^+$ effector T cells, whereas viral loads were only elevated in the Sm/HCV group (see section 3.1.1.1 and 3.1.1.3). This suggests that the effector $CD4^+$ and $CD8^+$ T-cell populations might not act properly on viral clearance and might be somehow influenced by the schistosome co-infection.

Another major finding within this study was the characterization and distribution of nTreg and iTreg within the Treg populations of the different groups. To discriminate between these Treg subsets, we employed the novel marker Helios, a transcription factor of the Ikaros family of transcription factors. This marker is currently proposed to be selectively expressed on nTreg and can therefore be used to discriminate between nTreg and iTreg [88, 89]. We found significantly higher frequencies of $Helios^{pos}$nTreg and decreased percentages of $Helios^{neg}$iTreg within the HCV mono-infected group, when compared to healthy individuals. Although a tendency towards higher frequencies of $Helios^{pos}$nTreg was observed within the Sm/HCV co-infected group compared to healthy controls, no significant differences could be determined, possibly due to the high variation within the group itself (see section 3.1.1.4). These data suggest that nTreg might increase during HCV infection, which is somewhat counterintuitive, and indeed, recently the selectiveness of Helios is being controversially discussed as it was also shown to be a marker of T cell activation and proliferation and was further detected in human and murine effector $CD4^+$ and $CD8^+$ T cells [88, 89, 266]. More specifically, *Akimova et al.* [89] reported that Helios expression within human and murine effector T cells regresses under resting conditions, whereas constantly high expression of the transcription factor could be detected within nTreg. In addition, *Gottschalk et al.* generated iTreg from naïve murine $CD4^+$ T cells *in vitro* and *in vivo* using different stimulatory

conditions and demonstrated that these iTreg only expressed Helios after being activated by antigen-presenting cells (APCs) and downregulated Helios expression under resting conditions. In contrast, nTreg constantly expressed the transcription factor Helios. iTreg generated without APCs but in the presence of TGF-β and TCR stimulation showed no Helios expression [266]. The study clearly demonstrates that Helios expression within iTreg is derived from an APC-dependent stimulus. In this regard, our findings of higher levels of Helios$^{pos}$Treg might not only pertain to the nTreg compartment as *in vivo* many iTreg will have been generated upon APC contact. We therefore believe that Helios might be a better marker to detect activated iTreg in humans rather than as a discrimination tool to dissect nTreg from iTreg. In this context, it will be interesting to investigate the phenotype of schistosome-induced 'Helios$^{pos}$' iTreg and moreover whether such cells simultaneously upregulate GrzB as well. Previous studies have shown that HCV/*S. mansoni* infected individuals have enhanced pathology when compared to *S. mansoni*-infected patients. Moreover, these studies have associated this pathology with differences in immune profiles of those groups including Treg numbers [105, 106, 108, 110, 151, 154, 156]. Expanding on those findings, we focused our study here on differences between HCV and HCV/*S. mansoni*-infected individuals and deciphered that Treg have a distinct immune profile: elevated frequencies of CD4$^{+}$CD127$^{lo}$Foxp3$^{+}$GrzB$^{+}$ Treg. In conclusion, this study provides additional knowledge on the broad influence that chronic helminthic infections have on immune responses to unrelated antigens such as HCV. As with their ability to suppress autoimmune diseases, this phenomenon probably stems from the nature of their general immunosuppressive features that arise due to the expansion and/or induction of regulatory populations such as Tregs [264, 267-270]. As in this co-infection scenario there is a detrimental effect on the patient's response to antiviral regimes, it will be important to study these immune responses after helminth treatment as this might improve the outcome of HCV therapy.

## 4.2 *Schistosoma mansoni* and hepatitis B virus co-infection in mice

To better understand plasticity of the liver microenvironment and its modulation by infection, analysing co-infection under defined experimental conditions is of imminent importance. Indeed, two very recent studies have addressed helminth-interaction with

γ-herpesvirus and mouse-norovirus for the first time and demonstrated a helminth-mediated effect on viral replication on a systemic as well as mucosal level [115, 116]. Therefore, to take our human study further and to expand on underlying mechanisms of interactions between hepatitis virus infections and schistosomiasis, in the second part of the thesis we experimentally investigated the development of an acute HBV infection acquired during the different immune phases ($T_H1$, $T_H2$, chronic) induced during *S. mansoni* infection. For this purpose we used the AdHBV-X$^-$ mouse model. As mentioned in section 3.2, murine HCV infections have long been analysed only in mice with human chimeric livers lacking an adaptive immune system, where the establishment of an anti-viral immune response and the resulting viral clearance in the presence of a concomitant schistosome infection cannot be investigated [254, 255]. Even though immuno-competent transgenic mice expressing the four main human HCV entry factors, such as CD81, scavenger receptor BI, claudin-1 and occludin were developed recently [271], a sustained and robust HCV infection was only achieved by crossing these animals with mice deficient for STAT1 [272]. Since HCV infection in these mice only elicited antiviral cellular and humoral immune responses but did not lead to the development of liver disease, this model only allows the study of HCV-induced immune responses and the preclinical evaluation of vaccine candidates [273]. To study the impact of schistosome-induced immune responses on liver disease development we took advantage of a fully immuno-competent mouse model where an acute HBV infection was established via adenoviral genome transfer (AdHBV-X$^-$ mouse model, see section 1.2.4) and liver disease develops. This mouse model allowed us to investigate the contribution of innate and adaptive immune responses present during the distinct immune phases of schistosome infection (see section 3.2.1.1) for viral clearance and persistence and further to analyse the influence of both pathogens on liver disease outcome.

### 4.2.1 The phase of immune response during *S. mansoni* infection determines the severity and outcome of concomitant acute HBV co-infection

In comparison to concomitant *S. mansoni* and HCV infections, where several epidemiological studies clearly report an accelerated onset of the liver disease with a higher incidence of liver cirrhosis and hepatocellular carcinoma in co-infected individuals [110, 148-151], the interrelationship between HBV and schistosomiasis is controversially discussed. While some

field studies observed prolonged viremia and worsening of liver damage [105, 106, 111-113, 177], other population based surveys revealed unaltered HBV infection rates and probability of HBV chronicity in schistosome co-infected patients [178-180] (see section 1.2.2.2). We hypothesized that these diverging epidemiological observations result from fluctuating immune responses induced during schistosome infection which influence the severity and outcome of a concomitant acute HBV co-infection. To address our hypothesis we analysed the development of a secondary acquired, acute HBV infection during the distinct immune phases ($T_H1$, $T_H2$, chronic) of *S. mansoni* infection. This reflects the situation in African schistosome-endemic areas, where children get in contact with the helminth before acquiring an HBV infection during adolescence [160]. The other scenario observed in Asia, is that viral infection is acquired mainly perinatally and contact to schistosomes occurs later in life [160]. To investigate this scenario, the HBV transgenic mouse model allowed us to study the impact of a secondary acquired schistosome infection on top of a pre-existing chronic HBV infection.

Taken together, in schistosome pre-infected animals, we indeed observed different outcomes of the secondary acquired viral infection. Compared to mice with a HBV mono-infection, we observed a faster viral clearance only in those animals who acquired the viral infection during IFN-γ-prone immune phases of the pre-existing schistosome infection (see *S. mansoni*-specific cytokine profile in C57Bl/6 mice, section 3.2.1.1). Mice that were acutely infected with HBV during the $T_H1$ (see section 3.2.2.1.2) and chronic phase (see section 3.2.2.3.1) of helminth infection displayed significantly decreased viral antigen levels and lower amounts of HBV genomes in the liver when compared to their HBV mono-infected counterparts, indicating that either viral entry or hepatocellular replication was inhibited. Moreover, elevated frequencies of HBV-specific $CD8^+$ IFN-γ secreting T cells were found locally in the liver and in the periphery, such as the spleen of co-infected animals. In addition, antigen-independent restimulated splenocytes (section 3.2.2.1.2) and mesenterial lymph node cells (section 3.2.2.3.1) of co-infected mice produced higher amounts of IFN-γ in comparison to animals with an HBV- or schistosome mono-infection, showing that concomitant helminth infection boosts the production of this cytokine in an antigen-independent manner.

Successful viral clearance is multifacetted but mainly involves intracellular and extracellular effects of interferones, especially IFN-γ. In an infected liver, viral elimination is therefore

mainly achieved by local production of IFN-γ, derived from $CD4^+$ and $CD8^+$ T cells, that allows the purging of virus from viable cells, and the induction of IFN-γ producing cytotoxic $CD8^+$ T-cells that destroy infected hepatocytes [162, 164-166, 274]. High levels of pre-existing schistosome-induced IFN-γ could therefore be responsible for the faster viral clearance in co-infected mice. In these animals, elevated levels of local schistosome-induced IFN-γ - predominantly produced by schistosome-specific $T_H1$ $CD4^+$ T cells - might on the one hand, immediately act on viral replication by binding to the IFN-γ receptor expressed on infected hepatocytes and on the other hand induce a faster priming and/or enhanced proliferation of virus-specific cytotoxic T cells. In this scenario, the Janus kinase-STAT (JAK/STAT) signalling pathway activation of the IFN-γ receptor can either trigger intracellular antiviral events that have the potential to interfere noncytophatically with the lifecycle of the virus or induce the production of an intracellular enzyme, protein kinase R, known to downregulate protein synthesis of both viral and host genes. While the latter finally destroys both the virus and infected host cells [167-169] the IFN-γ- dependent activation of 2'5' oligoadenylate synthase (2'5' OAS) induces RNAseL which degrades viral transcripts and therefore reduces intracellular RNA content of the virus [274]. This noncytolytic inhibition of viral replication in infected tissues and organs can be seen as an important host survival strategy to reduce the pathological consequences of the infection, such as the killing of all of the infected hepatocytes [274, 275].

Since IFN-γ secretion of virus-infected hepatocytes is furthermore known to induce the expression of intrinsic defense molecules, such as TRIM22 (tripartite motif-containing 22) and APOBEC 3G (Apolipoprotein B mRNA-editing enzyme-catalytic polypeptide-like 3G) in uninfected, bystander cells [171, 276, 277], we believe that in a schistosome pre-infected liver elevated levels of schistosome-induced IFN-γ additionally help to avoid the spread of the virus to other cells. Furthermore, we attribute the enhanced viral clearance in acutely and chronically schistosome co-infected mice also to the immunoregulatory properties of IFN-γ. Since this cytokine is known to induce an upregulation of MHC-I and MHC-II on antigen-presenting cells [171], in schistosome pre-infected animals elevated levels of this cytokine might lead to a faster presentation of processed viral antigens to naïve T cells and thereby contribute to a faster priming of virus-specific T cells. Moreover, IFN-γ is known to promote $T_H1$ cell differentiation and to suppress $T_H2$ cell differentiation by upregulating the transcription factor T-bet in naïve T cells. Consequently, $T_H1$ cells that secrete IFN-γ cause

more undifferentiated $CD4^+$ cells to differentiate into $T_H1$ cells, representing a positive feedback loop [171, 278]. In schistosome pre-infected animals one could therefore speculate, that elevated levels of IFN-γ moreover induce a faster proliferation of virus-specific $T_H1$ $CD4^+$ and $CD8^+$ T cells. Taken together, elevated frequencies of virus-specific $CD8^+$ IFN-γ secreting T cells in organs of acutely and chronically schistosome co-infected animals, possibly result from the faster priming and enhanced proliferation of these cells. This in turn is caused by elevated levels of schistosome-induced IFN-γ. In co-infected mice this increased HBV-specific T cell population might add to eliminate the virus in a faster manner by killing HBV-infected hepatocytes expressing viral antigens on MHC-I.

Co-infection experiments with animals being infected with HBV during the early $T_H1$ (see section 3.2.2.1.1), and $T_H2$ phase (see section 3.2.2.2.1), as well as co-infection experiments with IFN-γ-deficient mice (see section 3.2.5.2.2) where the production of IFN-γ was only instigated (early $T_H1$ phase), very low ($T_H2$ phase) or completely absent (IFN-γ-deficient mice) strengthened the pivotal role of schistosome-induced IFN-γ secretion on enhanced viral clearance. Since animals that were infected with HBV during the early $T_H1$ and $T_H2$ phase displayed similar viral loads and viral antigen levels as their HBV mono-infected counterparts throughout the whole course of co-infection, we attributed this phenotype to the absent schistosome-induced IFN-γ secretion during these immune phases of helminth co-infection. Whether these co-infected animals in turn had an enhanced liver inflammation will be analysed in the near future by measuring serum liver transaminase levels.

Experiments with *S. mansoni* infected C57BL/6 IFN-γ-deficient mice confirmed previous findings from *Straubinger et al.* [258] that schistosome infection in terms of parasite development and dynamics of $T_H2$ responses develop similarly to C57BL/6 wildtype mice (see section 3.2.5.2.1). Moreover, upon co-infection with HBV, we demonstrated that IFN-γ-deficient animals fail to show the enhanced viral clearance observed in co-infected wildtype counterparts (see section 3.2.5.2.2). Since we found comparable serum virus antigen levels and HBV genome titers between co-infected IFN-$\gamma^{-/-}$ mice and HBV mono-infected groups (IFN-γ-deficient and wildtype), we concluded that in co-infected IFN-γ-deficient animals the lack of schistosome-specific $CD4^+$IFN-$\gamma^+$ cells fails to provide the additional immunological boost amplifying virus-specific $CD4^+$ and $CD8^+$ T cell responses that could contribute to the faster virus elimination.

Moreover, in all co-infection experiments, absolute numbers of adenoviral genomes did not differ between co-infected and HBV mono-infected mice. These data indicate, that independent of the immune phase and the status of liver granuloma formation of the pre-existing helminth infection, an equal amount of adenoviral vectors carrying HBV DNA arrives into hepatocyte nuclei, showing that schistosome infected animals can initially be equally infected with HBV. We therefore exclude an HBV entry-inhibition in the schistosome pre-infected liver as a possible reason for different outcomes of concomitant acute HBV co-infection.

### 4.2.2 Depletion of schistosome-induced regulatory T cells does not additionally enhance the accelerated viral clearance in chronically schistosome co-infected mice

Since during schistosomiasis and other helminth infections, the importance of regulatory $CD4^+$ T cells in controlling exaggerated immunopathology as well as effector T cell responses is well documented [77, 78, 95], we further analysed the role of schistosome-induced Treg on the establishment of anti-viral immune responses during co-infection. Previous studies with HBV infected mice showed that Treg per se play an important role in the establishment of anti-viral immune responses. *Stross et al.* demonstrated, that 7 days post viral infection numbers of Treg increased locally in the liver and delayed the development of virus-specific immune responses leading to prolonged viremia. In Treg-depleted DEREG mice virus elimination occurred faster (lower viral load and viral antigen levels) when compared to wildtype mice infected with HBV, demonstrating a role for Treg in the liver in controlling virus-specific immune responses rather than acting directly on hepatocytes [114]. The importance of Treg in viral infections was also shown by various epidemiological studies, which demonstrated that chronically HCV/HBV infected individuals present elevated frequencies of peripheral $CD4^+CD25^+Foxp3^+$ Treg, which, in response to viral antigenic peptides (HBcAg; HCV core antigen, fragments of HCV NS3, NS4 or NS5 proteins) are able to suppress virus-specific T cell responses by secretion of TGF-$\beta$ *in vitro* [140-144, 279-281]. Since our human HCV/*S. mansoni* co-infection study, furthermore, clearly demonstrated, that schistosome-induced Treg with a unique phenotype do not only suppress schistosome-specific effector T cell responses but also act on bystander immune responses by influencing

virus-specific T cells [253], we wondered whether the depletion of Treg might have an impact on viral clearance in schistosome co-infected mice.

We therefore analysed viral replication and the development of virus-specific T cell responses in chronically schistosome co-infected C57BL/6 wildtype (S.m./HBV) and Treg-depleted C57BL/6 DEREG mice (S.m./HBV$^{DT}$) shortly after (3 days) and one week post viral infection (section 3.2.5.1). Both schistosome co-infected animal groups (S.m./HBV$^{DT}$ and S.m./HBV) displayed similar serum viral titers and amounts of HBV genomes in their livers, which, in comparison to HBV mono-infected mice with or without Treg depletion (HBV$^{DT}$ and HBV), were again significantly decreased. These data show, that 7 days post viral infection, Treg depletion per se does not further enhance the accelerated viral clearance in co-infected mice. Moreover, we showed that Treg depletion does not influence schistosome-specific immune responses, since antigen-specific restimulated splenocytes and mesenterial lymph node cells of both schistosome co-infected animal groups (S.m./HBV$^{DT}$ and S.m./HBV) responded with similar amounts of IFN-γ. Even though antigen-independent stimulation revealed significantly higher splenic and mesenteric IFN-γ secretion in S.m./HBV$^{DT}$ mice when compared to co-infected wildtype counterparts (S.m./HBV), viral replication does not seem to be affected by this circumstance as in comparison to HBV mono-infected animals (HBV$^{DT}$ and HBV), cells from both schistosome co-infected groups still secreted higher levels of this cytokine. The unaltered viral loads between both schistosome co-infected animal groups can be furthermore explained by the fact that while S.m./HBV$^{DT}$ mice had significantly elevated frequencies of HBV-specific CD4$^{+}$IFN-γ$^{+}$ T cells in the liver, populations of liver resident virus-specific CD8$^{+}$IFN-γ$^{+}$ T cells did not differ between both co-infected groups. Overall, since differences in antigen-independent IFN-γ secretion and populations of CD4$^{+}$IFN-γ$^{+}$ T cells were already observed between both co-infected animal groups (S.m./HBV$^{DT}$ and S.m./HBV), we still believe that Treg might influence viral clearance. In the complex mouse model of HBV/*S. mansoni* co-infection, 7 days of co-infection, however, might be too short to clearly visualize the potential effects of Treg depletion on viral elimination. Consequently, a longer time period of co-infection would be helpful to address the impact of Treg depletion on viral replication and on the establishment of anti-viral immune responses. However, since 6 days post diphtheria toxin (DT) administration populations of regulatory T cells start to re-expand in the DEREG mouse model [282, 283], longterm Treg depletion requires an administration of DT on a weekly basis. In the light of *S. mansoni* and HBV co-infection, however, these

experiments seem to not be feasible, since the high morbidity of co-infected animals that suffer from two infections will be additionally increased upon weekly DT administration. Moreover a potential anti-DT antibody formation and the presence of DT-insensitive $CD4^+Foxp3^+eGFP^-$ Treg populations needs to be considered in longterm depletion regimen, which additionally limit the effective long lasting depletion of Treg in this mouse model [284, 285].

In conclusion, our data indicate that 7 days post HBV infection the lower viral replication rate observed in schistosome co-infected animal groups (S.m./$HBV^{DT}$ and S.m./HBV) is independent of Treg and is more likely again attributed to the anti-viral effect of schistosome-induced IFN-γ.

### 4.2.3 Co-infected HBVtg mice show decreased HBV replication exclusively during the $T_H1$ phase of *S. mansoni* infection

The clinically very relevant scenario of a secondary schistosome infection acquired on top of a pre-existing chronic HBV infection was up to now addressed only once in a HBV transgenic (HBVtg) mouse model [217]. In this study HBV replication was suppressed during the $T_H1$ phase of *S. mansoni* infection and remained downregulated upon onset into the $T_H2$ phase 6-8 weeks post schistosome infection. The authors attributed the suppressed HBV replication to the antiviral activity of schistosome-induced IFN-γ and showed that the first appearance of $T_H2$ type cytokines does not counteract with the antiviral effect of IFN-γ [217]. *Guidotti et al.,* however, only monitored HBV replication up to the 8th week of schistosome infection during which the $T_H2$ phase has just begun to establish itself, and did not provide any information on whether this suppression persisted during the successive immune-suppressive phases of schistosome infection. We therefore took Guidotti's study further and monitored HBV replication in HBVtg mice with (HBVtg/Sm) or without (HBVtg) concomitant schistosome infection upon progression into the chronic phase of helminth co-infection (section 3.2.2.4.1). Like *Guidotti et al.* we found significantly lower viral replication rates in terms of lower viral antigen secretion exclusively during the $T_H1$ phase of *S. mansoni* co-infection. In addition, we found that the schistosome infection, possibly by secretion of IFN-γ, could break the peripheral tolerance in HBVtg mice, allowing the evolvement of anti-viral immunity. We therefore attribute the lower viral replication rates in co-infected mice to

the antiviral and immuneregulatory properties of schistosome-induced IFN-γ. These results were further validated by former studies with HBV transgenic IFN-γ-deficient mice that, in comparison to HBV transgenic mice lacking the IFN-α and β receptor, failed to show the suppressed HBV replication during the acute phase of schistosome co-infection [217].
However, the question whether viral replication relapses upon progression into the $T_H2$- and immune-suppressive phases of schistosome co-infection, was difficult to address with this mouse model. Since we used the transgenic mouse line C57BL/6 HBV1.3xfs with a low viral replication rate but less susceptibility to transgene silencing [256], the repetitive bleeding of these mice resulted in very low HBs and HBe titers in both animal groups (HBVtg/Sm and HBVtg) after the third bleeding round. This circumstance rendered the whole system inappropriate to observe little fluctuations in viral replication induced by the schistosome infection later on during the chronic phase of co-infection. Therefore, to address the question whether the suppression of HBV replication persists during the immune-suppressive phases of schistosome infection, one should consider to use HBV transgenic mice with a high replication rate, such as HBV 1.3.32 on a C57BL/6 background [199, 217].

### 4.2.4 Acute and chronic Hepatitis B virus infections have no impact on *S. mansoni* disease outcome

Since we observed that the distinct immune phases of *S. mansoni* infection led to differential outcomes in the case of acute and chronic HBV co-infection, we analysed if the latter had an impact on the helminth disease outcome as well. For this purpose, we monitored different parasitological parameters, such as egg count and granuloma formation within livers of *S. mansoni* infected animals with or without concomitant HBV infection. We found that the acute viral infection acquired during the distinct immune phases of *S. mansoni* infection, does not influence the helminth disease outcome in terms of infectivity and fecundity. Moreover, schistosome-specific immune responses in co-infected mice did not differ from those obtained from schistosome mono-infected animals (section 3.2.3.1). The same findings were obtained in the HBVtg mouse model, where the additional schistosome infection acquired on top of a pre-existing chronic HBV infection, developed normally in terms of parasite development and schistosome-specific immune responses (section 3.2.3.2). These results were in line with epidemiological studies that only reported an

accelerated onset of the viral (HCV/HBV) infection but never an aggravation of the helminth disease in schistosome co-infected individuals, which is however, considering the slow progress of the disease difficult to measure [105, 106, 110-113, 148-151, 177]. In contrast, in combination with another virus, such as lymphocytic choriomeningitis virus (LCMV), schistosome and viral infections were found to affect each other [117, 118]. In a murine *S. mansoni*/LCMV co-infection model, where the viral infection occurred during the $T_H2$ phase of schistosome infection, *Edwards et al.* reproduced the enhanced viral replication and liver pathology observed in human co-infections, and used this model to examine the mechanisms involved. The study demonstrated that both pathogens influenced each other in such a way that high numbers of infiltrating LCMV-specific IFN-$\gamma^+$ $CD8^+$ T cells suppressed the schistosome-induced production of $T_H2$ cytokines in the liver and led to an increased morbidity, linked to hepatotoxicity. On the other side, schistosome-egg antigens were found to suppress the type I Interferon response of bone-marrow-derived DCs locally in the liver and rendered the organ extremely susceptible to viral replication with ensuing immunopathological consequences [117, 118]. The potential of LCMV to induce a very strong $T_H1$ immune response might be a possible explanation why this virus, in contrast to HCV/HBV, is able to suppress the schistosome-induced production of $T_H2$ type cytokines.

### 4.2.5 Curing the helminth disease as an important prerequisite for successful viral treatment in co-infected individuals

Overall we have been able to show, that in *S. mansoni* and hepatitis virus (HCV and HBV) co-infected individuals, the helminth infection indeed influences the outcome of the viral infection, whereby the mutual influence is rather unidirectional since the schistosome infection per se seems to be nearly unaffected by the concomitant viral infection. We have shown that the development of a secondary acquired, acute HBV infection is highly dependent on the quality of the immune response during pre-existing schistosome infection, and that additionally, a schistosome infection acquired on top of a chronic HBV infection is able to suppress viral replication during its IFN-$\gamma$ prone immune phase. Therefore, in field studies, the assessment of the patient's immune profile can help to explain the differential outcomes of the viral disease in co-infected individuals. In schistosome endemic areas, however, it has to be considered that the constant exposure to the parasite as well as high

re-infection rates upon anti-helminthic treatment, lead to a high occurrence of chronic helminthic infections amongst the population [2, 42-46]. Since these individuals, in contrast to the experimental situation described here, only display very low levels of IFN-γ during the chronic phase of helminth infection [3, 286], the beneficial effect of this cytokine on a secondary acquired viral infection will be absent and an aggravation of the liver disease seems to be an expectable outcome. Therefore, in this scenario, curing the helminth disease first can be an important prerequisite for successful viral treatment.

In our murine *S. mansoni*/HBV co-infection study we have defined schistosome-induced IFN-γ as a key player in this parasite-virus interaction. Since IFN-γ is furthermore known to recruit also other cell types, such as natural killer cells (NK cells) and macrophages to sites of infection, which can also be involved in viral clearance by their additional production of IFN-γ and phagocytosis capacity [278, 287], we now hypothesize that also other cell types, triggered by schistosome-induced IFN-γ, might have similar effector functions. In this context the question arises how other inflammatory, liver-resident cell types, such as macrophages with or without an alternatively activated phenotype (AAMs, see section 1.1.4.2) and innate lymphoid cells additionally influence viral clearance by for example interacting with antiviral immune responses and/or directly with infected liver cells. In the near future we will therefore focus on those cells since they are known to be highly enriched in schistosome infected livers, and will determine the impact of these cells on viral clearance.

# 5 Registers

## 5.1 List of abbreviations

**A**

| | |
|---|---|
| AAM | alternatively activated macrophages |
| ACT | ammoniumchloride-tris |
| AdEmpty | adenoviral vector construct without insert |
| AdHBV-X$^-$ | adenoviral construct with HBV-X$^-$ insert |
| AFP | alpha-fetoprotein |
| ALT | alanine aminotransferase |
| AST | aspartate aminotransferase |
| APC | antigen presenting cells |
| Arg1 | Arginase 1 |

**B**

| | |
|---|---|
| BAC | bacterial artificial chromosome |
| BFA | Brefeldin A |
| bp | base pair(s) |
| Breg | regulatoy B cells |
| BSA | bovine serum albumin |

**C**

| | |
|---|---|
| cccDNA | covalently closed circular DNA |
| CD | cluster of differentiation |
| CTLA | cytotoxic T lymphocyte antigen |

**D**

| | |
|---|---|
| DC | dendritic cell |
| DEREG mouse | mouse model allowing the depletion of regulatory T cells |
| DHV | duck hepatitis virus |

| | |
|---|---|
| DMEM | Dulbecco's modified eagle medium |
| DMSO | dimethyl sulfoxide |
| DNA | deoxyribonucleic acid |
| DT | diphtheria toxin |
| DTR | diphtheria toxin receptor |
| dNTPs | deoxynucleoside triphosphate |
| DOI | degree of infection |
| dsRNA | double-stranded RNA |

**E**

| | |
|---|---|
| eGFP | enhanced green fluorescent protein |
| ELISA | enzyme linked immunosorbent assay |
| EMA | ethidium monoazid |
| ER | endoplasmatic reticulum |

**F**

| | |
|---|---|
| FACS | fluorescence-activated cell sorting |
| FCS | fetal calf serum |
| FITC | fluorescein isothiocyanate |
| Foxp3 | forkhead box P3 |

**H**

| | |
|---|---|
| HBcAg | hepatitis B virus core antigen |
| HBcP3 | HBcAg derived peptide pool (core pool 3) |
| HBeAg | hepatitis B virus early antigen |
| HBsAg | hepatitis B virus surface antigen |
| HBV | Hepatitis B virus |
| HBV-$X^-$ | hepatitis B virus with a stop codon in the HBx ORF |
| HCC | hepatocellular carcinoma |
| HCV | hepatitis C virus |
| HDI | hydrodynamic injection |
| HEK cells | human embryonic kidney cells |

| | |
|---|---|
| HRP | horseradish peroxidase |
| **I** | |
| ICS | intracellular cytokine staining |
| IFN | interferon |
| Ig | immunoglobulin |
| IL | interleukin |
| i.p. | intraperitoneal |
| IU | infectious units |
| i.v. | intravenously |
| **K** | |
| kb | kilobase |
| KCl | potassium chloride |
| kDa | kilo Dalton |
| KO | knockout |
| KOH | potassium hydroxide |
| **L** | |
| LAL | liver associated lymphocytes |
| **M** | |
| MHC | major histocompatibility complex |
| MIH | Institute of medical Mircrobiology, Immunology and Hygiene |
| mRNA | messenger RNA |
| **N** | |
| NaCl | sodium chloride |
| n.d. | not determined |
| NTCP | sodium taurocholate cotransporting polypetide |
| **P** | |
| PAMPs | pathogen-associated molecular pattern molecules |

| | |
|---|---|
| PBMCs | peripheral blood mononuclear cells |
| PBS | phosphate buffered saline |
| PCR | polymerase chain reaction |
| PE | phycoerythrin |
| PFA | paraformaldehyde |
| pgRNA | pregenomic RNA |
| p.i. | post infection |

**R**

| | |
|---|---|
| rc DNA | relaxed circular DNA |
| Reg | regulatory |
| Relmα | resisitn like molecule α |
| RNA | ribonucleic acid |
| RPMI | Roswell Park Memorial Institute medium |

**S**

| | |
|---|---|
| SCID | severe combined immunodeficiency |
| SD | standard deviation |
| SEA | soluble egg antigen |
| SEM | standard error of the mean |
| SLPI | secretory leukocyte peptidase inhibitor Abbreviations |
| *S. mansoni* | *Schistosoma mansoni* |
| STAT | signal transducer and activator of transcription |

**T**

| | |
|---|---|
| TGF | transforming growth factor |
| $T_H$ | T helper |
| TLR | Toll-like receptor |
| TMB | 3,3',5,5'-tetramethylbenzidine |
| TNF | tumor necrosis factor |
| Tris | tris(hydroxymethyl)aminomethane |
| Treg | regulatory T cells |

**V**

| | |
|---|---|
| v/v | volume per volume |

## 5.2 List of Figures

## 5.3 List of Tables

## 5.4 Bibliography


1. Gryseels, B., *Schistosomiasis.* Infect Dis Clin North Am, 2012. **26**(2): p. 383-97.
2. Chitsulo, L., et al., *The global status of schistosomiasis and its control.* Acta Trop, 2000. **77**(1): p. 41-51.
3. Pearce, E.J. and A.S. MacDonald, *The immunobiology of schistosomiasis.* Nat Rev Immunol, 2002. **2**(7): p. 499-511.
4. King, C.H., *Parasites and poverty: the case of schistosomiasis.* Acta Trop, 2010. **113**(2): p. 95-104.
5. Sangweme, D.T., et al., *Impact of schistosome infection on Plasmodium falciparum Malariometric indices and immune correlates in school age children in Burma Valley, Zimbabwe.* PLoS Negl Trop Dis, 2010. **4**(11): p. e882.
6. Doenhoff, M.J., et al., *Praziquantel: its use in control of schistosomiasis in sub-Saharan Africa and current research needs.* Parasitology, 2009. **136**(13): p. 1825-1835.
7. Fukuyama, K., et al., *The epidermal barrier to Schistosoma mansoni infection.* Curr Probl Dermatol, 1983. **11**: p. 185-93.
8. Hansell, E., et al., *Proteomic analysis of skin invasion by blood fluke larvae.* PLoS Negl Trop Dis, 2008. **2**(7): p. e262.
9. Gobert, G.N., M. Chai, and D.P. McManus, *Biology of the schistosome lung-stage schistosomulum.* Parasitology, 2007. **134**(Pt 4): p. 453-60.
10. Webster, J.P., et al., *Schistosome genomes: a wealth of information.* Trends Parasitol, 2010. **26**(3): p. 103-6.
11. Boros, D.L., *Immunopathology of Schistosoma mansoni infection.* Clin Microbiol Rev, 1989. **2**(3): p. 250-69.
12. Dunne, D.W. and A. Cooke, *A worm's eye view of the immune system: consequences for evolution of human autoimmune disease.* Nat Rev Immunol, 2005. **5**(5): p. 420-6.
13. Posey, D.L., et al., *High prevalence and presumptive treatment of schistosomiasis and strongyloidiasis among African refugees.* Clin Infect Dis, 2007. **45**(10): p. 1310-5.
14. Maizels, R.M. and M. Yazdanbakhsh, *Immune regulation by helminth parasites: cellular and molecular mechanisms.* Nat Rev Immunol, 2003. **3**(9): p. 733-44.
15. Wilson, R.A. and P.S. Coulson, *Immune effector mechanisms against schistosomiasis: looking for a chink in the parasite's armour.* Trends Parasitol, 2009. **25**(9): p. 423-31.
16. Webpage from http://www.merckmanuals.com/professional/infectious_diseases/trematodes_flukes/schistosomiasis.html.
17. Weinstock, J.V. and D.L. Boros, *Heterogeneity of the granulomatous response in the liver, colon, ileum, and ileal Peyer's patches to schistosome eggs in murine schistosomiasis mansoni.* J Immunol, 1981. **127**(5): p. 1906-9.
18. Andrade, Z.A. and S.G. Andrade, *Pathogenesis of schistosomal pulmonary arteritis.* Am J Trop Med Hyg, 1970. **19**(2): p. 305-10.
19. Martins, A.V., *Non-human vertebrate hosts of Schistosoma haematobium and Schistosoma mansoni.* Bull World Health Organ, 1958. **18**(5-6): p. 931-44.
20. Folster-Holst, R., et al., *Cercarial dermatitis contracted via contact with an aquarium: case report and review.* Br J Dermatol, 2001. **145**(4): p. 638-40.
21. Ross, A.G., et al., *Katayama syndrome.* Lancet Infect Dis, 2007. **7**(3): p. 218-24.
22. Gray, D.J., et al., *Diagnosis and management of schistosomiasis.* BMJ, 2011. **342**: p. d2651.
23. Cheever, A.W., K.F. Hoffmann, and T.A. Wynn, *Immunopathology of schistosomiasis mansoni in mice and men.* Immunol Today, 2000. **21**(9): p. 465-6.
24. Ross, A.G., et al., *Schistosomiasis.* N Engl J Med, 2002. **346**(16): p. 1212-20.

25. Yazdanbakhsh, M. and D.L. Sacks, *Why does immunity to parasites take so long to develop?* Nat Rev Immunol, 2010. **10**(2): p. 80-1.
26. Chabasse, D., et al., *[Developmental bilharziasis caused by Schistosoma mansoni discovered 37 years after infestation].* Bull Soc Pathol Exot Filiales, 1985. **78**(5): p. 643-7.
27. Watanabe, K., et al., *T regulatory cell levels decrease in people infected with Schistosoma mansoni on effective treatment.* Am J Trop Med Hyg, 2007. **77**(4): p. 676-82.
28. Teixeira-Carvalho, A., et al., *Cytokines, chemokine receptors, CD4+CD25HIGH+ T-cells and clinical forms of human schistosomiasis.* Acta Trop, 2008. **108**(2-3): p. 139-49.
29. Pearce, E.J. and A. Sher, *Mechanisms of immune evasion in schistosomiasis.* Contrib Microbiol Immunol, 1987. **8**: p. 219-32.
30. Maizels, R.M., et al., *Immunological modulation and evasion by helminth parasites in human populations.* Nature, 1993. **365**(6449): p. 797-805.
31. Auriault, C., et al., *Proteolytic cleavage of IgG bound to the Fc receptor of Schistosoma mansoni schistosomula.* Parasite Immunol, 1981. **3**(1): p. 33-44.
32. Soonawala, D., et al., *The immune response to schistosome antigens in formerly infected travelers.* Am J Trop Med Hyg, 2011. **84**(1): p. 43-7.
33. Pearce, E.J., et al., *Pillars article: downregulation of Th1 cytokine production accompanies induction of Th2 responses by a parasitic helminth, Schistosoma mansoni. J. Exp. Med. 1991. 173: 159-166.* J Immunol, 2012. **189**(3): p. 1104-11.
34. Grzych, J.M., et al., *Egg deposition is the major stimulus for the production of Th2 cytokines in murine schistosomiasis mansoni.* J Immunol, 1991. **146**(4): p. 1322-7.
35. *Immunology of schistosomiasis.* Bull World Health Organ, 1974. **51**(6): p. 553-95.
36. Duraes, F.V., et al., *IL-12 and TNF-alpha production by dendritic cells stimulated with Schistosoma mansoni schistosomula tegument is TLR4- and MyD88-dependent.* Immunol Lett, 2009. **125**(1): p. 72-7.
37. Samuelson, J.C. and J.P. Caulfield, *The cercarial glycocalyx of Schistosoma mansoni.* J Cell Biol, 1985. **100**(5): p. 1423-34.
38. Dias Da Silva, W. and M.D. Kasatchkine, *Schistosoma mansoni: activation of the alternative pathway of human complement by schistosomula.* Exp Parasitol, 1980. **50**(2): p. 278-86.
39. Paveley, R.A., et al., *The Mannose Receptor (CD206) is an important pattern recognition receptor (PRR) in the detection of the infective stage of the helminth Schistosoma mansoni and modulates IFNgamma production.* Int J Parasitol, 2011. **41**(13-14): p. 1335-45.
40. Rabello, A., *Acute human schistosomiasis mansoni.* Mem Inst Oswaldo Cruz, 1995. **90**(2): p. 277-80.
41. King, C.L., et al., *B cell sensitization to helminthic infection develops in utero in humans.* J Immunol, 1998. **160**(7): p. 3578-84.
42. Asaolu, S.O. and I.E. Ofoezie, *The role of health education and sanitation in the control of helminth infections.* Acta Trop, 2003. **86**(2-3): p. 283-94.
43. Hotez, P.J. and A. Fenwick, *Schistosomiasis in Africa: an emerging tragedy in our new global health decade.* PLoS Negl Trop Dis, 2009. **3**(9): p. e485.
44. Stothard, J.R. and A.F. Gabrielli, *Schistosomiasis in African infants and preschool children: to treat or not to treat?* Trends Parasitol, 2007. **23**(3): p. 83-6.
45. Fenwick, A., *New initiatives against Africa's worms.* Trans R Soc Trop Med Hyg, 2006. **100**(3): p. 200-7.
46. Garba, A., et al., *Present and future schistosomiasis control activities with support from the Schistosomiasis Control Initiative in West Africa.* Parasitology, 2009. **136**(13): p. 1731-7.
47. Lelo, A.E., et al., *No apparent reduction in schistosome burden or genetic diversity following four years of school-based mass drug administration in mwea, central kenya, a heavy transmission area.* PLoS Negl Trop Dis, 2014. **8**(10): p. e3221.
48. Caldas, I.R., et al., *Susceptibility and resistance to Schistosoma mansoni reinfection: parallel cellular and isotypic immunologic assessment.* Am J Trop Med Hyg, 2000. **62**(1): p. 57-64.

49. Farah, I.O., et al., *Schistosoma mansoni in mice: the pattern of primary cercarial exposure determines whether a secondary infection post-chemotherapy elicits a T helper 1- or a T helper 2-associated immune response.* Scand J Immunol, 2000. **51**(3): p. 237-43.
50. Wilson, M.S., et al., *IL-10 blocks the development of resistance to re-infection with Schistosoma mansoni.* PLoS Pathog, 2011. **7**(8): p. e1002171.
51. Wynn, T.A., et al., *Analysis of cytokine mRNA expression during primary granuloma formation induced by eggs of Schistosoma mansoni.* J Immunol, 1993. **151**(3): p. 1430-40.
52. Allen, J.E. and T.E. Sutherland, *Host protective roles of type 2 immunity: parasite killing and tissue repair, flip sides of the same coin.* Semin Immunol, 2014. **26**(4): p. 329-40.
53. Abdulla, M.H., et al., *Proteomic identification of IPSE/alpha-1 as a major hepatotoxin secreted by Schistosoma mansoni eggs.* PLoS Negl Trop Dis, 2011. **5**(10): p. e1368.
54. Hesse, M., et al., *The pathogenesis of schistosomiasis is controlled by cooperating IL-10-producing innate effector and regulatory T cells.* J Immunol, 2004. **172**(5): p. 3157-66.
55. Allen, J.E. and R.M. Maizels, *Diversity and dialogue in immunity to helminths.* Nat Rev Immunol, 2011. **11**(6): p. 375-88.
56. Harris, N. and W.C. Gause, *To B or not to B: B cells and the Th2-type immune response to helminths.* Trends Immunol. **32**(2): p. 80-8.
57. Terrazas, C.A., L.I. Terrazas, and L. Gomez-Garcia, *Modulation of dendritic cell responses by parasites: a common strategy to survive.* J Biomed Biotechnol, 2010. **2010**: p. 357106.
58. van Liempt, E., et al., *Schistosoma mansoni soluble egg antigens are internalized by human dendritic cells through multiple C-type lectins and suppress TLR-induced dendritic cell activation.* Mol Immunol, 2007. **44**(10): p. 2605-15.
59. Faveeuw, C., et al., *Schistosome N-glycans containing core alpha 3-fucose and core beta 2-xylose epitopes are strong inducers of Th2 responses in mice.* Eur J Immunol, 2003. **33**(5): p. 1271-81.
60. Kane, C.M., et al., *Helminth antigens modulate TLR-initiated dendritic cell activation.* J Immunol, 2004. **173**(12): p. 7454-61.
61. Kane, C.M., E. Jung, and E.J. Pearce, *Schistosoma mansoni egg antigen-mediated modulation of Toll-like receptor (TLR)-induced activation occurs independently of TLR2, TLR4, and MyD88.* Infect Immun, 2008. **76**(12): p. 5754-9.
62. Hewitson, J.P., J.R. Grainger, and R.M. Maizels, *Helminth immunoregulation: the role of parasite secreted proteins in modulating host immunity.* Mol Biochem Parasitol, 2009. **167**(1): p. 1-11.
63. van der Kleij, D., et al., *A novel host-parasite lipid cross-talk. Schistosomal lyso-phosphatidylserine activates toll-like receptor 2 and affects immune polarization.* J Biol Chem, 2002. **277**(50): p. 48122-9.
64. Everts, B., et al., *Schistosome-derived omega-1 drives Th2 polarization by suppressing protein synthesis following internalization by the mannose receptor.* J Exp Med, 2012. **209**(10): p. 1753-67, S1.
65. Steinfelder, S., et al., *The major component in schistosome eggs responsible for conditioning dendritic cells for Th2 polarization is a T2 ribonuclease (omega-1).* J Exp Med, 2009. **206**(8): p. 1681-90.
66. Klaver, E.J., et al., *Schistosoma mansoni Soluble Egg Antigens Induce Expression of the Negative Regulators SOCS1 and SHP1 in Human Dendritic Cells via Interaction with the Mannose Receptor.* PLoS One, 2015. **10**(4): p. e0124089.
67. Pesce, J.T., et al., *Arginase-1-expressing macrophages suppress Th2 cytokine-driven inflammation and fibrosis.* PLoS Pathog, 2009. **5**(4): p. e1000371.
68. Pesce, J.T., et al., *Retnla (relmalpha/fizz1) suppresses helminth-induced Th2-type immunity.* PLoS Pathog, 2009. **5**(4): p. e1000393.
69. Nair, M.G., et al., *Alternatively activated macrophage-derived RELM-{alpha} is a negative regulator of type 2 inflammation in the lung.* J Exp Med, 2009. **206**(4): p. 937-52.

70. Jenkins, S.J., et al., *Local macrophage proliferation, rather than recruitment from the blood, is a signature of TH2 inflammation.* Science, 2011. **332**(6035): p. 1284-8.
71. Vannella, K.M., et al., *Incomplete deletion of IL-4Ralpha by LysM(Cre) reveals distinct subsets of M2 macrophages controlling inflammation and fibrosis in chronic schistosomiasis.* PLoS Pathog, 2014. **10**(9): p. e1004372.
72. Broadhurst, M.J., et al., *Upregulation of retinal dehydrogenase 2 in alternatively activated macrophages during retinoid-dependent type-2 immunity to helminth infection in mice.* PLoS Pathog, 2012. **8**(8): p. e1002883.
73. Phillips, S.M. and P.J. Lammie, *Immunopathology of granuloma formation and fibrosis in schistosomiasis.* Parasitol Today, 1986. **2**(11): p. 296-302.
74. Pearce, E.J., *Priming of the immune response by schistosome eggs.* Parasite Immunol, 2005. **27**(7-8): p. 265-70.
75. Layland, L.E., H. Wagner, and C.U. da Costa, *Lack of antigen-specific Th1 response alters granuloma formation and composition in Schistosoma mansoni-infected MyD88-/- mice.* Eur J Immunol, 2005. **35**(11): p. 3248-57.
76. Silva, L.M., et al., *Significance of schistosomal granuloma modulation.* Mem Inst Oswaldo Cruz, 2000. **95**(3): p. 353-61.
77. Layland, L.E., et al., *Pronounced phenotype in activated regulatory T cells during a chronic helminth infection.* J Immunol. **184**(2): p. 713-24.
78. Layland, L.E., et al., *Immunopathology in schistosomiasis is controlled by antigen-specific regulatory T cells primed in the presence of TLR2.* Eur J Immunol, 2007. **37**(8): p. 2174-84.
79. Fallon, P.G., et al., *Schistosome infection of transgenic mice defines distinct and contrasting pathogenic roles for IL-4 and IL-13: IL-13 is a profibrotic agent.* J Immunol, 2000. **164**(5): p. 2585-91.
80. Mentink-Kane, M.M., et al., *IL-13 receptor alpha 2 down-modulates granulomatous inflammation and prolongs host survival in schistosomiasis.* Proc Natl Acad Sci U S A, 2004. **101**(2): p. 586-90.
81. Chiaramonte, M.G., et al., *An IL-13 inhibitor blocks the development of hepatic fibrosis during a T-helper type 2-dominated inflammatory response.* J Clin Invest, 1999. **104**(6): p. 777-85.
82. Jankovic, D., et al., *Schistosome-infected IL-4 receptor knockout (KO) mice, in contrast to IL-4 KO mice, fail to develop granulomatous pathology while maintaining the same lymphokine expression profile.* J Immunol, 1999. **163**(1): p. 337-42.
83. Morimoto, M., et al., *IL-13 receptor alpha2 regulates the immune and functional response to Nippostrongylus brasiliensis infection.* J Immunol, 2009. **183**(3): p. 1934-9.
84. Jankovic, D., et al., *CD4+ T cell-mediated granulomatous pathology in schistosomiasis is downregulated by a B cell-dependent mechanism requiring Fc receptor signaling.* J Exp Med, 1998. **187**(4): p. 619-29.
85. Workman, C.J., et al., *The development and function of regulatory T cells.* Cell Mol Life Sci, 2009. **66**(16): p. 2603-22.
86. Ziegler, S.F., *FOXP3: of mice and men.* Annu Rev Immunol, 2006. **24**: p. 209-26.
87. Kronenberg, M. and A. Rudensky, *Regulation of immunity by self-reactive T cells.* Nature, 2005. **435**(7042): p. 598-604.
88. Thornton, A.M., et al., *Expression of Helios, an Ikaros transcription factor family member, differentiates thymic-derived from peripherally induced Foxp3+ T regulatory cells.* J Immunol. **184**(7): p. 3433-41.
89. Akimova, T., et al., *Helios expression is a marker of T cell activation and proliferation.* PLoS One. **6**(8): p. e24226.
90. Battaglia, A., et al., *Neuropilin-1 expression identifies a subset of regulatory T cells in human lymph nodes that is modulated by preoperative chemoradiation therapy in cervical cancer.* Immunology, 2008. **123**(1): p. 129-38.
91. Hogquist, K.A., T.A. Baldwin, and S.C. Jameson, *Central tolerance: learning self-control in the thymus.* Nat Rev Immunol, 2005. **5**(10): p. 772-82.

92. Sakaguchi, S., *Regulatory T cells: key controllers of immunologic self-tolerance.* Cell, 2000. **101**(5): p. 455-8.
93. Sakaguchi, S., et al., *Foxp3+ CD25+ CD4+ natural regulatory T cells in dominant self-tolerance and autoimmune disease.* Immunol Rev, 2006. **212**: p. 8-27.
94. Sakaguchi, S., et al., *Regulatory T cells and immune tolerance.* Cell, 2008. **133**(5): p. 775-87.
95. McKee, A.S. and E.J. Pearce, *CD25+CD4+ cells contribute to Th2 polarization during helminth infection by suppressing Th1 response development.* J Immunol, 2004. **173**(2): p. 1224-31.
96. Yamaguchi, T., J.B. Wing, and S. Sakaguchi, *Two modes of immune suppression by Foxp3(+) regulatory T cells under inflammatory or non-inflammatory conditions.* Semin Immunol, 2011. **23**(6): p. 424-30.
97. Josefowicz, S.Z., L.F. Lu, and A.Y. Rudensky, *Regulatory T cells: mechanisms of differentiation and function.* Annu Rev Immunol, 2012. **30**: p. 531-64.
98. Apostolou, I., et al., *Peripherally induced Treg: mode, stability, and role in specific tolerance.* J Clin Immunol, 2008. **28**(6): p. 619-24.
99. Miyara, M. and S. Sakaguchi, *Natural regulatory T cells: mechanisms of suppression.* Trends Mol Med, 2007. **13**(3): p. 108-16.
100. Wynn, T.A., et al., *IL-10 regulates liver pathology in acute murine Schistosomiasis mansoni but is not required for immune down-modulation of chronic disease.* J Immunol, 1998. **160**(9): p. 4473-80.
101. Wynn, T.A., et al., *Analysis of granuloma formation in double cytokine-deficient mice reveals a central role for IL-10 in polarizing both T helper cell 1- and T helper cell 2-type cytokine responses in vivo.* J Immunol, 1997. **159**(10): p. 5014-23.
102. Hoffmann, K.F., A.W. Cheever, and T.A. Wynn, *IL-10 and the dangers of immune polarization: excessive type 1 and type 2 cytokine responses induce distinct forms of lethal immunopathology in murine schistosomiasis.* J Immunol, 2000. **164**(12): p. 6406-16.
103. Hesse, M., et al., *Differential regulation of nitric oxide synthase-2 and arginase-1 by type 1/type 2 cytokines in vivo: granulomatous pathology is shaped by the pattern of L-arginine metabolism.* J Immunol, 2001. **167**(11): p. 6533-44.
104. Yazdanbakhsh, M. and L.C. Rodrigues, *Allergy and the hygiene hypothesis: the Th1/Th2 counterregulation can not provide an explanation.* Wien Klin Wochenschr, 2001. **113**(23-24): p. 899-902.
105. Osada, Y. and T. Kanazawa, *Schistosome: Its Benefit and Harm in Patients Suffering from Concomitant Diseases.* Journal of Biomedicine and Biotechnology, 2011.
106. Chieffi, P.P., *Interrelationship between schistosomiasis and concomitant diseases.* Mem Inst Oswaldo Cruz, 1992. **87 Suppl 4**: p. 291-6.
107. Protzer, U., M.K. Maini, and P.A. Knolle, *Living in the liver: hepatic infections.* Nat Rev Immunol, 2012. **12**(3): p. 201-13.
108. Angelico, M., et al., *Chronic liver disease in the Alexandria governorate, Egypt: contribution of schistosomiasis and hepatitis virus infections.* J Hepatol, 1997. **26**(2): p. 236-43.
109. Strickland, G.T., et al., *Role of hepatitis C infection in chronic liver disease in Egypt.* Am J Trop Med Hyg, 2002. **67**(4): p. 436-42.
110. Kamal, S., et al., *Clinical, virological and histopathological features: long-term follow-up in patients with chronic hepatitis C co-infected with S. mansoni.* Liver, 2000. **20**(4): p. 281-9.
111. Hammad, H.A., et al., *Study on some hepatic functions and prevalence of hepatitis B surface antigenaemia in Egyptian children with schistosomal hepatic fibrosis.* J Trop Pediatr, 1990. **36**(3): p. 126-7.
112. Conceicao, M.J., et al., *Prognosis of schistosomiasis mansoni patients infected with hepatitis B virus.* Mem Inst Oswaldo Cruz, 1998. **93 Suppl 1**: p. 255-8.
113. Al-Freihi, H.M., *Prevalence of hepatitis B surface antigenemia among patients with schistosoma mansoni.* Ann Saudi Med, 1993. **13**(2): p. 121-5.

114. Stross, L., et al., *Foxp3+ regulatory T cells protect the liver from immune damage and compromise virus control during acute experimental hepatitis B virus infection in mice.* Hepatology, 2012. **56**(3): p. 873-83.
115. Osborne, L.C., et al., *Coinfection. Virus-helminth coinfection reveals a microbiota-independent mechanism of immunomodulation.* Science, 2014. **345**(6196): p. 578-82.
116. Reese, T.A., et al., *Coinfection. Helminth infection reactivates latent gamma-herpesvirus via cytokine competition at a viral promoter.* Science, 2014. **345**(6196): p. 573-7.
117. Edwards, M.J., et al., *Reciprocal immunomodulation in a schistosome and hepatotropic virus coinfection model.* J Immunol, 2005. **175**(10): p. 6275-85.
118. Rahman, A.H. and C. Aloman, *Dendritic cells and liver fibrosis.* Biochim Biophys Acta, 2013. **1832**(7): p. 998-1004.
119. Scheer, S., et al., *S. mansoni bolsters anti-viral immunity in the murine respiratory tract.* PLoS One, 2014. **9**(11): p. e112469.
120. Seeff, L.B., *Natural history of hepatitis C.* Hepatology, 1997. **26**(3 Suppl 1): p. 21S-28S.
121. Ray, S.C., et al., *Genetic epidemiology of hepatitis C virus throughout egypt.* J Infect Dis, 2000. **182**(3): p. 698-707.
122. Frank, C., et al., *The role of parenteral antischistosomal therapy in the spread of hepatitis C virus in Egypt.* Lancet, 2000. **355**(9207): p. 887-91.
123. Abdel-Aziz, F., et al., *Hepatitis C virus (HCV) infection in a community in the Nile Delta: population description and HCV prevalence.* Hepatology, 2000. **32**(1): p. 111-5.
124. Habib, M., et al., *Hepatitis C virus infection in a community in the Nile Delta: risk factors for seropositivity.* Hepatology, 2001. **33**(1): p. 248-53.
125. Shepard, C.W., L. Finelli, and M.J. Alter, *Global epidemiology of hepatitis C virus infection.* Lancet Infect Dis, 2005. **5**(9): p. 558-67.
126. Alter, M.J., *HCV routes of transmission: what goes around comes around.* Semin Liver Dis, 2011. **31**(4): p. 340-6.
127. http://www.who.int/mediacentre/factsheets/fs164/en/.
128. Bartenschlager, R. and V. Lohmann, *Replication of hepatitis C virus.* J Gen Virol, 2000. **81**(Pt 7): p. 1631-48.
129. Zeisel, M.B., et al., *Hepatitis C virus entry: molecular mechanisms and targets for antiviral therapy.* Front Biosci (Landmark Ed), 2009. **14**: p. 3274-85.
130. Yu, C.I. and B.L. Chiang, *A new insight into hepatitis C vaccine development.* J Biomed Biotechnol, 2010. **2010**: p. 548280.
131. Meier, V. and G. Ramadori, *Hepatitis C virus virology and new treatment targets.* Expert Rev Anti Infect Ther, 2009. **7**(3): p. 329-50.
132. Manns, M.P., et al., *The way forward in HCV treatment--finding the right path.* Nat Rev Drug Discov, 2007. **6**(12): p. 991-1000.
133. Manns, M.P. and T. von Hahn, *Novel therapies for hepatitis C - one pill fits all?* Nat Rev Drug Discov, 2013. **12**(8): p. 595-610.
134. Ciesek, S., T. von Hahn, and M.P. Manns, *Second-wave protease inhibitors: choosing an heir.* Clin Liver Dis, 2011. **15**(3): p. 597-609.
135. Wendt, A., et al., *Chronic hepatitis C: future treatment.* Clin Pharmacol, 2014. **6**: p. 1-17.
136. Kanda, T., et al., *New treatments for genotype 1 chronic hepatitis C - focus on simeprevir.* Ther Clin Risk Manag, 2014. **10**: p. 387-94.
137. Sulkowski, M.S., et al., *Faldaprevir combined with pegylated interferon alfa-2a and ribavirin in treatment-naive patients with chronic genotype 1 HCV: SILEN-C1 trial.* Hepatology, 2013. **57**(6): p. 2143-54.
138. Sulkowski, M.S., et al., *Faldaprevir combined with peginterferon alfa-2a and ribavirin in chronic hepatitis C virus genotype-1 patients with prior nonresponse: SILEN-C2 trial.* Hepatology, 2013. **57**(6): p. 2155-63.
139. Shoukry, N.H., A.G. Cawthon, and C.M. Walker, *Cell-mediated immunity and the outcome of hepatitis C virus infection.* Annu Rev Microbiol, 2004. **58**: p. 391-424.

140. Billerbeck, E., T. Bottler, and R. Thimme, *Regulatory T cells in viral hepatitis.* World J Gastroenterol, 2007. **13**(36): p. 4858-64.
141. Boettler, T., et al., *T cells with a CD4+CD25+ regulatory phenotype suppress in vitro proliferation of virus-specific CD8+ T cells during chronic hepatitis C virus infection.* J Virol, 2005. **79**(12): p. 7860-7.
142. Bolacchi, F., et al., *Increased hepatitis C virus (HCV)-specific CD4+CD25+ regulatory T lymphocytes and reduced HCV-specific CD4+ T cell response in HCV-infected patients with normal versus abnormal alanine aminotransferase levels.* Clin Exp Immunol, 2006. **144**(2): p. 188-96.
143. MacDonald, A.J., et al., *CD4 T helper type 1 and regulatory T cells induced against the same epitopes on the core protein in hepatitis C virus-infected persons.* J Infect Dis, 2002. **185**(6): p. 720-7.
144. Ward, S.M., et al., *Quantification and localisation of FOXP3+ T lymphocytes and relation to hepatic inflammation during chronic HCV infection.* J Hepatol, 2007. **47**(3): p. 316-24.
145. Strickland, G.T., *Liver disease in Egypt: hepatitis C superseded schistosomiasis as a result of iatrogenic and biological factors.* Hepatology, 2006. **43**(5): p. 915-22.
146. Mohamoud, Y.A., et al., *The epidemiology of hepatitis C virus in Egypt: a systematic review and data synthesis.* BMC Infect Dis, 2013. **13**: p. 288.
147. Edris, A., et al., *Seroprevalence and risk factors for hepatitis B and C virus infection in Damietta Governorate, Egypt.* East Mediterr Health J, 2014. **20**(10): p. 605-13.
148. Emam, E.A., et al., *Impact of Schistosoma mansoni co-infection on serum profile of interferon-gamma, interleukin-4 and interleukin-10 in patients with chronic hepatitis C virus infection.* Egypt J Immunol, 2006. **13**(2): p. 33-40.
149. Gad, A., et al., *Relationship between hepatitis C virus infection and schistosomal liver disease: not simply an additive effect.* J Gastroenterol, 2001. **36**(11): p. 753-8.
150. Van-Lume, D.S., et al., *Association between Schistosomiasis mansoni and hepatitis C: systematic review.* Rev Saude Publica, 2013. **47**(2): p. 414-24.
151. Gasim, G.I., A. Bella, and I. Adam, *Schistosomiasis, hepatitis B and hepatitis C co-infection.* Virol J, 2015. **12**: p. 19.
152. Kamal, S.M., et al., *Acute hepatitis C without and with schistosomiasis: correlation with hepatitis C-specific CD4(+) T-cell and cytokine response.* Gastroenterology, 2001. **121**(3): p. 646-56.
153. Kamal, S.M., et al., *Interferon therapy in patients with chronic hepatitis C and schistosomiasis.* J Hepatol, 2000. **32**(1): p. 172-4.
154. Chen, S.L. and T.R. Morgan, *The natural history of hepatitis C virus (HCV) infection.* Int J Med Sci, 2006. **3**(2): p. 47-52.
155. Li, Y., et al., *Severe hepatosplenic schistosomiasis: clinicopathologic study of 102 cases undergoing splenectomy.* Hum Pathol, 2011. **42**(1): p. 111-9.
156. Abdel-Rahman, M., et al., *Coinfection with hepatitis C virus and schistosomiasis: fibrosis and treatment response.* World J Gastroenterol, 2013. **19**(17): p. 2691-6.
157. Elrefaei, M., et al., *HCV-specific CD27- CD28- memory T cells are depleted in hepatitis C virus and Schistosoma mansoni co-infection.* Immunology, 2003. **110**(4): p. 513-8.
158. Kamel, M.M., et al., *P selectin and T cell profiles provide verification to understand the pathogenesis of liver cirrhosis in HCV and Schistosoma mansoni infections.* Microb Pathog, 2014. **73**: p. 19-24.
159. Schilsky, M.L., *Hepatitis B "360".* Transplant Proc, 2013. **45**(3): p. 982-5.
160. Fairley, C.K. and T.R. Read, *Vaccination against sexually transmitted infections.* Curr Opin Infect Dis, 2012. **25**(1): p. 66-72.
161. Yan, H., et al., *Sodium taurocholate cotransporting polypeptide is a functional receptor for human hepatitis B and D virus.* Elife, 2012. **1**: p. e00049.
162. Bertoletti, A. and A.J. Gehring, *The immune response during hepatitis B virus infection.* J Gen Virol, 2006. **87**(Pt 6): p. 1439-49.

163. Chang, M.H., *Hepatitis B virus infection.* Semin Fetal Neonatal Med, 2007. **12**(3): p. 160-7.
164. Xia, Y., et al., *Virology. Response to Comment on "Specific and nonhepatotoxic degradation of nuclear hepatitis B virus cccDNA".* Science, 2014. **344**(6189): p. 1237.
165. Fensterl, V. and G.C. Sen, *Interferons and viral infections.* Biofactors, 2009. **35**(1): p. 14-20.
166. Maini, M.K., et al., *The role of virus-specific CD8(+) cells in liver damage and viral control during persistent hepatitis B virus infection.* J Exp Med, 2000. **191**(8): p. 1269-80.
167. Platanias, L.C., *Mechanisms of type-I- and type-II-interferon-mediated signalling.* Nat Rev Immunol, 2005. **5**(5): p. 375-86.
168. Takaoka, A., et al., *Integration of interferon-alpha/beta signalling to p53 responses in tumour suppression and antiviral defence.* Nature, 2003. **424**(6948): p. 516-23.
169. Moiseeva, O., et al., *DNA damage signaling and p53-dependent senescence after prolonged beta-interferon stimulation.* Mol Biol Cell, 2006. **17**(4): p. 1583-92.
170. de Veer, M.J., et al., *Functional classification of interferon-stimulated genes identified using microarrays.* J Leukoc Biol, 2001. **69**(6): p. 912-20.
171. Schroder, K., et al., *Interferon-gamma: an overview of signals, mechanisms and functions.* J Leukoc Biol, 2004. **75**(2): p. 163-89.
172. Pungpapong, S., W.R. Kim, and J.J. Poterucha, *Natural history of hepatitis B virus infection: an update for clinicians.* Mayo Clin Proc, 2007. **82**(8): p. 967-75.
173. Lai, C.L. and M.F. Yuen, *The natural history and treatment of chronic hepatitis B: a critical evaluation of standard treatment criteria and end points.* Ann Intern Med, 2007. **147**(1): p. 58-61.
174. Lai, M.E., et al., *Markers of hepatitis C virus infection in Sardinian blood donors: relationship with alanine aminotransferase levels.* J Med Virol, 1993. **41**(4): p. 282-8.
175. Fox, Z., et al., *A randomized trial to evaluate continuation versus discontinuation of lamivudine in individuals failing a lamivudine-containing regimen: the COLATE trial.* Antivir Ther, 2006. **11**(6): p. 761-70.
176. Pramoolsinsup, C., *Management of viral hepatitis B.* J Gastroenterol Hepatol, 2002. **17 Suppl**: p. S125-45.
177. Andrade, J.R., et al., *Chronic hepatitis B and liver schistosomiasis: a deleterious association.* Trans R Soc Trop Med Hyg, 2014. **108**(3): p. 159-64.
178. Larouze, B., et al., *Absence of relationship between Schistosoma mansoni and hepatitis B virus infection in the Qalyub Governate, Egypt.* Ann Trop Med Parasitol, 1987. **81**(4): p. 373-5.
179. Ye, X.P., et al., *Absence of relationship between Schistosoma japonicum and hepatitis B virus infection in the Dongting lake region, China.* Epidemiol Infect, 1998. **121**(1): p. 193-5.
180. Al-Shamiri, A.H., M.A. Al-Taj, and A.S. Ahmed, *Prevalence and co-infections of schistosomiasis/hepatitis B and C viruses among school children in an endemic areas in Taiz, Yemen.* Asian Pac J Trop Med, 2011. **4**(5): p. 404-8.
181. Barker, L.F., et al., *Transmission of type B viral hepatitis to chimpanzees.* J Infect Dis, 1973. **127**(6): p. 648-62.
182. Dupinay, T., et al., *Discovery of naturally occurring transmissible chronic hepatitis B virus infection among Macaca fascicularis from Mauritius Island.* Hepatology, 2013. **58**(5): p. 1610-20.
183. Walter, E., et al., *Hepatitis B virus infection of tupaia hepatocytes in vitro and in vivo.* Hepatology, 1996. **24**(1): p. 1-5.
184. Mason, W.S., et al., *Experimental transmission of duck hepatitis B virus.* Virology, 1983. **131**(2): p. 375-84.
185. Summers, J., J.M. Smolec, and R. Snyder, *A virus similar to human hepatitis B virus associated with hepatitis and hepatoma in woodchucks.* Proc Natl Acad Sci U S A, 1978. **75**(9): p. 4533-7.
186. Tennant, B.C. and J.L. Gerin, *The woodchuck model of hepatitis B virus infection.* ILAR J, 2001. **42**(2): p. 89-102.
187. Gerin, J.L., *Experimental WHV infection of woodchucks: an animal model of hepadnavirus-induced liver cancer.* Gastroenterol Jpn, 1990. **25 Suppl 2**: p. 38-42.

188. Roggendorf, M., D. Yang, and M. Lu, *The woodchuck: a model for therapeutic vaccination against hepadnaviral infection.* Pathol Biol (Paris), 2010. **58**(4): p. 308-14.
189. Roggendorf, M. and T.K. Tolle, *The woodchuck: an animal model for hepatitis B virus infection in man.* Intervirology, 1995. **38**(1-2): p. 100-12.
190. Andrade, Z.A., et al., *Schistosomiasis mansoni and viral B hepatitis in woodchucks.* J Hepatol, 2001. **34**(1): p. 134-9.
191. Summers, J., *Three recently described animal virus models for human hepatitis B virus.* Hepatology, 1981. **1**(2): p. 179-83.
192. Di, Q., et al., *Major differences between WHV and HBV in the regulation of transcription.* Virology, 1997. **229**(1): p. 25-35.
193. Guha, C., et al., *Cell culture and animal models of viral hepatitis. Part I: hepatitis B.* Lab Anim (NY), 2004. **33**(7): p. 37-46.
194. Ogston, C.W., et al., *Cloning and structural analysis of integrated woodchuck hepatitis virus sequences from hepatocellular carcinomas of woodchucks.* Cell, 1982. **29**(2): p. 385-94.
195. Rogler, C.E., O. Hino, and C.Y. Su, *Molecular aspects of persistent woodchuck hepatitis virus and hepatitis B virus infection and hepatocellular carcinoma.* Hepatology, 1987. **7**(1 Suppl): p. 74S-78S.
196. Rogler, C.E. and J. Summers, *Cloning and structural analysis of integrated woodchuck hepatitis virus sequences from a chronically infected liver.* J Virol, 1984. **50**(3): p. 832-7.
197. Chen, M., et al., *Nondeletional T-cell receptor transgenic mice: model for the CD4(+) T-cell repertoire in chronic hepatitis B virus infection.* J Virol, 2000. **74**(16): p. 7587-99.
198. Chisari, F.V., et al., *A transgenic mouse model of the chronic hepatitis B surface antigen carrier state.* Science, 1985. **230**(4730): p. 1157-60.
199. Guidotti, L.G., et al., *High-level hepatitis B virus replication in transgenic mice.* J Virol, 1995. **69**(10): p. 6158-69.
200. Ando, K., et al., *Mechanisms of class I restricted immunopathology. A transgenic mouse model of fulminant hepatitis.* J Exp Med, 1993. **178**(5): p. 1541-54.
201. Guidotti, L.G., et al., *Intracellular inactivation of the hepatitis B virus by cytotoxic T lymphocytes.* Immunity, 1996. **4**(1): p. 25-36.
202. Guidotti, L.G., et al., *Cytotoxic T lymphocytes inhibit hepatitis B virus gene expression by a noncytolytic mechanism in transgenic mice.* Proc Natl Acad Sci U S A, 1994. **91**(9): p. 3764-8.
203. Nakamoto, Y., et al., *Differential target cell sensitivity to CTL-activated death pathways in hepatitis B virus transgenic mice.* J Immunol, 1997. **158**(12): p. 5692-7.
204. Milich, D.R., et al., *The secreted hepatitis B precore antigen can modulate the immune response to the nucleocapsid: a mechanism for persistence.* J Immunol, 1998. **160**(4): p. 2013-21.
205. Li, H., et al., *HBV life cycle is restricted in mouse hepatocytes expressing human NTCP.* Cell Mol Immunol, 2014. **11**(2): p. 175-83.
206. Hagenbuch, B. and P.J. Meier, *Molecular cloning, chromosomal localization, and functional characterization of a human liver Na+/bile acid cotransporter.* J Clin Invest, 1994. **93**(3): p. 1326-31.
207. Yan, H., et al., *NTCP opens the door for hepatitis B virus infection.* Antiviral Res, 2015.
208. Meier, A., et al., *Myristoylated PreS1-domain of the hepatitis B virus L-protein mediates specific binding to differentiated hepatocytes.* Hepatology, 2013. **58**(1): p. 31-42.
209. Schieck, A., et al., *Hepatitis B virus hepatotropism is mediated by specific receptor recognition in the liver and not restricted to susceptible hosts.* Hepatology, 2013. **58**(1): p. 43-53.
210. Yan, H., et al., *Molecular determinants of hepatitis B and D virus entry restriction in mouse sodium taurocholate cotransporting polypeptide.* J Virol, 2013. **87**(14): p. 7977-91.
211. Ni, Y., et al., *Hepatitis B and D viruses exploit sodium taurocholate co-transporting polypeptide for species-specific entry into hepatocytes.* Gastroenterology, 2014. **146**(4): p. 1070-83.

212. Yang, P.L., et al., *Hydrodynamic injection of viral DNA: a mouse model of acute hepatitis B virus infection.* Proc Natl Acad Sci U S A, 2002. **99**(21): p. 13825-30.
213. Sprinzl, M.F., et al., *Transfer of hepatitis B virus genome by adenovirus vectors into cultured cells and mice: crossing the species barrier.* J Virol, 2001. **75**(11): p. 5108-18.
214. Huang, L.R., et al., *An immunocompetent mouse model for the tolerance of human chronic hepatitis B virus infection.* Proc Natl Acad Sci U S A, 2006. **103**(47): p. 17862-7.
215. von Freyend, M.J., et al., *Sequential control of hepatitis B virus in a mouse model of acute, self-resolving hepatitis B.* J Viral Hepat, 2011. **18**(3): p. 216-26.
216. Dembek, C. and U. Protzer, *Mouse models for therapeutic vaccination against hepatitis B virus.* Med Microbiol Immunol, 2015. **204**(1): p. 95-102.
217. McClary, H., et al., *Inhibition of hepatitis B virus replication during schistosoma mansoni infection in transgenic mice.* J Exp Med, 2000. **192**(2): p. 289-94.
218. Baumert, T.F., H. Barth, and H.E. Blum, *Genetic variants of hepatitis B virus and their clinical relevance.* Minerva Gastroenterol Dietol, 2005. **51**(1): p. 95-108.
219. Shin, M.K., J. Lee, and W.S. Ryu, *A novel cis-acting element facilitates minus-strand DNA synthesis during reverse transcription of the hepatitis B virus genome.* J Virol, 2004. **78**(12): p. 6252-62.
220. Treichel, U., et al., *Receptor-mediated entry of hepatitis B virus particles into liver cells.* Arch Virol, 1997. **142**(3): p. 493-8.
221. Dane, D.S., C.H. Cameron, and M. Briggs, *Virus-like particles in serum of patients with Australia-antigen-associated hepatitis.* Lancet, 1970. **1**(7649): p. 695-8.
222. Pollicino, T., et al., *Hepatitis B virus PreS/S gene variants: pathobiology and clinical implications.* J Hepatol, 2014. **61**(2): p. 408-17.
223. Bruss, V., et al., *Myristylation of the large surface protein is required for hepatitis B virus in vitro infectivity.* Virology, 1996. **218**(2): p. 396-9.
224. Ishikawa, T. and D. Ganem, *The pre-S domain of the large viral envelope protein determines host range in avian hepatitis B viruses.* Proc Natl Acad Sci U S A, 1995. **92**(14): p. 6259-63.
225. Lenhoff, R.J. and J. Summers, *Coordinate regulation of replication and virus assembly by the large envelope protein of an avian hepadnavirus.* J Virol, 1994. **68**(7): p. 4565-71.
226. Bottcher, B., S.A. Wynne, and R.A. Crowther, *Determination of the fold of the core protein of hepatitis B virus by electron cryomicroscopy.* Nature, 1997. **386**(6620): p. 88-91.
227. Robinson, W.S., D.A. Clayton, and R.L. Greenman, *DNA of a human hepatitis B virus candidate.* J Virol, 1974. **14**(2): p. 384-91.
228. Howard, C.R., *The biology of hepadnaviruses.* J Gen Virol, 1986. **67 ( Pt 7)**: p. 1215-35.
229. Schulze, A., P. Gripon, and S. Urban, *Hepatitis B virus infection initiates with a large surface protein-dependent binding to heparan sulfate proteoglycans.* Hepatology, 2007. **46**(6): p. 1759-68.
230. Leistner, C.M., S. Gruen-Bernhard, and D. Glebe, *Role of glycosaminoglycans for binding and infection of hepatitis B virus.* Cell Microbiol, 2008. **10**(1): p. 122-33.
231. Huang, L.R., et al., *Transfer of HBV genomes using low doses of adenovirus vectors leads to persistent infection in immune competent mice.* Gastroenterology, 2012. **142**(7): p. 1447-50 e3.
232. Liu, Y.M., et al., *High expression of beta2-glycoprotein I is associated significantly with the earliest stages of hepatitis B virus infection.* J Med Virol, 2014. **86**(8): p. 1296-306.
233. Bock, C.T., et al., *Structural organization of the hepatitis B virus minichromosome.* J Mol Biol, 2001. **307**(1): p. 183-96.
234. Nassal, M., *Hepatitis B viruses: reverse transcription a different way.* Virus Res, 2008. **134**(1-2): p. 235-49.
235. Urban, S., et al., *The replication cycle of hepatitis B virus.* J Hepatol, 2010. **52**(2): p. 282-4.
236. Beck, J. and M. Nassal, *Hepatitis B virus replication.* World J Gastroenterol, 2007. **13**(1): p. 48-64.
237. Zlotnick, A., et al., *A theoretical model successfully identifies features of hepatitis B virus capsid assembly.* Biochemistry, 1999. **38**(44): p. 14644-52.

238. Bruss, V., *Hepatitis B virus morphogenesis.* World J Gastroenterol, 2007. **13**(1): p. 65-73.
239. Zhang, Y.Y., et al., *Single-cell analysis of covalently closed circular DNA copy numbers in a hepadnavirus-infected liver.* Proc Natl Acad Sci U S A, 2003. **100**(21): p. 12372-7.
240. Werle-Lapostolle, B., et al., *Persistence of cccDNA during the natural history of chronic hepatitis B and decline during adefovir dipivoxil therapy.* Gastroenterology, 2004. **126**(7): p. 1750-8.
241. Li, W., et al., *Hepatitis B virus X protein upregulates HSP90alpha expression via activation of c-Myc in human hepatocarcinoma cell line, HepG2.* Virol J, 2010. **7**: p. 45.
242. Rowe, W.P., et al., *Isolation of a cytopathogenic agent from human adenoids undergoing spontaneous degeneration in tissue culture.* Proc Soc Exp Biol Med, 1953. **84**(3): p. 570-3.
243. Robinson, C.M., et al., *Computational analysis and identification of an emergent human adenovirus pathogen implicated in a respiratory fatality.* Virology, 2011. **409**(2): p. 141-7.
244. Harrison, S.C., *Virology. Looking inside adenovirus.* Science, 2010. **329**(5995): p. 1026-7.
245. Thacker, E.E., et al., *A genetically engineered adenovirus vector targeted to CD40 mediates transduction of canine dendritic cells and promotes antigen-specific immune responses in vivo.* Vaccine, 2009. **27**(50): p. 7116-24.
246. Ross, P.J. and R.J. Parks, *Construction and characterization of adenovirus vectors.* Cold Spring Harb Protoc, 2009. **2009**(5): p. pdb prot5011.
247. Windheim, M., A. Hilgendorf, and H.G. Burgert, *Immune evasion by adenovirus E3 proteins: exploitation of intracellular trafficking pathways.* Curr Top Microbiol Immunol, 2004. **273**: p. 29-85.
248. Blair, G.E. and M.E. Blair-Zajdel, *Evasion of the immune system by adenoviruses.* Curr Top Microbiol Immunol, 2004. **273**: p. 3-28.
249. Lahl, K., et al., *Selective depletion of Foxp3+ regulatory T cells induces a scurfy-like disease.* J Exp Med, 2007. **204**(1): p. 57-63.
250. Wichmann, D., et al., *Diagnosing schistosomiasis by detection of cell-free parasite DNA in human plasma.* PLoS Negl Trop Dis, 2009. **3**(4): p. e422.
251. Gautheron, J., et al., *A positive feedback loop between RIP3 and JNK controls non-alcoholic steatohepatitis.* EMBO Mol Med, 2014. **6**(8): p. 1062-74.
252. Bruns, T., et al., *Hepatitis C virus RNA quantitation in venous and capillary small-volume whole-blood samples.* J Clin Microbiol, 2009. **47**(10): p. 3231-40.
253. Loffredo-Verde, E., et al., *Schistosome infection aggravates HCV-related liver disease and induces changes in the regulatory T-cell phenotype.* Parasite Immunol, 2015. **37**(2): p. 97-104.
254. Mercer, D.F., et al., *Hepatitis C virus replication in mice with chimeric human livers.* Nat Med, 2001. **7**(8): p. 927-33.
255. Bissig, K.D., et al., *Human liver chimeric mice provide a model for hepatitis B and C virus infection and treatment.* J Clin Invest, 2010. **120**(3): p. 924-30.
256. Dumortier, J., et al., *Liver-specific expression of interferon gamma following adenoviral gene transfer controls hepatitis B virus replication in mice.* Gene Ther, 2005. **12**(8): p. 668-77.
257. Buchmann, P., et al., *A novel therapeutic hepatitis B vaccine induces cellular and humoral immune responses and breaks tolerance in hepatitis B virus (HBV) transgenic mice.* Vaccine, 2013. **31**(8): p. 1197-203.
258. Straubinger, K., et al., *Maternal immune response to helminth infection during pregnancy determines offspring susceptibility to allergic airway inflammation.* J Allergy Clin Immunol, 2014.
259. Schmidt, J., H.E. Blum, and R. Thimme, *T-cell responses in hepatitis B and C virus infection: similarities and differences.* Emerg Microbes Infect, 2013. **2**(3): p. e15.
260. El-Kady, I.M., et al., *Interleukin (IL)-4, IL-10, IL-18 and IFN-gamma cytokines pattern in patients with combined hepatitis C virus and Schistosoma mansoni infections.* Scand J Immunol, 2005. **61**(1): p. 87-91.
261. Post, J., S. Ratnarajah, and A.R. Lloyd, *Immunological determinants of the outcomes from primary hepatitis C infection.* Cell Mol Life Sci, 2009. **66**(5): p. 733-56.

262. Spengler, U. and J. Nattermann, *Immunopathogenesis in hepatitis C virus cirrhosis.* Clin Sci (Lond), 2007. **112**(3): p. 141-55.
263. Langhans, B., et al., *Core-specific adaptive regulatory T-cells in different outcomes of hepatitis C.* Clin Sci (Lond). **119**(2): p. 97-109.
264. Wammes, L.J., et al., *Regulatory T cells in human geohelminth infection suppress immune responses to BCG and Plasmodium falciparum.* Eur J Immunol, 2010. **40**(2): p. 437-42.
265. Kamal, S.M., et al., *Progression of fibrosis in hepatitis C with and without schistosomiasis: correlation with serum markers of fibrosis.* Hepatology, 2006. **43**(4): p. 771-9.
266. Gottschalk, R.A., E. Corse, and J.P. Allison, *Expression of Helios in peripherally induced Foxp3+ regulatory T cells.* J Immunol, 2012. **188**(3): p. 976-80.
267. Specht, S. and A. Hoerauf, *Does helminth elimination promote or prevent malaria?* Lancet, 2007. **369**(9560): p. 446-7.
268. Borkow, G. and Z. Bentwich, *Chronic parasite infections cause immune changes that could affect successful vaccination.* Trends Parasitol, 2008. **24**(6): p. 243-5.
269. Cooper, P.J., et al., *Human infection with Ascaris lumbricoides is associated with suppression of the interleukin-2 response to recombinant cholera toxin B subunit following vaccination with the live oral cholera vaccine CVD 103-HgR.* Infect Immun, 2001. **69**(3): p. 1574-80.
270. Farid, A., et al., *Schistosoma infection inhibits cellular immune responses to core HCV peptides.* Parasite Immunol, 2005. **27**(5): p. 189-96.
271. Dorner, M., et al., *A genetically humanized mouse model for hepatitis C virus infection.* Nature, 2011. **474**(7350): p. 208-11.
272. Dorner, M., et al., *Completion of the entire hepatitis C virus life cycle in genetically humanized mice.* Nature, 2013. **501**(7466): p. 237-41.
273. Tawar, R.G., L. Mailly, and T.F. Baumert, *A new HCV mouse model on the block.* Cell Res, 2014. **24**(10): p. 1153-4.
274. Guidotti, L.G. and F.V. Chisari, *Cytokine-induced viral purging--role in viral pathogenesis.* Curr Opin Microbiol, 1999. **2**(4): p. 388-91.
275. Chisari, F.V., *Rous-Whipple Award Lecture. Viruses, immunity, and cancer: lessons from hepatitis B.* Am J Pathol, 2000. **156**(4): p. 1117-32.
276. Peng, G., et al., *Induction of APOBEC3 family proteins, a defensive maneuver underlying interferon-induced anti-HIV-1 activity.* J Exp Med, 2006. **203**(1): p. 41-6.
277. Gao, B., et al., *Tripartite motif-containing 22 inhibits the activity of hepatitis B virus core promoter, which is dependent on nuclear-located RING domain.* Hepatology, 2009. **50**(2): p. 424-33.
278. Schoenborn, J.R. and C.B. Wilson, *Regulation of interferon-gamma during innate and adaptive immune responses.* Adv Immunol, 2007. **96**: p. 41-101.
279. Peng, G., et al., *Circulating CD4+ CD25+ regulatory T cells correlate with chronic hepatitis B infection.* Immunology, 2008. **123**(1): p. 57-65.
280. Stoop, J.N., et al., *Regulatory T cells contribute to the impaired immune response in patients with chronic hepatitis B virus infection.* Hepatology, 2005. **41**(4): p. 771-8.
281. Ye, B., et al., *T-cell exhaustion in chronic hepatitis B infection: current knowledge and clinical significance.* Cell Death Dis, 2015. **6**: p. e1694.
282. Christiaansen, A.F., P.M. Boggiatto, and S.M. Varga, *Limitations of Foxp3(+) Treg depletion following viral infection in DEREG mice.* J Immunol Methods, 2014. **406**: p. 58-65.
283. Lahl, K. and T. Sparwasser, *In vivo depletion of FoxP3+ Tregs using the DEREG mouse model.* Methods Mol Biol, 2011. **707**: p. 157-72.
284. Mayer, C.T., et al., *Advantages of Foxp3(+) regulatory T cell depletion using DEREG mice.* Immun Inflamm Dis, 2014. **2**(3): p. 162-5.
285. Berod, L., et al., *Rapid rebound of the Treg compartment in DEREG mice limits the impact of Treg depletion on mycobacterial burden, but prevents autoimmunity.* PLoS One, 2014. **9**(7): p. e102804.
286. Caldas, I.R., et al., *Human schistosomiasis mansoni: immune responses during acute and chronic phases of the infection.* Acta Trop, 2008. **108**(2-3): p. 109-17.

287. Pak-Wittel, M.A., et al., *Interferon-gamma mediates chemokine-dependent recruitment of natural killer cells during viral infection.* Proc Natl Acad Sci U S A, 2013. **110**(1): p. E50-9.

## 5.5 Publications

***Schistosoma mansoni-mediated suppression of allergic airway inflammation requires patency and Foxp3$^{+}$ Treg cells.***

**Layland LE[1,2,§], Straubinger K[1,§]**, Ritter M[1], Loffredo-Verde E[1], Garn H[3], Sparwasser T[4], Prazeres da Costa C[1].

[1]Institute of Medical Microbiology, Immunology and Hygiene, Technische Universität München, Munich, Germany. [2]Institute of Medical Microbiology, Immunology and Parasitology (IMMIP), University Clinic Bonn, Bonn, Germany, [3]Institute of Laboratory Medicine and Pathobiochemistry, Medical Faculty, Philipps- University Marburg, Marburg, Germany, [4]Institut für Infektionsimmunologie TWINCORE - Zentrum für Experimentelle und Klinische Infektionsforschung GmbH, Hannover, Germany

§ - shared first authorship

**PlosNTD (accepted 2013)**

***Lack of host gut microbiota alters immune responses and intestinal granuloma formation during schistosomiasis.***

**Holzscheiter M[1,§], Layland LE[1,4,§]**, Loffredo-Verde E[1], Mair K[2], Vogelmann R[2], Langer R[3], Wagner H[1], Prazeres da Costa C[1].

[1]Institute of Medical Microbiology, Immunology and Hygiene, Technische Universität München, Munich, Germany. [2]II Medizinische Klinik und Poliklinik (Gastroenterlologie) and [3]Institute of Pathology, Technische Universität München, Munich, Germany and [4]Institute of Medical Microbiology, Immunology and Parasitology (IMMIP), University Clinic Bonn, Bonn, Germany

§ - shared first authorship

**Clin Exp Immunol. (accepted 2014)**

## *Schistosome infection aggravates HCV-related liver disease and induces changes in the regulatory T-cell phenotype.*

**Loffredo-Verde E[1,§]**, Abdel-Aziz I[2], Albrecht J[1,3], El-Guindy N[4], Yacob M[4], Solieman A[5], Protzer U[3,6], Busch DH[1,3], Layland LE[7], Prazeres da Costa CU[1].

[1]Institute for Medical Microbiology, Immunology and Hygiene, Technische Universität München, Munich, Germany. [2]Medical Parasitology, Kasr El-Eini University Clinic Cairo, Cairo, Egypt, [3]Clinical Cooperation Group 'Immune Monitoring', Helmholtz Zentrum München and Technische Universität München, Munich, Germany, [4]Clinical & Chemical Pathology, Kasr El-Eini School of Medicine Hospitals, University of Cairo, Cairo, Egypt, [5]Tropical Medicine Departments, Kasr El-Eini School of Medicine Hospitals, University of Cairo, Cairo, Egypt, [6]Institute of Virology, Technische Universität and Helmholtz Zentrum München, Munich, Germany, [7]Institute of Medical Microbiology, Immunology and Parasitology (IMMIP), University Clinic Bonn, Bonn, Germany

§ - first authorship

**Parasite Immunology (accepted 2015)**

## Declaration

I, Eva Loffredo-Verde, hereby declare that I independently prepared the present thesis, using only the references and resources stated. This work has not been submitted to any examination board, yet. Parts of this work are already published (human HCV/*S. mansoni* study; Journal *Parasite Immunology*, accepted 2015), others will be published in scientific journals as well.

Munich, October 2015

## Acknowledgement

This dissertation would not have been possible without the help of so many people in so many ways. Firstly, I would like to thank my advisor Dr. Clarissa Prazeres da Costa for her continuous support of my Ph.D. research, for her patience, motivation, infectious enthusiasm and instilling in me the qualities of being a good scientist. Without her guidance, encouragement and persistent help this dissertation would not have been possible.

I would like to thank Prof. Dr. Dirk Busch for giving me the possibility to do my Ph.D. thesis at the Institute of Medical Microbiology, Immunology and Hygiene. In addition, I would like to take this opportunity to thank Dr. Laura Layland whose assistence and immense knowledge helped to finalize and publish our human co-infection study. Thanks also go out to Prof. Dr. Ulrike Protzer for initiating a very interesting murine side project through which I discovered my passion for virology. I thank her for the nice collaboration, help and supporting discussions.

I would like to thank my second supervisor and thesis committee member, Prof. Dr. Martin Klingenspor for his insightful comments and stimulating discussions.

A warm appreciation goes to my teammates for supporting me both on and off the water. Particularly, I am indebted to Sonakshi Bhattacharjee, who gave me so much joy and fun in the lab and carefully proofread this manuscript. A special thanks goes also to Dr. Elisabeth Maier who recently joined the institute and gave this manuscript a second proofread. I thank Marija Ram, Sabine Paul and Natalie Röder for excellent technical support and Ulla Henn and Stephanie Fetzer for taking care of the schistosome cycle. I would also like to thank Antje Malo for all the fruitful discussions and the great cooperation in the murine project.

I cannot find words to express my gratitude to Bruno Piochacz, whose love, support and encouraging words helped me to survive all the stress from these years and not letting me give up. Last but not least, I owe my deepest gratitude to my mother for her unconditional love and support that helped to finalize this work.